Molecular mechanisms regulating B lymphocyte polarization

Dorian Obino

UNIVERSITE PARIS DESCARTES

THESE DE DOCTORAT

Spécialité Immunologie

Ecole doctorale BioSPC

Soutenue le 16 juin 2016 par

Dorian OBINO

Pour obtenir le titre de

DOCTEUR EN SCIENCES

DE L'UNIVERSITE PARIS DESCARTES

Molecular mechanisms regulating B lymphocyte polarization

Thèse dirigée par **Ana-Maria LENNON-DUMENIL**
Institut Curie, INSERM - U932
12 Rue Lhomond
75005 PARIS

Devant le jury composé de:

Pr. Catherine ALCAÏDE-LORIDAN	Président du jury
Dr. Federica BENVENUTI	Rapporteur
Dr. Stéphanie MISEREY-LENKEI	Rapporteur
Dr. Marion ESPELI	Examinateur
Dr. Philippe BOUSSO	Examinateur
Dr. Jérôme DELON	Examinateur
Dr. Ana-Maria LENNON-DUMENIL	Directeur de thèse

UNIVERSITÉ PARIS DESCARTES

Bio Sorbonne Paris Cité

FONDATION RECHERCHE MÉDICALE

institut Curie

Ensemble, prenons le cancer de vitesse.

A Arnaud,

A mes Parents,

A mes Grands-Parents,

Aux membres du jury

Tout d'abord, mes sincères remerciements sont dirigés vers les membres du jury qui ont gentiment accepté d'évaluer mon travail de thèse. Merci au Pr. Catherine Alcaïde-Loridan de présider ce jury, ainsi qu'aux Dr. Federica Benvenuti et Stéphanie Miserey-Lenkei pour le temps passé à lire mon manuscrit et pour vos précieux commentaires. Merci aux Dr. Marion Espéli, Philippe Bousso et Jérôme Delon d'avoir accepté d'examiner mon travail de thèse. Enfin, merci à tous d'être parmi nous pour la soutenance de ma thèse et pour les belles discussions que nous allons avoir ensemble.

A mon incroyable Chef

Ana, quel moment difficile… Ces quelques pages représentent l'aboutissement de plus de 4 ans de collaboration… Je tiens à te remercier pour toute la confiance que tu m'as accordée. Merci de m'avoir donné l'opportunité de réaliser ma thèse dans ton équipe. J'ai grandi à tes côtés, scientifiquement et personnellement, et je garderai toujours au fond de moi le souvenir de nos moments partagés. Ton excellence scientifique et ta renommée ne sont plus à faire, mais je tiens ici à les souligner. Grâce à toi j'ai ''découvert le monde'', je me suis forgé une solide expérience et j'ai énormément appris. Même si tout n'a pas été facile tous les jours, quelle belle aventure nous avons vécue… C'est le cœur serré que je vais quitter ton laboratoire et que je vais m'envoler vers de nouvelles aventures… Je ne serai pas très loin et j'espère sincèrement que nos chemins se recroiseront. Enfin, juste MERCI !

A la ''Lennon Team''

Je tiens ici à remercier l'ensemble de l'équipe Lennon pour les nombreux échanges, discussions, coups de main qui ont fait que mon passage dans le labo a été si fructueux. Je remercie tout particulièrement Maria-Isabel et Danielle qui m'ont tout appris quand je suis arrivé et qui ont été d'une précieuse aide. Merci à Mélanie C., Marine, Pablo et Pablo, Odile, Hélène et Violaine pour votre soutien sans faille, pour votre disponibilité, vos conseils, merci d'avoir été là dans les moments de doute pour me remotiver, enfin merci d'avoir été juste vous-même ! Ne changez rien !!!

Mél ma râleuse née, qu'est-ce que tu me manques depuis que tu es partie… Et oui c'est dur de perdre son alter ego féminin… Merci en tout cas pour tout… Il n'y aurait pas assez de

place pour parler de tout et tout écrire, mais tu sais déjà tout !! Merci, merci et encore merci (nieuh, snif, nieuh !) !!!

Marnie Bertour, Ah Marnie… Ma première voisine de bureau, ma rousse préférée… Merci pour ton humour inébranlable (oui oui, j'ai mis ce mot dans mes remerciements…), pour avoir été si fidèle et toujours présente à mes côtés (pas comme Mélanie qui est partie à l'autre bout du monde… ! Nah, nieuh !), merci de m'avoir supporté et soutenu !

Pablo V., la force tranquille… Discret mais toujours présent ! Une source intarissable de bonnes idées et de bons conseils, une connaissance de nos sujets et de la biblio incroyable… Merci pour tous tes conseils, pour nos longues discussions toujours utiles et pleines de sens… Je suis content d'avoir partagé tant de bons moments avec toi et d'avoir été à tes côtés pour l'obtention de ton poste de CR… Je te souhaite tout plein de bonnes choses pour la suite de ta carrière mais je ne me fais pas trop de soucis pour toi…

Enfin, Odile, ma Dilou adorée, la dernière arrivée mais surement la plus importante… A la fois lab-manager (heureusement que tu es là… !) et amie, voisine de bureau depuis plus de 2 ans… Qu'est-ce que l'on rigole tous les 2 ! Un vrai plaisir de travailler à tes côtés et d'apprendre de ton expérience (et oui tu es vieille, mais ça a des avantages !!! lol). Merci pour ton aide précieuse et ton implication dans mes projets! J'ai découvert une chouette personne et j'ai de suite accroché avec toi ! J'espère qu'on aura encore l'occasion de travailler ensemble !!!!

Une petite pensée amicale aussi à notre nouvelle mascotte, Margot Golito, qui représente l'avenir du Génotypage de souris en France. Heureux d'avoir eu la chance de faire ta connaissance. Je te souhaite bonne chance pour la suite…

A l'U932 et l'Institut Curie

Un grand merci à l'ensemble des membres de l'unité U932 pour leurs conseils qui m'ont souvent aidé, pour les discussions scientifiques (ou non…) et pour cette incroyable interaction qui existe au sein de cette ‘‘famille’’. Un merci particulier à Armelle, Mélanie D., Aymeric, Joao, Florence et ceux que j'oublie pour votre aide et pour tous les moments partagés. J'ai découvert de vraies belles personnes ici, et j'espère sincèrement qu'on se reverra…

Merci à Matthieu Piel et Franck Perez ainsi qu'à leurs équipes pour les interactions toujours très enrichissantes que nous avons pu avoir. Merci de m'avoir accompagné à des moments clés de ma thèse, vos connaissances et votre vision de la Science resteront pour moi une source d'inspiration…

Un merci particulier à Sandrine Mout'Moutel pour nos longues discussions, toujours très instructives. Merci de m'avoir fait bénéficier de ta grande connaissance du clonage qui m'a énormément aidée… Je me demande bien comment tu vas faire pour surmonter le vide après mon départ… Qui viendra à l'improviste te déranger dans TON labo pour râler et papoter ?

Je remercie également Isabelle, Céline et l'ensemble de l'équipe de l'animalerie de l'Institut Curie qui fournissent un travail de qualité et sont toujours aux petits soins pour nos petites bêtes à 4 pattes ! Un grand merci à Edwige pour son sourire, sa disponibilité et son aide précieuse. Ton ''Bonjour'' du matin et nos discussions dans ton ''bocal'' vont me manquer…

Enfin, je souhaite remercier Frédérique Deshayes, ma Prêtresse de stage adorée, et Stéphanie Ghislin. Vous avez été là à mes débuts, vous m'avez encadré, formé, dégrossi en quelque sorte et préparé à devenir un jeune chercheur. Vous m'avez transmis votre rigueur scientifique et une passion absolue pour les contrôles de manip… De vieux réflexes qui ne m'ont plus quitté et que j'applique avec beaucoup de soin au quotidien. Juste Merci de m'avoir mis sur de si bons rails…

A mes Amis

Manue, enfin devrais-je dire Docteur Manue, toi tu as pris un peu d'avance sur moi et tu as déjà plié ta thèse !!! Quelle chance ! Merci pour tous les dimanches (et les autres jours aussi) passés à discuter de nos thèses, à faire des hypothèses de folies et essayer de griffonner des théories (parfois foireuses) sur le coin d'une feuille. Merci pour ton soutien, tes coups de boost quand j'étais démotivé. Juste merci d'avoir été là pour moi et cela depuis bien longtemps maintenant. Après avoir vécu les tornades à Memphis, Tennessee, on a retrouvé la France pour notre M2 et notre thèse et nous voilà aujourd'hui enfin sorti du système éducatif !!! On est des Grands !

Ma Florie, ma Môôôôche !!! Qui aurait cru en ce matin de septembre 2007, lorsque je t'ai demandé une clope sur le parvis de la Fac de Médecine de Nice, qu'on en serait là aujourd'hui ! Te voilà Maman, mariée à un beau Catalan et Ostéopathe à Barcelone… Et moi je suis sur le point de devenir Docteur… (Et oui c'est la classe, non ?! lol)… Quel chemin parcouru.

Arthur et Hicham, merci les gars pour nos bons moments partagés, souvent chez Cath à parler Science, avenir et à faire des plans pour notre futur… C'est toujours un plaisir de discuter avec vous et d'apprendre de vous. Arthur, tiens-toi prêt, j'arrive dans ton labo… lol.

Et je vous souhaite plein de courage et de réussite pour vos dernières années de thèse. On touche le bout !!!

A ma Famille et Belle-Famille

Je remercie mes Parents et mes Grands-Parents pour leur bienveillance et leur soutien. Merci de m'avoir permis de réaliser de si longues études, parfois au prix de quelques sacrifices. Merci de m'avoir accompagné et porté depuis tout ce temps. Rien n'aurait été possible sans vous, alors juste Merci !

A mes petits frères, Jimmy et Tom, je tiens ici à vous dire combien je suis fier de vous. Il m'est souvent difficile d'être aussi loin de vous et de ne pas être aussi présent à vos côtés que je ne le voudrais, mais sachez que je serais toujours là pour vous. Je vous aime de tout mon cœur.

Je remercie également mes beaux-parents, Françoise et Jacques, ainsi que Pauline, Jérôme, Véro et les petits bouts pour leur bienveillance à mon égard et leur présence à mes côtés depuis près de 10 ans maintenant.

A Arnaud

Toi qui partage ma vie depuis bientôt 10 ans et qui m'as toujours connu étudiant… Et bien c'est sur le point de changer !! Merci pour tout. Merci pour ton soutien sans faille tout au long de ces années, merci de prendre soin de moi au quotidien et de m'écouter (enfin j'espère !) me plaindre le plus souvent (oui oui, je râle beaucoup !). Ton Amour me remplit de bonheur chaque jour et je n'aurais pu accomplir tout ce long chemin sans ta présence à mes côtés. J'ai beaucoup appris de toi, et notamment à ''lâcher prise'', même si j'ai encore du boulot de ce côté-là. Merci de relativiser les choses à ma place lorsque je panique (parfois sans raison). Merci de m'avoir soutenu et épaulé lors des moments de doute, d'angoisse et/ou de stress. Juste, Merci Merci et Merci pour tout. Je t'aime…

Abstract

In secondary lymphoid organs, B cells acquire antigens that are tethered at the surface of neighboring cells. Engagement of the B cell receptor (BCR) with such immobilized antigens leads to the formation of an immune synapse and the subsequent polarization of B cells. This includes the repositioning of the centrosome towards the immune synapse as well as the recruitment and local secretion of lysosomes required for efficient antigen extraction, processing and presentation onto class II major histocompatibility complex (MHC-II) molecules to primed $CD4^+$ T cells. Pioneer work performed in the lab has highlighted the first molecular players involved in this process. However, the precise mechanism governing centrosome polarization remains to be fully elucidated. The work performed during this thesis aimed at identifying new regulators supporting centrosome polarization in B lymphocytes upon BCR engagement with immobilized antigens. In addition, in view of the emerging role played by the tissue microenvironment in shaping B cell activation and functions we investigated whether extracellular Galectin-8 modulates the ability of B cells to polarize, extract and present immobilized antigens.

We show here that, in resting lymphocytes, centrosome-associated Arp2/3 (actin related protein-2/3) locally nucleates F-actin, which is needed for centrosome tethering to the nucleus via the LINC (linker of nucleoskeleton and cytoskeleton) complex. Upon lymphocyte activation, Arp2/3 is partially depleted from the centrosome as a result of its HS1-dependent recruitment to the immune synapse. This leads to a reduction in F-actin nucleation at the centrosome and thereby allows its detachment from the nucleus and polarization to the synapse. In addition, we show that extracellular Galectin-8 favors lysosome recruitment and secretion at the immune synapse, hence providing B cells with an enhanced capacity to extract and present immobilized antigens.

Our findings highlight unexpected mechanisms that tune B cell polarity in response to antigenic stimulation and raise exciting questions concerning the coordinated regulation of these mechanisms to provide B cells with the capacity to efficiently extract, process and present surface-tethered antigens.

Résumé

Dans les organes lymphoïdes secondaires, les lymphocytes B acquièrent des antigènes immobilisés à la surface de cellules voisines. L'engagement du BCR (récepteur des cellules B) avec de tels antigènes induit la formation d'une synapse immunologique et la polarisation des lymphocytes B. Cette polarisation inclut le repositionnement du centrosome à la synapse immunologique ainsi que le recrutement et la sécrétion locale des lysosomes qui sont nécessaires à l'extraction, l'apprêtement et la présentation des antigènes sur les molécules du complexe majeur d'histocomptabilité de classe II (CMH-II) aux lymphocytes T $CD4^+$ pré-activés. Des travaux précurseurs menés dans le laboratoire ont permis de mettre en évidence les premiers acteurs moléculaires impliqués dans ce processus. Cependant, le mécanisme précis gouvernant la polarisation du centrosome demeure encore aujourd'hui inconnu. Le travail réalisé pendant cette thèse avait pour objectif d'identifier de nouveaux régulateurs contrôlant la polarisation du centrosome dans les lymphocytes B après engagement du BCR avec des antigènes immobilisés. De plus, au regard du rôle grandissant joué par le microenvironnement tissulaire dans l'activation des lymphocytes B ainsi que dans la modulation de leurs fonctions, nous avons étudié l'effet de la protéine extracellulaire Galectine-8 sur la régulation de la capacité des lymphocytes B à se polariser et à extraire et présenter des antigènes immobilisés.

Le travail présenté dans ce manuscrit montre que la présence du complexe Arp2/3 au centrosome des lymphocytes B non activés permet la nucléation locale de filaments d'actine qui permettent, grâce à leur interaction avec le complexe LINC, de lier le centrosome au noyau. L'activation des lymphocytes B induit la déplétion partielle du complexe Arp2/3 du centrosome qui est recruté à la synapse immunologique par la protéine HS1. Ceci induit une diminution de la nucléation d'actine au centrosome entraînant la séparation entre le centrosome et le noyau et permettant la polarisation du centrosome vers la synapse. De plus, nous montrons que la présence de la protéine Galectine-8 dans le milieu extracellulaire favorise le recrutement et la sécrétion des lysosomes à la synapse immunologique, conférant aux lymphocytes B une meilleure capacité à extraire et présenter des antigènes immobilisés.

Nos résultats mettent en évidence des mécanismes inattendus régulant la polarisation des lymphocytes B en réponse à une stimulation antigénique et soulèvent des questions intéressantes concernant la régulation coordonnée de ces mécanismes qui confèrent aux lymphocytes B la capacité d'extraire, d'apprêter et de présenter des antigènes immobilisés efficacement.

INTRODUCTION

RESULTS

DISCUSSION

Abp-1	actin-binding protein 1
Akt	protein kinase B (PKB)
APCs	antigen-presenting cells
aPKC	atypical protein kinase C
Arp2/3 / ArpC1-5	actin-related protein-2/3 / Arp2/3 complex component 1-5
ATOC	actin-organizing center
ATP/ADP	adenosine triphosphate/diphosphate
Bcl-6	B-cell lymphoma 6 protein
BCR	B cell antigen receptor
Blimp-1	B lymphocyte-induced maturation protein 1
Btk	Bruton's tyrosine kinase
CCL19/21	C-C chemokine ligand 19/21
CCR7	C-C chemokine receptor type 7
CD4/8/40/169	cluster of differentiation 4/8/40/169
Cdc42	cell division control protein 42
CFSE	carboxyfluorescein succinimidyl ester
Chmp2b	charged multivesicular body protein 2b
CLPs	common lymphoid progenotors
CRD	carbohydrate recognition domain
CSR	class switch recombination
CXCL13	C-X-C chemokine ligand 13
CXCR5	C-X-C chemokine receptor type 5
DAG	diacylglycerol
DAMPs	damage-associated molecular patterns
Dlg1	discs large homolog 1
DNA	deoxyribonucleic acid
Erk1/2	extracellular signal-regulated kinases 1/2
ERM	ezrin, radixin, moesin
ESCRT	endosomal sorting complexes required for transport
F-actin	filamentous actin
FDR	false discovery rate
G-actin	globular actin
Gal8	galectin-8
GCs	germinal centers
GDP/GTP(ase)	guanosine diphosphate/triphosphate(ase)
GEF	guanine exchange factor
(e)GFP	(enhanced) green fluorescent protein
GO term	genome ontology term
GST	glutathione S-transferase
HEL	hen egg lysozyme
HS1	hematopoietic lineage cell-specific protein 1
HSCs	hematopoietic stem cells
ICAM-1	intracellular adhesion molecule-1
Ig(H/L)	immunoglobulin (heavy/light chain)
Ii	invariant chain
IL-2/21	interleukin-2/21
IP3	inositol-1,4,5-triphosphate
ITAM	immunoreceptor tyrosine-based activation motif
KASH domain	klarsicht, ANC-1, syne homology domain
KO	knock out

LAMP-1	lysosomal-associated membrane protein 1
LC-MS/MS	liquid chromatography–tandem mass spectrometry
LFA-1	lymphocyte function-associated antigen-1
LINC complex	linker of nucleoskeleton and cytoskeleton complex
LPS	lipopolysaccharide
MHC-I/II	class I/II major histocompatibility complex
MTs	microtubules
MTOC	microtubule-organizing center
MVBs	multivesicular bodies
NF-κB	nuclear factor-kappa B
NLRs	nod-like receptors
NPFs	nucleation promoting factors
OVA	ovalbumin
PAMPs	pathogen-associated molecular patterns
Par(1/2/3/6)	partinioning defective (1/2/3/6)
PAX5	paired box 5
PCM	pericentriolar matrix
PDPN	podoplanin
pH	power of hydrogen
PI3K	phosphoinositide 3-kinase
PIP_2	phosphatidylinositol(4,5)-bisphosphate
PRRs	pattern recognition receptors
(m/si)RNA	(messenger/small interfering) ribonucleic acid
SCS	sub-capsular sinus
SDS-PAGE	sodium dodecyl sulfate - polyacrylamide gel electrophoresis
SHM	somatic hypermutation
SILAC	stable isotope labelling by amino acids in cell culture
SLOs	secondary lymphoid organs
(c/p/d)SMAC	(central/peripheral/distal) supramolecular activation cluster
SNARE	soluble n-éthylmaleimide-sensitive-factor attachment protein receptor
TAN lines	transmembrane actin-associated nuclear lines
TCR	T cell receptor
Tfh	follicular helper T cells
TGFβ	Transforming growth factor beta
TGS101	tumour susceptibility gene 101
TLRs	toll-like receptors
Vamp-7	Vesicle-associated membrane protein 7
VCA domain	verprolin homology or WH2-Connector-Acidic domain
V(D)J	variable (diversity) joining
Vps	vacuolar protein sorting
WASH	Wiskott–Aldrich syndrome protein family homolog 1
(N-)WASP	(neuronal) Wiskott–Aldrich syndrome protein
WT	wild type
WAVE	Wiskott-Aldrich syndrome protein family member 1
γTuRC	γ-tubulin ring complex
µm	micrometer
µM	micromolar
min	minutes
p.i.	post immunization

INTRODUCTION

Figure 1. Ehlrlich's side-chain theory. Drawings of the formation and effector functions of antibodies according to the side-chain theory. Reproduced from [Kaufmann, 2008].

1. From Metchnikoff and Ehlrlich …

Following on pioneer discoveries made by Edward Jenner on smallpox vaccination in the late 1700's, Louis Pasteur believed that vaccines might be used to efficiently prevent other diseases. He succeeded in the 1880's when he showed that chickens vaccinated with a weakened form of the cholera bacteria could survive to a later exposure to virulent cholera bacteria. He then defined the term "immunity" to characterize this resistance to infections. Whereas Jenner, Pasteur and Koch's discoveries had revolutionized the way physicians envisioned medicine, nobody was able to explain how and why immunity occurred. Elie Metchnikoff and Paul Ehrlich were the firsts to develop theories describing the putative mechanisms leading to an efficient immunity.

In Italy, Metchnikoff studied immunity in the starfish larvae in which he pinned thrones from a Christmas tree. He observed the formation of pus and the recruitment of white blood cells at the site of inflammation leading him to hypothesize that those particular cells possessed the unique capacity to surround and kill microbes. Following advices of one of his friends, Metchnikoff named this process "phagocytosis".

At that time in Germany, Ehrlich developed his side-chain theory. Spending part of his career studying the ability of components of certain sera to neutralize the effect of toxins, he postulated that cells possess "side-chains" that are specifically recognized by toxins, "as a key in a lock". He theorized that in response to side-chain binding by a toxin, cells produce more side-chains that can be released in the blood as "magic bullets" looking for the toxin (**Figure 1**).

Despite their opposing theories, Metchnikoff and Ehrlich shared the Nobel Prize of Physiology and Medicine in 1908 for their contribution to the understanding of Immunology. To date, the actual view of Immunology reconciles both theories that constitute the cellular and humoral branches of immunity.

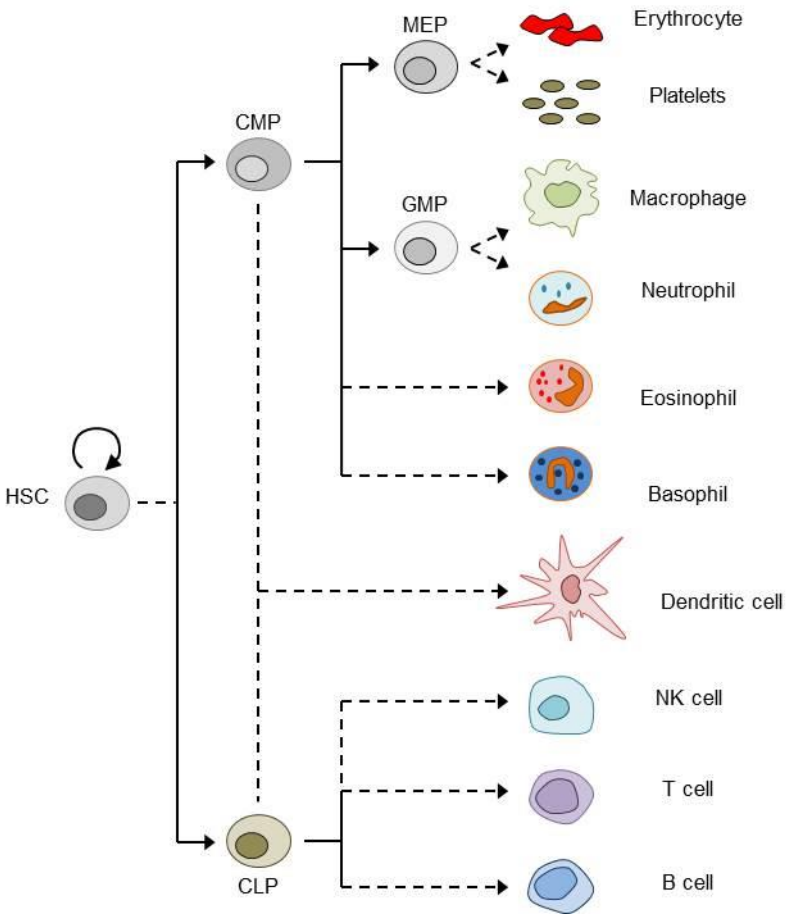

Figure 2. Overview of hematopoiesis. HSC, hematopoietic stem cell; CMP, common myeloid progenitor; CLP, common lymphoid progenitor; MEP, megakaryocyte/erythroid progenitor; GMP, granulocyte-macrophage progenitor. Adapted from [Larsson and Karlsson, 2005].

2. … to innate and adaptive immunity

Since these early theories on immunity, increasing amounts of data had helped us to understand how the immune system works. In Mammalian, the immune system has evolved in such a way that it is formed of two branches: innate immunity and adaptive immunity, which are highly interconnected to efficiently fight pathogens. Cells from both the innate and adaptive immune systems are generated in the bone marrow by the differentiation of hematopoietic stem cells (HSCs) through a process called hematopoiesis (**Figure 2**). Interestingly, in mouse embryos, HSCs derive from endothelial cells of the dorsal aorta within the aorta-gonads-mesonephros (AGM) region [Robin et al., 2003].

Innate immunity represents the first line of defense within peripheral tissues. There, tissue-residing macrophages and/or dendritic cells patrol their environment in search for pathogens. Their capacity to internalize high amounts of extracellular fluid, by a process related to phagocytosis, provides to these cells a key role in the immune surveillance of peripheral tissues. The activation of cells from the innate immune system is triggered by the engagement of specific receptors, called pattern recognition receptors (PRRs), such as toll-like receptors (TLRs) or NOD-like receptors (NLRs), which are either expressed at the plasma-membrane, within the cytosol or at the surface of intracellular vesicles. PRRs recognize two kinds of signals: first they detect molecules that derive from exogenous pathogens, such as bacteria or viruses, which are called pathogen-associated molecular patterns, or PAMPs. They also possess the ability to recognize endogenous signals such as DNA or ATP from damaged or dead cells that are named damage-associated molecular patterns (DAMPs). PRR-mediated activation of macrophages and dendritic cells results in the local clearance of pathogens or infected cells that are internalized (**Figure 3**①). Other cells, such as natural killer cells or granulocytes (eosinophils, basophiles and neutrophils) that also recognize PAMPs and DAMPs are locally recruited and activated and their mobilization participates locally to struggle against invaders.

Once activated, dendritic cells that are professional antigen-presenting cells leave the periphery, travel through the lymph (**Figure 3**②) and reach secondary lymphoid organs, such as lymph nodes, where they present processed antigens to antigen-specific T lymphocytes (**Figure 3**③,④). This launches the adaptive immune response. In contrast to innate immunity that relies on the recognition of conserved patterns between microorganisms

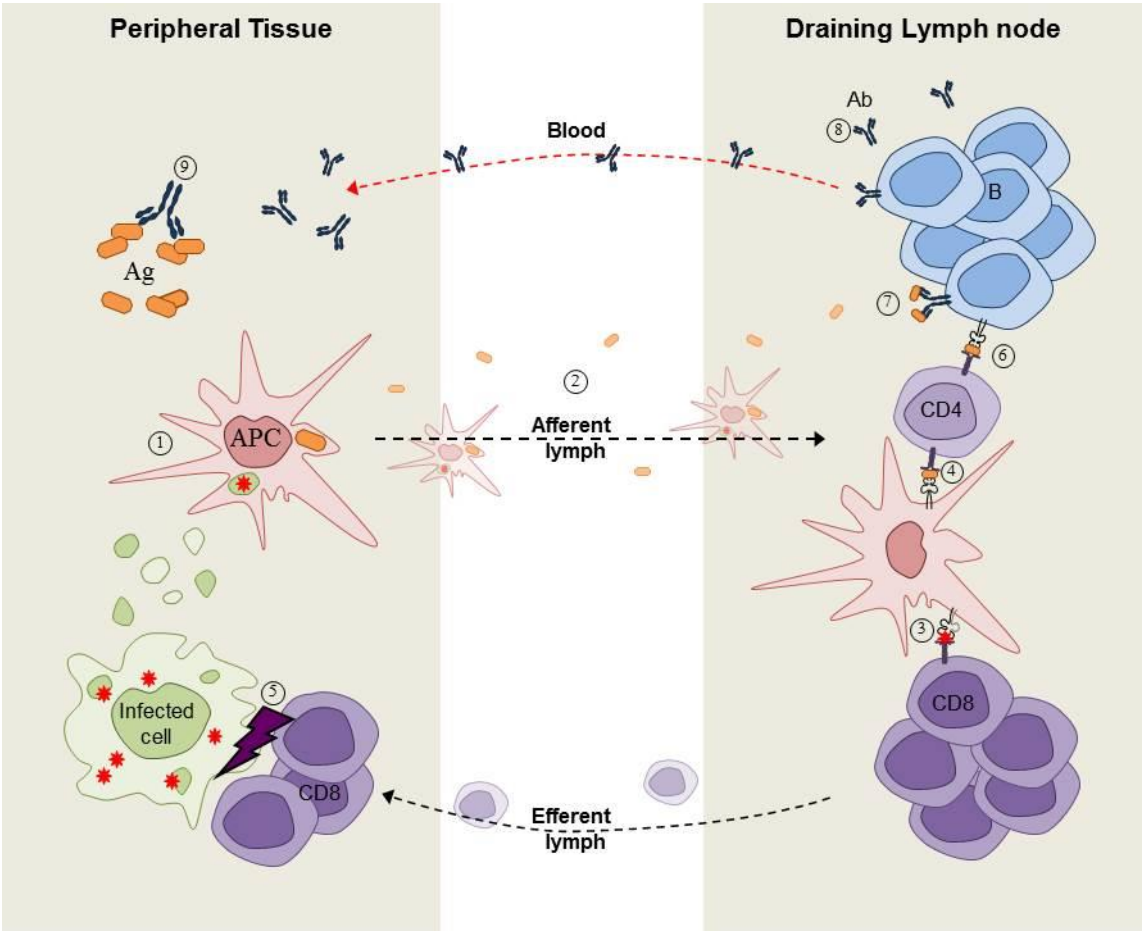

Figure 3. Overview of immune responses. Antigen-presenting cells (APCs) that have internalized pathogens and/or infected cells ① leave peripheral tissues and reach, via the lymph, secondary lymphoid organs such as the spleen and lymph nodes ②. There, depending on its origin, the antigen will be presented to either $CD8^+$ T cells ③ or $CD4^+$ T cells ④. While $CD8^+$ T cell activation results in the cytotoxicity-mediated killing of target cells ⑤, $CD4^+$ T cells provide help ⑥ to antigen-stimulated B cells ⑦. B cell activation induces the production and secretion of antigen-specific antibodies ⑧ that recirculate through the blood to fight against pathogen within peripheral tissues ⑨.

or common molecular signals, adaptive immune responses rely on the engagement of antigen-specific receptors. In a simplistic view, antigens derived from intracellular pathogens are loaded onto class I major histocompatibility complex (MHC-I) molecules and presented to $CD8^+$ T cells (**Figure 3**③). These cells, also called cytotoxic T cells, possess the unique capacity to travel back to the periphery to kill infected cells by the release of perforin and granzymes that induce apoptosis of the target cells (**Figure 3**⑤).

Extracellular pathogens are internalized in endo-lysosomal compartments where they are processed and loaded onto class II MHC (MHC-II) molecules for further presentation to $CD4^+$ T cells (**Figure 3**④). The main effector function of these cells, often referred to as helper T cells, is to provide secondary signals to antigen-specific B cells (**Figure 3**⑥), which have already encountered their cognate antigen through their B cell antigen receptor (BCR) (**Figure 3**⑦). This B cell/T cell cooperation is strictly required for B cells to be fully activated and produce high affinity antibodies of the same specificity than the BCR they carry at their surface (**Figure 3**⑧) and generate B cell memory [Mitchison, 2004]. Secreted antibodies finally recirculate within the blood circulation and ‘‘neutralize’’ extracellular pathogens present within peripheral tissues (**Figure 3**⑨).

Thus, B cells are considered as key players of the adaptive immune system and play a pivotal role in the outcome of immune responses. Therefore, identifying the mechanisms underlying B cell activation and functions is crucial for the better understanding of humoral immune responses. This represents the main goal of the work presented in this manuscript and therefore this Introduction will mostly be centered on B lymphocyte biology.

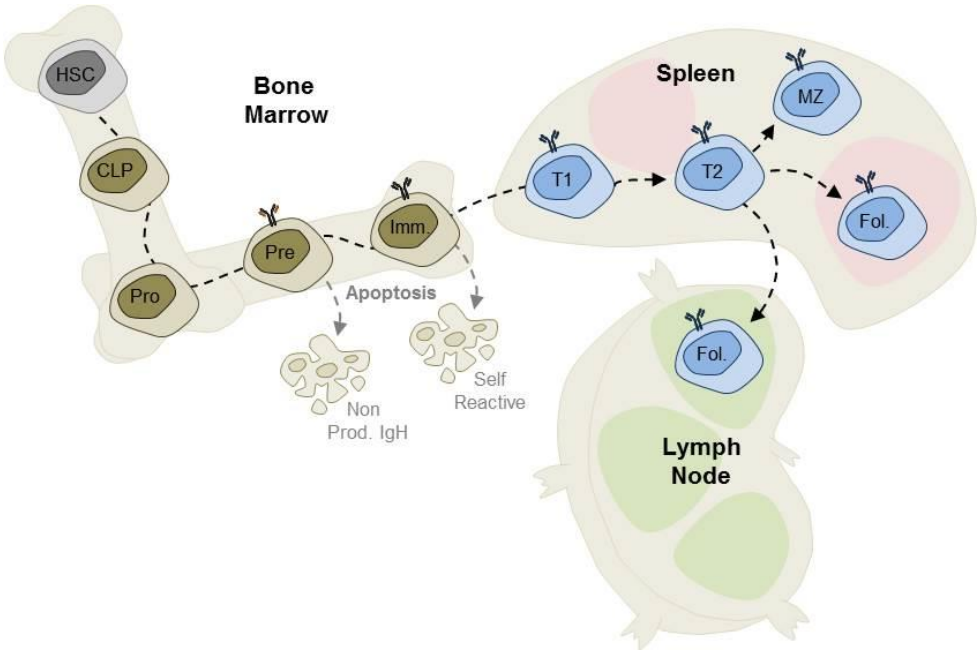

Figure 4. Schematics of B cell development. Hematopoietic stem cells (HSC) differentiate into common lymphoid progenitor (CLP), which will further generate pro-B cells (Pro) and then pre-B cells (Pre). Pre-B cells expressing a functional pre-BCR will further give rise to immature B cells (Imm.) expressing a mature BCR. There, autoreactive immature B cells are eliminated. Selected immature B cells differentiate into transitional 1 and 2 B cells (T1 and T2) before becoming mature B cells that reside within either the spleen marginal zone (MZ) or spleen and lymph-node B cell follicles (Fol.). Adapted from [Nagasawa, 2006].

1. Generation of B cells

In Mammalian, B cells mainly differentiate within the bone marrow from hematopoietic stem cells (HSCs) that are characterized by their ability to divide asymmetrically and to self-renew. In particular, HSCs give rise to common lymphoid progenitors (CLPs) that possess the unique capacity to differentiate into either T or B lymphocytes. The up-regulation of the transcription factor PAX5, irreversibly engages CLPs towards the B cell lineage (B cell commitment) leading to the generation of pro-B cells that will further mature into pre-B cells. Then pre-B cells become immature B cells expressing a mature BCR at their surface. At that time, immature B cells exit the bone marrow and reach the spleen. There they complete their maturation process as they become transitional 1 and 2 B cells to finally develop into mature B cells residing within B cell follicles (follicular B cells) or the marginal zone (marginal zone B cells). At that stage, a pool of mature B cells egress from the spleen, gains access to the blood circulation and colonize lymph nodes [Nagasawa, 2006] (**Figure 4**).

The BCR is a "Y"-shaped transmembrane receptor protein composed of a cell-surface immunoglobulin facing the extracellular environment. As all immunoglobulins (Igs), the BCR can be subdivided into two main regions: at the N-terminus, the variable region is formed of two paratopes involved in antigen binding, whereas the C-terminus part of the protein corresponds to the constant region and defines the isotype (IgM, IgD, IgA, IgE or IgGs) and function of Igs **(Figure 5)**. For the BCR, the constant region, which is made of the μ or δ chain (IgM or IgD), is involved in anchoring the immunoglobulin at the cell surface and promotes its association with the Igα-Igβ signaling module [Cambier et al., 1994, Reth and Wienands, 1997]. During the course of B cell differentiation, genes of the immunoglobulin loci undergo multiple rearrangements in order to generate a mature BCR. The heavy chain of the immunoglobulin locus (IgH) is composed of numerous coding sequences, divided in variable (V), diversity (D) and joining (J) segments that assemble in a unique combination at the pro-B cell stage. This rearranged VDJ segment then associates with the μ chain of the constant region (Cμ) of IgH to form the pre-BCR. At this stage, a first checkpoint leads to the selection of pre-B cells with functional pre-BCRs. Following allelic exclusion – a process by which only one allele of the IgH locus is expressed by the cell to ensure a unique antigen-specificity of the BCR – pre-B cells rearrange V and J segments of the light chain

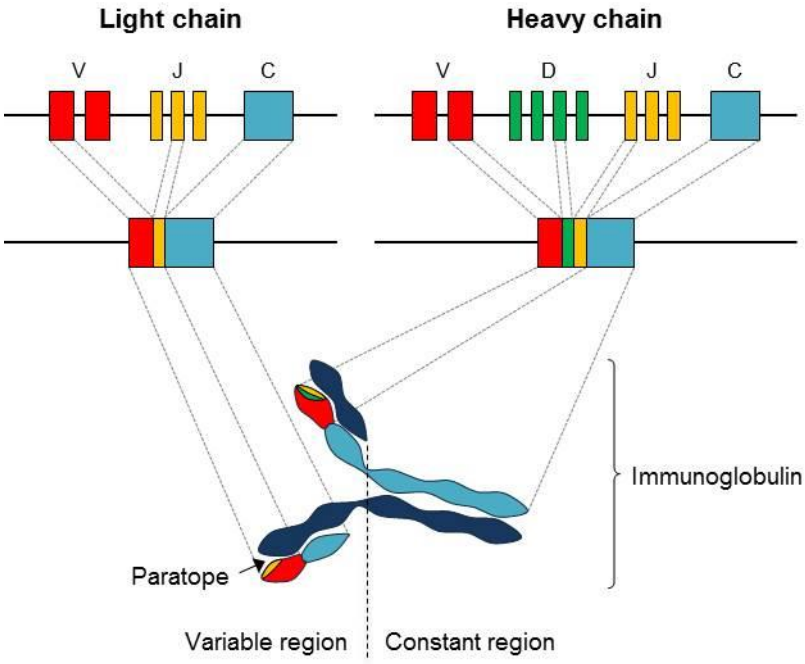

Figure 5. Structure and assembly of immunoglobulins. Immunoglobulins are composed of two light chains associated with two heavy chains. These chains are generated by an unique combination of rearranged coding sequences, divided in variable (V), diversity (D) and joining (J) segments through a process called V(D)J recombination.

immunoglobulin locus (IgL) to form a mature BCR with a unique variable region (reviewed in [Roth, 2014]) (**Figure 5**). Of note, at this stage, the BCR is tested for its ability to bind to self antigens and autoreactive B cells are eliminated.

Because the BCR is composed of two paratopes, it can bind to two identical epitopes allowing the cross-linking of multiple BCRs that is required for efficient signal transduction [Metzger et al., 1992]. The strength of epitope binding to its specific paratope is called affinity. However, when several epitopes cross-link multiple BCRs, the strength of interaction is defined by the avidity that might overcome impaired BCR signaling in the case of antigen with too low affinity [Batista and Neuberger, 1998].

2. Antigen encounter by B cells

Due to the antigenic specificity of each BCR, the probability for a given B cell to encounter its cognate antigen by patrolling the body is very low. In contrast, the follicles of secondary lymphoid organs (SLOs) where B cells reside provide the appropriate environment for them to encounter their specific antigens. Indeed, SLOs act as antigen reservoirs where antigens coming from the periphery accumulate; thus increasing the probability for a given B cell to encounter its cognate antigen. Efficient antigen sampling by B cells relies on their capacity to explore entire follicles within lymph nodes. This is achieved by a random-walking amoeboid mode of migration of CXCR5-expressing B cells that is constrained to the follicle by the local presence of the chemokine CXCL13 [Miller et al., 2002, Saez de Guinoa et al., 2011, Lammermann and Sixt, 2009].

The fate of antigens that are present within peripheral tissues is mainly dependent on their nature [Batista and Harwood, 2009]. First, within peripheral tissues antigens can be taken-up by tissue-patrolling dendritic cells that transport them towards lymph nodes. There, antigens can be transferred onto lymph node-resident dendritic cells or macrophages or directly presented to B cells [Qi et al., 2006] [Suzuki et al., 2009] [Gonzalez et al., 2010] (**Figure 6a**). In contrast, antigens may also reach draining lymph nodes passively, through the lymph or the blood circulation, where B cells encounter them by different means. Small antigens (smaller than 70 kDa) from afferent lymph vessels diffuse into the lymph node follicle where B cells acquire them in a soluble form [Pape et al., 2007] (**Figure 6b**). The mechanisms by which soluble antigens gain access to B cell follicles are not totally understood, but it has been proposed that their ingress is promoted by tiny pores [Batista and Harwood, 2009] and/or a

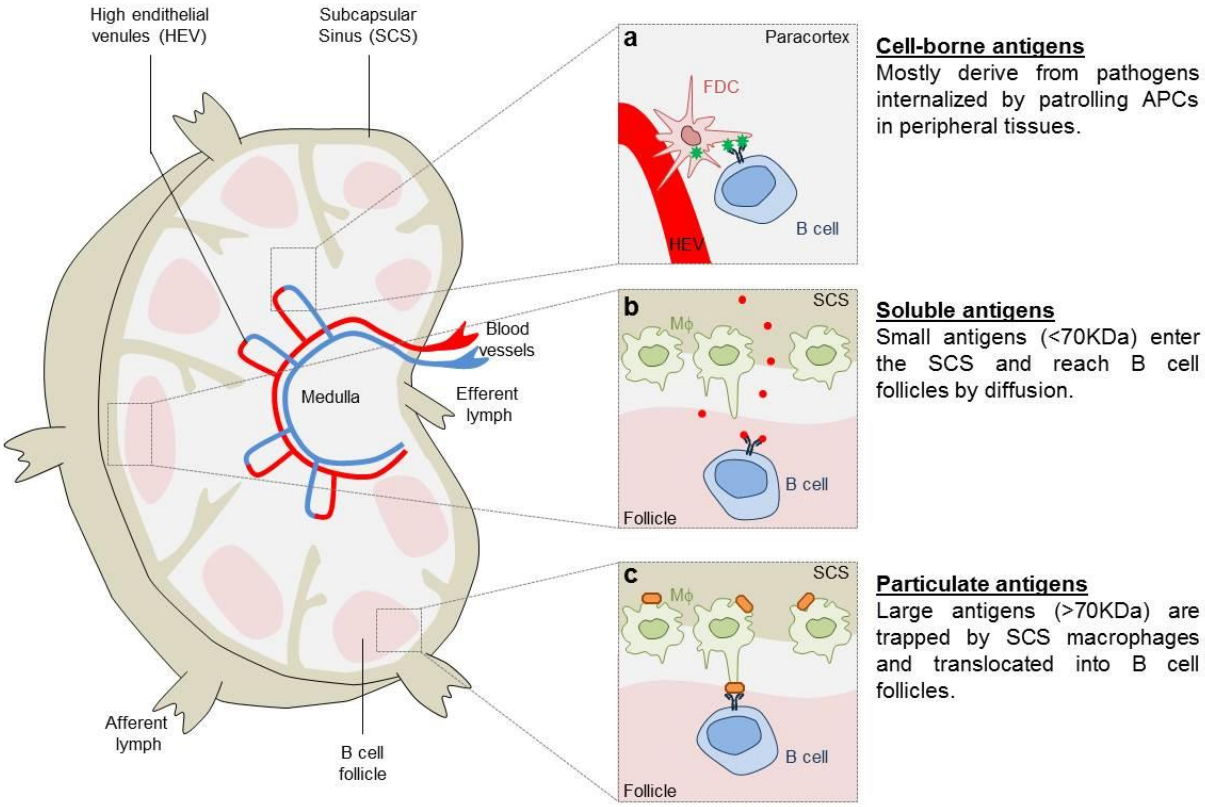

Figure 6. Antigen encounter by B cells. Depending on their nature and origin, antigens follow different routes to be presented to B cells. Pathogen-derived antigens generated within antigen-presenting cells (APCs) are presented to B cells in areas close to high endothelial venules (**a**). Small soluble antigens reach B cell follicles by diffusion where they encounter antigen-specific B cells (**b**). In contrast, large/particulate antigens reaching the sub-capsular sinus of lymph nodes are trapped at the surface of specialized macrophages (SCS $CD169^+$ macrophages), translocated within B cell follicles and presented to antigen-specific B cells in their native form (unprocessed antigens) (**c**). Adapted from [Harwood and Batista, 2010].

conduit network that directly connects the sub-capsular sinus (SCS) with B cell follicles [Roozendaal et al., 2009].

On the contrary, large antigens (bigger than 70 kDa) have been shown to be trapped at the surface of specialized $CD169^+$ macrophages located at the SCS floor site, which transfer them to follicular B cells [Carrasco and Batista, 2007, Junt et al., 2007] (**Figure 6c**). How antigens are transferred from the SCS floor plate to B cell follicles is unclear. Two routes have been suggested: first, prior to expose them in their native form at their cell surface, sub-capsular $CD169^+$ macrophages that display a poor phagocytic capacity could internalize antigens and recycle them back to the cell surface. Alternatively, antigens that are immobilized at the surface of $CD169^+$ macrophages could be directly translocated from the lumen of the SCS to B cell follicles through macrophage protrusions [Martinez-Pomares and Gordon, 2007].

These antigens are referred to as particulate, immobilized or surface-tethered antigens and are, to date, considered as the main pathway of antigen encounter by B cells. Indeed, taking into account the complexity of the extracellular environment (constrained geometry, presence of matrix proteins and conjunctive network); it is unlikely that big particulate antigens freely "float" within tissues but instead are immobilized on cell surfaces. Therefore, surface-tethered antigens were used all along the work presented in this manuscript to stimulate B cells.

Antigen encounter by B cells results in the formation of BCR-antigen complexes that initiate a complex signaling cascade downstream the BCR. These early events of B cell activation induce a drastic remodeling of the B-cell cytoskeleton leading to the internalization of BCR-antigen complexes into endo-lysosomal compartments for further presentation to primed $CD4^+$ T cells.

3. Early events of B cell activation

In addition to its role during B cell development, BCR-mediated signaling plays a crucial role in the activation of B cells upon antigen encounter. BCR engagement with antigens initiates a cascade of signaling events that ultimately launches the transcription of genes required for B cell function [Baba and Kurosaki, 2011]. First, it triggers the activation of Lyn, a member of the Src-family kinases, which phosphorylates the immunoreceptor tyrosine-based activation motifs (ITAM) present on the cytoplasmic tail of the Igα/Igβ heterodimer. This in turn leads to the recruitment and phosphorylation of adaptor proteins, among which

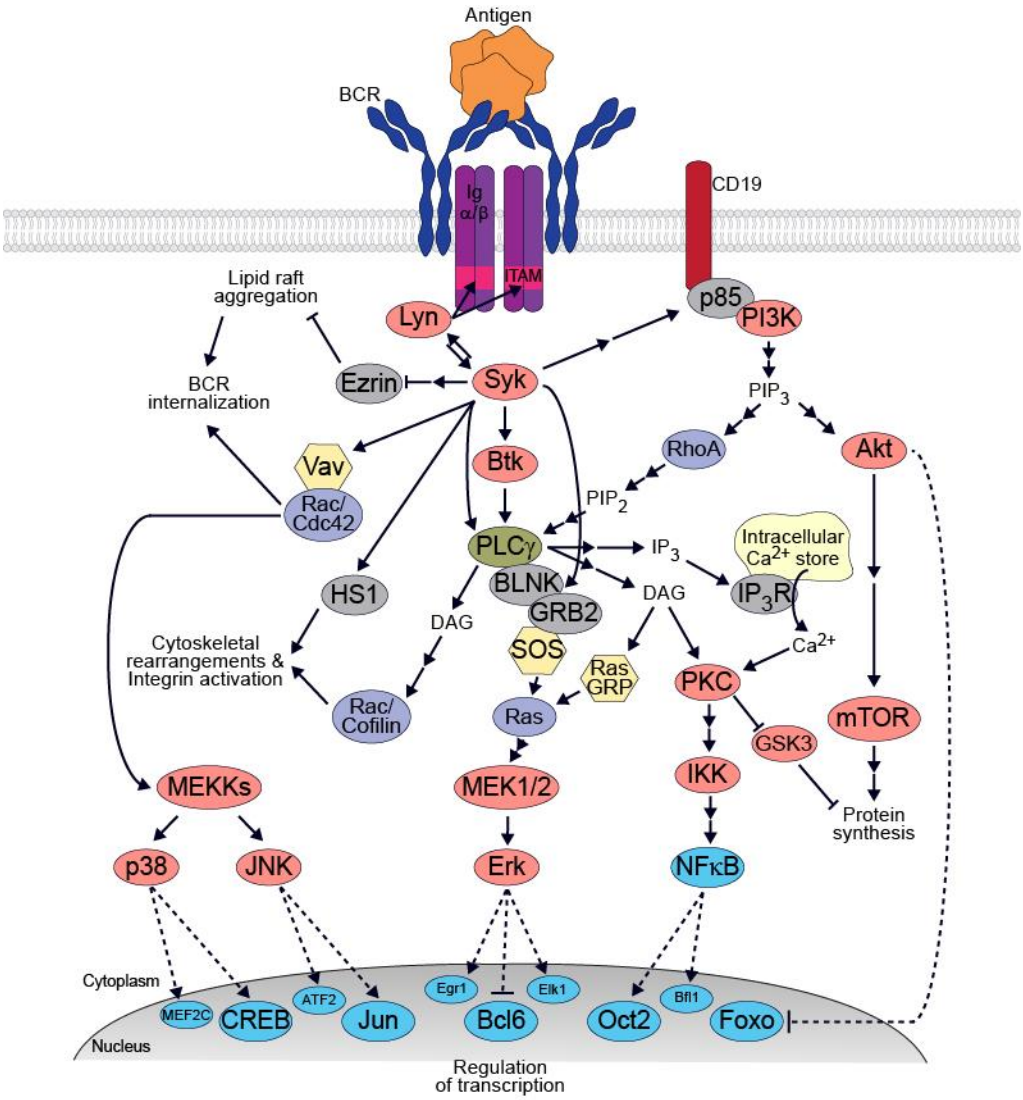

Figure 7. BCR-mediated signaling. BCR cross-linking by antigens (top) induces a signaling cascade that ultimately leads to BCR-antigen internalization, cytoskeletal rearrangements (middle) and activation of transcription factors (bottom) required for B cells to acquire their specific effector functions. Adapted from http://www.cellsignal.com/pathways/Lymphocyte.jsp

Syk, Btk and Vav [Reth and Wienands, 1997, Depoil et al., 2009], leading to the release of endoplasmic reticulum calcium stores and the generation of secondary messengers, mainly inositol-1,4,5-triphosphate (IP3) and diacylglycerol (DAG) [Tolar et al., 2008, Cambier et al., 1994]. Then secondary messengers propagate BCR-mediated signaling that ultimately leads to the activation of transcription factors, such as Erk1/2, Akt and NF-κB, which regulate the transcription of genes required for B cell functions and induce a drastic remodeling of the cytoskeleton [Yuseff et al., 2009]. In addition, Lyn and Syk have been described to recruit and activate the Cortactin-like protein HS1 to the BCR signalosome, which in turn regulates local actin dynamics [Uruno et al., 2003, Hao et al., 2004] (**Figure 7**).

Local actin remodeling at the antigen-contact site participates in the internalization of BCR-antigen complexes into endo-lysosomal compartments for them to be processed, loaded onto MHC-II molecules and presented to primed $CD4^+$ T cells.

4. Antigen uptake and processing by B cells

Although antigen internalization for presentation by B cells can involve Fc or complement receptors, as well as surface lectins [Cyster, 2010], the most efficient pathway remains the one mediated by the BCR [Lanzavecchia, 1990] as it not only allows antigen uptake but further triggers B cell activation. As mentioned above, B cells mainly encounter antigens that are immobilized at the surface of neighbouring cells [Carrasco and Batista, 2007, Junt et al., 2007]. This results in the establishment of an immune synapse that corresponds to an adhesive structure allowing the tight interaction between antigen-specific B cells and antigen-presenting cells [Batista et al., 2001] (see Section 3.3 for more details on the immune synapse). Establishment of the immune synapse has been shown to be strictly required for the uptake of BCR-antigen complexes where they are internalized through clathrin-mediated endocytosis [Lanzavecchia and Bove, 1985, Cherukuri et al., 2001, Stoddart et al., 2002, Stoddart et al., 2005]. Then, BCR-antigen complexes reach endo-lysosomal compartments where antigenic peptides are generated before being loaded onto MHC-II molecules for presentation to primed $CD4^+$ T cells.

Once internalized, BCR-antigen complexes reach $MHC\text{-}II^+$ endo-lysosomes (**Figure 8**①**,** ②), where antigens undergo limited proteolysis that preserves T-cell epitopes from excessive

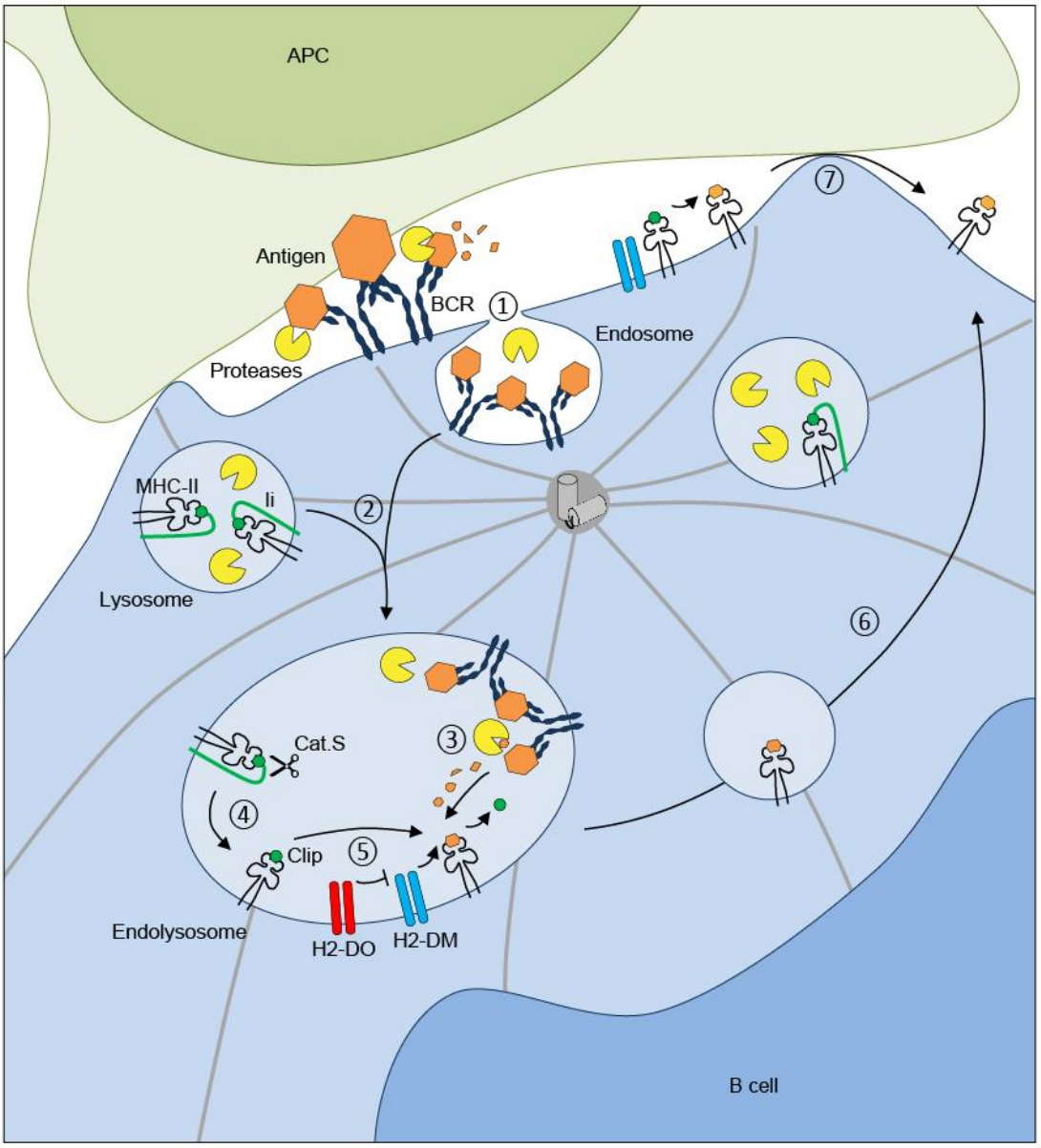

Figure 8. Antigen processing by B cells. BCR cross-linking by antigens induces the internalization of BCR-antigen complexes within B cell–endosomes ①. Endolysosomes that are formed by the fusion ② of antigen-containing endosomes with lysosomes that carry MHC-II molecules allow the efficient processing of antigens ③. In the same compartment, Cathepsin S (Cat.S) cleaves the invariant chain (Ii) resulting in MHC-II–CLIP complex formation ④. Finally, H2-DM molecules promote the exchange between CLIP and antigenic peptides for them to be loaded onto MHC-II molecules ⑤. The catalysis of CLIP released by H2-DM is regulated by another non-classical MHC-II molecule, H2-DO. Peptide–MHC-II complexes are exported to the B-cell surface ⑥. Of note antigenic peptides might also be generated within the synaptic space where they are directly loaded onto MHC-II molecules at the cell surface ⑦. Adapted from [Obino and Lennon-Dumenil, 2014].

degradation [Delamarre et al., 2005] (**Figure 8**③). Interestingly, it has been shown that the arrival of BCR-antigen complexes into MHC-II$^+$ endo-lysosomes was regulated by the activation of the cytoplasmic tyrosine kinase Syk and facilitated by the actin-based molecular motor Myosin IIA that interacts with the cytosolic tail of invariant chain (Ii) [Le Roux et al., 2007, Vascotto et al., 2007]. Ii associates with MHC-II molecules during biogenesis in the endoplasmic reticulum, preventing the premature binding of endogenous peptides onto MHC-II molecules [Bakke and Dobberstein, 1990, Lotteau et al., 1990, Roche and Cresswell, 1990, Roche and Cresswell, 1991]. Once in endo-lysosomes, Ii undergoes sequential proteolysis ultimately leading to the generation of the Ii CLIP fragment that occupies the MHC-II peptide-binding groove [Driessen et al., 1999, Riese et al., 1996, Villadangos et al., 1997] (**Figure 8**④). CLIP exchange with antigenic peptides is regulated by the non-classical MHC-II molecules, H2-DM and H2-DO [Denzin and Cresswell, 1995, Denzin et al., 1997] (**Figure 8**⑤). Of note, antigen processing and peptide loading onto MHC-II molecules can also directly take place at the B cell surface, where H2-DM molecules are equally found [Moss et al., 2007] (**Figure 8**⑦). Finally, peptide–MHC-II complexes are exported to the B cell surface for further presentation to primed CD4$^+$ T cells (**Figure 8**⑥). This step, known as T-cell/B-cell cooperation, is pivotal for the ultimate formation of germinal centers (GCs), production of high-affinity antibodies by B lymphocytes and generation of B cell memory [Mitchison, 2004].

5. Antigen presentation to CD4$^+$ T cells and germinal center reaction

Following antigen internalization and processing, a pool of B cells differentiates into short-lived plasmablasts producing antibodies with relative low affinity [Cunningham et al., 2007]. Another pool migrates toward the T cell boundary and receives signals, mainly CD40 ligand, from helper T cells that differentiate into follicular helper T cells. This T-cell/B-cell cooperation is required for B cells to be fully activated, proliferate, and form GCs [Mitchison, 2004]. B cell migration is supported by the upregulation of the chemokine receptor CCR7 that senses the chemokines CCL19 and CCL21 produced by stromal cells in the T-cell zone [Reif et al., 2002, Okada et al., 2005]. Interestingly, while migrating towards the T cell-zone, B cells concentrate internalized antigens in their uropod [Carrasco and Batista, 2007]. This asymmetric distribution of antigens leads to their unequal inheritance among daughter B cells following cell division, providing them with different antigen presentation capacities [Thaunat et al., 2012]. Why such mechanism has been selected instead of providing to all the daughter

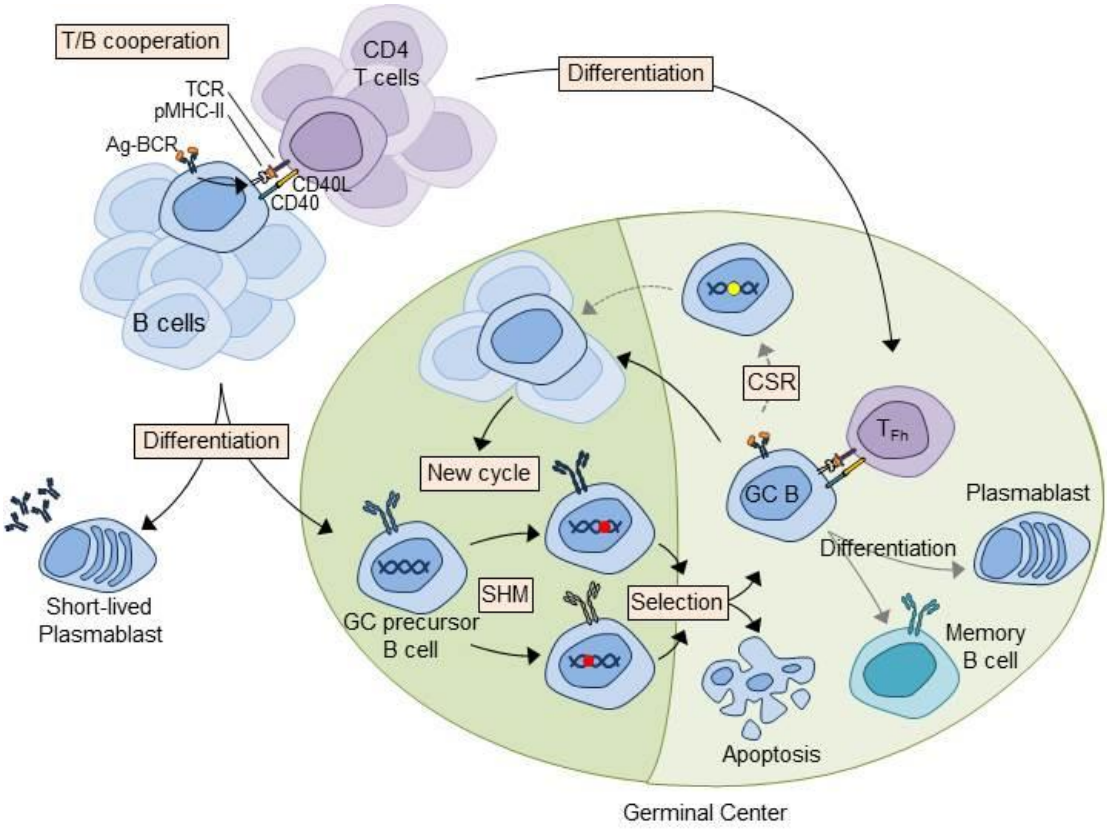

Figure 9. Antigen presentation to CD4$^+$ T cells and germinal center reaction. Following antigen internalization and processing, a pool of B cells receives secondary signals, mainly CD40 ligand, from helper T cells that are required for B cells to be fully activated and enter the germinal center reaction. There, while proliferating, antigen-activated B cells undergo i) affinity maturation through a process named somatic hypermutation (SHM) and ii) eventually immunoglobulin class switch recombination (CSR) leading to the generation of either plasma cells, which produce antigen-specific high-affinity antibodies of different classes, or memory B cells. Adapted from [De Silva and Klein, 2015].

cells with the same antigen presentation capacities remains an open question. One could speculate that it may be more efficient to enter the germinal center reaction with a restricted number of B cells displaying a high antigen presentation capacity instead of a myriad of cells with low/intermediate presentation capacities.

During the GC reaction, while proliferating, antigen-activated B cells undergo affinity maturation through a process named somatic hypermutation (SHM). This consists in the introduction of point-mutations within the V(D)J segment of immunoglobulin variable region leading to changes in the affinity of the BCR for its cognate antigen. Following their selection, B cells with a higher affinity for the antigen go through immunoglobulin class switch recombination (CSR) leading to the generation of different classes of high-affinity Igs [De Silva and Klein, 2015]. Following successive rounds of GC reactions, selected class-switched B cells differentiate into either plasma cells, which produce antigen-specific high-affinity antibodies, or memory B cells [Allen et al., 2007, MacLennan, 1994] (**Figure 9**).

6. Modulation of B cell responses: a role for Galectins?

Beyond B-cell intrinsic properties that define the way a B cell respond to antigen stimulation, B cell follicles contain a diversity of stromal cells and extracellular matrix components that might modulate the outcome of B lymphocyte responses. Although such clues have been poorly studied; during the last decade, glycan-binding proteins have emerged as key regulators of immune cell homeostasis and response to antigens [Rabinovich and Croci, 2012]. Among these proteins is the Galectin family that has the ability to cross-link cell-surface glycol proteins in the extracellular space upon secretion, thereby impacting a wide range of biological processes [Rabinovich and Toscano, 2009] (**Figure 10**).

For instance, during B cell development, Galectin-1 supports the formation of an immune developmental synapse between pre-B cells and stromal cells [Gauthier et al., 2002], required for the proper differentiation of B cells [Rossi et al., 2006, Espeli et al., 2009]. It was also described that the lack of Galectin-3 in *Schistosoma mansoni* chronically infected mice promotes plasma cell formation [Oliveira et al., 2011], suggesting a role for this galectin in the negative regulation of B cell responses. In contrast, Galectin-1 and 8 were shown to bind to mature B cells and promote the differentiation of LPS-treated B cells into antibody-secreting plasma cells *in vitro* [Tsai et al., 2008, Tsai et al., 2011]. On the same line, it has been shown that Galectin-1 expression was required to maintain antigen-specific antibody

Figure 10. Mode of actions of Galectins. Functional interactions of galectins with cell-surface glycoconjugates and extracellular glycoconjugates can lead to cell adhesion and cell signaling. Interactions of galectins with intracellular ligands may also contribute to the regulation of intracellular pathways. Reproduced from [Cummings and Liu, 2009].

titers as well as the number of plasma cells following mouse immunization [Anginot et al., 2013]. Of note, while Galectin-1 expression increases during the course of B cell differentiation upon LPS stimulation, the expression of Galectin-8 decreases [Tsai et al., 2011], suggesting an important role for Galectin-8 in the early steps of B cell activation. In addition, high concentration of Galectin-8 was reported to trigger antigen-independent proliferation of $CD4^+$ T cells, whereas lower quantity of the protein provides costimulatory signals that synergize antigen-specific $CD4^+$ T-cell responses [Cattaneo et al., 2011, Tribulatti et al., 2009].

Interestingly, Galectin-8 was also described to promote cell adhesion [Cueni and Detmar, 2009] and migration of endothelial cells *in vivo* [Delgado et al., 2011]. Moreover, the presence of function-blocking autoantibodies against Galectin-8 in the sera of patients suffering from systemic lupus erythematosus correlates with acute lymphopenia [Massardo et al., 2009].

During the last decade, extracellular clues that are present within the lymphoid tissue microenvironment have emerged as key regulators of B cell activation and responses. However, the mechanisms underlying such regulation and how they affect the outcome of an immune response are poorly understood and shall now be addressed. More specifically, the data presented above suggest that Galectin-8 binding to glycosylated proteins might regulate B cell homeostasis and function. However, its involvement in antigen uptake, processing and presentation by B cells upon surface-tethered antigen stimulation remains to be determined. The second part of the results presented in this manuscript challenges these questions and highlights the first mechanism of action of Galectin-8 in tuning B cell responses upon immobilized antigen stimulation.

The cell skeleton or cytoskeleton is a highly interconnected network that regulates most of cellular functions, cell shape and division. Whereas it has gained in complexity during evolution, the cytoskeleton is present in all organisms from basic prokaryotes to archaea and eukaryotes. In eukaryotic cells, the cytoskeleton is mainly composed of three structures: microfilaments made of actin, intermediate filaments and microtubules [Wickstead and Gull, 2011]. Of note, it is now well-admitted that proteins belonging to the Septin family form the fourth component of the cytoskeleton (reviewed in [Mostowy and Cossart, 2012]). In the following sections, I will focus on both the actin and microtubule cytoskeletons and their role in shaping B cell functions that has been at the heart of the work presented in this manuscript.

1. The actin cytoskeleton

1.a. Assembly of actin filaments

Actin is one of the most abundant proteins in eukaryotic cells and its concentration can reach up to 300 µM [Blanchoin et al., 2014]. Cytoplasmic actin monomers, or globular actin (G-actin), assemble in protofilaments. The association of two protofilaments in a right-handed helix forms an actin microfilament, referred to as filamentous actin or F-actin [Gardel et al., 2008, Pollard and Cooper, 2009]. The intrinsic structure of F-actin given by the arrangement of the actin monomers that are oriented in the same direction provides to actin filaments a polar phenotype. Whereas actin polymerization might occurs at both extremities, the filament displays a fast-growing end, referred to as the barbed end, and a slow-growing end called the pointed end [Pollard and Cooper, 2009]. Elongation of actin filaments results from the addition of ATP-G-actin at the barbed end that is quickly hydrolyzed in ADP following its incorporation within the growing filament. In contrast, filament depolymerization occurs at the pointed end where ADP-G-actin is removed [Baum and Kunda, 2005]. The length of actin filaments is regulated by capping proteins that stop filament elongation as well as severing proteins (including ADF/Cofilin) that induce their depolymerization.

Spontaneous F-actin assembly rarely occurs within cells and rather relies on the activity of specific proteins referred to as actin nucleators. Indeed, it has been shown that Profilin, a protein that binds G-actin with high affinity, prevents the spontaneous polymerization of F-actin [Pollard et al., 2000]. Among the different type of actin nucleators described in the last

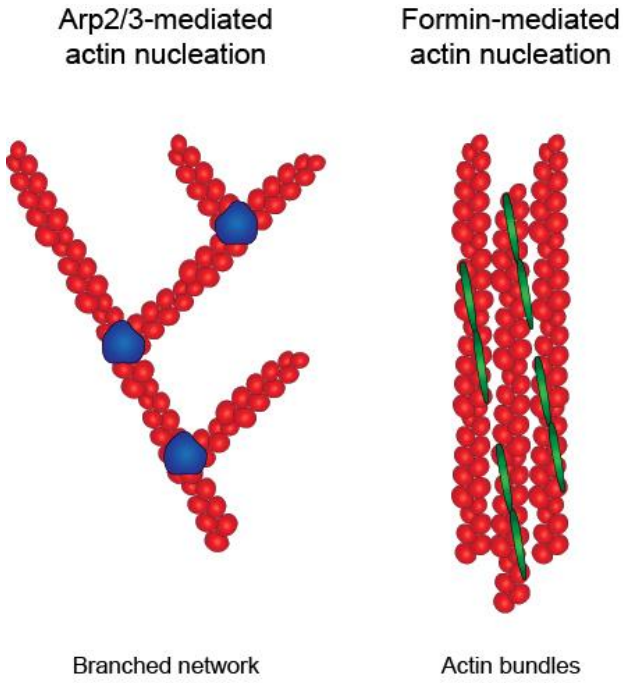

Figure 11. Arp2/3- versus Formin-mediated actin nucleation. While the Arp2/3 complex induces the formation of branched actin networks, Formin activity results in the generation of actin bundles. Adapted from [Le Clainche and Carlier, 2008].

Figure 12. Structure and function of the Arp2/3 complex. Left. Cartoon representation of the subunit organization in the inactive Arp2/3 complex. Arp2, Arp3 and Arp complex-1 (ArpC1) through ArpC5 are shown (labelled as 1–5). **Right.** Cartoon diagram of Arp2/3 complex binding to the side of the mother filament and the pointed end of the daughter filament in the Y-branch. The two filaments are oriented at ~70° angle. Reproduced and modified from [Goley and Welch, 2006]

twenty years, proteins from the Formin family and the Actin-Related Protein-2/3 (Arp2/3) complex [Chesarone and Goode, 2009, Carlier et al., 2015] are the most studied in eukaryotic cells. Actin nucleation supported by either Formins or Arp2/3 results in the generation of different actin structures. Formins mainly stabilize already formed actin oligomers, hence promoting their elongation in bundles (not detailed in this manuscript). On the opposite, Arp2/3, which is structurally related to G-actin, binds to the side of an existing actin filament and promotes the polymerization of a new filament [Chesarone and Goode, 2009] (**Figure 11**).

1.b. Focus: the Arp2/3 complex

In the mid-1990's, MACHESKY and co-workers identified seven polypeptides that interact with the actin-binding protein Profilin and form a complex composed of one of each subunit [Machesky et al., 1994] (**Figure 12**). Interestingly, two of these subunits are structurally similar to G-actin and were named actin-related protein 2 and 3 (Arp2 and Arp3), respectively. This was at the origin of the name of the Arp2/3 complex. The other five subunits – termed ArpC1 to 5 (for Arp2/3 complex component 1-5) – act as scaffold proteins providing to the Arp2/3 complex the proper organization to support actin nucleation. Indeed, whereas ArpC2 and ArpC4 (and maybe other subunits) bind the side of an existing actin filament to anchor the complex, Arp2 and Arp3 form the first actin dimer promoting the nucleation of a new filament with a characteristic branch angle of ~70°. Thus, the Arp2/3 complex caps the pointed end of the newly formed filament while its elongation occurs at the barbed end [Mullins et al., 1998, Amann and Pollard, 2001, Beltzner and Pollard, 2004, Egile et al., 2005].

Activation of the Arp2/3 complex requires the action of nucleation promoting factors (NPFs) (reviewed in [Rotty et al., 2013]). NPFs are categorized into two classes depending on their mode of action. Whereas the mechanism leading to Arp2/3 activation by class II NPFs, which include Cortactin, is not well understood (not detailed in this manuscript); class I NPFs offer a more comprehensive view of their mode of action. Class I NPFs are composed by members of the Wiskott-Aldrich Syndrome protein (WASP, neural WASP and WASH) and suppressor of cyclic AMP repressor (SCAR, also known as WASP-family verpolin-homologous protein (WAVE)) [Goley and Welch, 2006]. They all possess a WCA (or VCA) domain comprising a WASP-homology-2 domain (WH2 or W) that binds to G-actin as well

Figure 13. Model for activation and recycling of the Arp2/3 complex. The Arp2/3 complex starts in an inactive, open conformation. 1) Binding of WCA domain promotes a conformational change that primes the complex for activation, which occurs upon binding of the WCA–actin–Arp2/3 assembly to the mother filament, preferentially near the barbed end. WCA domain presents an ATP–actin monomer to the complex and/or possibly to the barbed end of the mother filament. 2) ATP is hydrolyzed on Arp2 concomitant with or shortly after nucleation of the daughter filament. The WCA dissociates, although the trigger for this is unknown. 3) Phosphate is released from Arp2. Mother and daughter filaments elongate and age by ATP hydrolysis and phosphate release. 4) Phosphate release from Arp2 and filament ageing weaken the interactions between Arp2/3 and the daughter and/or mother filament, 5) allowing branch disassembly and release of the Arp2/3 complex, presumably in an inactive, ADP-bound conformation. 6) Nucleotide exchange on Arp2 (and possibly on Arp3) occurs and the cycle begins again. Reproduced from [Goley and Welch, 2006]

as a central domain (C) and an acidic domain (A), both mediating the interaction with Arp2/3 [Goley and Welch, 2006]. The precise mechanism enabling Arp2/3 activation by class I NPFs is still lacking. However a common model has emerged and is now well-accepted. Upon Arp2/3 binding by the acidic domain, the central region induces a conformational change in the Arp2/3 complex that brings Arp2 and Arp3 closer to each other, hence mimicking a dimer of G-actin (**Figure 13**). This dimer acts as a "root" to support the incorporation of new actin monomers that are presented by the coordinated action of the WH2 and central regions (**Figure 13**). This results in the net elongation of the new filament at the barbed end [Goley and Welch, 2006, Chesarone and Goode, 2009].

NPF-mediated activation of the Arp2/3 complex is a highly regulated process that is mainly controlled by the Rho family of small GTP-binding proteins that includes Rho, Rac and Cdc42 [Ridley and Hall, 1992, Nobes and Hall, 1995a, Nobes and Hall, 1995b, Raftopoulou and Hall, 2004, Pellegrin and Mellor, 2007, Heasman and Ridley, 2008]. For instance, the NPF WASP exists into two states: a close autoinhibitory state where its WCA domain is not accessible since it interacts with the GTPase-binding-domain (GBD) of the protein and an open active state, which is mediated by the binding of Rho-GTPases (mainly Rac or Cdc42) to the WASP GBD domain, thus releasing the WCA domain that might now be accessible to bind to Arp2/3 [Rotty et al., 2013]. Of note, not all NPFs contain a GBD domain (such as WAVE) and the mechanism presented above might not be applicable for them. Other models, such as the trans- regulation by interacting proteins, have been proposed to explain such other mechanisms [Lebensohn and Kirschner, 2009, Ismail et al., 2009] (not detailed in this manuscript).

The complexity of such regulatory mechanisms as well as the increasing number of protagonists involved in these mechanisms highlight how it is crucial for the cell to tightly control in time and space the assembly of actin filaments. Further work is still needed to better understand the precise mechanisms allowing the fine regulation of Arp2/3 by NPFs. Interestingly, the local activation of specific NPFs at different subcellular localizations represents another level of regulation that allows building particular actin networks that serve specific cellular functions (reviewed in [Suetsugu, 2013]).

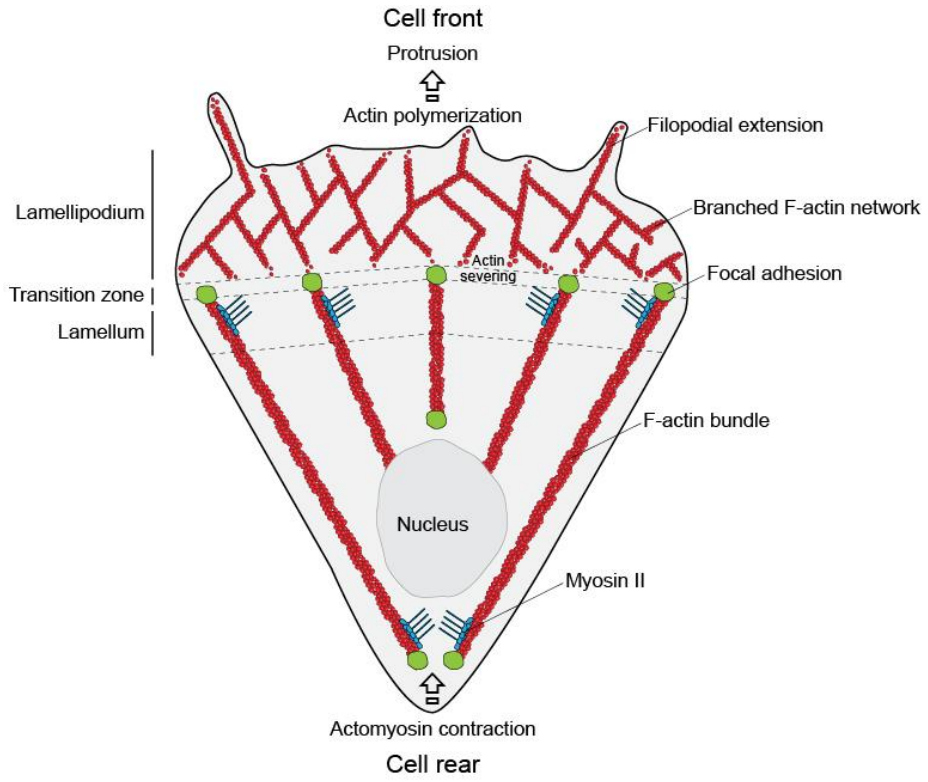

Figure 14. The actin cytoskeleton in cell locomotion. Cell migration is supported by the generation of membrane protrusions at the cell front resulting from actin polymerization at the leading edge. Concomitantly, Myosin II-mediated contractions at the rear of the cell allow back retraction resulting in the forward movement of the cell. Adapted from [Parsons et al., 2010].

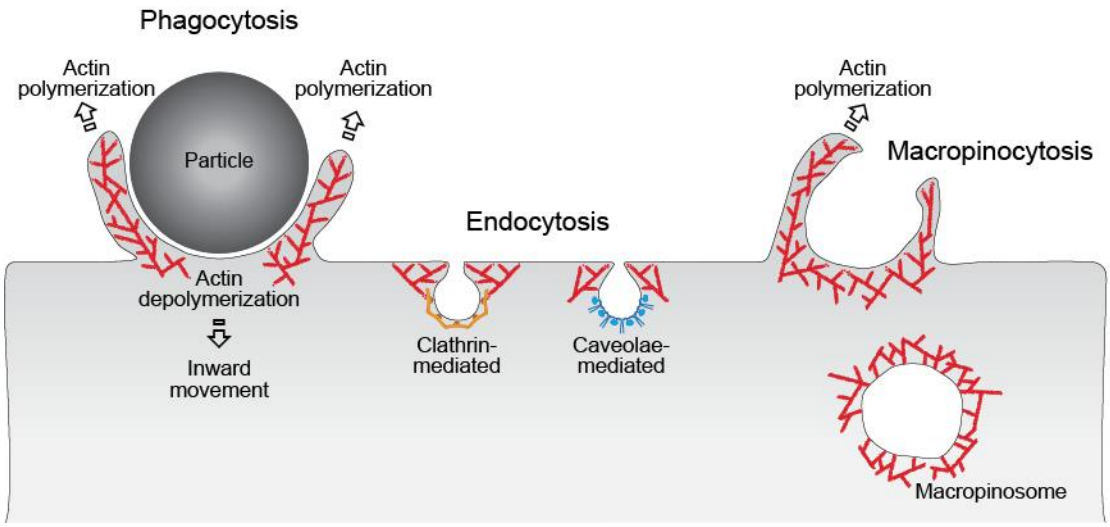

Figure 15. The actin cytoskeleton in internalization processes. Large particles can be taken-up by phagocytosis, whereas fluid uptake occurs through macropinocytosis. Both processes are triggered by and rely on actin-mediated remodeling of the plasma membrane. Actin filaments might also play a role in the closure of endocytic vesicles. Adapted from [Kaksonen et al., 2006, Mayor and Pagano, 2007].

1.c. Actin networks & key biological processes

- **Cell migration**

One of the most studied actin-dependent processes over the world is cell migration. Amoeboid cell migration relies on cycles of actin polymerization at the leading edge and contractility at the rear of the cell. At the cell front, polymerization of Arp2/3-mediated branched actin networks underneath the plasma membrane, referred to as the lamellipodium, promotes membrane protrusion leading to the net extension of the cell front. Just behind the lamellipodium, the lamellum is formed of actin bundles that extend throughout the cells and transmit the contractile forces, generated at the rear of the cell, required for cell movement. Force generation in migrating cells is ensured by the actin-based motor myosin II that associates with anti-parallel actin filaments [Burnette et al., 2011, Ennomani et al., 2016] (**Figure 14**). Thus the coordinated assembly of different actin networks within specific subcellular localizations provides to the cell with the machinery required for its movement.

- **Cell division**

Actin dynamics play also a key role during cell division where actin-dependent mechanisms occur throughout the progression of the cell cycle. In adherent cells, reorganization of the cortical actin network modifies cell shape and induces them adopting the roundish morphology characteristic of dividing cells. In addition, both Myosin II and F-actin have been shown to play crucial role in centrosome separation for the establishment of the mitotic spindle [Rosenblatt et al., 2004, Uzbekov et al., 2002]. The reorganization and stabilization of cortical F-actin, which increases the rigidity of the cell cortex, was also described to drive the correct positioning of the spindle [Kaji et al., 2008]. Another key role played by F-actin during cell division is its involvement in the formation of the contractile ring at the cleavage furrow required for the completion of cytokinesis (reviewed in [Heng and Koh, 2010]).

- **Internalization processes**

Internalization of extracellular fluid/particles represents an important path of entry within cells and particularly applies for cells of the immune system. Among these processes, endocytosis, phagocytosis and macropinocytosis are key entry routes. Of note, while endocytosis and phagocytosis are mediated by the engagement of specific receptors at the cell surface, macropinocytosis rather represents a non-specific entry route. Whereas actin was

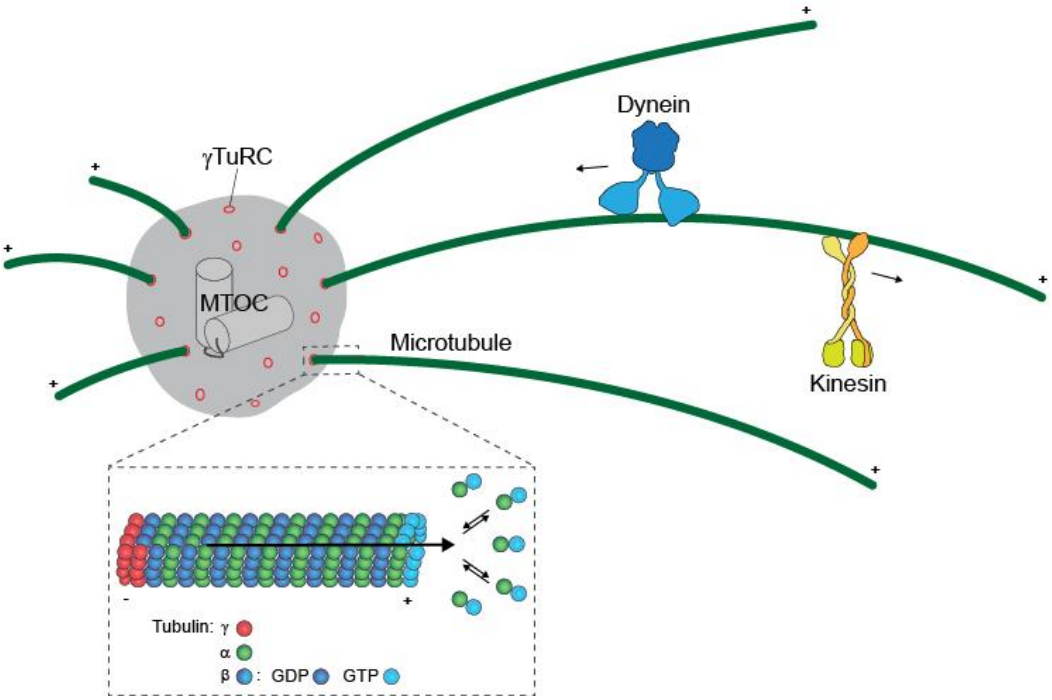

Figure 16. Organization of the microtubule cytoskeleton and intracellular trafficking. Microtubules are composed of α and β-tubulin dimers and are assembled from γ-tubulin ring complexes (γTuRC) present within the pericentriolar matrix that surrounds the centrioles. The centrosome serves as the main microtubule-organizing center (MTOC) within animal cells. Microtubules are the support of directed trafficking where the Dynein motor moves towards the centrosome (microtubule minus ends) and Kinesins move towards the cell periphery (microtubule plus ends).

.

thought to be dispensable for endocytosis in mammalian cells (what might be due to artefacts following clathrin overexpression), increasing evidences suggest that actin is involved in vesicles closure/scission (reviewed in [Smythe and Ayscough, 2006, Mooren et al., 2012]). In contrast, the role of the actin cytoskeleton in both phagocytosis and macropinocytosis is well described. First, actin remodeling underneath the plasma membrane leads to the formation of membrane protrusions that are pivotal for the initiation of the internalization process. During phagocytosis, following receptor binding, actin polymerization occurs within the protruding membrane enveloping the particle to be phagocytosed. In parallel, actin depolymerization at the base of the nascent phagosome allows its inward movement (reviewed in [Freeman and Grinstein, 2014]). During macropinocytosis, actin polymerization is sustained throughout the process of membrane extension until protrusions fold back and fuse with the plasma membrane leading to the formation of actin-coated macropinosomes (reviewed in [Lim and Gleeson, 2011]) (**Figure 15**).

2. The microtubule cytoskeleton

2.a. Assembly of microtubules

Similar to actin microfilaments, microtubules (MTs) are assembled from protofilaments made of heterodimers of α- and β-tubulin. In its common form, a microtubule is composed of thirteen protofilaments forming a hollow tube. The intrinsic structure of MTs given by the head-to-tail assembly of α- and β-tubulin provides to MTs a polar phenotype with α-tubulin oriented toward the minus-end and β-tubulin toward the plus-end. Whereas MT elongation might occurs at both extremities, the rate of tubulin incorporation is sensibly higher at their plus-end. This might result from the fact that MT minus-ends are anchored to the microtubule-organizing center (MTOC) that promotes MT assembly from γ-tubulin rings (γ-TuRC) [Moritz et al., 1995, Moritz et al., 2000]. MTs are also characterized by their dynamic instability that represents their high capacity to assemble and disassemble [Mitchison and Kirschner, 1984]. Indeed, the presence of GTP-bound tubulin polymers, referred to as the GTP cap, at the plus-end of MTs promotes fast polymerization. Conversely, the loss of this cap triggers their immediate depolymerization, since GDP-bound tubulin quickly dissociates [Erickson and O'Brien, 1992, Howard and Hyman, 2009] (**Figure 16, inset**).

Figure 17. Centriole and cartwheel architecture. The ultrastructure of a resin-embedded centriole and cartwheel within it purified from *Chlamydomonas reinhardtii.* **c**) Side view of the centriole with indicated proximal and distal ends. The arrow points to the ~100 nm high cartwheel. **d**) Cross-section of the proximal part of a *C. reinhardtii* centriole onto which a ninefold rotational symmetry was applied to highlight repeated features. The A-microtubule, B-microtubule and C-microtubule are indicated and the arrow points to the A–C linker. Reproduced from [Gonczy, 2012].

2.b. Focus: the centrosome, the main microtubule-organizing center

The centrosome is the main microtubule-organizing center within eukaryotic cells. It is composed of a pair of centrioles, generally oriented in a perpendicular manner, and surrounded by a network of proteins named the pericentriolar matrix (PCM) (**Figure 16**). The centrioles are "*ninefold-symmetrical barrels*" usually composed of nine microtubule triplets and measure between 0.1–0.5 µm long and 0.1–0.2 µm in diameter [Preble et al., 2000, Marshall, 2001] (**Figure 17**). They are assembled from a specific structure, termed the cartwheel and enriched in Centrin, which acts as the central hub for the assembly of the microtubule triplets (reviewed in [Hirono, 2014] and [Dong, 2015]) (**Figure 17**). The PCM can be seen as an amorphous mass surrounding the centrioles that appeared in the earliest electron micrographs as densely stained material [Robbins et al., 1968]. It is composed of scaffold proteins thought to form the base of the PCM and effector proteins, including kinases, phosphatases and proteins of the γ-tubulin ring complex, which localize more at the periphery and are involved in microtubule organization (reviewed in [Woodruff et al., 2014]). Due to its protein content, the PCM can serve as signaling platform regulating organelle trafficking, protein degradation and mitotic spindle assembly [Woodruff et al., 2014].

Through its pivotal role in promoting MT nucleation, the centrosome has been described to affect a wide range of biological processes by impacting on the intracellular organization. For instance, the Golgi apparatus is most of the time associated with the centrosome and this association was described to regulate biological processes as different as directional cell migration or ciliogenesis [Hurtado et al., 2011]. In addition, the term centrosome was used to name this organelle because it is mainly found at the center of resting cells, often in close association with the nucleus [Burakov and Nadezhdina, 2013] to which it is tethered by the LINC (Linker of Nucleoskeleton and Cytoskeleton) complex [Tapley and Starr, 2013]. The core of this complex results from the interaction of KASH-domain proteins, such as Nesprins, and SUN-domain proteins, which are anchored to the outer and inner nuclear membrane, respectively [Kim et al., 2015]. Whereas Nesprins link the microtubule and actin cytoskeleton within the cytoplasm, SUN proteins bind to the nucleoskeleton.

2.c. Microtubules/Centrosome & key biological processes

- **Intracellular trafficking**

The network of MTs defines intracellular routes that support directed-trafficking of organelles and vesicles. These trafficking events rely on the activity of microtubule-based molecular motors, which are mainly defined by their direction of movement (**Figure 16**). Kinesins represent a large family of proteins (around 40 different kinesins have been described) that preferentially move towards the plus-end of MTs, hence bringing organelles or vesicles from the centrosome at the cell center towards the cell periphery. In contrast, the Dynein motor moves towards the minus-end of MTs, i.e. from the periphery to the cell center. Of note vesicle trafficking might also occur independently of MTs, and rather relies on actin nucleation at one side of the vesicle, e.g. phagosomes or endosomes [Zhang et al., 2002], by a process similar to actin rockets assembled by *Listeria monocytogenes* [Machesky, 1999].

- **Cell division**

One important feature of cell division is the symmetric segregation of chromosomes within the two daughter cells. This is achieved through the assembly of a sophisticated microtubule-based machine called mitotic spindle. As a cell enters in mitosis, the centrosome duplicates, hence forming two MTOCs within the cell. Meanwhile, the rate of microtubule shrinkage greatly increases transforming the relatively stable interphase microtubules into two radial arrays of dynamic microtubules. Then microtubules elongate and depolymerize until they are captured by chromosome kinetochores, linking the chromosomes to one of the two centrosomes. This process has been theorized in the mid-1980's by KIRSCHNER and MITCHISON, who named it the "search and capture" model [Kirschner and Mitchison, 1986]. Few years later, microtubule capture has been observed in live cells [Hayden et al., 1990, Rieder and Alexander, 1990]. To date, our knowledge on the mechanisms underlying spindle assembly and function has increased and explain how chromosome segregation is properly orchestrated to ensure the proper division of the cell (reviewed in [Heald and Khodjakov, 2015]).

- **Ciliogenesis**

Cilia are membrane-bound sensory organelles made of dynamic microtubules. A large variety of cell types (but not lymphocytes) bear cilia at their cellular surface. Cilia sense changes in the extracellular environment and transmit the information within the cell

Figure 18. *In vivo* coorganization of F-actin and microtubules. A) Fluorescence micrograph of part of a 3T3 fibroblast with fluorescent labels showing the distinct organization of F-actin (cyan) and microtubules (red). Actin forms rigid stress fibers and dense networks underneath the plasma membrane (top), whereas microtubules grow toward the cell periphery and form a sparse network. B) Schematic showing how dynamic microtubules can encounter different F-actin architectures within a cell. Scale bar: 5 μm. Reproduced from [Preciado Lopez et al., 2014].

[Christensen et al., 2007] for it to control biological processes ranging from organ development, cell differentiation and cell polarity [Goetz and Anderson, 2010, Badano et al., 2006]. The base of a cilium corresponds to modified centrioles, termed basal bodies, anchored to the plasma membrane thanks to specialized structures at their distal part referred to as appendages (reviewed in [Kobayashi and Dynlacht, 2011]). Once basal bodies are anchored at the membrane, nine microtubule doublets linked by Dynein assemble and elongate to form the axoneme (reviewed in [Keeling et al., 2016]). Of note, axonemal extension might also occur at the surface of intracellular vesicles as observed in migrating neurons [Baudoin et al., 2012].

2.d. Crosstalk between microtubule and actin cytoskeletons

As illustrated on **Figure 18**, in living cells microtubules and F-actin might be in close association within specific subcellular localizations where a real crosstalk between both cytoskeletal components occurs. Several proteins have been shown to crosslink F-actin and microtubules such as members of the Spectraplakin family. These proteins share the characteristic of both Spectrin and Plakin proteins that possess the ability to bind F-actin and microtubules, respectively [Roper et al., 2002, Suozzi et al., 2012, Huelsmann and Brown, 2014](not discussed in this manuscript).

Interestingly, members of the Formin family of actin nucleators have been described to regulate microtubule dynamics. For instance, overexpression of a constitutive active form of mDia2 that is unable to support actin nucleation induced the stabilization of microtubules marked by a decrease in their rates of elongation and depolymerization [Bartolini et al., 2008, DeWard and Alberts, 2008]. In addition, alignment of MTs to actin fibres has been reported in HeLa cells expressing a constitutively active form of mDia1 [Ishizaki et al., 2001]. Thus, through their dual role in regulating both the actin and microtubule cytoskeletons, Formins might influence the global organization of the cytoskeleton.

Conversely, microtubules might also influence actin networks. In the late 1980's, DANOWSKI brings evidences that microtubule polymerization counter-acts actin-based contractility [Danowski, 1989]. Indeed, treatment of different fibroblastic cell lines with inhibitors of MT assembly resulted in the increase of actin-mediated contractility [Danowski, 1989]. Although the mechanism underlying such a regulation was not known at that time, one could imagine that MT-dependent regulation of cell contractility might occur through the

modulation of Myosin II activity. Later, KRENDEL and co-workers showed that the activity of the guanine exchange factor GEF-H1, which activates RhoA thus promoting Formin and Myosin II activation, was regulated through its interaction with microtubules. Indeed, the availability of GEF-H1 within the cytoplasm to promote RhoA activation is directly linked to the amount of polymerized microtubules within the cells since GEF-H1 by interacting with microtubules is no longer able to activate RhoA [Krendel et al., 2002]. Upon microtubule depolymerization, GEF-H1 is released within the cytoplasm, hence promoting RhoA activation and the subsequent simulation of Myosin II-mediated contractility [Krendel et al., 2002]. Thus, by controlling the local assembly/disassembly of microtubules, a cell might finely tune actin networks and cell contractility, hence highlighting the pivotal role of actin/microtubule crosstalk in the regulation of cellular processes.

Of note, F-actin and components of the Arp2/3 complex have also been described to be in close association with the centrosome in different studies without any clear identified-function [Hubert et al., 2011, Vaughan and Dawe, 2011, Tang and Marshall, 2012]. Whether such association also serves specific co-regulatory mechanisms involved in the tuning of cellular processes remains to be determined. A specific focus on this F-actin/centrosome interaction has been made during my thesis and the first part of the results presented in this manuscript highlights a new mechanism of F-actin/centrosome cooperation in the regulation of B lymphocyte polarization.

3. Role of the cytoskeleton in antigen uptake, processing and presentation by B cells

As mentioned in the above sections, B cells must encounter, internalize and process antigens as well as migrate towards the T cell zone to exert their immune function. All these processes rely on their actin and microtubule cytoskeletons, which associate with cellular membranes to regulate all these events that need membrane deformation to occur.

3.a. Antigen encounter and immune synapse formation

As mentioned earlier, the engagement of BCRs with cell surface-tethered antigens induces the formation of an immune synapse that serves as a local platform to coordinate BCR-mediated signaling and antigen uptake [Batista et al., 2001]. B cell synapse resembles the one originally described in T cells [Grakoui et al., 1999, Yuseff et al., 2009]. Its establishment represents a key step in the process of B cell activation [Carrasco et al., 2004, Fleire et al., 2006] and is initiated as soon as immobilized antigens engage BCRs leading to their cross-

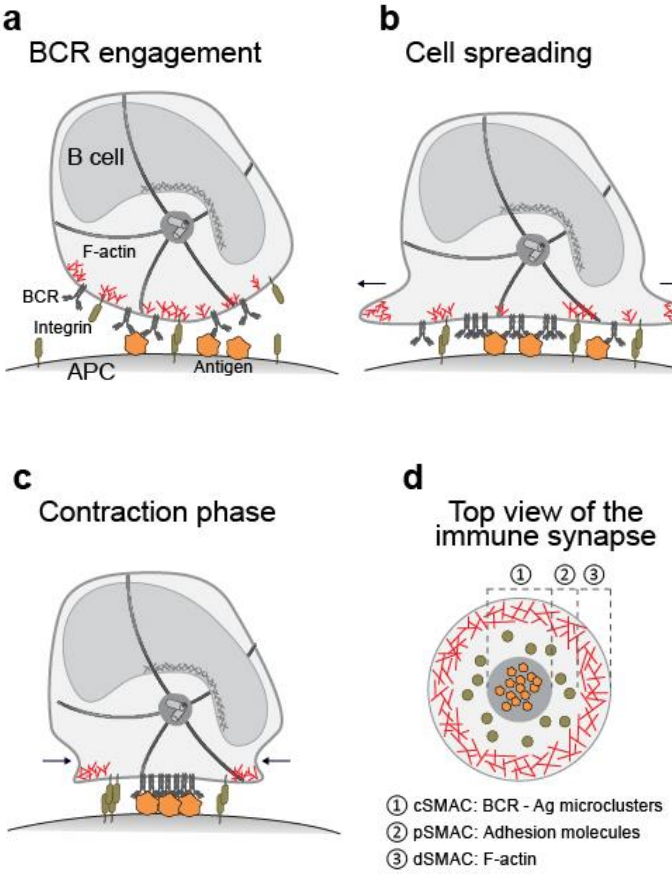

Figure 19. Formation of the B cell immune synapse. BCR engagement with surface-tethered antigens induces the formation of BCR-antigen microclusters (**a**) that are required for the initiation of BCR-mediated signaling ultimately leading to cytoskeleton remodeling. Then through cycles of spreading (**b**) and contraction (**c**) microclusters coalesce within the center of the synapse and form the central supramolecular activation cluster (cSMAC). Whereas integrins concentrate within the peripheral SMAC (pSMAC), F-actin accumulates in the distal SMAC (dSMAC) (**d**). Adapted from [Kuokkanen et al., 2015].

linking and the formation of BCR-microclusters (reviewed in [Harwood and Batista, 2010]) (**Figure 19a**). The actin cytoskeleton plays a key role in the formation of the B cell synapse as well as in antigen capture [Hartwig et al., 1995]. In particular, BCR stimulation initiates a rapid cofilin-dependent actin depolymerization at the antigen-contact site, allowing the local increase of BCR diffusion within the membrane [Freeman et al., 2011]. This is followed by polarized actin re-polymerization that promotes B cell spreading onto the antigen-carrying cell [Sumoza-Toledo et al., 2006] (**Figure 19b**). This process facilitates the formation of BCR microclusters that are required for sustained BCR signaling [Treanor et al., 2010]. Rearrangements of the actin cytoskeleton occur through the BCR-dependent activation of Syk, the small GTPases Cdc42 and Rac1/Rac2 and their GEF factors Dock8 and Vav1/Vav2, respectively [Le Roux et al., 2007, Arana et al., 2008, Randall et al., 2009, Burbage et al., 2015]. In the case of Cdc42, this occurs through the activation of the actin nucleation promoting factor (NPF) WASP, which activates the Arp2/3 complex for polymerization of branched actin networks [Sharma et al., 2009]. Actin dynamics at the synapse are also critical for the attenuation of BCR signaling. Indeed, Abp1 (actin-binding protein 1) is needed for antigen internalization but further acts as a negative regulator of BCR signaling by activating inhibitory signaling molecules [Seeley-Fallen et al., 2014].

At that stage, through a contraction phase mediated by Myosin II, BCR microclusters merge together in the center of the immune synapse and form the central supramolecular activation cluster (cSMAC) [Fleire et al., 2006] (**Figure 19c**). This implies that the actin cortex might associate to the membrane to allow its deformation. This physical interaction does not only define the cell shape but also regulates the tension of the plasma membrane, which has been linked to receptor signaling in various cell types [Masters et al., 2013]. Actin-membrane association depends on different molecules including the Ezrin Radixin Moesin (ERM) family as well as the atypical class I Myosins. In resting B cells, the ERM network creates boundaries that restrict BCR diffusion. Compromising ERM proteins is sufficient to induce a robust intracellular signaling and a concomitant increase in BCR motility [Treanor et al., 2010]. Upon B cell activation, ERM proteins are transiently inactivated to increase BCR diffusion allowing the formation of the cSMAC. Then they are re-activated to further immobilized BCR microclusters at the center of the B cell synapse [Treanor et al., 2011]. The short-tailed Myosin IC and IG were also shown to be recruited to F-actin rich domains at the B cell synapse and to regulate cell spreading and antigen internalization [Sumoza-Toledo et al., 2006, Maravillas-Montero et al., 2011, Maravillas-Montero et al., 2014]. Cortical actin

rearrangements also trigger the formation of a second concentric region called the peripheral SMAC (pSMAC) that contains adhesion molecules such as LFA-1 (lymphocyte function-associated antigen 1, also known as $\alpha_L\beta_2$ integrin). The engagement of this integrin with its counter-receptor intercellular adhesion molecule 1 (ICAM-1, also known as CD54) promotes B cell adhesion to the antigen-carrying cell, facilitating the formation of the immune synapse and decreasing the antigen-affinity threshold required for BCR-mediated cell activation [Carrasco et al., 2004]. While the cSMAC and the pSMAC display low concentrations of polymerized actin, F-actin concentrates in a third concentric region called the distal SMAC (dSMAC) (**Figure 19d**).

In vivo, B cell spreading onto antigen-presenting cells and immune synapse formation are coupled to an arrest phase in B cell migration, which is required for B cells to acquire immobilized antigens [Carrasco and Batista, 2007, Junt et al., 2007]. Thereby, the tight regulation of the interplay between cell motility and antigen internalization is critical for B cell function. It has been recently shown that recruitment to the immune synapse of the scaffold protein vinculin, which links integrins at the plasma membrane with the actin cytoskeleton [Humphries et al., 2007], regulates adhesion between the B cell and the antigen-presenting cell [Saez de Guinoa et al., 2013]. Vinculin is recruited to the immune synapse in parallel to a phosphatidylinositol (4, 5)-bisphosphate (PIP_2) wave and stabilizes LFA-1 cluster within the pSMAC. This process relies on the activity of the Myosin IIA motor, which is also required for CXCL13-mediated migration [Saez de Guinoa et al., 2011]. Vinculin and Myosin IIA are therefore critical for B lymphocytes to switch between random motility and antigen internalization. Thus, B cells possess the machinery required to integrate incoming information and adapt their response to maximize antigen acquisition by regulating the balance between cell migration and cell adhesion to antigen-presenting cells. This leads to the formation of either stable immune synapses characterized by a firm adhesion of the B cell to the antigen-presenting cell and very poor migratory capacities or of CXCL13- and LFA-1-mediated kinapses where B cells establish successive short interactions with multiple antigen-presenting cells, alternating between adhesion and motility phases. This resembles what have been described in T cells that form either synapses or kinapses depending on the affinity of the TCR for their cognate peptide-MHC complexes [Moreau et al., 2012]. Whether and how synapse versus kinapse formation impacts on the ability of B cells to extract, process and present immobilized antigens to primed $CD4^+$ T cells remains an open question.

Microtubules are also essential regulators of BCR signaling as well as of the uptake of surface-tethered antigens by B cells. In particular, the dynamics of BCR-antigen complexes and their internalization at the immune synapse were shown to rely on the microtubule minus-end molecular motor Dynein [Schnyder et al., 2011]. Impaired Dynein recruitment to the B cell synapse does not alter microcluster formation or actin-dependent cell spreading but compromises the centripetal movement of BCR microclusters as well as their internalization [Schnyder et al., 2011], suggesting that microcluster uptake might preferentially take place at the synapse center.

3.b. Antigen processing and presentation

Both vesicles containing internalized BCR-antigen complexes and MHC-II$^+$ endo-lysosomes undergo active intracellular transport in antigen-presenting cells to ultimately converge. Depolymerization of the actin cytoskeleton was shown to alter this convergence as well as Ii degradation [Barois et al., 1998, Brown and Song, 2001], highlighting the requirement of an intact actin cytoskeleton for antigen processing. Interestingly, actin depolymerization in B cells leads to excessive antigen degradation [Gondre-Lewis et al., 2001], suggesting that actin filaments are needed for antigen transport to MHC-II-containing compartments rather than to terminal lysosomes. In agreement with a key role for the actin network in antigen processing, our laboratory has identified Myosin II as the first motor protein involved in this process [Vascotto et al., 2007]. By interacting with the cytosolic tail of Ii, this actin-based motor protein allows the convergence between MHC-II-containing endo-lysosomes and vesicles loaded with taken-up antigens [Vascotto et al., 2007]. Later, two atypical class I Myosins, Myosin IC and IE, were also implicated in MHC-II trafficking in B cells [Maravillas-Montero et al., 2011, Santos-Argumedo et al., 2013]. However, the precise mechanisms by which class I Myosins interact with MHC-II$^+$ vesicles to regulate antigen processing remain to be determined.

Once generated, MHC-II-peptide complexes are exported to the antigen-presenting cell surface for presentation to primed CD4$^+$ T cells. In B cells both Kinesins and Dynein are used for the proper export of MHC-II-containing vesicles towards the cell surface, which traffic bi-directionally along microtubules [Wubbolts et al., 1996, Wubbolts and Neefjes, 1999, Wubbolts et al., 1999]. How these motor proteins interact with each other to coordinate the transport of MHC-II-containing endo-lysosomes towards the cell surface and whether actin networks participate in this process are interesting questions to be addressed.

The findings presented above indicate that both the actin and microtubule cytoskeletons control the trafficking of antigens and MHC-II-containing vesicles, suggesting that both networks might functionally interact. Accordingly, there are growing evidences for the dynamics of these two types of filaments being tightly coupled in most cell types [Small et al., 1999, Palazzo and Gundersen, 2002, Rodriguez et al., 2003, Etienne-Manneville, 2004a, Lasserre and Alcover, 2010, Schneider and Persson, 2015]. They further suggest that the use of common cytoskeleton elements at distinct subcellular locations might help coupling various cellular processes. How such coupling is used to coordinate in time and space the various events that are needed for B cell function remains to be precisely determined.

Establishment of the immune synapse also gives the first cues of asymmetrical cell organization leading *in fine* to the polarization of B cell organelles towards the synaptic interface. This process is strictly required for B cells to extract, process and present surface-tethered antigens to primed $CD4^+$ T cells.

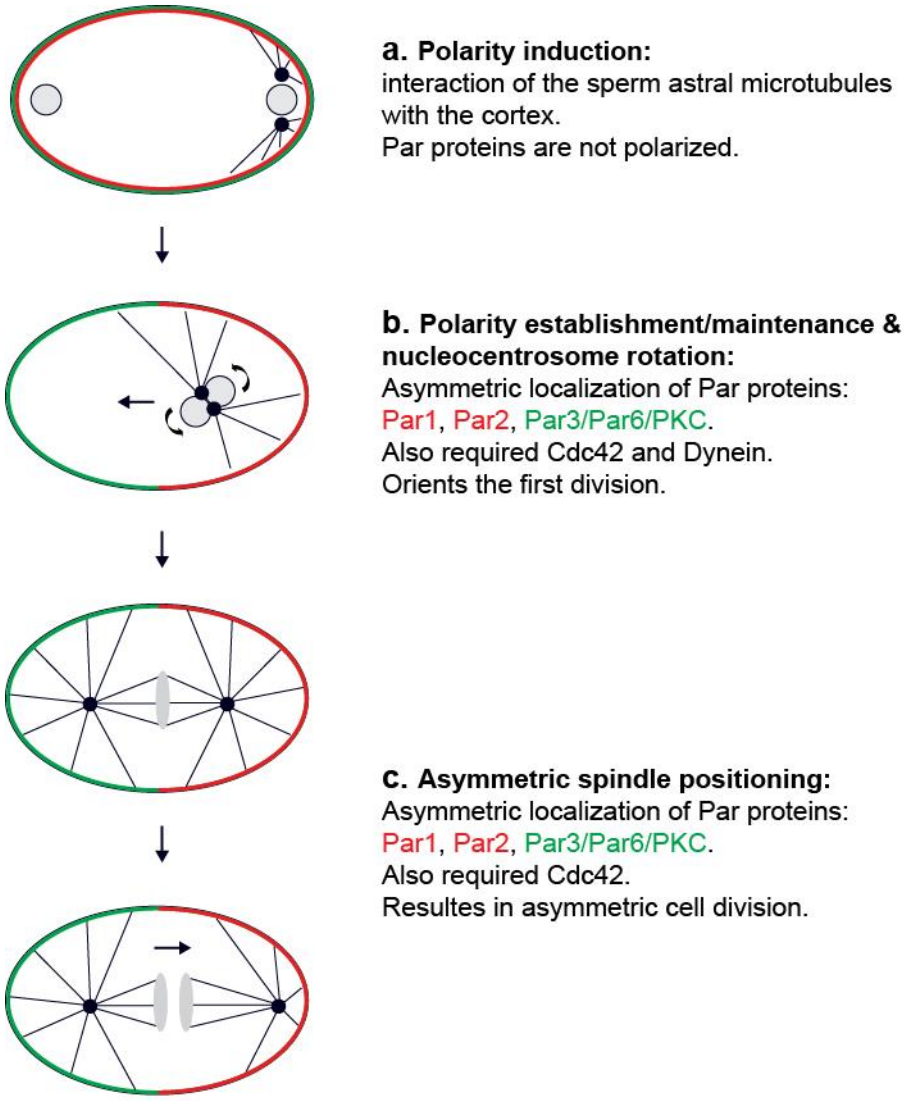

Figure 20. Establishment of cell polarity: asymmetric segregation of PAR proteins. Asymmetric localization of the Par proteins is required for the polarization of *C. elegans* embryos at the one-cell stage. In addition, polarized localization of Par proteins regulates asymmetric cell division of the embryo providing the daughter cells with different fates. Adapted from [Ahringer, 2003].

1. Cell polarity: a simple definition

Cell polarity is defined by the non-symmetric organization of a cell and regulates a broad range of biological processes such as cell division, cell fate and cell migration [Barnett et al., 2012, Thaunat et al., 2012, Schmoranzer et al., 2009] and allows the definition of polarity axis within cells and tissues. For instance, the asymmetric segregation of cellular components confers to epithelial cells a "top" and a "bottom", called the apical and basal pole, respectively, which regulate the main functions of these cells (reviewed in [Lee and Streuli, 2014]). Migrating cells also display a polarized phenotype with a front, or leading edge, and a rear, which thus defines a front-back polarity axis [Parsons et al., 2010]. Cell polarity also regulates cell division as the positioning of the mitotic spindle defines the axis of cell division and the asymmetric partitioning of proteins, mRNA and/or organelles providing different fates to the daughter cells.

Establishment of cell polarity relies on the integration of polarity cues that mainly dictate the reorganization of the microtubule cytoskeleton, hence defining the cell polarity axis and the directionality of intracellular trafficking [Elric and Etienne-Manneville, 2014]. As the centrosome drives the nucleation and organization of MTs, this organelle was found to play an essential role in the polarization of a variety of cell types ranging from yeast to specialized cells in multicellular organisms [Yuseff et al., 2013].

2. The hallmark of polarity: the PAR polarity complex

One of the polarity proteins most studied over the world and in almost all animal models, from worms to mammalian cells, are members of the PAR (partitioning defective) polarity complex. These polarity proteins were discovered in the late 1980's in the nematode *Caenorhabditis elegans* by genetic studies of embryos impaired for asymmetric cell division. Mutants lacking genes of the PAR polarity complex failed to establish an anterior-posterior polarity axis, preventing the proper positioning of the mitotic spindle and thus impairing embryo development [Kemphues et al., 1988]. Following on this early study, members of the PAR polarity complex were classified into two major groups based on their cellular localization: the anterior PAR complex composed of Par3, Par6 and aPKC and PAR proteins localized at the posterior pole such as Par1 and Par2 [Ahringer, 2003] (**Figure 20**).

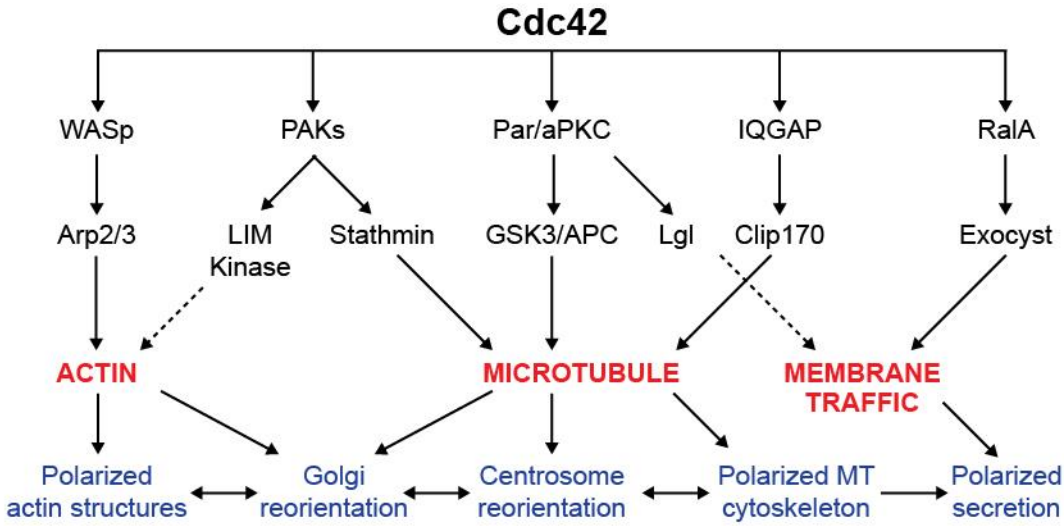

Figure 21. Cdc42, the master regulator of cell polarity. Cdc42 regulates multiple signaling pathways leading to the polarization of cellular components as well as to the polarized secretion of proteins. Adapted from [Etienne-Manneville, 2004b].

In *C. elegans* embryos, asymmetric segregation of the PAR proteins results in the polarized positioning of the mitotic spindle thus providing the daughter cells with different fate. Interestingly, beside its role in the regulation of the actin cytoskeleton, the small Rho GTPase Cdc42 has been described to activate the PAR polarity complex [Joberty et al., 2000], hence providing to Cdc42 a key role in the reorganization of both actin and microtubule cytoskeletons (**Figure 21**). Although the Cdc42-dependent activation of the PAR complex was first identified as a key factor for budding yeast polarization, its pivotal function in polarity establishment in all eukaryotes is now well admitted [Etienne-Manneville, 2004b, Macara, 2004, Jaffe and Hall, 2005].

3. B cell polarization upon surface-tethered antigen stimulation

Similarly to observations that were made in natural killer and cytotoxic T cells [Stinchcombe et al., 2011], upon BCR engagement, B cells rapidly polarize their centrosome towards the antigen-contact site. Concomitantly, MHC-II$^+$/Lamp-1$^+$ lysosomes are recruited to the immune synapse, where they cluster [Yuseff et al., 2011] (**Figure 22**). Interestingly, using MHC-II-expressing human melanoma cells, WUBBOLTS *et al.* had found that MHC-II$^+$ lysosomes traffic along microtubules to reach the plasma membrane [Wubbolts et al., 1996, Wubbolts et al., 1999]. Accordingly, we have shown that laser ablation of the centrosome following B cell stimulation with immobilized antigens prevents the polarized recruitment of lysosomes to the immune synapse [Yuseff et al., 2011]. There, lysosomes are locally secreted leading to the acidification of the extracellular synaptic space and promoting the release of proteases in this confined environment. Both synapse alkalinization and extracellular inhibition of proteases lead to a drastic decrease in the capacity of B cells to extract antigens, indicating that synapse acidification and protease secretion are required for efficient surface-tethered antigen extraction [Yuseff et al., 2011]. Although the molecular mechanisms underlying B cell polarization upon BCR engagement with immobilized antigens are not fully understood, former lab-members have identified the conserved polarity machinery Cdc42/Par3/aPKC-ζ as required for B cell polarization [Yuseff et al., 2013]. Indeed, BCR engagement with surface-tethered antigens leads to the Cdc42-dependent activation of aPKC-ζ that localizes at the surface of Lamp-1$^+$ lysosomes. Both Cdc42 and aPKC-ζ inhibition impairs centrosome polarization and lysosome recruitment at the immune synapse, thus preventing B cells to efficiently extract and present immobilized antigens to primed CD4$^+$ T cells. In addition, they have shown that the polarity protein Par3 together with the

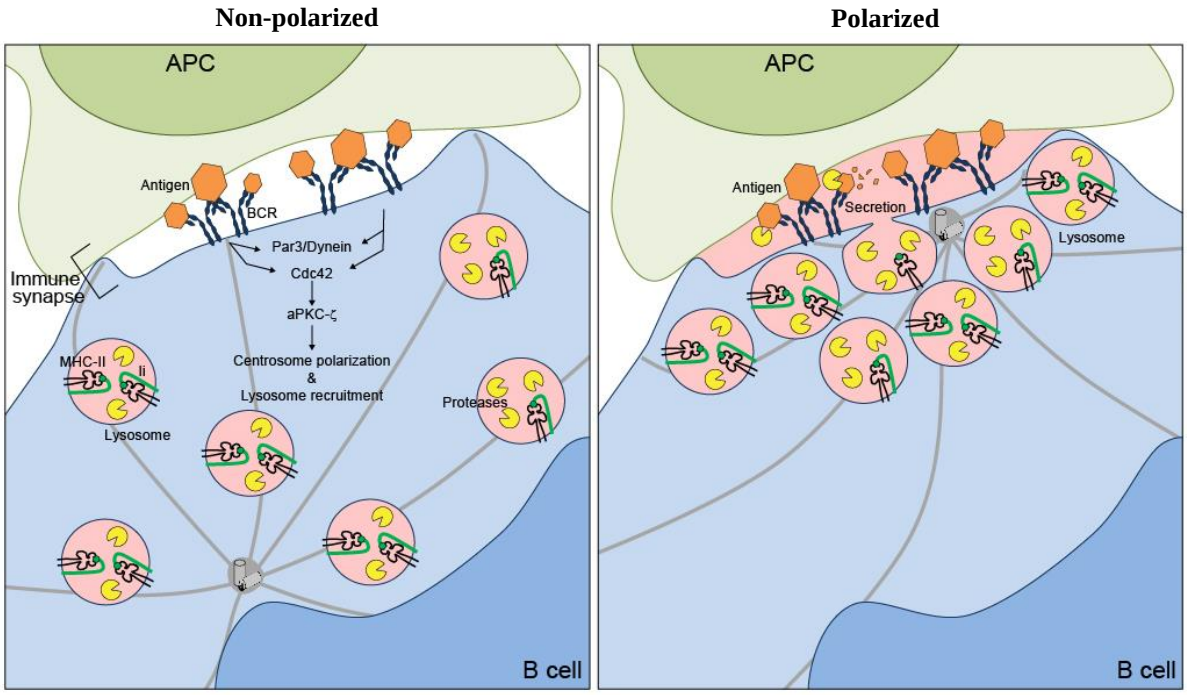

Figure 22. B cell polarization upon immobilized antigen stimulation. Upon BCR engagement with immobilized antigens, the coordinated action of the Par polarity complex and Dynein induces centrosome repositioning towards the antigen-contact site. Centrosome polarization in turn dictates the recruitment and local secretion of lysosomes within the synaptic cleft, which is required for the efficient extraction and processing of immobilized antigens. Adapted from [Yuseff et al., 2013].

microtubule-based motor Dynein accumulate at the antigen-contact site and act in concert to promote centrosome polarization and docking at the immune synapse [Reversat et al., 2015, Yuseff et al., 2011] (**Figure 22**).

Thus, B cell polarization in response to BCR engagement with immobilized antigens emerges as pivotal in the initiation of B cell responses and is required for the efficient extraction and presentation of surface-tethered antigens. How is precisely regulated centrosome polarization in B cells upon surface-tethered antigen stimulation remained an open question and represents the main goal of my work.

4. Cell polarity and lymphocyte functions

As mentioned above, the establishment of cell polarity often relies on the repositioning of the centrosome at a specific location within cells. This in turn imposes the reorganization of both the actin and microtubule cytoskeleton, thus defining new routes within polarized cells that support directed trafficking events. Such a feature is used by all polarized cells in order to maintain their polarized phenotype and/or achieve their specific effector functions.

In lymphocytes, centrosome re-orientation to one cell pole was shown to be required for cell migration [Schmoranzer et al., 2009], asymmetric division [Barnett et al., 2012, Thaunat et al., 2012, Chang et al., 2007] and immune synapse formation [Stinchcombe and Griffiths, 2014]. While Cdc42, Par3 and aPKC-ζ localize at their leading edge, Scribble and Dlg1, two other well-described polarity proteins, accumulate at the rear of migrating T cells when searching for their cognate peptide [Ludford-Menting et al., 2005]. It has been shown that T cell migration in response to a chemokine gradient leads to Cdc42 activation at the cell front, hence promoting local actin remodeling that support directed cell migration (reviewed in [Rougerie and Delon, 2012]). In addition, aPKC-ζ and Par6 have also been described to play a crucial role in the polarization of T cells in response to chemokine stimulation [Real et al., 2007].

The formation of the immune synapse between T cells and antigen-presenting cells represents another key polarization event regulating T cell functions. The immune synapse refers to the zone of tight interactions that forms once a T cell encounters its cognate antigen loaded on MHC molecules at the surface of APCs [Grakoui et al., 1999]. It is viewed as a

signaling platform where both exocytotic and endocytotic events needed for lymphocytes to perform their specific effector functions, take place [Harwood and Batista, 2011].

The engagement of the T cell receptor (TCR) with such peptide-MHC complexes triggers the reorganization of the actin cytoskeleton leading to the spreading of the T cell onto the APC. This is followed by the rapid repositioning of the centrosome towards the newly establish immune synapse where the polarity protein Par3 accumulates [Ludford-Menting et al., 2005]. Of note, both microtubules and actin structures have been shown to regulate centrosome polarization. Indeed, inhibition of Dynein activity impairs centrosome translocation to the synapse [Combs et al., 2006] and Formin-dependent actin nucleation is required for its proper polarization [Gomez et al., 2007]. In $CD4^+$ T cells, centrosome polarization has been described to rely on the polarity protein aPKC and regulates cytokine secretion [Bertrand et al., 2010, Tourret et al., 2010]. Similarly, in $CD8^+$ T cells, centrosome polarization and docking at the immune synapse allows sustained TCR signaling [Martin-Cofreces et al., 2008] and regulates the local release of cytotoxic granules [Stinchcombe et al., 2006, Stinchcombe and Griffiths, 2007, Angus and Griffiths, 2013].

Thus cell polarization in response to antigenic stimulation emerges as a pivotal feature regulating the effector functions of lymphocytes and thus impacting on the outcome of immune responses. Many features in the mechanisms underlying T and B lymphocyte polarization are similar. However, some cell-specific particularities deserve to be highlighted and are mentioned in the Discussion of this manuscript.

Since the 2000's, the concept that B cells encounter their cognate antigen in an immobilized form has emerged and is now well accepted. Therefore, the lab and others have focused their work in understanding the key steps leading to B cell activation by such cell-surface tethered antigens. Whereas others have been particularly interested in the formation of the B cell synapse as well as in BCR dynamics and its signaling, the lab has focused its studies in understanding the fundamental cell biological events enabling B cells to extract, process and present cell surface-tethered antigens.

Before my arrival, my colleagues have found that upon BCR engagement with immobilized antigens, B cells rapidly repositioned their centrosome towards the immune synapse. Centrosome repositioning was shown to be required for the proper recruitment and local secretion of lysosomes within the synaptic cleft providing the adequate environment (pH, presence of hydrolases and MHC-II molecules) to B cells to efficiently extract, process and present antigens to primed $CD4^+$ T cells. They have shown that B cell polarization relies on the coordinated action of the conserved polarity axis Cdc42/aPKC-ζ/Par3 and the microtubule-dependent motor Dynein, which acts at the immune synapse as a polarity cue defining the axis of polarity. However, not much was known about the basic molecular mechanisms regulating centrosome polarization and thus this aspect of centrosome repositioning remained to be fully elucidated. In addition, the increasing pieces of data suggesting that tissue microenvironment might regulate various steps of B cell differentiation, activation and functions prompted us to investigate whether such cues would modulate the ability of B cells to polarize in response to immobilized antigen stimulation.

Therefore, the main goals of my work were (1) to identify and decipher new molecular mechanisms regulating B cell polarization with a special emphasis given to mechanisms controlling centrosome repositioning and (2) to study whether extracellular Galectin-8 modulates B cell polarization and activation upon BCR engagement with immobilized antigens.

RESULTS

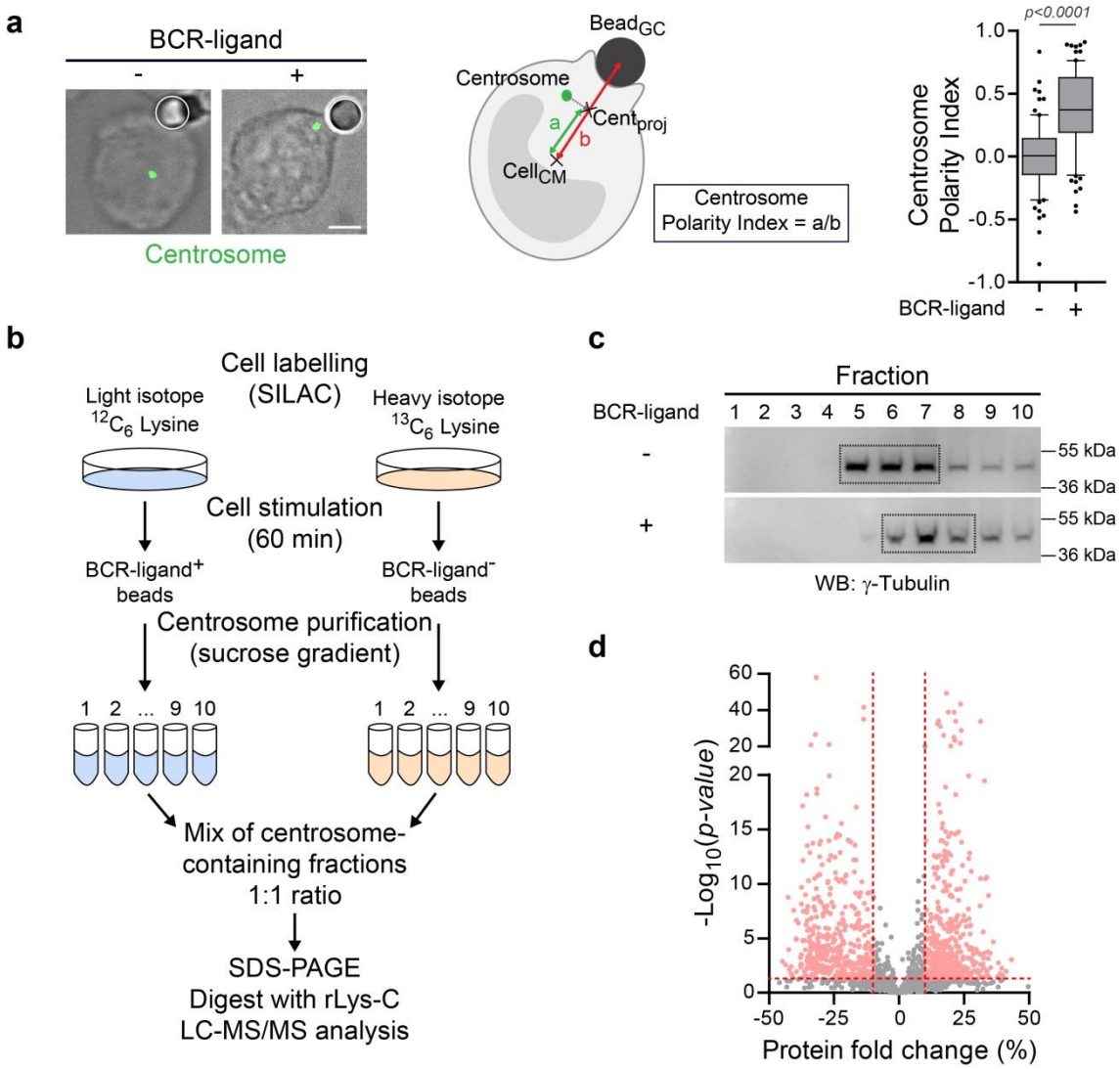

Figure 23. B cell stimulation modifies the centrosome proteome. (**a**) **Left.** Representative images of non-polarized (BCR-ligand$^-$) and polarized (BCR-ligand$^+$) B cells. B cells were incubated for 60 min with beads coated with either BCR ligands or with proteins that do not engage the BCR, fixed and the centrosome was stained (γ-Tubulin). White circles indicate bead position. Scale bar, 3 µm. **Middle.** Schematics depicting centrosome polarity index measurement. **Right.** Quantification of centrosome polarity index. Data are pooled from 3 independent experiments with *n*=80 and 85 cells for BCR-ligand$^-$ and BCR-ligand$^+$, respectively. Unpaired Student's t-test was used to determine statistical significance. (**b**) SILAC-based mass spectrometry workflow used to identify proteins differentially associated with the centrosome of B cells stimulated with either BCR-ligand$^-$ or BCR-ligand$^+$ beads. (**c**) Western blots highlighting centrosome-containing fractions after centrosome isolation on discontinuous sucrose gradient. Immunoblots are representative of 3 independent experiments. (**d**) Volcano plot showing the 835 proteins considered for further analysis (light red) among the total of the 1600 quantified proteins. Horizontal red line represents the threshold for statistical significance (*adjusted p-value*≤0.05). Vertical red lines represent the biological threshold used to select proteins (-10% and +10% of protein fold change).

B lymphocyte polarization and especially centrosome repositioning towards the immune synapse is a key step in the initiation of B cell activation. However, little is known regarding the molecular mechanisms regulating this process. We therefore hypothesized that variations in the composition of centrosome-associated proteins between polarized and non-polarized B cells might reveal valuable candidates to be involved in this process. Centrosome polarization in these cells can be triggered by engaging their BCR with surface-tethered ligands (anti-BCR antibodies, BCR-ligand^{+}) coated on latex beads [Yuseff et al., 2011, Reversat et al., 2015], giving access to a simplified model for the calculation of centrosome polarity indexes (**Figure 23a**).

1. Analysis of centrosomal proteome of activated and non-activated B cells

To identify proteins differentially associated with the centrosome of polarized and non-polarized B cells, a stable isotope labelling by amino acids in cell culture- (SILAC-) based quantitative proteomic approach was developed [Hoedt et al., 2014]. For this, B cells were grown in cultures containing lysine labelled with light or heavy carbon isotopes and incubated for 60 min with BCR-ligand^{+} or with beads coated with a protein that does not engage the BCR (BCR-ligand^{-}), respectively (**Figure 23b**). Cells were lysed, centrosomes were isolated by sequential centrifugations on sucrose gradients and the 3 main γ-Tubulin-containing fractions were pooled for each sample (**Figure 23c**). Resulting pools were mixed 1:1 to be separated by SDS-PAGE followed by reverse-phase liquid chromatography and analyzed by high-resolution mass spectrometry (LC-MS/MS) (**Figure 23b**). This led to the identification of 2743 proteins with a false discovery rate (FDR) of 1%. The relative quantification of the 1600 proteins (among the 2743) for which at least 3 peptides were recovered was then performed by computing peptide SILAC ratios between both conditions. Strikingly, among the 1600 quantified proteins, we found that 835 proteins were differentially associated with the centrosome of activated B cells (absolute fold change ≥10% and adjusted p-value of quantification ≤ 0.05, **Figure 23d, light red**).

We conclude that BCR engagement induces multiple changes in the centrosome proteome providing potential candidates involved in the regulation of centrosome polarization.

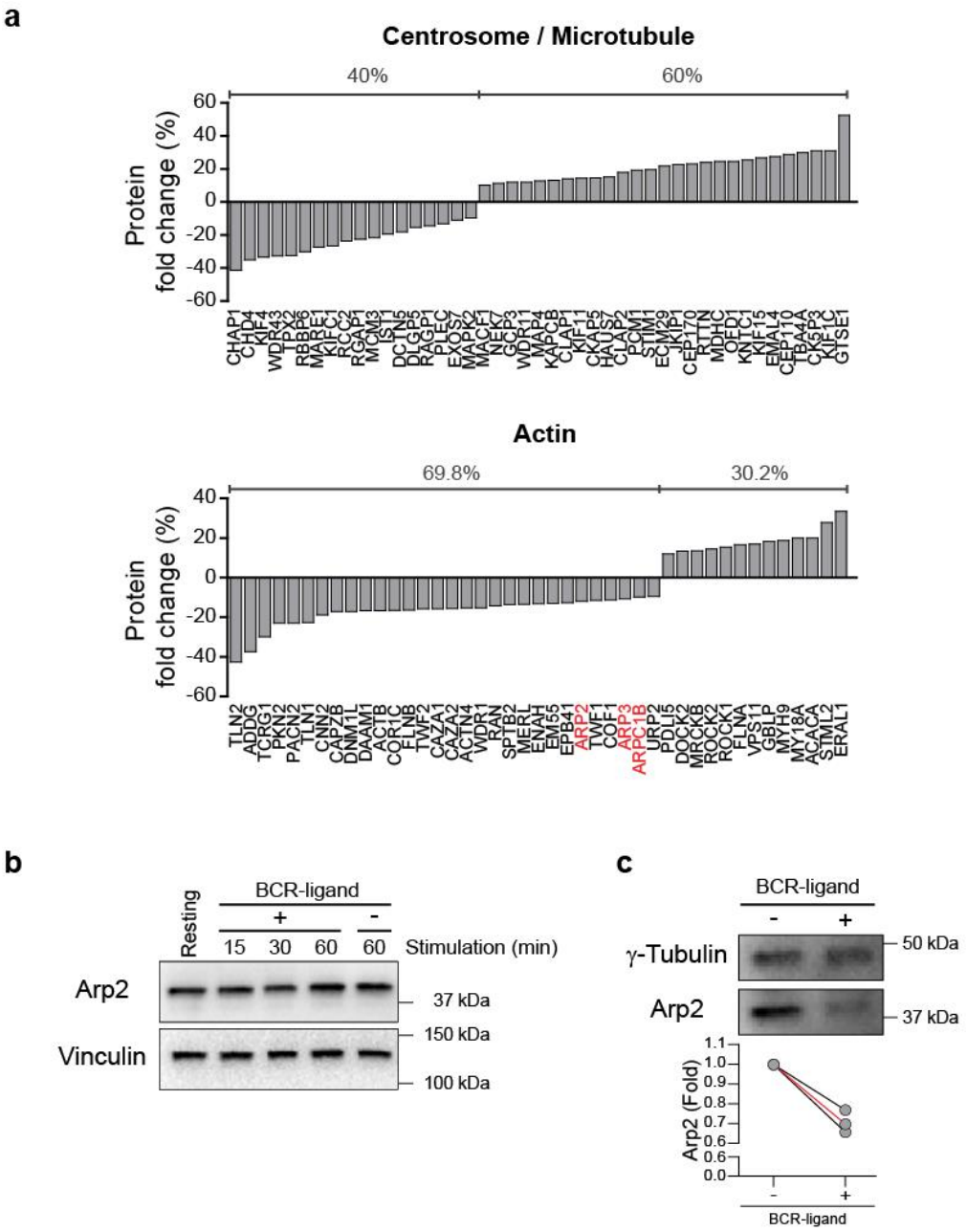

Figure 24. Reduced Arp2/3 subunits in centrosome preparations from activated B cells. (**a**) Protein fold change (%) for each of the 45 proteins belonging to the "Centrosome / Microtubule" sub-group (top) and the 43 belonging to the "Actin" one (bottom). (**b**) The total amount of Arp2 in B cells under resting conditions or stimulated with either BCR-ligand^{-} or BCR-ligand^{+} beads for indicated time was assessed by immunoblot. Vinculin was used as loading control. Western blots shown are representative of 3 independent experiments. (**c**) Centrosomes purified from B cells stimulated with either BCR-ligand^{-} or BCR-ligand^{+} beads for 60 min were assessed by immunoblot for their associated amounts of Arp2. γ-Tubulin was used as loading control. Bottom panel shows the relative quantification of 3 independent experiments. Red line corresponds to the quantification of the blot presented above.

2. Reduced Arp2/3 subunits in centrosome preparations of activated lymphocytes

To identify key networks, Genome Ontology (GO) term enrichment was performed on the 835 proteins differentially associated with the centrosome of activated B cells. As expected, this analysis highlighted components of the microtubule-organizing center (enrichment factor: 1.9, p-value = $3.56x10^{-05}$) and the cytoskeleton (enrichment factor: 1.8, p-value = $2.65x10^{-11}$) as two major groups of proteins enriched in centrosome preparations. More surprisingly, zooming on proteins belonging to the GO Term "Cytoskeleton" showed that while microtubule-related components were either increased or decreased in polarized cells, the majority of actin cytoskeleton components were reduced (69.8%, **Figure 24a**). Noticeably, this particularly applied to 3 subunits of the branched actin nucleating complex Arp2/3 [Rotty et al., 2013] (10% and 12% decrease, **Figure 24a, red**). To confirm the reduced amounts of Arp2/3 at the centrosome of activated lymphocytes, immunoblot analysis of centrosomes purified from non-activated and activated B cells were performed. Whereas no reduction in the total amount of Arp2 was observed in cells between both conditions (**Figure 24b**), we observed an even more pronounced reduction of the Arp2/3 subunit Arp2 in centrosome preparations isolated from activated lymphocytes (**Figure 24c**).

Altogether, these data suggest that B cell activation induces a significant reduction in the pool of centrosomal Arp2/3. Although the presence of this complex at the centrosome has been described in the past [Hubert et al., 2011], whether it regulates centrosome function remains unclear. We therefore focused our analysis on exploring the putative role of Arp2/3 reduction at the centrosome of activated lymphocytes in the polarization of this organelle.

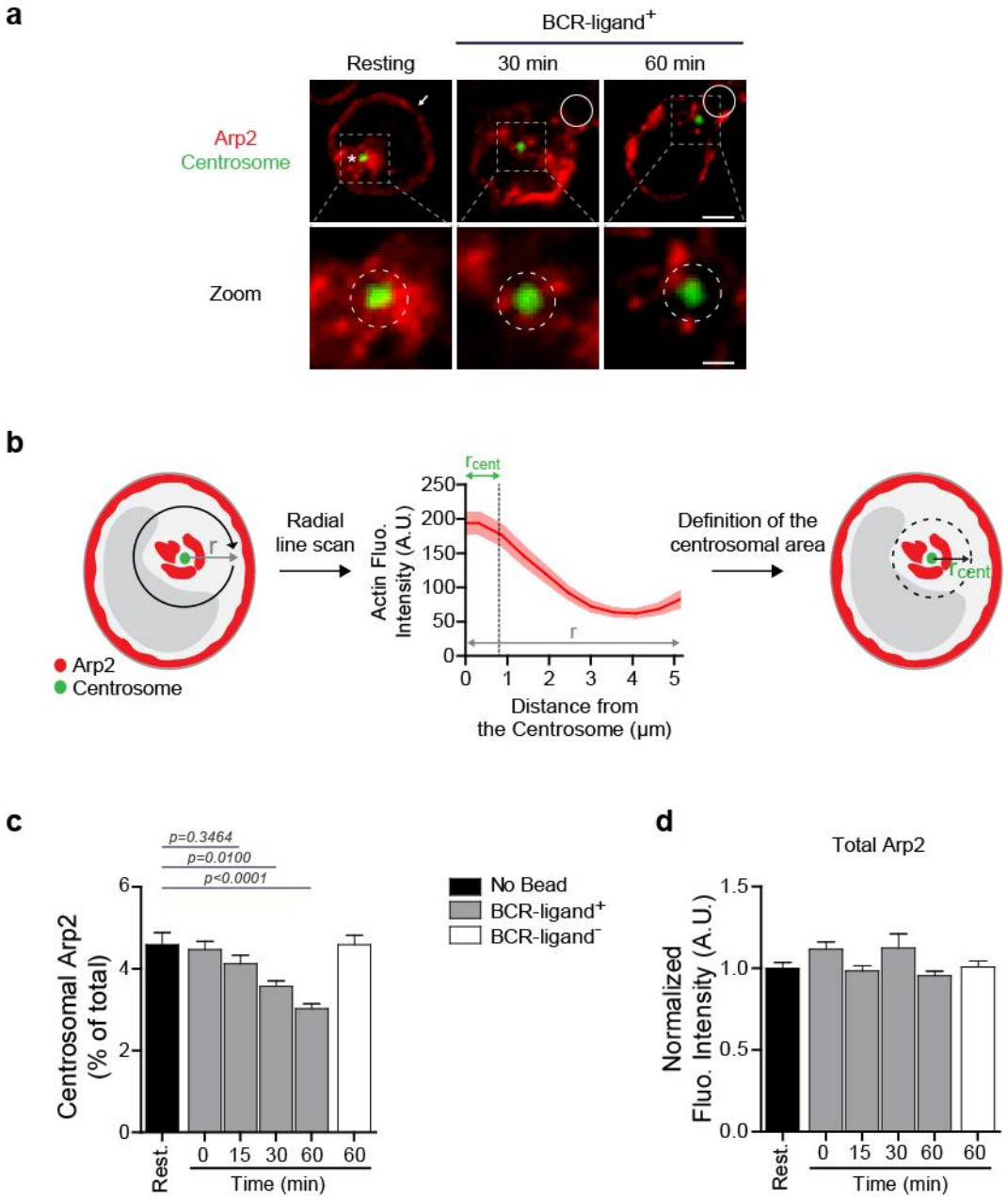

Figure 25. Reduced centrosomal Arp2/3 in activated lymphocytes. (**a**) Representative images of B cells under resting conditions or stimulated with BCR-ligand^{+} beads for indicated time, fixed and co-stained for Arp2 (white arrow: cortical pool; *: centrosomal pool) and the centrosome (α-Tubulin). White circles indicate bead position. Dashed grey squares indicate the centrosomal region magnified below each image. Dashed circles on bottom panel highlight the centrosomal area used for quantification. Scale bar, top: 3 µm; bottom: 1 µm. (**b**) Schematics depicting the pipeline used to quantify centrosome-associated Arp2. (**c**) Quantification of centrosome-associated Arp2 from cells shown in (a). Data are pooled from 3 independent experiments with *n*=67, 62, 64, 72, 61 and 69 cells from left to right. (**d**) Quantification of the total Arp2 fluorescence intensity in B cells under resting conditions or stimulated with either BCR-ligand^{-} or BCR-ligand^{+} beads for indicated time. Data are pooled from 3 independent experiments and were normalized with respect to the mean fluorescence intensity of resting cells in each replicate. *n*=67, 71, 64, 68, 72 and 69 cells from left to right.

3. Lymphocyte activation decreases the amounts of Arp2/3 at the centrosome

We next asked whether reduction of Arp2/3 at the centrosome was equally observed in intact lymphocytes. Immunofluorescence analysis revealed the presence of two pools of Arp2/3 in resting B cells: a cortical pool (**Figure 25a, white arrow**) and a cytosolic pool that surrounded the centrosome (**Figure 25a, white star**).

To accurately quantify this centrosome-associated pool of Arp2/3, we computed the radial distribution of cytoplasmic Arp2 fluorescence intensity from the centrosome of resting lymphocytes and, based on this result, we defined a "centrosomal area" (**Figure 25b**). The amount of Arp2/3 in this centrosomal area was then quantified at different time points after BCR engagement. In agreement with our proteomic and immunoblot data, we found that this centrosome-associated pool of Arp2/3 gradually decreased in time upon lymphocyte stimulation with BCR-ligand^{+} beads (**Figure 25a, c**). Of note, no reduction in the total amount of Arp2/3 was found (**Figure 25d**).

We conclude from these data that the amount of Arp2/3 associated with the centrosome is decreased upon BCR engagement.

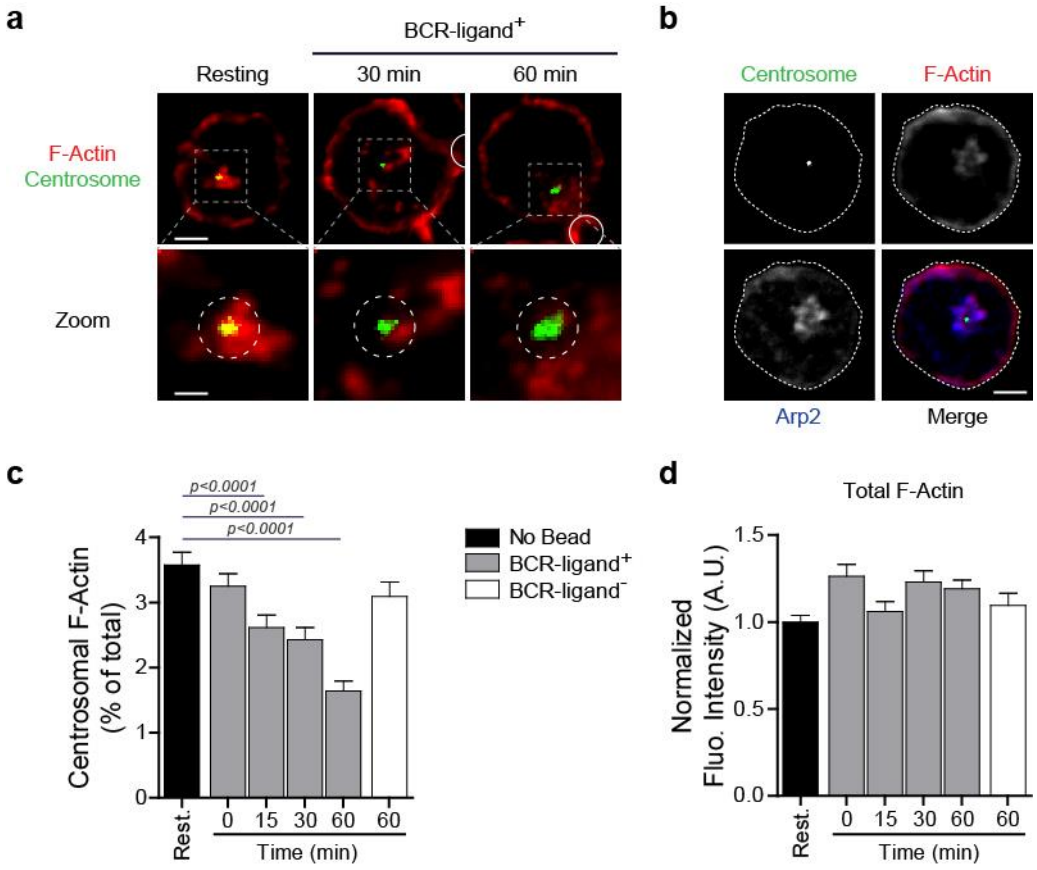

Figure 26. Reduced centrosomal F-Actin in activated lymphocytes. (**a**) Representative images of B cells under resting conditions or stimulated with BCR-ligand$^+$ beads for indicated time, fixed and co-stained for F-actin (Phalloidin) and the centrosome (α-Tubulin). White circles indicate bead position. Dashed grey squares indicate the centrosomal region magnified below each image. Dashed circles on bottom panel highlight the centrosomal area used for quantification. Scale bar, top: 3 µm; bottom: 1 µm. (**b**) Representative images of resting B cells expressing the F-actin probe Utrophin-RFP, fixed and stained for Arp2 and an anti-RFP (Utrophin). The merge image shows the co-localization of F-actin (Utrophin) and Arp2 at the centrosome. Images are representative of 2 independent experiments. Scale bar, 3 µm. (**c**) Quantification of centrosome-associated F-actin from cells shown in (a). Data are pooled from 3 independent experiments with *n*=54, 63, 64, 62, 59 and 64 cells from left to right. (**d**) Quantification of the total F-actin fluorescence intensity in B cells under resting conditions or stimulated with either BCR-ligand$^-$ or BCR-ligand$^+$ beads for indicated time. Data are pooled from 3 independent experiments and were normalized with respect to the mean fluorescence intensity of resting cells in each replicate. *n*=60, 59, 64, 66, 59 and 64 cells from left to right.

4. Lymphocyte activation decreases the amounts of F-actin at the centrosome

Arp2/3 being a well-characterized complex involved in the nucleation of branched actin networks, we asked whether its decreased association with the centrosome of activated B cells reflected different levels of F-actin at the centrosome of these cells.

In resting B lymphocytes, we observed the presence of a pool of F-actin in close vicinity of the centrosome, which co-localized with Arp2/3 (**Figure 26a, b**). In contrast, in lymphocytes incubated for 30 min with BCR-ligand^{+} beads, F-actin was observed as patches dispersed in the cytosol rather than gathered around the centrosome (**Figure 26a**). After 60 min of stimulation, the centrosome polarized to the cell-bead interface and was therefore found in proximity of the cortical F-actin pool (**Figure 26a**). Nonetheless, the pool of centrosome-associated F-actin, whose quantification was performed as for Arp2/3 fluorescence intensity, was decreased in these cells (**Figure 26c**). Of note, no reduction in the total amount of F-actin in cells was observed (**Figure 26d**).

Altogether, these results show that resting B cells display a pool of Arp2/3 and F-actin at their centrosome that decreases upon BCR engagement with immobilized antigens while this organelle polarizes to the immune synapse.

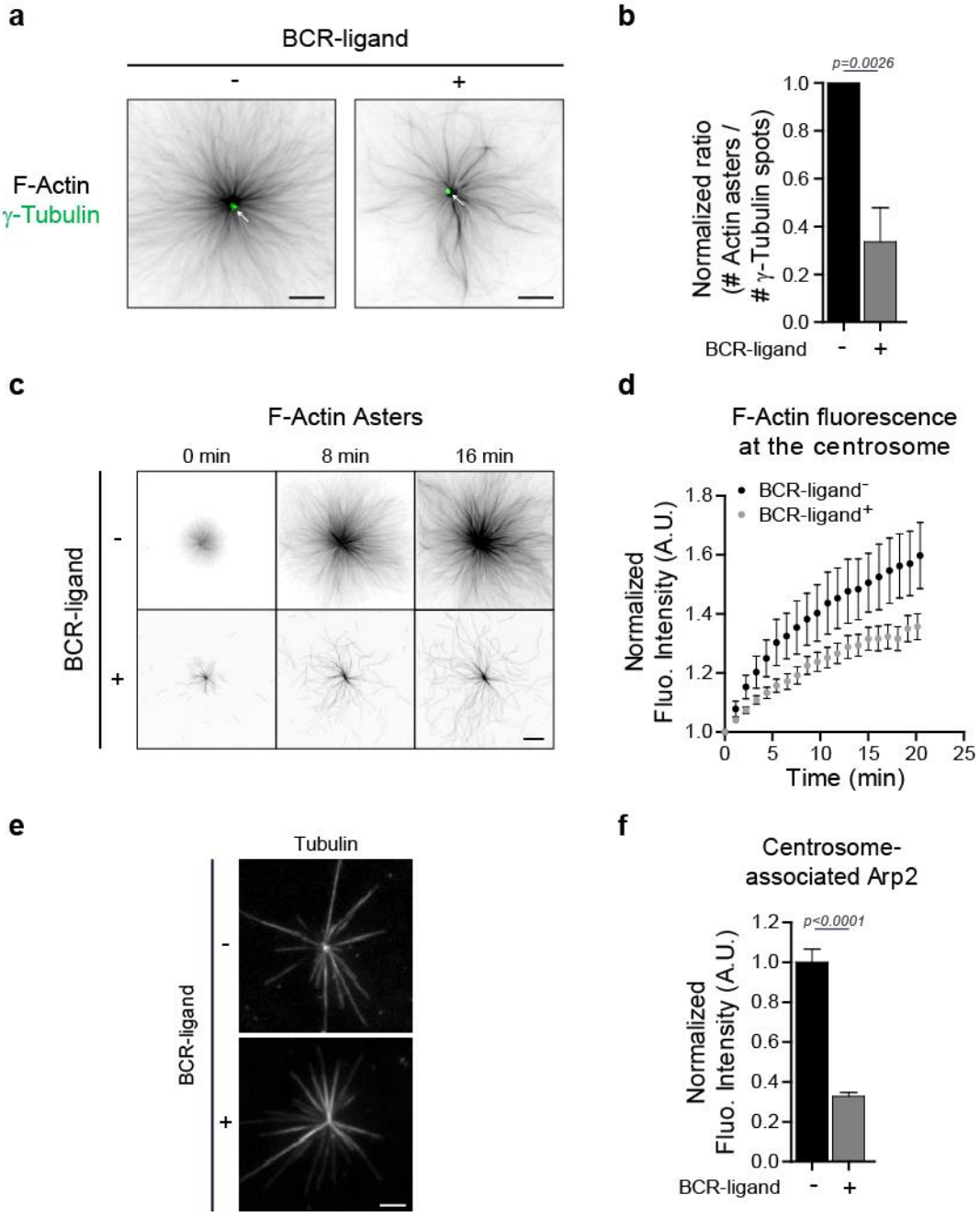

Figure 27. Reduced F-actin nucleation by centrosomes of activated B lymphocytes. (**a**) Representative images of actin asters nucleated from isolated centrosomes (white arrow). Scale bar, 8 µm. (**b**) Actin nucleation efficiency was calculated as the ratio of the number of actin asters divided by the number of γ-Tubulin spots. >200 actin asters and >450 γ-Tubulin spots per condition pooled from 4 independent experiments. (**c**) Sequential images of F-actin assembly by centrosomes isolated from B cells stimulated with indicated beads. Scale bar, 5 µm. (**d**) Quantification of F-actin nucleation activity. (*n*=14 and 12 actin asters per condition. Data are representative of 4 independent experiments). (**e**) Centrosomes isolated from B cells stimulated for 60 min with indicated beads were assessed for their ability to nucleate microtubules *in vitro*. Scale bar, 16 µm. (**f**) Quantification of Arp2 fluorescence intensity associated with purified centrosomes. *n*=100 and 190 centrosomes per condition pooled from 2 independent experiments.

5. Lymphocyte activation decreases the ability of centrosomes to nucleate F-actin

It has been recently shown that centrosomes possess an intrinsic actin-nucleating activity in various cell types including T lymphocytes [Farina et al., 2016]. We therefore investigated whether the distinct amounts of centrosome-associated F-actin observed in resting and BCR-stimulated B lymphocytes reflected different actin nucleation capacities.

For this, centrosomes purified from resting and activated B lymphocytes were compared for their ability to nucleate actin filaments *in vitro*. Strikingly, we observed that both centrosome preparations assembled actin asters from γ-Tubulin spots (**Figure 27a**), indicating that B lymphocyte centrosomes also possess an intrinsic actin nucleation capacity.

In agreement with our hypothesis, actin nucleation by centrosomes purified from BCR-stimulated cells was strongly diminished as compared to centrosomes purified from resting lymphocytes. Indeed, both the number of actin asters and the actin fluorescence intensity at the aster center were significantly decreased when using centrosomes from activated cells (**Figure 27a-d**). Importantly, centrosome integrity was not affected in preparations from activated lymphocytes as shown by their ability to nucleate microtubules (**Figure 27e**). Consistent with these results and with our proteomic and immunofluorescence data, the amount of Arp2/3 associated with centrosomes purified from BCR-stimulated lymphocytes was also found to be strongly decreased as compared to centrosomes of resting B cells (**Figure 27f**).

We conclude from these data that centrosomes possess an intrinsic capacity to nucleate F-actin that is down-regulated upon BCR engagement with immobilized antigens.

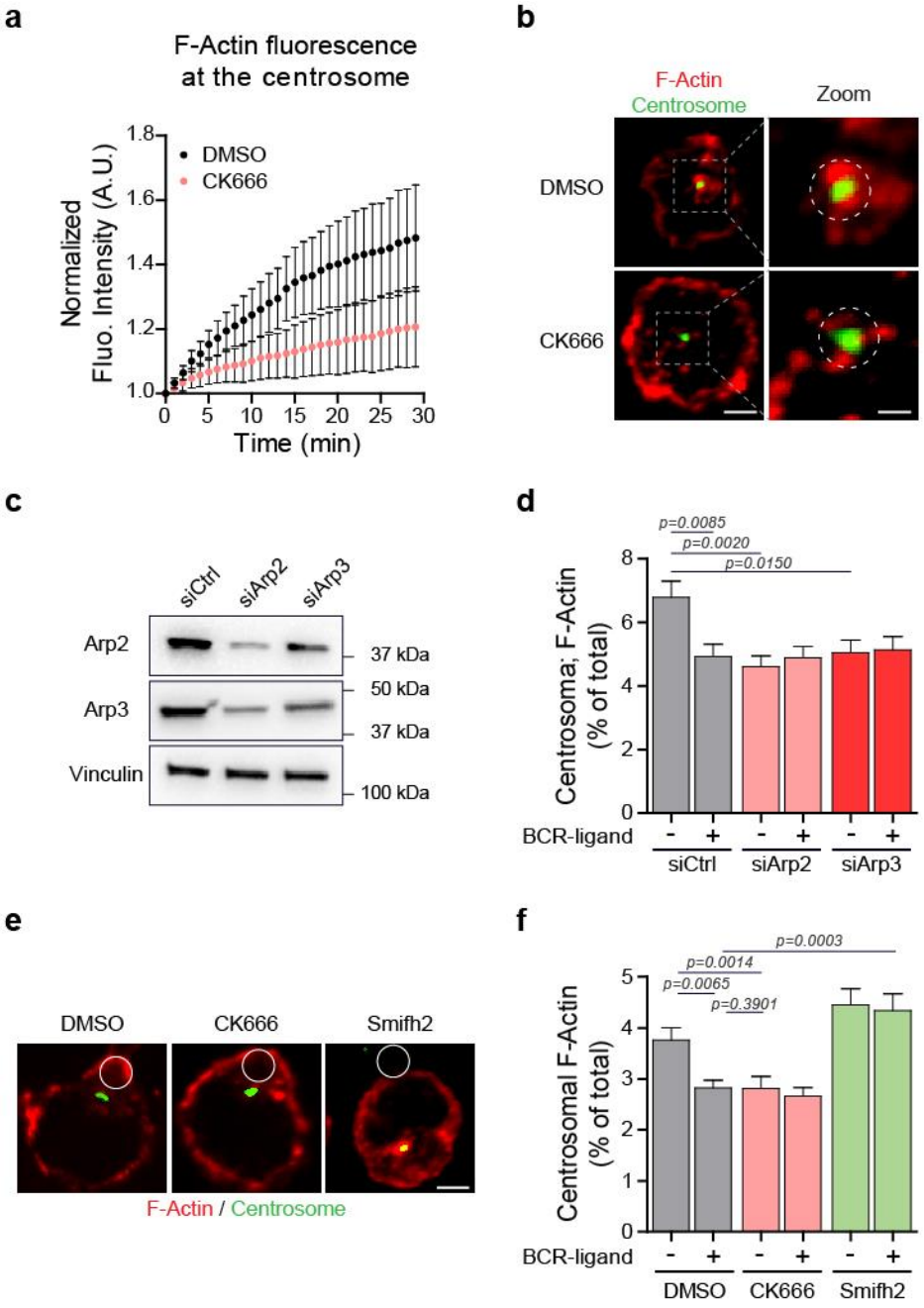

Figure 28. Centrosomes nucleate F-Actin in an Arp2/3-dependent manner. (**a**) Quantification of actin nucleation activity of centrosomes purified from resting lymphocytes in presence of CK666 or DMSO. *n*=12 and 22 actin asters, respectively from 2 independent experiments. (**b**) Representative images of resting B cells treated with DMSO or CK666 for 60 min, fixed and co-stained for F-actin (Phalloidin) and the centrosome (α-Tubulin). Dashed grey squares indicate the region magnified on the right panel. Dashed circles on the right panel highlight the centrosomal area used for quantification. Scale bar, left: 3 µm; right: 1 µm. (**c**) Western blot analysis of the efficiency of Arp2 and Arp3 silencing. Vinculin was used as loading control. Immunoblot presented is representative of 2 independent experiments. (**d**) Quantification of centrosome-associated F-actin in control, Arp2- and Arp3-silenced B cells stimulated with indicated beads for 60 min. Data are pooled from 2 independent experiments with *n*=44, 45, 45, 46, 46 and 42 cells from left to right. (**e**) Representative images of B cells pre-treated with DMSO, CK666 or Smifh2 for 30 min prior to be stimulated with BCR-ligand^{+} beads for 60 min, fixed and stained for F-actin (Phalloidin) and the centrosome (α-Tubulin). White circles indicate bead position. Scale bar, 3 µm. (**f**) Quantification of centrosome-associated F-actin from cells shown in (e). Data are pooled from 3 independent experiments with *n*=82, 81, 68, 62, 76 and 69 cells from left to right.

6. Centrosomes nucleate F-actin in an Arp2/3-dependent manner

The involvement of the Arp2/3 complex in F-actin nucleation by centrosomes purified from resting lymphocytes was confirmed by using the CK666 Arp2/3 inhibitor [Nolen et al., 2009], which significantly reduced F-actin assembly (**Figure 28a**).

On the same line, treatment of resting B cells with CK666 decreased the amount of centrosome-associated F-actin to the levels observed in BCR-stimulated lymphocytes (**Figure 28b**). Equivalent results were obtained when silencing Arp2/3 with two different siRNA (**Figure 28c, d**). Smifh2-mediated inhibition of Formin proteins, the other family of actin nucleators, did not decrease F-actin nucleation at the centrosome, indicating that it most likely did not play a direct role in this process. Interestingly, Formin inhibition even increased the amount of F-actin at the centrosome (**Figure 28e, f**), what might result from the recently reported competition between Arp2/3 and Formins [Burke et al., 2014].

We conclude that lymphocyte centrosomes nucleate F-actin in an Arp2/3-dependent fashion and that this property of centrosomes is down regulated upon lymphocyte activation as a result of Arp2/3 local depletion.

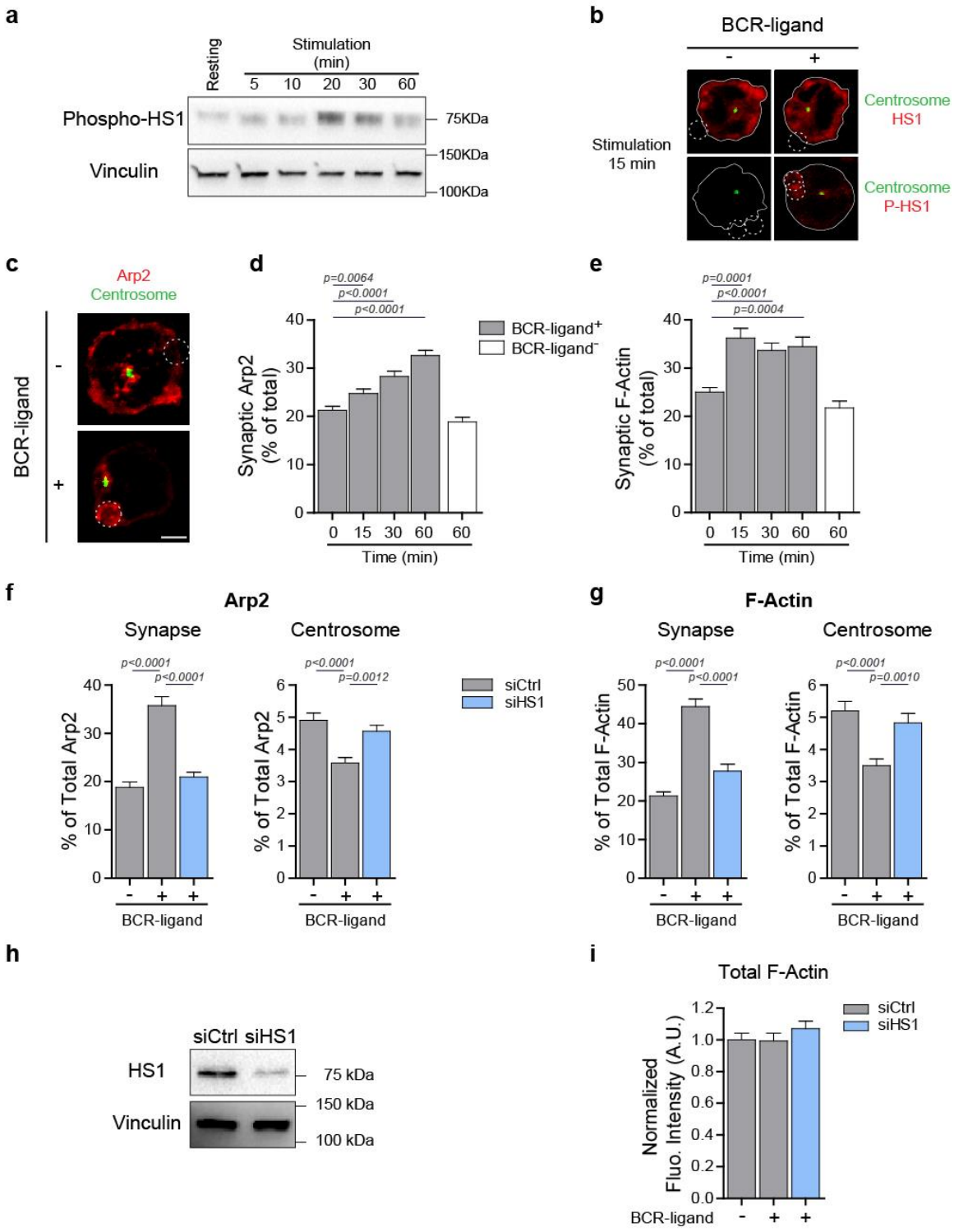

Figure 29. Depletion of Arp2/3 from the centrosome results from its HS1-dependent recruitment at the immune synapse. (**a**) Western blot showing the phosphorylation of HS1 during the course of B cell stimulation. Representative of 2 independent experiments. (**b**) Representative images of B cells stimulated with indicated beads for 15 min, fixed and co-stained for total HS1 (top) or phosphorylated HS1 (bottom) and the centrosome (α-Tubulin). Dashed white circles indicate bead position. Scale bar, 3 µm. Images are representative of 2 independent experiments. (**c**) Representative images of B cells stimulated with indicated beads for 60 min, fixed and co-stained for Arp2 and the centrosome (α-Tubulin). Dashed white circles indicate bead position. Scale bar, 3 µm. Representative of 3 independent experiments. (**d**, **e**) Quantification of synapse-associated Arp2 (**d**) and F-actin (**e**). (**d**) *n*=71, 64, 68, 72 and 69 cells and (**e**) *n*=55, 60, 66, 59 and 57 cells from left to right, pooled from 3

7. Depletion of centrosome-associated Arp2/3 results from its HS1-dependent recruitment to the immune synapse

We next searched for the molecular mechanisms responsible for this partial depletion of Arp2/3 from the centrosome of BCR-stimulated lymphocytes. It was shown that the Cortactin homolog Hematopoietic Lineage Cell-Specific Protein (HS1), which is predominantly expressed in hematopoietic cells [Gomez et al., 2006], recruits Arp2/3 to the BCR signalosome upon antigenic stimulation [Hao et al., 2004]. Consistently, we observed that BCR engagement with BCR-ligand^{+} beads induced HS1 phosphorylation and accumulation at the cell-bead interface (**Figure 29a, b**).

We therefore hypothesized that phospho-HS1-dependent recruitment of Arp2/3 at the immune synapse might lead to its partial depletion from the centrosome and thereby to a local decrease in F-actin nucleation. Consistent with this hypothesis, we found that the gradual decrease in the pool of centrosome-associated Arp2/3 and F-actin was concomitant to the accumulation of both proteins at the cell-bead interface (**Figure 29c-e**). This was also observed for F-actin in time-lapse imaging experiments: upon BCR stimulation, F-actin gradually decreased at the centrosome but progressively increased at the synapse (not shown). Noticeably, both the decrease of Arp2/3 and F-actin at the centrosome and their increase at the synapse were severely impaired when silencing HS1 (**Figure 29f-h**). No reduction in the total amount of F-actin was observed between control and HS1-silenced lymphocytes (**Figure 29i**).

Hence, HS1-dependent recruitment of Arp2/3 at the cell-bead interface is associated with its partial depletion from the centrosome, thus decreasing the actin nucleation capacity of this organelle.

---

independent experiments. (**f**, **g**) Quantification of Arp2 (**f**) and F-actin (**g**) associated with the synapse (left) and the centrosome (right) in control and HS1-silenced B cells stimulated for 60 min with indicated beads. Data are pooled from 2 (**f**) and 3 (**g**) independent experiments with (**f**) Synapse: *n*=51, 46 and 53 cells; Centrosome: *n*=51, 52 and 47 cells and (**g**) Synapse: *n*=72, 74 and 66 cells; Centrosome: *n*=73, 72 and 67 cells from left to right. (**h**) Immunoblot analysis of the efficiency of HS1 silencing. Vinculin was used as loading control. The blot presented is representative of at least 4 independent experiments. (**i**) Quantification of the total F-actin fluorescence intensity in control and HS1-silenced B cells stimulated with indicated beads for 60 min. Pooled from 3 independent experiments and normalized with respect to the mean fluorescence intensity of control cells stimulated with BCR-ligand^{-} beads in each replicate. *n*=72, 75 and 66 cells from left to right.

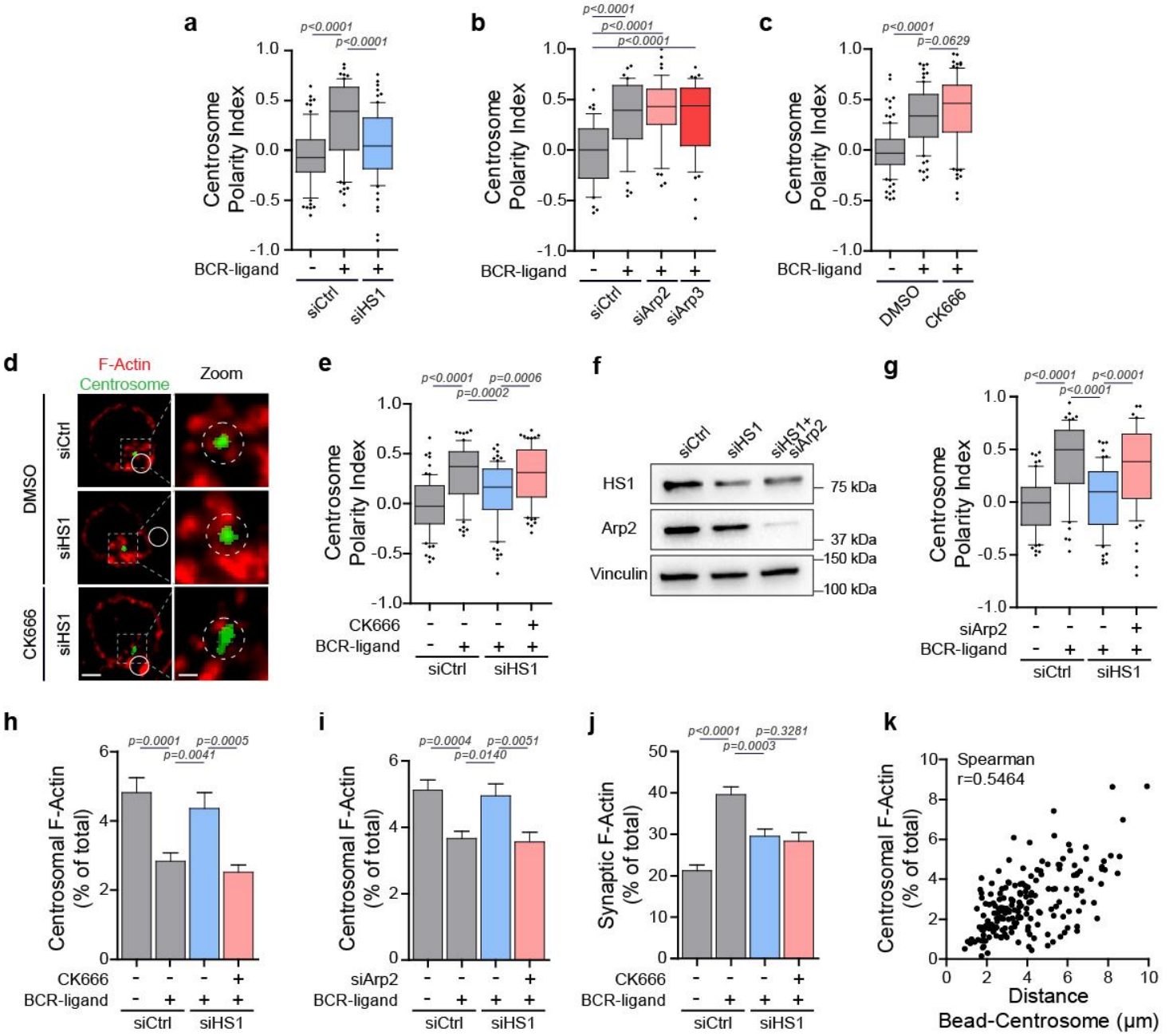

Figure 30. Centrosomal Arp2/3 and F-actin impair centrosome polarization. (**a**-**c**) Quantification of centrosome polarity index of control and HS1-silenced (**a**), control, Arp2- and Arp3-silenced (**b**) or DMSO and CK666-treated (**c**) B cells stimulated with indicated beads for 60 min. (**a**) *n*=77, 71 and 75 cells; (**b**) *n*=43, 46, 47 and 43 cells and (**c**) *n*=103, 80 and 87 cells from left to right, pooled from 2 (**b**) and 3 (**a**, **c**) independent experiments. (**d**) Representative images of control and HS1-silenced B cells treated with DMSO or CK666, stimulated with BCR-ligand^{+} beads for 60 min, fixed and co-stained for F-actin (Phalloidin) and the centrosome (α-Tubulin). Scale bar, left: 3 µm; right: 0.9 µm. (**e**) Quantification of centrosome polarity index of control and HS1-silenced B cells treated or not with CK666. *n*=77, 69, 72 and 75 cells from left to right, pooled from 3 independent experiments. (**f**) Immunoblot analysis of the efficiency of HS1 and HS1 plus Arp2 silencing. Vinculin was used as loading control. Representative of 3 independent experiments. (**g**) Quantification of centrosome polarity index of control, HS1- and HS1 plus Arp2-silenced B cells stimulated for 60 min with indicated beads. Data are pooled from 3 independent experiments with *n*=64 cells per condition. (**h**, **i**) Quantification of centrosome-associated F-actin from (**h**) cells shown in (d) and (**i**) control, HS1- and HS1 plus Arp2-silenced B cells stimulated for 60 min with indicated beads. (**h**) *n*=41, 47, 38 and 45 cells and (**i**) *n*=58, 65, 65 and 63 cells from left to right, pooled from 2 and 3 independent experiments, respectively. (**j**) Quantification of synapse-associated F-actin from cells shown in (d). *n*=41, 47, 38 and 45 cells from left to right, pooled from 2 independent experiments. (**k**) Correlation analysis of centrosome-associated F-actin and the bead-centrosome distance (*n*=185 cells). Spearman correlation test, P<0,0001.

8. Regulation of centrosome polarization by centrosomal F-actin nucleation

8.a. Maintaining high levels of centrosomal F-actin prevents centrosome polarization

We next used HS1-silenced lymphocytes that maintained high levels of centrosomal Arp2/3 and F-actin upon BCR stimulation to investigate whether Arp2/3 and F-actin depletion from the centrosome regulates the ability of this organelle to polarize to the immune synapse.

We found that most HS1 knock down B cells did not reposition their centrosome at the cell-bead interface (**Figure 30a**). However, because these cells displayed not only more Arp2/3 and F-actin at the centrosome but also less Arp2/3 and F-actin at the synapse as compared to control cells, we could not exclude that impaired centrosome polarization resulted from decreased Arp2/3 and F-actin at the synapse. To address this question, we investigated the effect of Arp2/3 inhibition on centrosome polarity. We found that both Arp2/3 silencing and inhibition with CK666 had no impact on centrosome polarization to the synapse (**Figure 30b, c**) and, even more importantly, rescued the non-polarized phenotype of HS1-silenced activated lymphocytes (**Figure 30d-g**). Of note, Arp2/3 inhibition in these cells reduced the centrosomal pool of F-actin (**Figure 30h-i**) but had no significant effect on the amounts of synapse-associated F-actin (**Figure 30j**).

These results suggest that the centrosomal pool of Arp2/3 and F-actin prevents centrosome polarization while its synaptic counterpart is not required for this process. In support of this conclusion, a significant correlation was found between the levels of centrosomal F-actin and the distance between this organelle and the bead geometrical center (**Figure 30k**).

Hence, HS1-dependent recruitment of Arp2/3 at the synapse partially depletes this complex from the centrosome, leading to a local reduction in F-actin that is needed for centrosome polarization to the synapse.

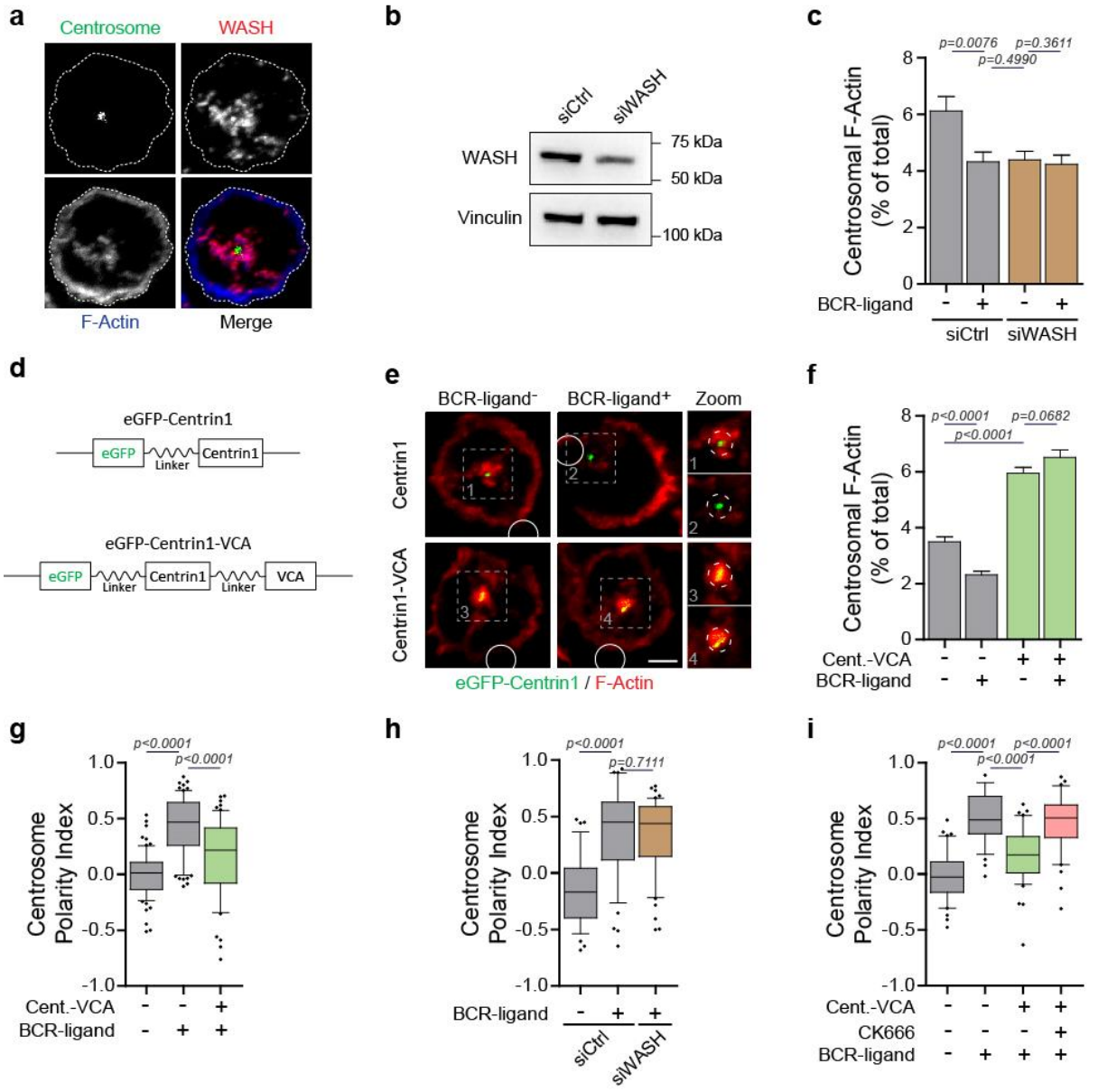

Figure 31. WASH promotes F-actin nucleation at the centrosome. (**a**) Representative images of resting B cells stained for WASH, F-actin (Phalloidin) and the centrosome (α-Tubulin). Images are representative of 2 independent experiments. (**b**) Immunoblot analysis of the efficiency of WASH silencing. Vinculin was used as loading control. Representative of 2 independent experiments. (**c**) Quantification of centrosomal F-actin of control and WASH-silenced B cells, stimulated with indicated beads for 60 min. Data are pooled from 2 independent experiments with *n*=36, 46, 41 and 50 cells from left to right. (**d**) Schematics depicting the construct used to over-activate the Arp2/3 complex at the centrosome (bottom). (**e**) Representative images of control and eGFP-Centrin1-VCA-expressing B cells, stimulated with indicated beads for 60 min, fixed and co-stained for F-actin (Phalloidin) and the centrosome (GFP). White circles indicate bead position. Dashed grey squares indicate the region magnified on the right. Dashed circles on magnifications highlight the centrosomal area used for quantification. Scale bar, 3 µm. (**f**, **g**) Quantification of centrosomal F-actin (**f**) and centrosome polarity index (**g**) of cells shown in (e). (**f**) *n*=74, 66, 68 and 64 cells and (**g**) *n*=75, 71 and 64 cells from left to right, pooled from 3 independent experiments. (**h**) Quantification of centrosome polarity index of control and WASH-silenced B cells, stimulated with indicated beads for 60 min. Data are pooled from 2 independent experiments with *n*=37, 46 and 50 cells from left to right. (**i**) Quantification of centrosome polarity index of control and eGFP-Centrin1-VCA-expressing B cells, treated or not with CK666 and stimulated with indicated beads for 60 min. *n*=41, 39, 42 and 42 cells from left to right, pooled from 2 independent experiments.

8.b. WASH-dependent F-actin nucleation at the centrosome prevents its polarization

WASH, an actin nucleation promoting factor (NPF) that activates Arp2/3 through its VCA (Verprolin homology or WH2-Connector-Acidic) domain, was shown to associate with the centrosome [Monfregola et al., 2010]. We thus asked whether WASH was responsible for Arp2/3 activation at the centrosome of B cells.

In resting lymphocytes, we observed WASH as discrete punctuated structures mainly gathered around the centrosome (**Figure 31a**). In addition, WASH silencing in resting cells decreased the amount of F-actin at the centrosome to the levels observed in activated cells (**Figure 31b, c**), indicating that it participates to local Arp2/3 activation.

We next reasoned that targeting the WASH VCA domain to the centrosome would result in the exacerbation of local Arp2/3 activity and F-actin nucleation, giving us the opportunity to directly assess whether actin nucleation by Arp2/3 at the centrosome prevents the polarization of this organelle to the immune synapse. We therefore developed a chimeric protein composed of the VCA domain of WASH fused to the centrosomal protein Centrin1 tagged with an enhanced Green Fluorescent Protein (eGFP) (**Figure 31d**). Accordingly, expression of this eGFP-Centrin1-VCA fusion protein strongly increased the amount of F-actin at the centrosome (**Figure 31e, f**). More importantly, expression of the eGFP-Centrin1-VCA fusion protein compromised the ability of the centrosome to polarize to the immune synapse (**Figure 31g**). As observed for Arp2/3 inhibition or silencing, WASH silencing had no impact on centrosome polarity (**Figure 31h**). Consistently, centrosome polarization in eGFP-Centrin1-VCA-expressing cells was rescued by inhibiting Arp2/3 activity (**Figure 31i**).

Together these data strongly support a model where F-actin nucleation at the centrosome prevents its translocation to the synapse and must therefore be down regulated upon lymphocyte activation.

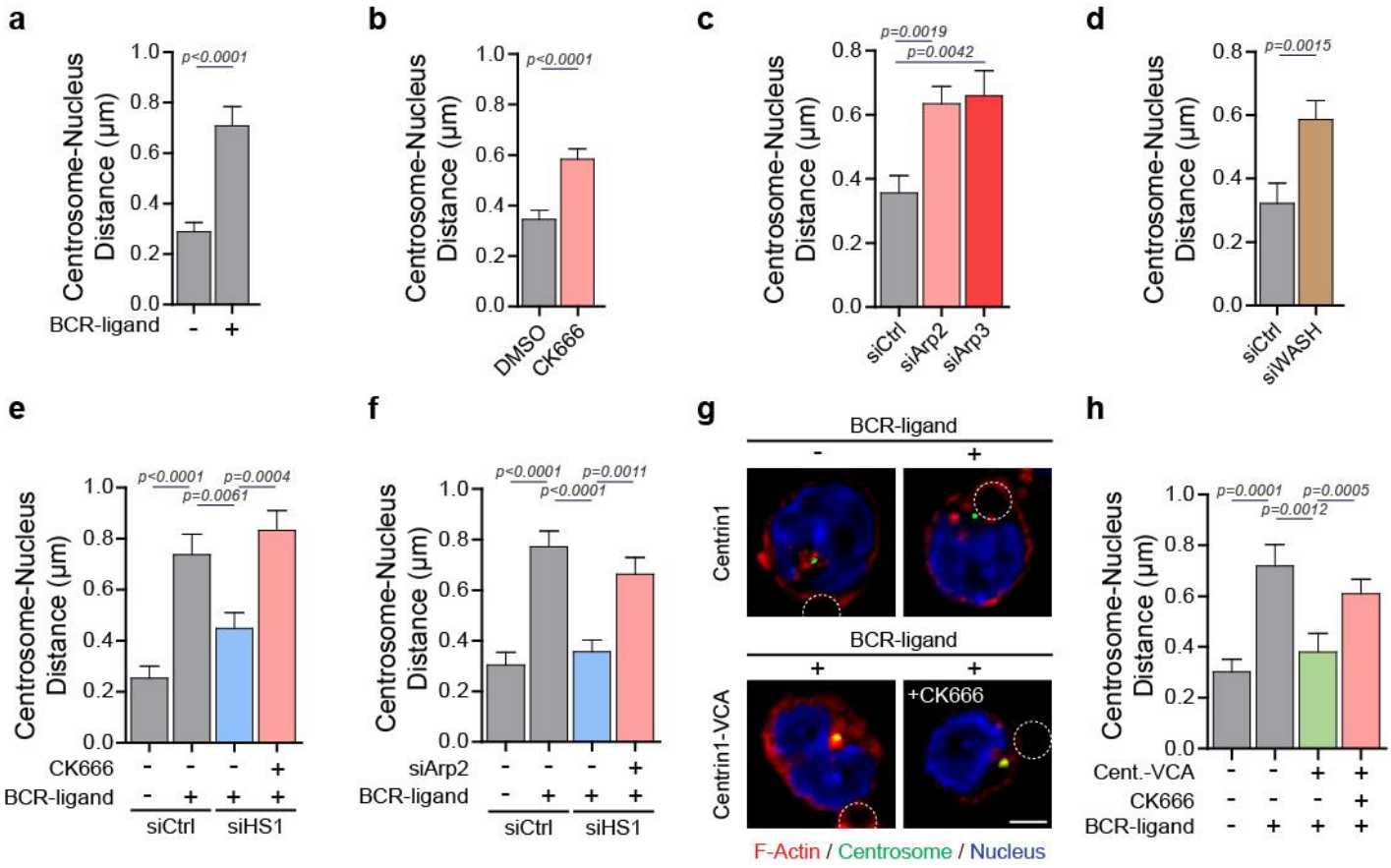

Figure 32. Increased centrosome-nucleus distance upon centrosome polarization. (**a**-**f**) The shorter distance in three dimensions between the centrosome and the edge of the nucleus was measured in: (**a**) B cells stimulated with either BCR-ligand^{-} or BCR-ligand^{+} beads for 60 min; (**b**) resting B cells treated with DMSO or CK666 for 60 min; (**c**) control, Arp2- and Arp3-silenced resting B cells; (**d**) control and WASH-silenced resting B cells; (**e**) control and HS1-silenced B cells, treated with either DMSO or CK666 and stimulated with indicated beads for 60 min and (**f**) control, HS1- and HS1 plus Arp2-silenced B cells stimulated for 60 min with indicated beads. Data are pooled from 2 (**c**, **d**, **e**) and 3 (**a**, **b**, **f**) independent experiments with (**a**) *n*=90 cells per condition; (**b**) *n*=93 and 78 cells for DMSO and CK666, respectively; (**c**) *n*=43, 35 and 31 cells from left to right; (**d**) *n*=37 and 42 cells for siCtrl and siWASH; (**e**) *n*=56, 53, 52 and 54 cells and (**f**) *n*=64, 63, 61 and 64 cells from left to right. (**g**) Representative images of B cells over-expressing the eGFP-Centrin1 protein or the eGFP-Centrin1-VCA fusion protein treated or not with CK666, stimulated with indicated beads for 60 min, fixed and co-stained for F-actin (Phalloidin), the centrosome (GFP) and the nucleus (DAPI). Dashed circles indicate bead position. Scale bar, 3 µm. (**h**) Quantification of the distance between the centrosome and the nucleus edge from cells shown in (g). Data are pooled from 2 independent experiments with *n*=41, 39, 42 and 43 cells from left to right.

9. Centrosomal F-actin tethers the centrosome to the nucleus via the LINC complex

9.a. Increased centrosome-nucleus distance upon centrosome polarization

We next searched for the cellular basis of the negative impact of Arp2/3-dependent actin nucleation at the centrosome on its ability to polarize. Based on recent work indicating that F-actin controls centrosome positioning by inducing the retrograde transport of the nucleus in polarized fibroblasts [Luxton et al., 2010], we postulated that actin nucleation at the centrosome might regulate its physical interaction with the nucleus [Burakov and Nadezhdina, 2013]. To test this hypothesis, we measured the shorter distance in three dimensions between both organelles in lymphocytes that exhibited different levels of centrosomal F-actin.

We found that reduction of centrosomal F-actin upon BCR engagement not only stimulated centrosome polarization but was also accompanied by an increase in the distance between the nucleus edge and this organelle (**Figure 32a**). Strikingly, such increase was equally observed when inhibiting or depleting Arp2/3 in non-stimulated cells (**Figure 32b, c**), indicating that the mere reduction of centrosomal F-actin is sufficient to induce its physical separation from the nucleus. Similarly, the distance between the centrosome and the nucleus edge of resting WASH-silenced cells, whose centrosomes have low levels of centrosomal F-actin, was also increased (**Figure 32d**).

In contrast, in activated HS1-silenced lymphocytes that maintained high levels of F-actin at their centrosome, the centrosome-nucleus distance was as short as in non-stimulated cells (**Figure 32e, f**). This result equally applied to lymphocytes expressing the eGFP-Centrin1-VCA construct, which displayed increased centrosomal actin and impaired centrosome polarization (**Figure 32g, h**). However, centrosome-nucleus separation was rescued in these cells by reducing centrosomal F-actin with CK666 or by silencing Arp2/3 (**Figure 32e-h**).

These results strongly suggest that the pool of F-actin at the centrosome maintains it in close proximity to the nucleus and must therefore be depleted for these two organelles to physically separate.

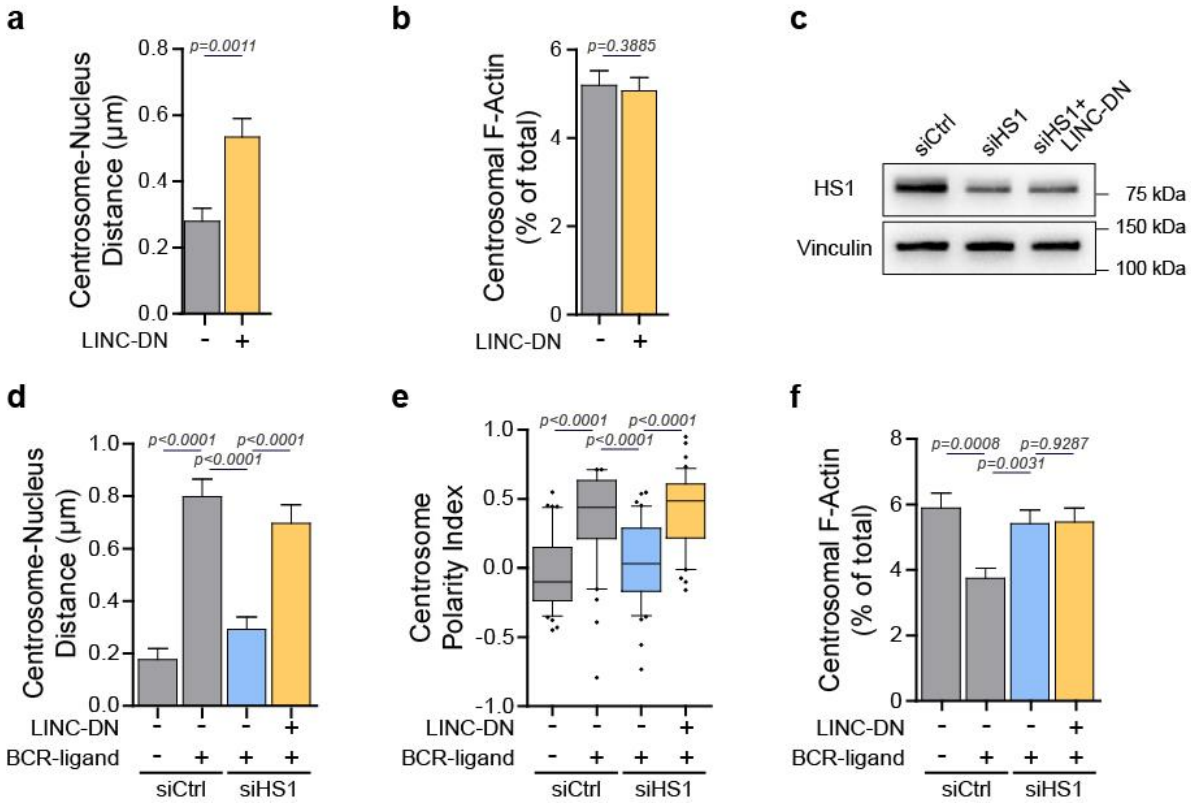

Figure 33. F-Actin-mediated centrosome-nucleus tethering relies on the LINC complex. (**a**, **b**) Quantification of the distance between the nucleus edge and the centrosome (**a**) and the amount of centrosome-associated F-actin (**b**) in resting B cells over-expressing or not the LINC-DN construct. Data are pooled from 3 independent experiments with (**a**) *n*=64 cells per condition and (**b**) *n*=69 and 64 cells from left to right. (**c**) Immunoblot analysis of the efficiency of HS1 silencing in cells over-expressing or not the LINC-DN construct. Vinculin was used as loading control. The blot presented is representative of 2 independent experiments. (**d-f**) Quantification of centrosome-nucleus distance (**d**), centrosome polarity index (**e**) and centrosomal F-actin (**f**) of control and HS1-silenced B cells, over-expressing or not the LINC-DN construct and stimulated for 60 min with indicated beads. Data are pooled from 2 independent experiments with (**d**) *n*=41, 44, 41 and 45 cells; (**e**) *n*=41, 40, 42 and 42 cells and (**f**) *n*=40, 37, 43 and 41 cells from left to right, respectively.

9.b. F-actin-mediated centrosome tethering to the nucleus relies on the LINC complex

Important molecules involved in the physical association of the centrosome to the nucleus are components of the Linker of Nucleoskeleton and Cytoskeleton (LINC) complex. This complex includes Nesprin proteins that bind both the MT and actin cytoskeleton networks. We therefore investigated whether detachment of the centrosome from the nucleus as a result of LINC complex disruption might rescue centrosome polarity.

Over-expression of a dominant-negative mutant of Nesprin-2 that does not bind F-actin [Luxton et al., 2010] was sufficient to increase the distance between the centrosome and the nucleus edge in resting cells without affecting the amounts of centrosome-associated F-actin (**Figure 33a, b**).

More importantly, expression of this dominant-negative version of the LINC complex rescued both centrosome separation from the nucleus (**Figure 33c, d**) and centrosome polarization (**Figure 33e**) in HS1-silenced activated lymphocytes despite their high levels of centrosomal F-actin (**Figure 33f**). Hence, the need to deplete F-actin at the centrosome to detach it from the nucleus and allow its polarization to the immune synapse can be bypassed by disrupting the LINC complex.

These results strongly suggest that F-actin nucleation at the centrosome is required for its physical association to the nucleus by the LINC complex. Altogether, these data further provide a putative mechanism for the need to deplete centrosomal Arp2/3 and F-actin in order to allow centrosome translocation to the immune synapse.

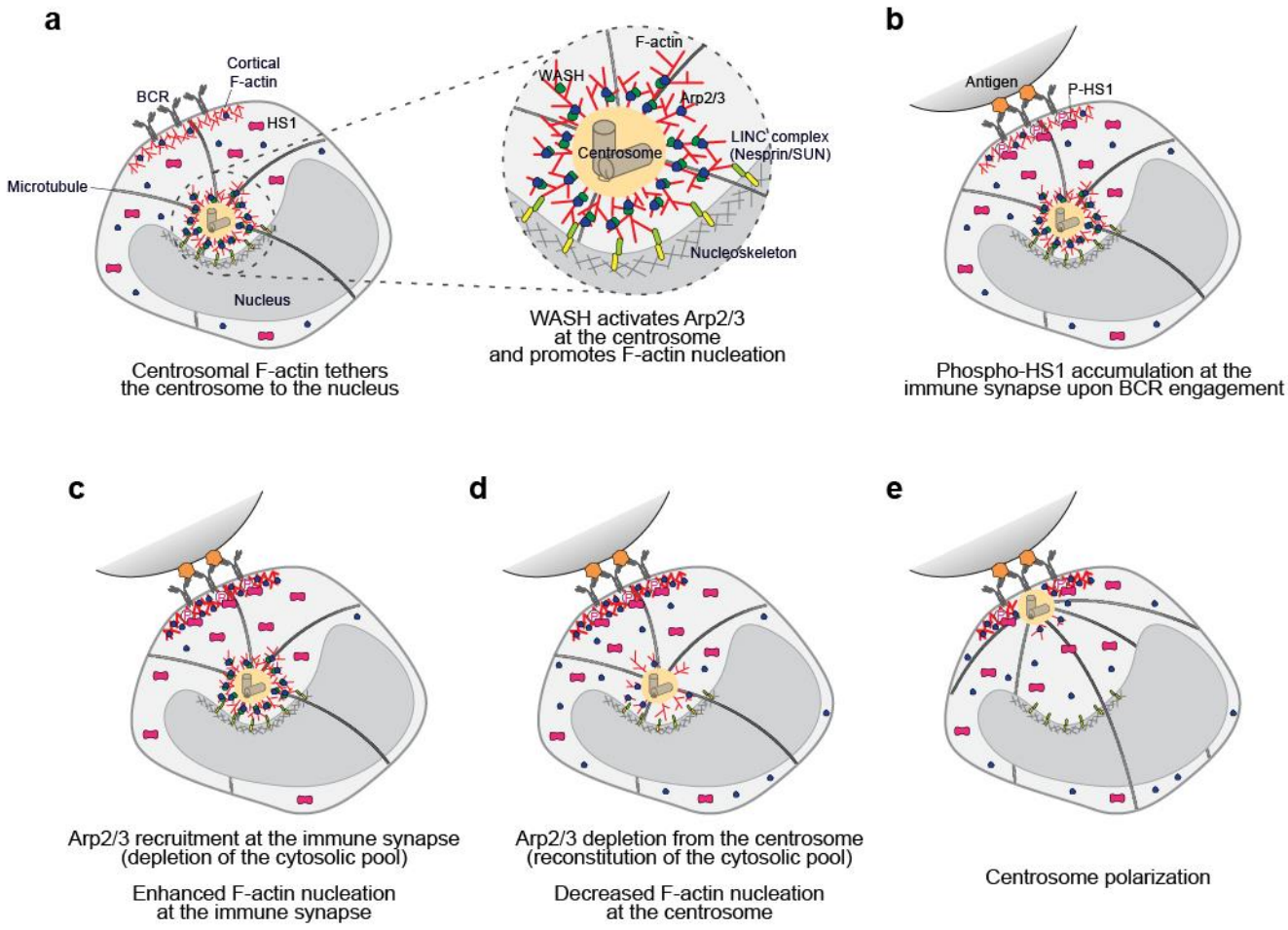

Figure 34. Model of F-actin-mediated regulation of centrosome polarization.

10. Conclusion

We here found that the centrosomes of resting B cells nucleate F-actin in a WASH- and Arp2/3-dependent manner (**Figure 34a**). The engagement of the BCR with immobilized antigens induces the accumulation of the Cortactin-like protein HS1 at the immune synapse (**Figure 34b**), which recruits Arp2/3, promoting the local enrichment of F-actin (**Figure 34c**). Of note, although inhibition of Arp2/3 does not impair centrosome polarization, its activity is nonetheless required for B lymphocytes to process and present BCR-internalized antigens to T-lymphocytes (see **Figure 41** of the Discussion, page 114), suggesting a function for this complex at the B cell synapse. Recruitment of Arp2/3 at the synapse would in turn lead to its partial depletion from the centrosome, thereby reducing the pool of centrosome-nucleated F-actin (**Figure 34d**). The centrosome would then be free to physically separate from the nucleus and move towards the immune synapse (**Figure 34e**). Importantly, we found that an intact LINC complex is required for centrosomal F-actin to maintain centrosome attachment to the nucleus (**Figure 34a**). Interestingly, although the molecular players that allow interaction between the LINC complex and the nucleoskeleton were described, the one that link this complex to the centrosome remained unclear [Burakov and Nadezhdina, 2013]. Our results suggesting that F-actin nucleation at the centrosome might be a key player in this process therefore brings an interesting new piece to this puzzle.

Taken together the results presented above highlight an unexpected role for Arp2/3-mediated F-actin nucleation by the centrosome in the control of centrosome polarization in response to immobilized antigen stimulation. Whether such a mechanism regulates centrosome positioning in other polarization processes as well as in other cellular systems would be an interesting field of future investigations.

This work has been published in Nature Communications in March 2016

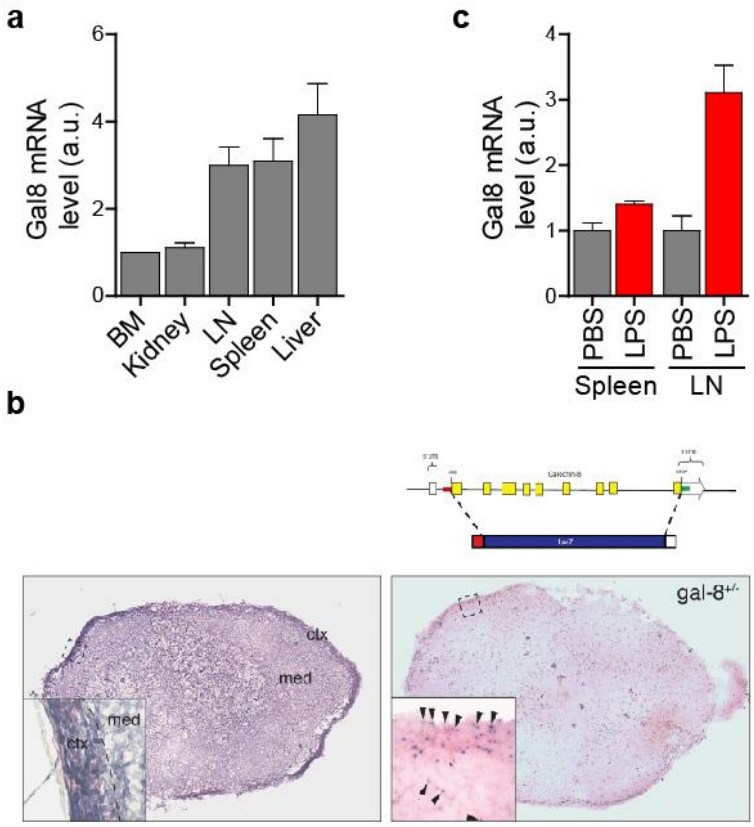

Figure 35. Galectin-8 is upregulated in lymphoid tissues upon inflammation. (**a**) Quantitative RT-PCR analysis of Galectin-8 (*Lgals8*) mRNA levels in bone marrow (BM), kidney, lymph nodes (LN), spleen and liver of wild-type mice. Values were normalized with respect to the BM value for each mouse. Bars represent the mean±S.E.M. of 3 mice. (**b**) **Left.** Representative picture of hematoxylin-eosin staining of LN cryosection. **Right.** Representative image of β-galactosidase staining of LN cryosection from mouse bearing a LacZ expression cassette at the Galectin-8 locus. Arrowheads on the inset highlight β-galactosidase staining within the sub-capsular sinus area. (**c**) Quantitative RT-PCR analysis of Galectin-8 (*Lgals8*) mRNA levels in spleen and lymph nodes (LN) of wild-type mice 6 h following *i.v.* injection of PBS (vehicle control) or 50 µg LPS. Values were normalized with respect to the PBS condition for each organ. Bars represent the mean±S.E.M..

As discussed throughout this manuscript, the acquisition of polarity is pivotal for B cells to achieve their effector functions. In this second part of my thesis, I explored whether extracellular cues present within the lymphoid tissue microenvironment are involved in the regulation of B cell responsiveness upon immobilized antigen stimulation. A special focus was made on the role of the glycan-binding protein Galectin-8 in the regulation of centrosome and lysosome polarization towards the immune synapse.

1. Galectin-8 is upregulated in lymphoid tissues upon inflammation

We first sought to determine whether Galectin-8 was expressed in lymphoid tissues at steady state. We found that *Lgals8* mRNA was expressed in spleen and lymph nodes (**Figure 35a**) and accumulates within the sub-capsular sinus area (**Figure 35b**), which has been described to be the site of dynamic cell-cell interactions between B cells and specialized macrophages carrying immobilized antigens at their surface [Carrasco and Batista, 2007, Junt et al., 2007]. Strikingly, upon LPS-induced systemic inflammation, Galectin-8 expression was up-regulated in lymph nodes (**Figure 35c**). Of note, this increase was less important in the spleen.

The presence of Galectin-8 in lymphoid tissues and its up-regulation upon inflammation prompted us to assess whether Galectin-8 acts as an extracellular co-signal that modulates BCR-dependent cell polarization and could thus have an impact on the antigen extraction and processing capacity of B cells.

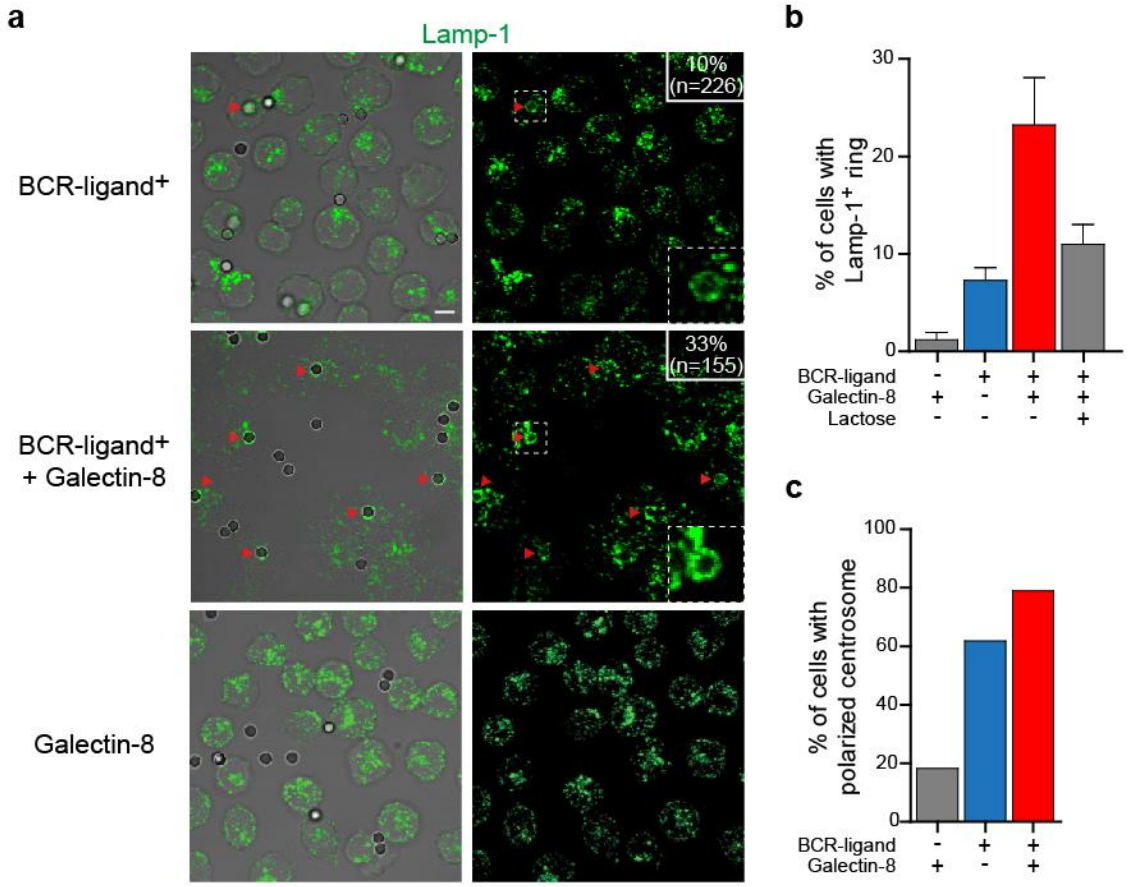

Figure 36. Galectin-8 enhances lysosome recruitment to the immune synapse. (**a**) Representative images of B cells stimulated for 60 min with indicated beads and stained for lysosomes (Lamp-1). Insets show a zoom of Lamp-1^+ rings. (**b**) Quantification of the percentage of cells displaying Lamp-1^+ rings upon stimulation with indicated beads for 60 min. (**c**) Quantification of the percentage of cells having repositioned their centrosome towards the bead-contact site upon stimulation with indicated beads for 60 min. Data are representative of at least 2 independent experiments.

2. Galectin-8 enhances BCR-mediated recruitment of lysosomes to the synapse

Upon BCR engagement with immobilized antigens, the recruitment and local secretion of lysosomes at the immune synapse enable B cells to efficiently extract and present antigens [Yuseff et al., 2011]. We thus asked whether extracellular Galectin-8 might potentiate lysosome polarization, thus enhancing antigen extraction. B cell polarization was studied by incubating these cells for different time with BCR-ligand$^+$ beads coated or not with Galectin-8 and both centrosome and lysosome polarization was monitored by immunofluorescence.

As mentioned in the Introduction of this manuscript, BCR engagement with surface-tethered antigens induces the recruitment and local secretion of Lamp-1$^+$ lysosomes within the synaptic interface [Yuseff et al., 2011]. This leads to the appearance of a characteristic Lamp-1$^+$ ring at the antigen-contact site reflecting the local fusion of lysosomes, a process that relies on BCR signaling [Yuseff et al., 2011]. Strikingly, when B cells were incubated with BCR-ligand$^+$ beads coated with Galectin-8 (BCR-ligand$^+$-Gal8 beads), the presence of Lamp-1$^+$ rings around the beads was increased, suggesting that Galectin-8 promotes the recruitment and secretion of lysosomes at the synaptic interface (**Figure 36a, b**). Importantly, the effect of Galectin-8 on lysosome polarization was not observed when BCR-ligand$^+$-Gal8 beads were pre-incubated with lactose, a saccharide which binds Galectin sugar binding domains, thereby blocking their biological activity (**Figure 36b**). However, no major differences in the polarization of the centrosome were observed upon stimulation with BCR-ligand$^+$ beads containing or not Galectin-8 (**Figure 36c**). Of note, lysosome recruitment and clustering was not observed in B cells stimulated with BCR-ligand$^-$ coated or not with Galectin-8 beads, suggesting that Galectin-8 does not trigger B cell polarization independently of BCR engagement (**Figure 36a, b**).

These results suggest that Galectin-8 is an extracellular cue that cooperates with BCR signaling to promote lysosome polarization at the B cell synapse.

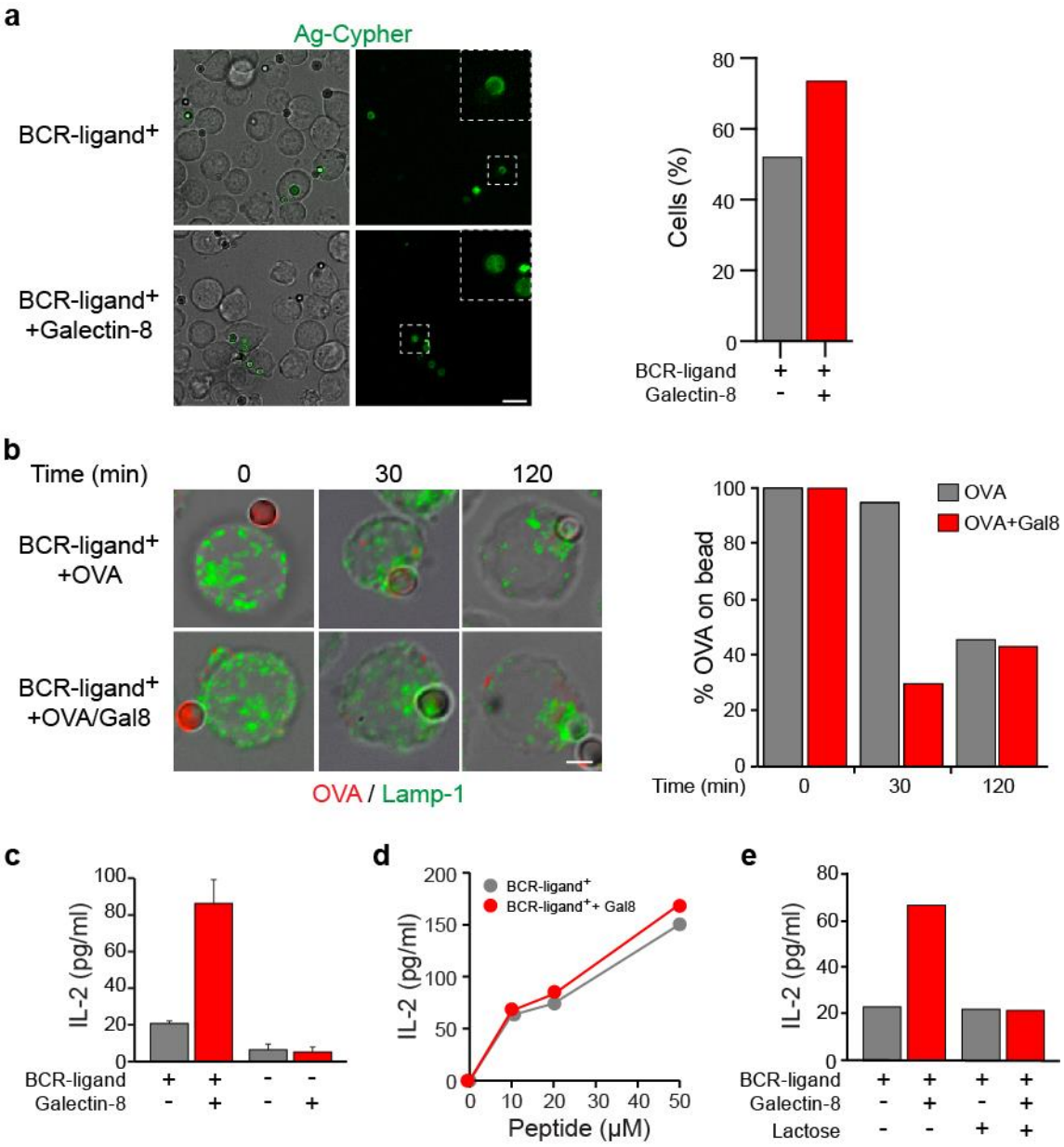

Figure 37. Galectin-8 promotes efficient antigen extraction and presentation. (**a**) **Left.** B cells were incubated 90 min with indicated beads plus Cypher5E and the appearance of Cypher5E fluorescence signal on beads was monitored as a read-out of lysosome secretion within the synaptic interface. Insets show a zoom of Cypher5E$^+$ beads. Scale bar, 12 µm. *n*= 132 and 123 bead/cell conjugates per condition. **Right.** Quantification of the percentage of cells harboring acidic synapses (only beads displaying a Cypher5E fluorescence intensity superior at 10% of the background fluorescence intensity were considered as acidic synapses). (**b**) **Left.** B cells were incubated with BCR-ligand$^+$ beads plus the model antigen OVA in the presence or not of Galectin-8 for indicated time and the amounts of OVA remaining on beads were assessed as a read-out of B cell antigen extraction capacity. Scale bar, 3µm. **Right.** Quantification of the amounts of OVA remaining on beads from cells shown in the left panel. (**c**) B cells were incubated with indicated beads plus the model antigen Lack for 3 h, fixed and co-cultured for 16 h with a Lack-specific T cell hybridoma and the amounts of IL-2 within culture supernatants were assessed by ELISA. (**d**) Presentation of the Lack peptide control for cells used in (c). (**e**) Lack antigen presentation as described in (c) in presence or not of lactose to inhibit Galectin-8 activity. Data are representative of at least 2 independent experiments.

3. Galectin-8 promotes efficient antigen extraction and presentation

We next investigated whether the enhanced recruitment of lysosomes to the synapse observed in the presence of Galectin-8 translated into a rapid acidification of the synaptic interface, thereby promoting more efficient antigen extraction. Synapse acidification was quantified by using Cypher5E, a dye whose fluorescence increases at acidic pH [Adie et al., 2002, Yuseff et al., 2011]. Beads coated with Cypher5E-coupled BCR ligand ± Galectin-8 were incubated with B cells for 90 min and the appearance of a fluorescence signal on the bead was quantified. Remarkably, a higher number of BCR-ligand^{+}-Gal8 beads showed high levels of fluorescence compared to control beads, strongly suggesting that Galectin-8 promotes a faster secretion of lysosomes at the B cell synapse (**Figure 37a**).

We next assessed the capacity of B cells to extract antigens in the presence of Galectin-8 by monitoring the disappearance of ovalbumin (OVA) from beads, as previously described [Yuseff et al., 2011]. Strikingly, the amount of OVA extracted from beads at early time points was significantly higher when Galectin-8 was present (**Figure 37b**). Of note, after 120 min the total amount of OVA extracted reached a plateau and was equal in both conditions, suggesting that, in agreement with the ability of Galectin-8 to trigger rapid lysosome secretion at the synapse, it prompts cells to extract antigens at a faster rate. Similar results were obtained when monitoring the ability of primary spleen B cells to extract antigens (not shown).

We next sought to determine the impact Galectin-8 has on the ability of cells to process and present immobilized antigens. For this, B cells were incubated with BCR-ligand^{+} beads coated with the *LACK* antigen from *Leishmania major* plus Galectin-8 or not. Their ability to present *LACK*-derived MHC-II-peptide complexes to a specific T cell hybridoma was then measured by monitoring interleukin-2 (IL-2) secretion, as previously described [Yuseff et al., 2011]. Consistent with the results shown above, antigen presentation was significantly higher in the presence of Galectin-8 (**Figure 37c**). Noticeably, peptide presentation showed no major differences indicating that Galectin-8 does not affect cell surface levels of MHC-II or co-stimulatory molecules and does not influence B cell/T cell interactions (**Figure 37d**). In the presence of lactose, the effect of Galectin-8 was blocked and the levels of antigen presentation were comparable to the ones shown by controls where Galectin-8 is absent (**Figure 37e**). Similar results were obtained when assessing the ability of primary spleen B cells to present antigens in presence of extracellular Galectin-8 (not shown).

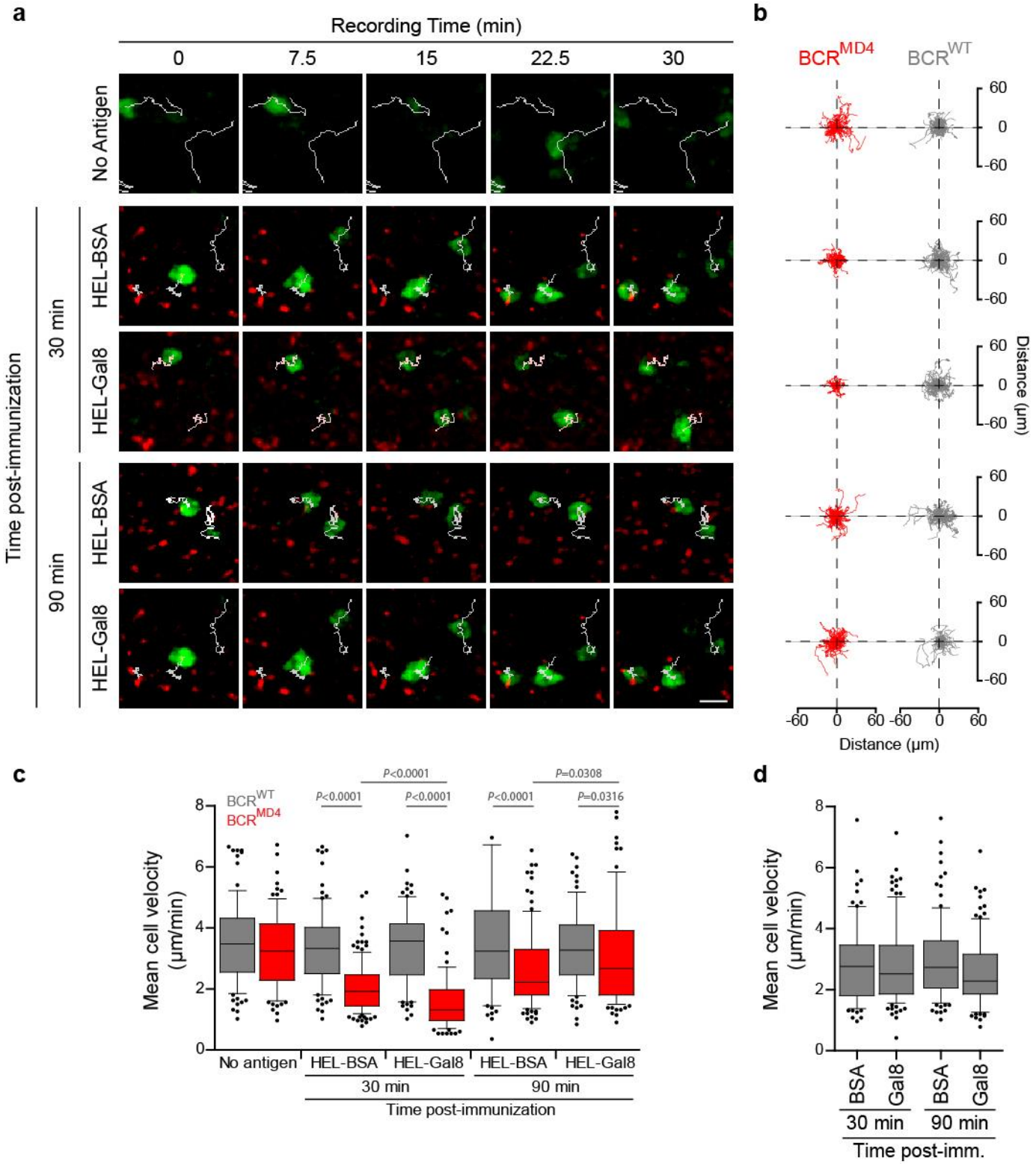

Figure 38. Galectin-8 favors B cell synapse formation *in vivo*. IAβ-GFP-expressing MD4 (BCR^{MD4}) or WT (BCR^{WT}) B cells were adoptively transferred within wild-type recipient mice prior to be immunized with indicated microspheres by footpad injection. 30 or 90 min post-immunization, mice were anesthetized and the popliteal lymph node draining the site of injection was prepared for two-photon imaging. (**a**) Representative images of migrating B cells within the sub-capsular region of lymph nodes. Cells were then tracked and the length of their migratory paths (**b**) as well as their mean velocity (**c**) was assessed. (**d**) Mean cell velocity of MD4 B cells migrating within the sub-capsular area upon immunization with beads coated with non-relevant antigen (BSA) or Galectin-8 alone. Data are pooled from at least 3 independent experiments with at least 70 cells and 4 mice per condition.

Collectively, these results show that extracellular Galectin-8 cooperates with BCR signaling to enhance the capacity of B cells to extract and present antigens.

4. Galectin-8 favors B cell responses *in vivo*

We next sought to determine the impact of extracellular Galectin-8 on B cell responses *in vivo* and thus analyzed how this lectin, presented together with antigen affected both B cell motility and antigen recognition within the sub-capsular sinus region of lymph nodes. For this purpose, we first generated mice with antigen-specific B cells expressing a fluorescent tag by crossing the MD4 mouse model, whose B cells express a transgenic BCR specific for the hen egg lysozyme (HEL) protein, with mice bearing a green fluorescent protein (GFP) fused to the IAβ chain of the MHC-II molecules (IAβ-GFP). This allowed us to distinguish and track antigen-specific B cells within lymph nodes when adoptively transferred into wild type (WT) recipient mice.

We then immunized those mice by injecting into their footpad 0.2 µm red fluorescent microspheres coated with HEL in combination or not with Galectin-8. Intravital imaging (movie duration: 30 min) of the lymph node draining the site of injection using two-photon microscopy was then performed 30 or 90 min post-immunization (p.i.). Tracking of IAβ-GFP$^+$ B cells within the sub-capsular sinus area showed that B cells displayed shorter trajectories when microspheres containing both HEL and Galectin-8 were presented compared to B cells that encountered HEL-coated microspheres (**Figure 38a, b**), suggesting that under these conditions B cells were no longer in the antigen "searching" phase. Accordingly, B cells showed reduced mean velocity after antigen administration (**Figure 38c**), as previously described [Carrasco and Batista, 2007]. This effect was even more drastic when Galectin-8 was also present suggesting that, in addition to promote antigen extraction and presentation *in vitro*, Galectin-8 favors the formation of the B cell immune synapse *in vivo*. Importantly, consistent with our *in vitro* data, no effect on B cell behavior was observed after administrating microspheres coated with non-specific antigen (BSA) or Galectin-8 alone (**Figure 38d**). Interestingly, higher mean velocity values were observed in B cells 90 min after antigen injection compared to earlier time points (**Figure 38c**). Increased motility was more noticeable when Galectin-8 was also present on microspheres and most likely reflect the pool of B cells that have already acquired antigens and are migrating towards the T cell boundary.

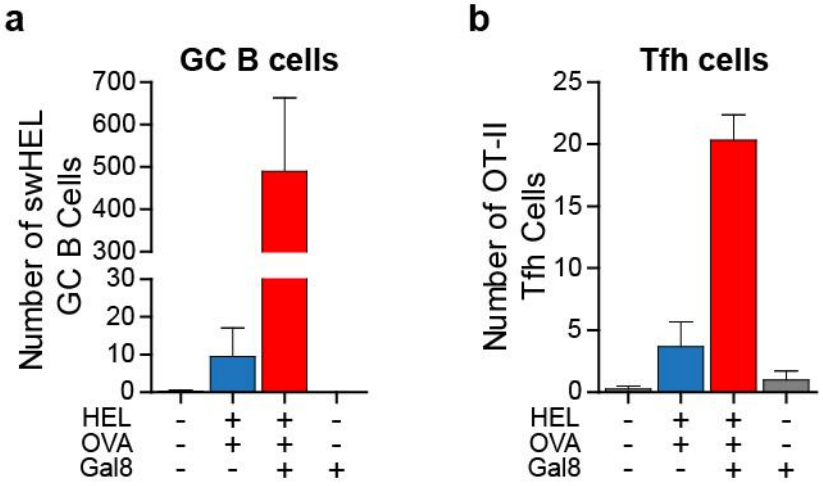

Figure 39. Galectin-8 enhances antigen presentation *in vivo*. CD45.2$^+$ swHEL B cells and OT-II CD4$^+$ T cells were adoptively transferred into CD45.1$^+$ wild-type recipient mice and 8 days post-immunization by footpad injection of indicated microspheres, draining popliteal lymph nodes were recovered. Lymph node-cell suspensions were then analyzed by flow cytometry to monitor the emergence of antigen-specific germinal center B cells (swHEL GC B cells, gated on CD45.2$^+$, B220$^+$, HEL$^+$, GL7$^+$, FAS$^+$) (**a**) as well as antigen-specific follicular helper T cells (OT-II Tfh cells, gated on CD45.2$^+$, CD4$^+$, CXCR5$^+$, PD-1$^+$) (**b**). 4 mice per group, 1 experiment.

We conclude from these data that Galectin-8 acts as an extracellular cue promoting the arrest phase of B cells, which is known to be required for B cells to extract and present antigen [Carrasco and Batista, 2007]. Given that extracellular Galectin-8 also promotes antigen extraction and presentation *in vitro*, one could envision that *in vivo* Galectin-8 favors these processes by promoting B cell arrest upon antigen encounter.

5. Galectin-8 enhances antigen presentation *in vivo*

We next asked whether Galectin-8 promotes antigen presentation *in vivo*. Antigen presentation to T lymphocytes induces the formation of germinal center (GC) characterized by the emergence of GC B cells and follicular helper T cells (Tfh). We thus assessed whether the enhanced capacity of B cells to form immune synapses in presence of extracellular Galectin-8 also reflected a higher capacity to present antigen to $CD4^+$ T cells in such conditions. For this purpose, swHEL B cells, whose cells are able to class switch and enter the GC reaction upon HEL stimulation, and OT-II $CD4^+$ T cells that recognized OVA peptide loaded on MCH-II molecules, were co-adoptively transferred into WT recipients. Mice were then immunized with microspheres coated with HEL/OVA plus Galectin-8 or not and 8 days post-immunization, the generation of GC B cells as well as Tfh cells was assessed. Strikingly, both GC B cells and Tfh generation were enhanced in the presence of Galectin-8 compared to mice having received only HEL/OVA microspheres (**Figure 39a, b**). As previously, neither non-specific antigen nor Galectin-8 alone was able to induce the generation of GC B and Tfh cells (**Figure 39a, b**), suggesting that extracellular Galectin-8 potentiates BCR stimulation.

We conclude from these data that Galectin-8 cooperates with BCR signaling to favor the presentation of antigens to helper T cells and favors the formation of germinal centers *in vivo*.

6. Conclusion

We here showed that extracellular Galectin-8 potentiates the effect of BCR signaling induced by BCR engagement with immobilized antigens, thereby resulting in the faster recruitment and secretion of lysosomes at the immune synapse. This in turn provides to B cells an enhanced capacity to extract and present immobilized antigens. The recent generation in the lab of a mouse strain knock-out for Galectin-8 will now allow us to assess whether the lack of extracellular Galectin-8 impairs immune responses.

Overall, our results highlight a new level in the regulation of B cell functions, whereby extracellular cues present within the tissue microenvironment tune the responsiveness of lymphocytes upon encounter of surface-tethered antigens.

This work is on-going and will soon be submitted for publication in a peer-reviewed journal

DISCUSSION

Since the first observation of centrosome polarization toward target cells in cytotoxic T cells [Kupfer and Dennert, 1984] and the description of the main features of the T cell immune synapse [Grakoui et al., 1999], numerous studies have focused their interests in understanding how these particular processes regulate the functions of T lymphocytes. Even through pioneer work carried out by Facundo BATISTA in the early 2000's have highlighted the establishment of an immune synapse upon B cell stimulation with surface-tethered antigens [Batista et al., 2001], the basic cell biological events controlling B cell functions were for a long time under-studied. To date, we and others have equilibrated the balance since the formation of the B cell immune synapse and the polarization of the centrosome and lysosomes appear to be crucial in the initiation of adaptive immune responses [Yuseff et al., 2011, Reversat et al., 2015, Obino et al., 2016].

In that context, the main goal of this work was to identify and decipher new molecular mechanisms involved in the regulation of B lymphocyte polarization and functions with a special emphasis given to both extracellular cues and cell intrinsic properties. In the last part of this manuscript, the main findings of my work will be first summarized. Then the results presented will be discussed around three axes that I would like to highlight: 1) the ability of the centrosome to nucleate Arp2/3-dependent F-actin, 2) the molecular mechanism(s) underlying lymphocyte polarization and 3) the emergence of the concept that the immune synapse might be assimilated to an adhesive structure.

About F-actin, Cell Polarity and B Lymphocyte Functions

Centrosome repositioning towards the immune synapse represents a key step of B cell activation. Indeed, this early event redefines the intracellular routes within B lymphocytes, which support the directed transport and local secretion of lysosomes within the synaptic interface [Yuseff et al., 2011]. Hence, centrosome translocation towards the immune synapse is strictly required for B cells to acquire their antigen extraction, processing and presentation capacities [Yuseff et al., 2011]. Therefore, understanding the mechanisms underlying centrosome polarization upon B cell stimulation with surface-tethered antigens represents a crucial accomplishment. In addition, whether and how extracellular cues present within the lymphoid microenvironment might contribute/help in tuning B cell functions represents an interesting field of investigations. These questions have been challenged during my PhD. We first hypothesized that B cell activation might modify the centrosome proteome.

Consequently, the identification of such changes might reveal valuable candidates involved in the regulation of centrosome polarization.

The main findings of this work rely on the identification of an F-actin-dependent mechanism regulating centrosome polarization in B lymphocytes. By using multiple approaches, including quantitative mass spectrometry and immunofluorescence, we show that in addition to its well-known cortical localization, Arp2/3 also associates with the centrosome of resting B lymphocytes. This allows the centrosome to assemble a network of F-actin that tethers the centrosome to the nucleus via the LINC complex. Upon B cell stimulation with surface-tethered antigens, Arp2/3 is recruited to the immune synapse thanks to the local activation of the Cortactin-like protein HS1. This in turn induces the depletion of Arp2/3 from the centrosome, hence decreasing its ability to assemble F-actin. Thus, the centrosome detaches from the nucleus and is free to polarize towards the immune synapse.

In a second time, we investigated whether the presence within the lymphoid environment of Galectin-8, a protein involved in immune cell homeostasis and responses [Rabinovich and Toscano, 2009], regulates B cell polarization and functions. We first show that Galectin-8 expression increases within lymphoid tissues upon inflammation, strongly suggesting an immunomodulatory function for this protein in this particular context. Accordingly, our results demonstrate that the arrest phase of B cells, which is observed upon antigen encounter by B cells and strictly required for these cells to acquire antigens [Carrasco and Batista, 2007], is potentiated in presence of extracellular Galectin-8 *in vivo*. This correlates with an enhanced capacity of B cells to extract and present antigens to $CD4^+$ T cells when the antigen is presented to B cells together with Galectin-8. The increased capacity of B cells to extract and present antigens in presence of extracellular Galectin-8 results from the enhanced recruitment and secretion of lysosomes within the synaptic space.

Taken together those findings highlight 1) a new cell intrinsic mechanism that regulates the ability of the centrosome to polarize in response to external stimuli (e.g. surface-tethered antigens) and 2) the involvement of extracellular cues present within the environment of B cells in tuning the capacity of these cells to respond to such stimulation. These two new mechanisms have important implications in our understanding of the basic cell biology events regulating B cell functions and raise new concepts that may have a major impact in cell biology as they might control cell polarization in many different cellular systems.

1. The centrosome: from MTOC to ATOC

Since the mid-1960's, the idea that microtubules (MTs) were not randomly arranged within cells has emerged. Even if the structure supporting MT nucleation has been initially named differently – such as MT initiating sites (Porter 1966) or MT generators (Wolfe 1972) (reviewed in [Brinkley, 1985]) – the concept that the centrosome was the main microtubule-organizing center (MTOC) is now well accepted. Therefore most of the studies carried out in this field have focused their work in understanding the basics of centrosome functions based on this picture (reviewed in [Bornens, 2012]).

In contrast, although the actin cytoskeleton and the Arp2/3 complex have been described to be in close association with the centrosome in different studies [Hubert et al., 2011, Vaughan and Dawe, 2011, Tang and Marshall, 2012], they have been most of the time considered as "sticky" contaminants and little efforts have been made to understand such association. However, taking into account the crosstalk that exist between both the microtubule and actin cytoskeletons as well as the growing evidences suggesting that they are tightly coupled [Rodriguez et al., 2003], it was unlikely that centrosome-associated F-actin and Arp2/3 did not serve specific cellular processes. Following on this reasoning, these observations pushed the labs of Manuel THÉRY and Laurent BLANCHOIN to investigate whether the centrosome was intrinsically able to assemble actin filaments. This pioneer work has led to the recent discovery of a new function for the centrosome that is, in addition to its well-known capacity to induce MT polymerization, the support of Arp2/3-dependent F-actin nucleation in different cellular systems, including T lymphocytes [Farina et al., 2016] (**Figure 40a**). Following on this study, we found in collaboration with their groups that B lymphocyte centrosomes also assemble actin filaments in an Arp2/3-dependent manner.

Hence, in addition to its function as MTOC, the centrosome might also be seen as an actin-organizing center, or ATOC, providing for the first time an explanation for the recurrent but unexplained observation of F-actin and Arp2/3 at the centrosome. In addition, this finding opens new fields of investigations and raises new questions: How are (co-)regulated these two functions of the centrosome? In which cellular processes centrosomal F-actin is involved?...

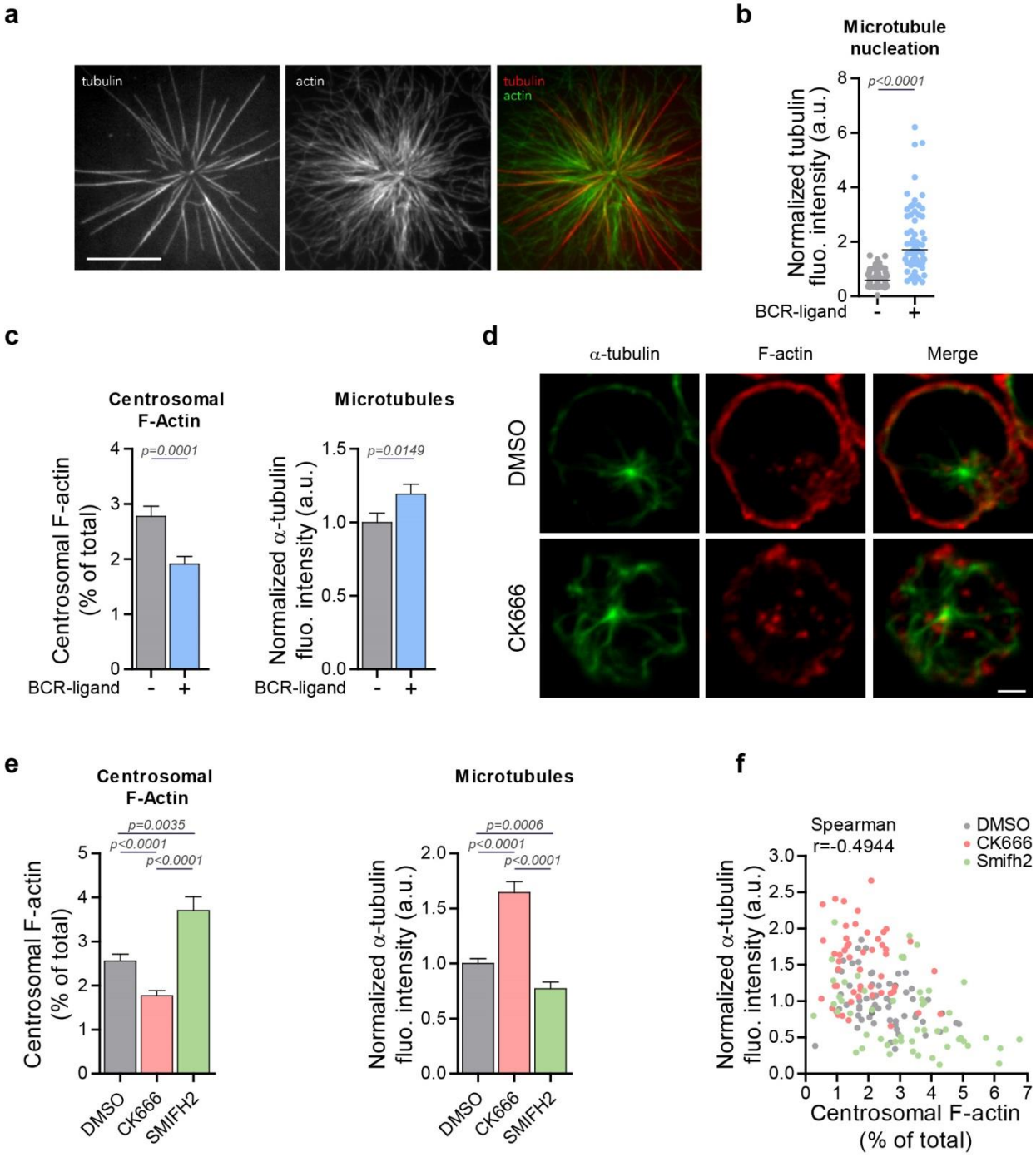

Figure 40. Microtubules or F-actin: the centrosome must choose... (**a**) The assembly of both microtubules and actin filaments from isolated centrosomes. Scale bars, 10 µm. Reproduced from [Farina et al., 2016]. (**b**) Quantification of microtubule nucleation activity of centrosomes purified from B cells stimulated with indicated beads for 60 min. *n*=59 and 62 tubulin asters respectively. Data are representative of 3 independent experiments. (**c**) Quantification of centrosome-associated F-actin (left) and microtubule fluorescence intensity (right) from cells stimulated for 60 min with indicated beads. (**d**) Representative images of B cells treated with DMSO or CK666, fixed and stained for microtubules (α-tubulin) and F-actin (Phalloidin). Scale bar, 3 µm. (**e**) Quantification of centrosome-associated F-actin (left) and microtubule fluorescence intensity (right) of cells treated with DMSO, CK666 or Smifh2 for 60 min. (**f**) Correlation analysis between the amounts of centrosomal F-actin and the fluorescence intensity of microtubule staining from cells quantified in (e). Spearman correlation analysis, p-value<0.0001. α-tubulin fluorescence intensity was normalized with respect to the mean fluorescence intensity of cells stimulated with BCR-ligand$^-$ beads in each replicate. Data were pooled from 2 independent experiments.

2. Microtubules or F-actin: the centrosome must choose…

The identification of this dual property of centrosomes in nucleating both MTs and F-actin raises an additional question: How centrosomes deal with these two functions? To investigate this question we first assessed the ability of centrosomes purified from either non-activated or activated B cells to assemble MTs *in vitro*. We observed that centrosome preparations from BCR-stimulated lymphocytes, which we have shown are less efficient in nucleating actin filaments than their control counterparts, possess a greater capacity to nucleate MTs (**Figure 40b**). Interestingly, similar observations have been made by the group of M. THÉRY. Treatment of centrosomes that have co-assembled actin filaments and MTs with actin-depolymerizing drugs results in the increase in MT nucleation *in vitro*.

This has been also observed in intact cells displaying various amounts of centrosomal F-actin, e.g. between non-activated and activated B cells, wherein I quantified the fluorescence intensity of MTs. Strikingly, activated B cells, whose cells have lower levels of centrosome-associated F-actin, showed increased amounts of MTs compared to non-activated lymphocytes (**Figure 40c**). One could speculate that such increase in MT nucleation upon B cell stimulation is likely to contribute to centrosome polarization. Similarly, Arp2/3 inhibition with CK666, which decreases the amounts of centrosomal F-actin in resting B cells, promotes the nucleation of MTs (**Figure 40d, e**). Conversely, promoting F-actin nucleation at the centrosome using the Formin inhibitor Smifh2 decreases the ability of centrosomes to assemble microtubules (**Figure 40d**).

These data strongly suggest that the amount of centrosomal F-actin regulates the ability of centrosomes to nucleate MTs. In line with this hypothesis, we found a significant anti-correlation between the level of F-actin associated with centrosomes and their capacity to assemble MTs (**Figure 40f**). However, how centrosomal F-actin regulates MT polymerization by centrosomes remains to be determined. Different hypotheses may be envisioned: first, the steric hindrance resulting from the F-actin cage around the centrosome might negatively impact on the ability of centrosomes to nucleate MTs. Second, the presence of the Arp2/3 complex at the centrosome may compete with other factors that are required to enhance MT assembly. This represents an exciting field of investigations that is currently under study in collaboration between our two groups.

3. Centrosome-nucleus interaction: implications for cell polarity

The idea that the actin cytoskeleton links the centrosome to the nucleus was initially proposed in the eighties based on observations showing that nucleus purification or cell enucleation required the addition of F-actin depolymerizing drugs [Maro and Bornens, 1980, Karsenti et al., 1984]. However, the precise nature and origin of this actin network remained unclear. Different F-actin structures have been reported in association with the centrosome and/or the nucleus. This includes "actin clouds" that position centrosomes and mitotic spindles [Kwon et al., 2015] and resemble the F-actin structures we observed at the centrosome of B lymphocytes. In addition, the nucleus of migrating fibroblasts associates to a "perinuclear actin cap" [Kim et al., 2014] or to "linear actin arrays" referred to as TAN lines, which regulate nucleus retrograde transport and centrosome polarity through the LINC complex [Luxton et al., 2010, Kutscheidt et al., 2014]. Although we did not observe TAN lines in B lymphocytes, what might be due to their non-adherent properties, whether and how Arp2/3-dependent F-actin nucleation at the centrosome contributes to the formation and/or function of these actin structures will be an important point to investigate in the future.

Consistently with previous findings [Burakov and Nadezhdina, 2013], our results strongly suggest that F-actin nucleation at the centrosome of B lymphocytes tethers the centrosome to the nuclear envelop via the LINC complex, thus determining its position at the cell center. Upon stimulation, this capacity of centrosomes to nucleate F-actin must decrease for this organelle to detach from the nucleus and acquire a polarized localization. Of note, we do not exclude that actin depletion at the centrosome may control additional processes required for efficient centrosome polarization than centrosome-nucleus attachment. In particular, reduction of F-actin nucleation at the centrosome might induce local changes to favor its MT-dependent translocation to the synapse. For example, it may facilitate Dynein recruitment and/or local centrosome docking at the immune synapse. Consistent with these hypotheses, we and others have shown that Dynein is indeed required for centrosome reorientation to the synapse in both B and T lymphocytes [Reversat et al., 2015, Liu et al., 2013, Yi et al., 2013, Combs et al., 2006]. Further work is needed to unravel the role played by centrosome-nucleated F-actin in the biology of resting lymphocytes as well as to fully understand how depletion of this F-actin pool facilitates centrosome polarity.

In conclusion, our results highlight an unexpected role for the regulation of centrosome-associated F-actin in the control of cell polarization. Whether and how this novel regulatory mechanism applies to additional biological systems that rely on cell polarity is an open question. This would be of particular interest in the context of cilium biogenesis that involves signaling pathways also used in immune synapse formation by lymphocytes [Finetti et al., 2009, de la Roche et al., 2013].

4. Centrosome-nucleus interaction: a role for microtubules?

Beyond the role of centrosomal F-actin in promoting the tethering of the centrosome to the nuclear envelop, several studies suggest a role for the microtubule network in this process (reviewed in [Burakov and Nadezhdina, 2013]). Indeed, similarly to observations made in mice during neurogenesis and neural migration [Zhang et al., 2009], the opposite direction of movement of Dynein and Kinesins has been proposed to regulate nuclear positioning relative to the centrosome. While Kinesin activity moves the nucleus away from the centrosome, Dynein, which might be anchored at the nuclear envelop by the LINC complex, exerts pulling forces on microtubules bringing the centrosome in close vicinity of the nucleus. This process has been referred to as the "Magnet" model and has been opposed to the "Velcro" model wherein centrosome-nucleus interaction is mediated by other cytoskeleton components, most likely F-actin since Cytochalasin D treatment is required to obtain centrosome preparations devoid of nucleus [Maro and Bornens, 1980].

Our findings strongly support the latter model since centrosome tethering to the nuclear envelop in B cells is mediated by centrosomal F-actin. Indeed, both centrosomal F-actin inhibition and expression of a dominant-negative mutant of the LINC complex that does not bind F-actin induce the separation of the centrosome from the nucleus, which is highlighted by the increased distance between both organelles. Although it is unlikely that microtubules and Dynein play a major role in centrosome-nucleus attachment in B cells, their contribution to this process shall now be precisely determined. For instance, this might be assessed by monitoring centrosome positioning within cells upon chemical inhibition of Dynein activity or depolymerization of microtubules.

Since the 2000's, lot of efforts have been made to describe and understand the basic cell biological events regulating the ability of B lymphocytes to acquire, process and present antigens. The discovery that, similarly to T cells, B lymphocytes form an immune synapse upon BCR engagement with immobilized antigens represented the first piece of data in this puzzle [Batista et al., 2001]. The immune synapse is seen as a signaling platform where both exocytotic and endocytotic events take place (reviewed in [Yuseff et al., 2009, Obino and Lennon-Dumenil, 2014, Delon, 2000]). The general organization of both B and T cell synapses is similar, with the formation of concentric supramolecular activation clusters (SMACs) supporting BCR- and TCR-mediated signaling required for the proper activation of those cells [Alarcon et al., 2011, Grakoui et al., 1999, Batista et al., 2001]. Of note, the modulation of ERM protein activity is required to promote both B and T cell spreading onto APCs [Faure et al., 2004, Treanor et al., 2011].

Another important set of data bringing forward our understanding of B cell functions has been made by the description of B cell polarization triggered by surface-tethered antigen stimulation by our group [Yuseff et al., 2011, Reversat et al., 2015]. B cell polarization mainly relies on the repositioning of the centrosome towards the newly established immune synapse that dictates the local recruitment of lysosomes and their subsequent secretion to promote antigen extraction and processing [Yuseff et al., 2011]. We have highlighted the conserved polarity machinery Cdc42/Par3/aPKC-ζ as the main complex regulating centrosome repositioning, as well as the microtubule minus-end motor protein Dynein [Reversat et al., 2015]. While Cdc42 is required to promote centrosome repositioning, Par3 and aPKC-ζ play a major role in docking the centrosome at the immune synapse. In addition, we have shown that Dynein recruitment at the immune synapse relies on Par3, regulates BCR microcluster coalescence required for B cell activation and its inhibition impairs centrosome polarization [Reversat et al., 2015].

1. How is B cell polarization coordinated?

The results presented in this manuscript bring new data into this picture. Indeed, we found that upon BCR engagement with immobilized antigens, the Cortactin-like protein HS1 is phosphorylated and accumulates at the immune synapse. This in turn induces the local

recruitment of the Arp2/3 complex, thereby depleting it from the centrosome and decreasing the ability of this organelle to nucleate F-actin. Consequently, the centrosome detaches from the nucleus and polarizes toward the immune synapse. However, the identification of this new mechanism regulating centrosome polarization raises new questions. In particular, how the Cdc42/Par3/aPKC-ζ polarity axis and Dynein activity impact on/cooperate with this new molecular mechanism to efficiently support centrosome polarization remains to be determined. As speculations, we can envision that both pathways are activated downstream of the BCR upon immobilized antigen stimulation and act in parallel to efficiently drive centrosome polarization. While Cdc42/Par3/aPKC-ζ will allow the local recruitment of Dynein, thus promoting BCR microcluster merging at the synapse center and providing the forces required to pull the centrosome forward, HS1-dependent depletion of Arp2/3 from the centrosome will free it from the nucleus to allow its movement. Thus, the polarity cue made by the PAR polarity complex together with the HS1-mediated recruitment of Arp2/3 at the immune synapse might ensure the proper polarization of the centrosome, thereby defining new intracellular routes that are the support of directed lysosome trafficking for them to be recruited and secreted within the synaptic interface. In addition, whereas Arp2/3 recruitment to the immune synapse is dispensable for centrosome polarization, its local activity is nonetheless required for B cells to fulfill their functions, since Arp2/3 inhibition impairs the antigen presentation capacity of B cells (**Figure 41**).

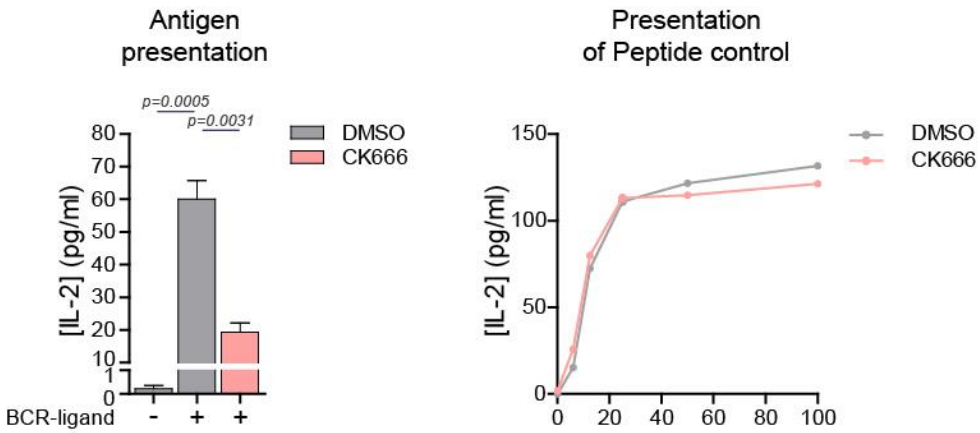

Figure 41. Arp2/3 activity is required for efficient antigen presentation by B cells. Left. Antigen presentation assay with control (DMSO) and CK666-treated B cells stimulated with indicated beads plus the *Lack* antigen. Bar graphs show the mean ± s.e.m. of triplicates. **Right.** Peptide control for cells used in the antigen presentation assay. Graph shows the mean of duplicates. Data are representative of 2 independent experiments.

Therefore, it would be of interest to define the precise role of Arp2/3 at the immune synapse as well as the interconnections that might exist between the two axes in order to complete our view of B cell polarization. For instance, HS1 phosphorylation relies on both Syk and Lyn kinases that are activated downstream the BCR [Hao et al., 2004, Brunati et al., 2005], but whether its accumulation at the immune synapse and subsequent Arp2/3 recruitment only relies on these two kinases or involved the Cdc42/Par3/aPKC-ζ polarity axis remains to be determined.

Interestingly, similarly to their key role in B cells [Arana et al., 2008, Yuseff et al., 2011, Reversat et al., 2015], the Rho GTPases Rac and Cdc42 as well as the polarity protein aPKC-ζ play crucial functions in regulating T cell adhesion, polarization and migration (reviewed in [Rougerie and Delon, 2012]). For instance, aPKC-ζ has been shown to be activated at the T cell immune synapse and regulate the polarization of the secretory machinery [Bertrand et al., 2010]. This is similar to what we have described in B cells [Yuseff et al., 2011]. Together these data highlight the similar mechanisms used by B and T cells to spread and form immune synapses that represent the first step of asymmetric cell organization leading *in fine* to the drastic reorganization of the actin and microtubule cytoskeletons as well as the polarization of organelles, and especially the centrosome, towards the antigen-contact site (reviewed in [Martin-Cofreces et al., 2014, Kumar et al., 2014, Obino and Lennon-Dumenil, 2014]).

2. Mechanisms of centrosome positioning

The precise molecular machinery involved in centrosome polarization towards the immune synapse is not totally elucidated. Although increasing piece of data highlights a key role for Dynein and microtubule-mediated forces in the regulation of centrosome positioning, how precisely this process occurs remains to be determined. In the early eighties, BAJER and coworkers brought the first "*evidence that elongating microtubules can exert a pushing force in living cells*" [Bajer et al., 1982]. Later, microtubule-mediated pushing and pulling forces in association with motor proteins have been involved in chromosome, mitotic spindle and nuclear positioning (reviewed in [Dogterom et al., 2005]). This is mediated by the generation of asymmetric forces supported by the combined capacities of microtubules to contact specific cellular locations, regulate their differential polymerization/depolymerization rates at the level of individual filaments as well as to be assembled in an asymmetric fashion [Burakov et al., 2003, Daga et al., 2006].

Interestingly, when immobilized on substrates, Dynein has been shown to generate pulling forces that are exerted on shrinking MT plus-ends, thus regulating centrosome positioning. Indeed, whereas balanced pulling forces have been involved in centrosome centering, induction of symmetry breaking by locally depolymerizing MTs promotes centrosome displacement and off-centering [Laan et al., 2012, Burakov et al., 2003]. This was also supported by a computational study predicting that forces generated by a strong Dynein activity (and weak Myosin contractility) pull centrosome inward and are required to balance MT plus-end pushing forces that tend to move the centrosome outward, thus resulting in the positioning of the centrosome at the cell center [Zhu et al., 2010].

In T lymphocytes, centrosome polarization relies on the concerted action of both the MT-dependent motor protein Dynein and the actin-based motor protein Myosin II. Dynein localizes at the center of the immune synapse together with TCR microclusters and its local activity induces microtubule end-on capture-shrinkage, thus pulling the centrosome forward [Yi et al., 2013, Liu et al., 2013]. Conversely, Myosin II localizes at the back of T cells, mainly behind the moving centrosome, and potentiates centrosome repositioning through cycles of contraction [Liu et al., 2013]. The coordinated action of both Dynein and Myosin II results in the biphasic polarization of the centrosome towards the T cell synapse, which includes first its directed movement and second its stable docking at the synapse [Yi et al., 2013] (**Figure 42**).

In B cells, whereas Dynein recruitment at the immune synapse and its involvement in centrosome polarization have been shown [Schnyder et al., 2011, Reversat et al., 2015], it is unlikely that Myosin II plays a similar role in these cells than in T lymphocytes. Indeed, unpublished but recurrent observations from the lab highlight the dispensable role of Myosin II in centrosome polarization towards the B cell synapse. Neither its chemical inhibition with Blebbistatin nor its siRNA-mediated silencing impaired centrosome repositioning towards the antigen-contact site. This might result from the major contribution played by Myosin II at the B cell synapse in generating contractile forces required for antigen internalization [Natkanski et al., 2013] (**Figure 42**). However, how Dynein is locally anchored and whether the motor protein induces imbalanced forces upon BCR engagement with surface-tethered antigens that promotes centrosome polarization is an interesting question that shall now be addressed.

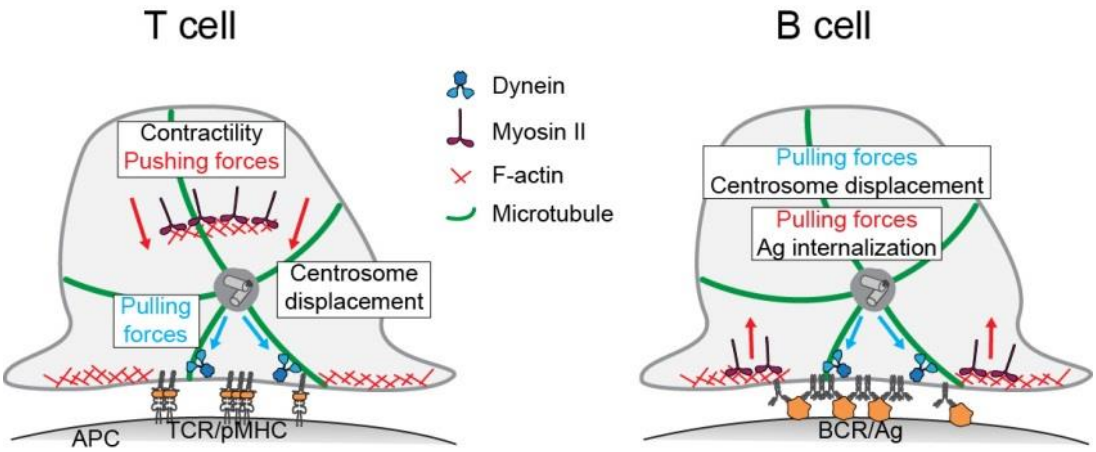

Figure 42. Mechanisms of centrosome positioning in T and B lymphocytes. In T cells, Dynein at the immune synapse pulls on microtubules to promote the forward movement of the centrosome, which is potentiated by Myosin II-dependent contractions at the cell rear. Conversely, both Dynein and Myosin II localize at the B cell synapse where they promote centrosome repositioning and antigen internalization, respectively.

Nevertheless, centrosome polarization in B and T cells shares common features. For instance, GOMEZ and colleagues have shown that Arp2/3 was not required for centrosome repositioning in T cells that rather relies on Formin activity [Gomez et al., 2007]. In the same line, data presented in this manuscript highlight the dispensable role of Arp2/3 in centrosome polarization towards the B cell immune synapse, which was prevented by chemical inhibition of Formins. Interestingly, in T cells, Formin activity has been associated with the regulation of centrosome repositioning by promoting post-translational modification of microtubules. Indeed, the authors showed that Formin-dependent detyrosination of MTs breaks the symmetry of the microtubule network, thus promoting pushing forces that induce centrosome movement [Andres-Delgado et al., 2013, Andres-Delgado et al., 2012].

Whether Formin-dependent polarization of the centrosome in B cells relies on the actin nucleation capacity of Formin proteins or is rather supported by MT-mediated pushing forces induced by MT detyrosination remains to be addressed.

3. Mechanisms of vesicle secretion

Another important aspect in the regulation of B and T cell functions relies on the directed trafficking of vesicles. In B cells, we have shown that BCR engagement with immobilized antigens induces the recruitment and local secretion of lysosomes within the synaptic cleft, which is required for the efficient extraction, processing and presentation of antigens to primed $CD4^+$ T cells [Yuseff et al., 2011]. Similarly, recruitment and secretion of lysosomes and secretory granules at the T cell synapse promote cell-specific functions [Stinchcombe et al., 2006, Lettau et al., 2015].

A common theme in vesicle trafficking and secretion is the involvement of proteins from the SNARE family. These proteins, located at the surface of both vesicle (vSNARE) and acceptor or target compartment (tSNARE), form a complex that promotes the docking and the subsequent fusion of vesicles with their specific acceptor compartments (reviewed in [Bombardier and Munson, 2015]). Of note, the vSNARE protein Vamp-7, initially involved in vesicle exocytosis in neurons (reviewed in [Chaineau et al., 2009]), has been associated with the membrane of secretory lysosomes in NK cells and described to play a critical role in the release of granzyme B by these cells [Casey et al., 2007, Marcet-Palacios et al., 2008]. In T cells, Vamp-7 regulates the trafficking and recruitment of vesicles containing the scaffold protein Lat to the immune synapse and is required for the proper TCR-dependent signaling and activation of T cells [Larghi et al., 2013]. Interestingly, we found that this vSNARE protein plays also a crucial role in the regulation of lysosome secretion at the B cell synapse. Indeed, while lysosome polarization was not affected, Vamp-7 silencing prevents their secretion at the B cell synapse, hence abrogating the ability of B cells to extract and present immobilized antigens to primed $CD4^+$ T cells (unpublished data from M.-I. YUSEFF and J. DIAZ).

Together these observations highlight a determinant function for the vSNARE protein Vamp-7 in the regulation of vesicle trafficking in leukocytes. Whether these Vamp-7-mediated trafficking events are regulated by the same machinery in both B and T cells remains to be elucidated.

4. Cell polarity: the driving ‘‘force’’ of B lymphocyte functions?

Once antigens are extracted and internalized for them to be processed, B cells migrate toward the B-cell/T-cell boundary in order to present MHC-II-peptide complexes to primed $CD4^+$ T cells. While migrating towards the T-cell zone, B cells concentrate internalized antigens in their uropod [Carrasco and Batista, 2007], suggesting that they reverse the polarized phenotype acquired upon BCR engagement with immobilized antigens. This polarized concentration of antigens leads to their asymmetrical distribution among daughter B cells following cell division, providing them with differential antigen presentation capacities [Thaunat et al., 2012]. Noticeably, the contact between B cells and T cells also results in the establishment of an immune synapse, where both cells harbor polarized phenotypes [Duchez et al., 2011].

Interestingly, asymmetrical polarized division of B cells was also observed during the GC reaction and shown to regulate the survival of daughter cells through the unequal inheritance of Bcl-6, IL-21 receptor, and the polarity protein aPKC-ζ [Barnett et al., 2012]. Thus, cell polarity is likely to play an essential role in shaping B cell responses to surface-tethered antigens at their various activation stages. Whether the initial polarity adopted by B cells upon BCR engagement with immobilized antigens drives the overall cell polarity that B cells maintain throughout asymmetric cell division as well as GC reaction remains to be determined.

5. Toward the identification of new mechanisms regulating B cell polarity

The identification of proteins differentially associated with the centrosome between non-activated and activated B lymphocytes has given to us the unique opportunity to identify additional mechanisms involved in the regulation of B cell polarization. To this end, I developed a medium-throughput screening based on cell imaging and siRNA-mediated silencing of individual proteins. Among the proteins we identified as differentially associated with the centrosome of activated cells, we selected 187 of them that were described to regulate the cytoskeleton, vesicle or protein trafficking as well as motor proteins (**Figure 43a**). We completed this list with 45 proteins coming from the actin and microtubule literature, which were not identified by our mass spectrometry analysis. Following the silencing of each of these 232 proteins, cells were stimulated with BCR-$ligand^+$ beads and the polarization of the centrosome and lysosomes have been assessed (**Figure 43b, c**).

We first used control cells to perform a correlation analysis between centrosome and lysosome polarization. As expected, polarization of both the centrosome and lysosomes displayed a strong correlation in most of the cells (~85%, **Figure 43d**). Intriguingly, while we thought that centrosome repositioning towards the immune synapse was strictly required for lysosome recruitment and secretion, we found more cells for which lysosomes, but not the centrosome, were polarized towards the immune synapse (~12% versus ~3% of cells having polarized their centrosome and not their lysosomes, **Figure 43d**). These observations suggest that centrosome and lysosome polarization does not occur in a sequential manner but rather results from the concomitant repositioning of both compartments towards the immune synapse.

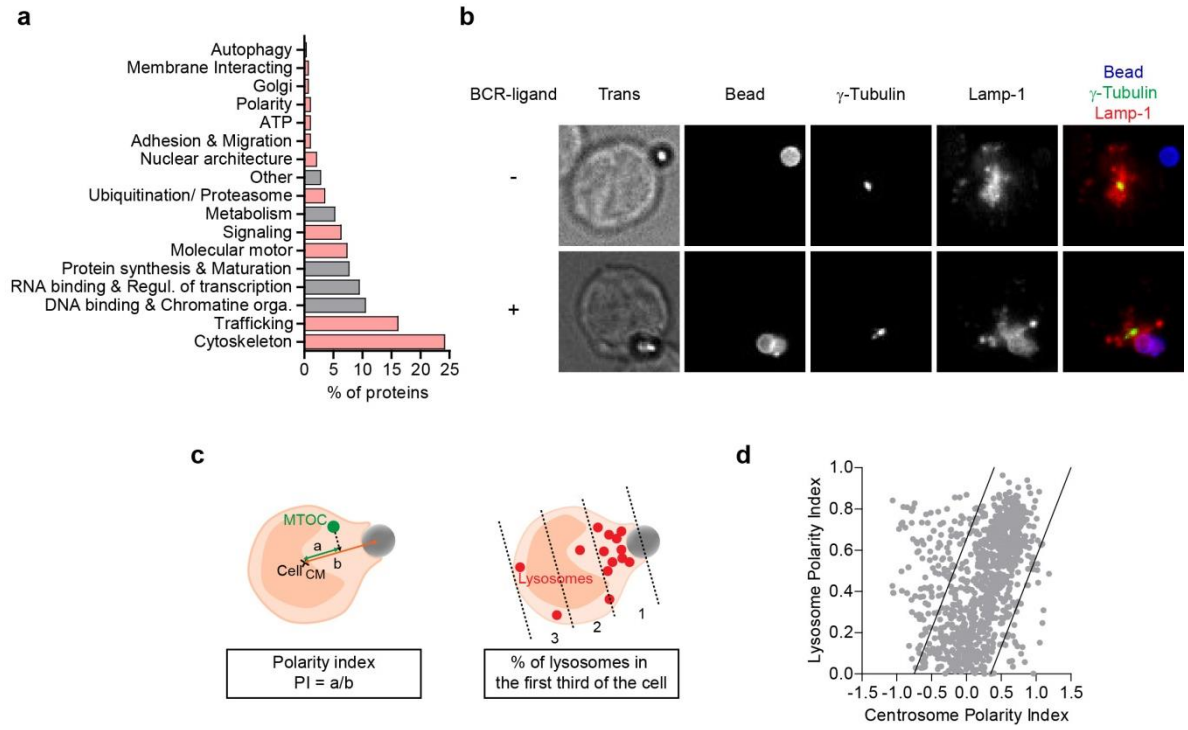

Figure 43. Medium-throughput screening to uncover new mechanisms of B cell polarization. (**a**) Functional classification (Uniprot database) of the proteins differentially associated with the centrosome between non-activated and activated B cells. Functional groups included in the screen are shown in red. (**b**) Representative images of B cells stimulated with either BCR-ligand^{-} or BCR-ligand^{+} beads for 90 min, fixed, stained for the bead, the centrosome and lysosomes and acquired using the XPress automatized microscope. (**c**) Schematics depicting the calculation of centrosome (left) and lysosome (right) polarity indexes. (**d**) Correlation analysis between centrosome and lysosome polarity indexes of control cells (siCtrl). Data were pooled from 3 independent experiments. n > 1000 cells.

Among the 232 tested proteins, we found 9 hits whose silencing affects the polarization of both the centrosome and lysosomes, 6 affecting only lysosome polarization and 14 affecting only centrosome polarization. The latter comprised 4 components (Snf8 or Vps22, Vps24 or Chmp3, Vps2 or Chmp2b and Ist1) of the endosomal sorting complexes required for transport (ESCRT) machinery involved in the formation of intralumenal vesicles within multi-vesicular bodies (MVBs) (reviewed in [Henne et al., 2013, Woodman, 2016]), viral particle budding or plasma membrane repair (reviewed in [Olmos and Carlton, 2016]). We therefore focused our study in understanding the role of Chmp2b (Charged multi-vesicular body protein 2b) as potential regulator of B cell polarization (**Figure 44a, red dot**), since this protein belongs to the core of the ESCRT-III complex. As mentioned above, while we thought that centrosome polarization was required for the recruitment of lysosomes to the immune synapse, impaired centrosome but not lysosome polarization was confirmed by immunofluorescence in primary spleen B cells lacking Chmp2b expression (**Figure 44b**). Two hypotheses might explain this apparent discrepancy. First, laser ablation was used to assess whether centrosome repositioning to the immune synapse was required to support local lysosome recruitment. This approach might be too harsh for the cells and might induce side-effects, such as MT depolymerization, leading to the observed phenotype. Second, the ESCRT-III complex might act as a "linker" between the lysosomal compartment and the centrosome/MTs thus connecting both structures. The breaking of such link by silencing one subunit of the complex, which has been shown to inhibit the function of the whole complex, might result in the removal of the apparent centrosome dependency observed during lysosome polarization. Having access to the dynamics of lysosome polarization in that context (e.g. by time-lapse imaging) might highlight valuable information regarding the way lysosome trafficking occurs in the absence of Chmp2b.

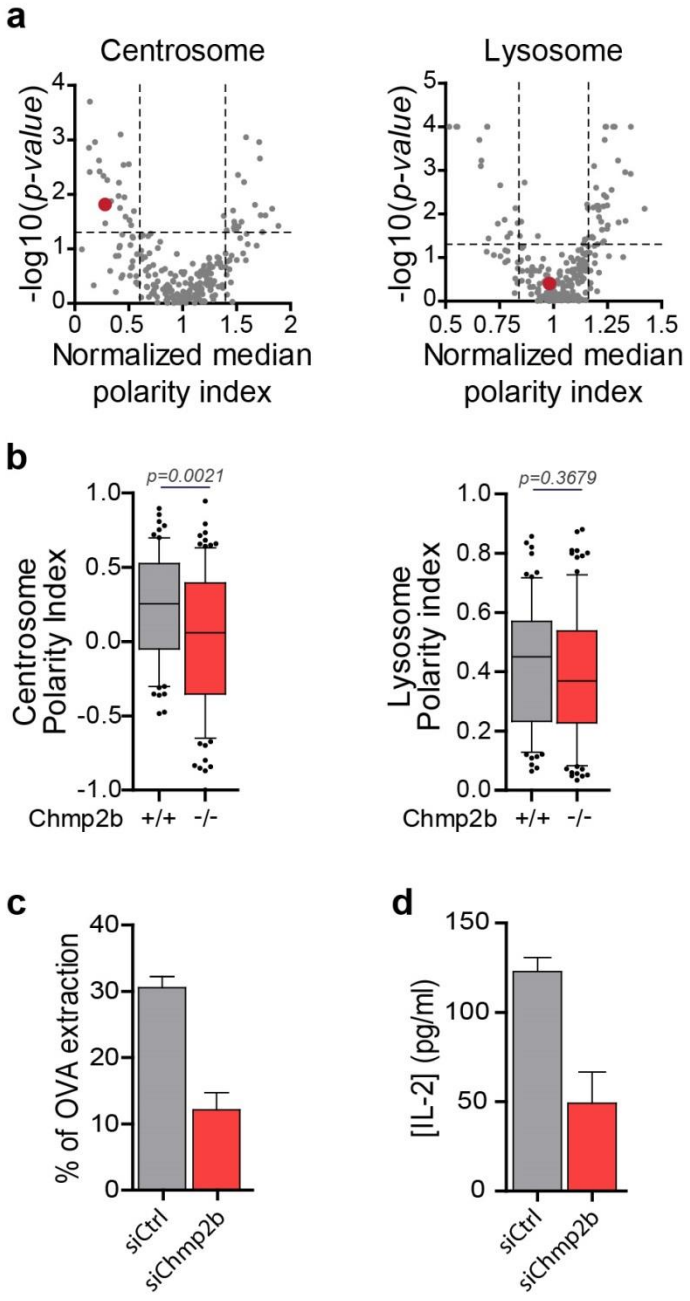

Figure 44. Impaired centrosome but not lysosome polarization in B lymphocytes lacking Chmp2b. (**a**) Normalized median centrosome (left) and lysosome (right) polarity indexes of each of the 232 proteins assessed. Data were pooled from 3 independent experiments and normalized with respect to control condition (siCtrl=1) by plate and by replicate. Horizontal dashed line represents the threshold for statistical significance (p-value ≤ 0.05). Vertical dashed lines represent the biological threshold used to select candidates (± 1 standard deviation). Red dots highlight polarity indexes of cells lacking Chmp2b expression. (**b**) Centrosome (left) and lysosome (right) polarity indexes of control (+/+) or Chmp2b-KO (-/-) spleen B cells. Data were pooled from 3 mice. (**c, d**) Antigen extraction (**c**) and presentation (**d**) assays of control and Chmp2b-silenced B cells. Data were pooled from 2 independent experiments.

Despite their ability to polarize lysosomes, B cells lacking Chmp2b displayed a reduced capacity to extract and present immobilized antigens (**Figure 44c, d**). Interestingly, an unexpected function for the ESCRT machinery has been reported as regulator of centrosome integrity. Indeed, the absence of the ESCRT-III complex results in the generation of multiple and/or fragmented centrosomes in interphase cells [Morita et al., 2010]. It is likely that centrosome integrity is a pre-requisite for its repositioning and may thus impact on its ability to polarize. In addition, in *Drosophila melanogaster*, the lack of ESCRT components has been described to induce the loss of apical-basal polarity and result in the mislocalization of aPKC [Lobert and Stenmark, 2011]. Knowing the crucial role of aPKC-ζ in the regulation of centrosome repositioning to the B cell immune synapse, it would be of special interest to assess whether Chmp2b deficiency affects aPKC-ζ localization and/or activation in B cells.

How lysosome polarization can be achieved in the absence of centrosome repositioning represents another interesting point that remains to be elucidated. One could envision that the lack of ESCRT components might disrupt the proper interaction between microtubules and lysosomes. Indeed, in the hypothesis where ESCRT components regulate the interaction between lysosomes and Dynein (or adaptor proteins), the lack of the complex will prevent vesicle loading with Dynein thus giving the opportunity to Kinesins to bind to lysosomes. This would results in the transport of lysosomes from the cell center towards the periphery, thus bypassing the need to polarize the centrosome to orient vesicle trafficking.

Finally, why B cells lacking Chmp2b are not able to efficiently extract and present antigens? Two non–exclusive hypotheses might be envisioned. First, knowing the key role played by the ESCRT machinery in membrane remodeling, the observed decrease in antigen extraction might result from a default in lysosome secretion at the immune synapse. Second, it might also results from the well-described abnormal phenotype of the endo-lysosomal compartment in the absence of the ESCRT machinery. Indeed, yeast lacking *Vps* (Vacuolar protein sorting) components and especially *Vps2*, the Chmp2 homologous in yeast, harbors exaggerated endosome-like compartments referred to as Class E compartments [Raymond et al., 1992] (and reviewed in [Coonrod and Stevens, 2010]). Interestingly such compartments have also been identified in mammalian cells [Doyotte et al., 2005]. In the latter study, silencing of *tumour susceptibility gene 101* (TGS101), another member of the ESCRT machinery, impairs protein sorting to MVBs as well as their proper transport towards lysosomes. This might be a possible explanation for the defect in antigen extraction and

presentation we observed in B cells lacking Chmp2b expression and would need to be addressed. In line with this hypothesis, preliminary electron microscopy observations suggest that Chmp2b KO spleen B cells display an abnormal endo-lysosomal compartment (not shown). One could envision studying the whole endo-lysosomal compartment in WT and Chmp2b-deficient B cells, for instance by assessing the number/percentage of intracellular vesicles harboring specific markers of early and late endosomes, mature lysosomes or recycling endosomes (Rab5, Rab7 and EEA1, Lamp-1 or Rab11, respectively), the lysosomal pH as well as the capacity of those lysosomes to be secreted at the immune synapse upon surface-tethered antigen stimulation.

The role of Chmp2b in the regulation of B cell polarity and functions is currently under study in the lab and might reveal unexpected new mechanisms controlling such processes.

1. Competition for the Arp2/3 complex

Our observations that the decrease of centrosomal F-actin upon B cell stimulation correlates with the concomitant increased of F-actin at the immune synapse suggest that the centrosome and the immune synapse compete for the Arp2/3 complex. Although we cannot formally exclude that there is a direct exchange between centrosomal and synaptic Arp2/3, we think that this is unlikely in view of data showing that most Arp2/3 resides in the cytosol [Higgs et al., 1999]. We therefore propose that both the centrosome and the synapse are rather competing for the cytosolic pool of Arp2/3 highlighting the existence of an effective competition between distinct subcellular locations for this actin nucleating complex (**Figure 45**). As a result of this competition, cells would respond to extracellular stimuli by favoring one biological process over another, what might provide a simple mechanism for cells to coordinate their functions in time and space. One could speculate that increasing the amounts of Arp2/3 available within the cytosol might be therefore sufficient to release this apparent competition. Even though we tempted to assess this particular point, the overexpression of components of the Arp2/3 complex in B cells resulted in the loss of Arp2/3 subcellular localizations and the generation of aberrant cytoplasmic F-actin structures, which had not allow us monitoring the impact of Arp2/3 recruitment at the immune synapse on its centrosomal counter-part in this particular context.

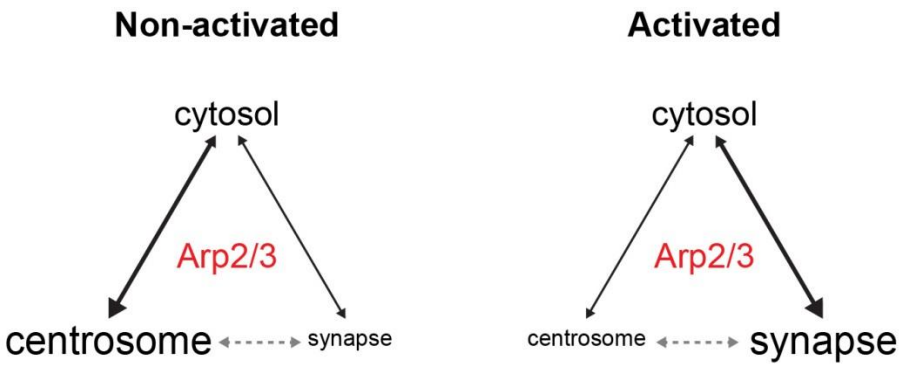

Figure 45. Proposed model for the competition of Arp2/3 by distinct subcellular localizations. Under resting conditions, Arp2/3 is mainly recruited to the centrosome and controls centrosome positioning. Upon B cell activation, Arp2/3 is recruited to the immune synapse where it regulates effector functions. It is unlikely that a direct exchange between the centrosome and the synapse occurs. We propose that the two subcellular localizations are rather competing for the cytosolic pool of Arp2/3.

In addition, the existence of a competition for cytosolic Arp2/3 implies that the pool of centrosome-associated Arp2/3 might be minor in adherent cells as compared to lymphocytes, given that they use the Arp2/3 complex to form adhesive structures such as lamellipodia. Interestingly, it has been shown that immune synapses share many features with lamellipodia [Sims et al., 2007] (**Figure 46**). Indeed, the radial symmetry of the immune synapse can be seen as a "folded" lamellipodium thus preventing cell motion. In contrast, it has been shown that immune synapse symmetry breaking induces T cell migration [Sims et al., 2007]. Based on these observations, we can speculate that the competition between the centrosome and the immune synapse for Arp2/3 might also apply to the centrosome and the lamellipodium of migrating cells. Whether the centrosome of migrating cells is able to assemble actin networks and how the regulation of this centrosomal F-actin might be influenced by actin dynamics within the lamellipodium remain interesting questions that shall now be addressed.

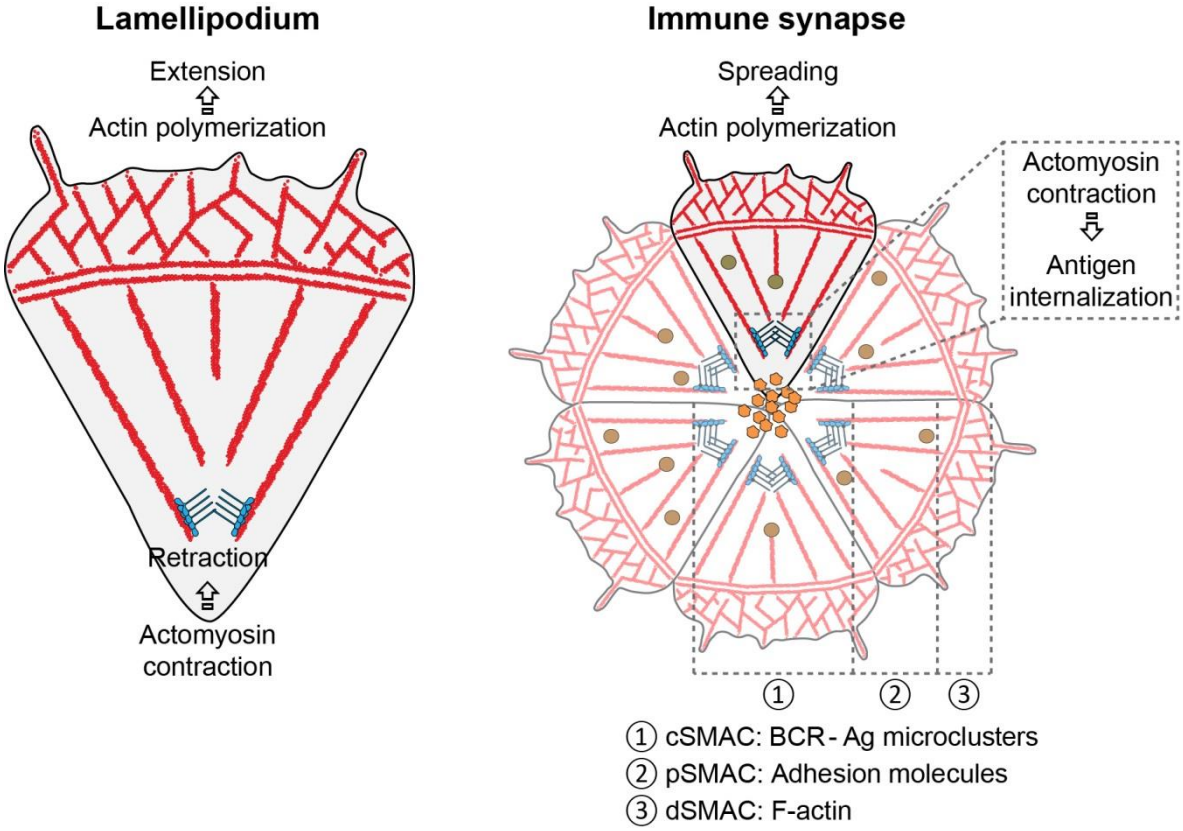

Figure 46. Structural organization of the lamellipodium and the immune synapse. The immune synapse might be seen as a "folded" lamellipodium where symmetric actin polymerization at the leading edge promotes cell spreading and actomyosin contractility at the rear/center allows antigen internalization.

Taking into account the similarities between the immune synapse and the lamellipodium, immune synapses might be viewed as particular adhesive structures that support specific cellular functions. In other words, as the lamellipodium promotes cell migration by orchestrating cytoskeleton dynamics and cell contractility; the immune synapse might act as a platform connecting intracellular trafficking with extracellular stimuli to ensure the proper function of the cell. This might imply that cells have the capacity to divert cellular machineries to adapt their responses to their needs. To which extend such regulatory mechanism is conserved in different biological processes that require centrosome polarization and different cellular systems represent very exciting fields of future investigations.

2. Modulation of cell adhesion to tune B lymphocyte functions

Based on the concept described above – wherein the immune synapse is assimilated to an adhesive structure – an intimate communication shall exist between the immune synapse and B cell function. Accordingly, modulation of cell adhesion shall impact on B lymphocyte functions. In line with this hypothesis, the engagement of the integrin LFA-1 with its counter-receptor ICAM-1 has been shown to enhance BCR-dependent cell spreading onto lipid-bilayers, thus promoting the establishment of the immune synapse and decreasing the threshold of B cell activation [Carrasco et al., 2004]. Another piece of data arguing in this direction is brought by our work on the role of extracellular Galectin-8 in the modulation of B cell functions. Indeed, Galectin-8 has been described to promote or inhibit adhesion in a wide range of cell types. Several studies converge to highlight a dual role for this sugar-binding protein in modulating cell adhesion. While surface-immobilized Galectin-8 promotes cell spreading, its addition in solution tempts to decrease adhesion mainly by counter-acting the effect of integrins [Zick et al., 2004]. The pro-adhesive properties of Galectin-8 are mediated by its ability to bind glycosylated surface proteins, since truncation of one of its carbohydrate recognition domains (CRD, involved in sugar binding) or addition within the milieu of β-lactose (a well-described competing sugar) drastically reduces cell adhesion [Levy et al., 2001, Diskin et al., 2009]. Of note, upon interaction with integrins, Galectin-8 potentiates the integrin-mediated signaling cascade that ultimately induces the remodeling of the actin cytoskeleton to enhance cell adhesion [Levy et al., 2003, Carcamo et al., 2006]. Preliminary results obtained in the lab show that surface-immobilized Galectin-8 also favors the spreading of B cells, even independently of BCR engagement (**Figure 47**). These data suggest that

Galectin-8 might promote the formation of the immune synapse upon BCR engagement with immobilized antigens, thus enhancing B cell functions.

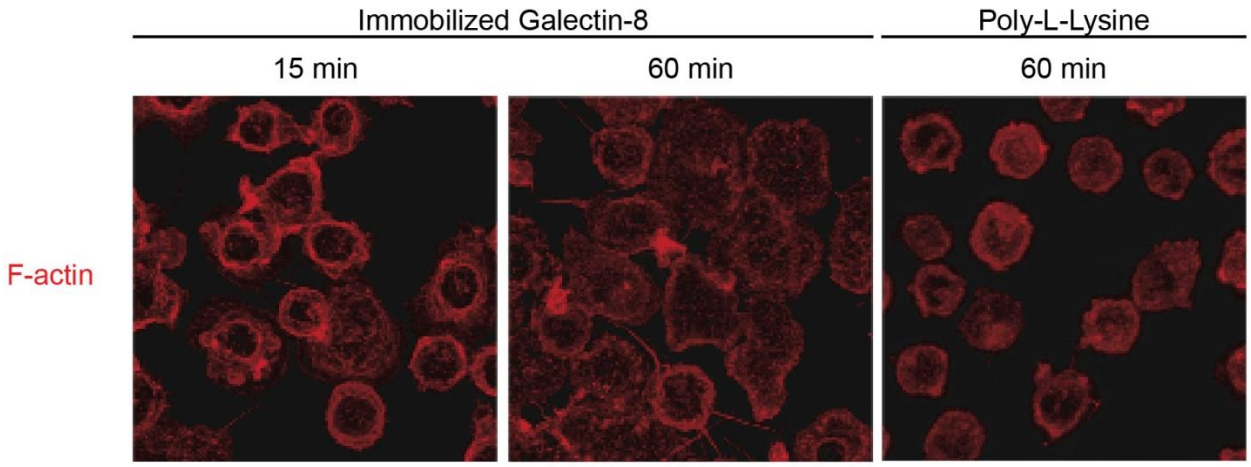

Figure 47. Galectin-8 enhances B cell spreading. B cells were plated on poly-L-lysine- or Galectin-8-coated surfaces for indicated time, fixed and stained for F-actin (Phalloidin).

In agreement with this hypothesis, we here show that the presence of Galectin-8 in the extracellular space, e.g. coated at the surface of beads, promotes the arrest phase of B cells upon antigen encounter *in vivo*, a process shown to be required for immune synapse formation and antigen internalization by B cells [Carrasco and Batista, 2007]. The presence of Galectin-8 in the B cell microenvironment also enhances the secretion of lysosomes at the immune synapse induced by the engagement of the BCR with surface-tethered antigens. Consequently to this increase in lysosomal secretion, B cells extract and present peptide-MHC-II complexes to primed $CD4^+$ T cells more efficiently. However, the precise mechanism involved in this process remains to be determined. One could envision that by modulating B cell adhesion, extracellular Galectin-8 potentiates the formation of the immune synapse, hence providing B cells with a better capacity to polarize, extract and present peptide-MHC-II complexes to primed $CD4^+$ T cells. Indeed, the enhanced adherent properties of B cells in presence of extracellular Galectin-8 would imply that the recruitment of Arp2/3 at the immune synapse might be more important in this particular context, since this actin nucleation complex support cell spreading. This might result in an exaggerated subcellular competition for Arp2/3 leading to the strong decrease of this complex from the centrosome.

3. The integrin LFA-1: a putative receptor for Galectin-8?

As mentioned above, numerous studies have highlighted the key role of integrins in supporting Galectin-8-mediated cell adhesion. Interestingly, Galectin-8 has been shown to interact with the integrin Lymphocyte Function-Associated Antigen-1 (LFA-1) [Vicuna et al., 2013], a well-characterized integrin involved in cell adhesion and immune synapse formation in T cells (reviewed in [Springer and Dustin, 2012]). Whether Galectin-8 promotes B cell functions by interacting with LFA-1 remains to be addressed but this would provide a putative mechanism of action. In line with this hypothesis, we have identified both subunits (α_L and β_2) of LFA-1 as Galectin-8-interacting proteins in a GST-Pull down experiment. Of note, this experiment has also highlighted that the BCR itself might interact with Galectin-8, providing another possible mechanism to explain the observed effect of Galectin-8 on B cell functions. The use of LFA-1 blocking antibodies or LFA-1 silencing in B cells might be useful tools to precisely determine whether Galectin-8 acts through this integrin to promote B cell functions.

The interaction between extracellular Galectin-8 and a B cell surface protein, providing B cells with a better capacity to extract and present antigens, implies that Galectin-8 is present within this particular environment. As shown in Figure 35b (Results section), Galectin-8 is expressed within the sub-capsular sinus (SCS) area of lymph nodes, where B cells acquire antigens immobilized at the surface of $CD169^+$ SCS macrophages [Carrasco and Batista, 2007, Junt et al., 2007]. Whether and how Galectin-8 is immobilized at the surface of those cells to promote B cell spreading and support immune synapse formation remain open questions. Interestingly, it has been reported that in addition to its ability to bind integrins, Galectin-8 interacts with the transmembrane glycoprotein Podoplanin (PDPN, also known as gp38, T1α) [Cueni and Detmar, 2009]. Preliminary data I obtained suggest that both the RAW macrophage mouse cell line and primary $CD169^+$ SCS macrophages express Podoplanin (**Figure 48**), giving a potential mechanism for such immobilization of Galectin-8 at the cell surface of antigen-carrying cells. In order to test this hypothesis, one could envision first to add soluble Galectin-8 in the culture medium of PDPN-expressing macrophages and monitor whether Galectin-8 is immobilized at the surface of these cells. Obviously, other experiments would be required to demonstrate the specificity of the Galectin-8/PDPN interaction. For instance, we could use similar assays but with macrophages lacking PDPN expression, this would result in the loss of Galectin-8 immobilization at their cell surface. This simple setting might be complemented with particulate antigens tethered at the surface of those macrophages

and B cells to assess whether PDPN-mediated immobilization of Galectin-8 at the surface of macrophages is sufficient to recapitulate the effect of Galectin-8 on B cell functions we observed when this protein is immobilized at the surface of beads.

The identification of one extracellular protein promoting B cell functions raises new questions and especially does Galectin-8 act alone or in concert with other extracellular and/or matrix proteins present within the lymphoid tissue microenvironment to modulate cell adhesion and tune B cell functions?

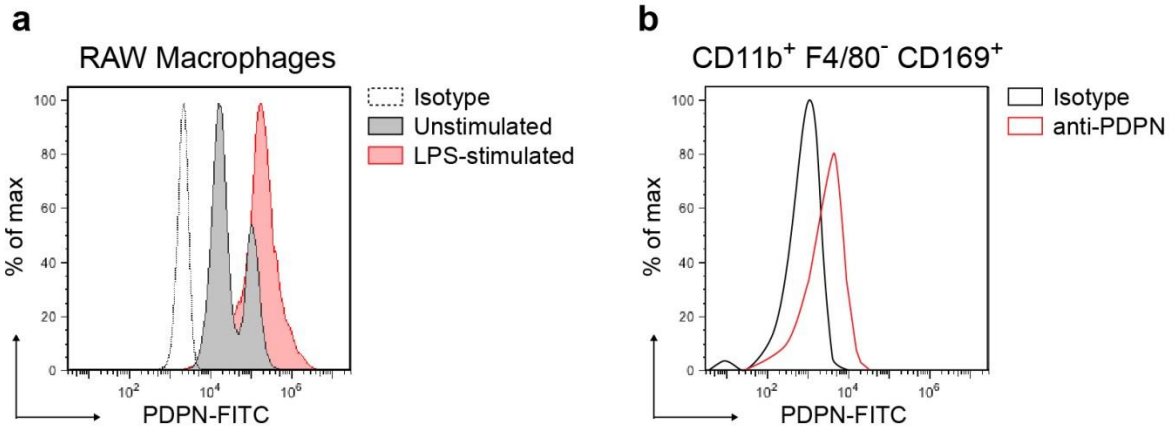

Figure 48. Putative interactants of Galectin-8. (**a**) RAW macrophages were stimulated or not with 1 µg/ml LPS for 16 h before assessing their surface levels of Podoplanin. (**b**) Surface levels of Podoplanin expressed by sub-capsular macrophages (defined as $CD11b^{+}$, $F4/80^{-}$, $CD169^{+}$) in lymph node-cell suspension.

4. Role of Galectins in modulating lymphocyte functions

Beyond Galectin-8, other members of the Galectin family have been described to modulate lymphocyte functions. For instance, stromal-cell-derived Galectin-9 secreted in the extracellular milieu possesses anti-proliferative properties on B and T cells resulting in the decrease of immunoglobulin (Ig) secretion [Ungerer et al., 2014]. Conversely, upon antigenic challenge, the up-regulation of the transcription factor B lymphocyte-induced maturation protein-1 (Blimp-1) promotes the production and secretion of Galectin-1 by B cells that binds glycosylated proteins at their surface and promotes Ig production [Tsai et al., 2008, Zuniga et al., 2001]. This might result from the enhanced phosphorylation of Syk, Btk and PI3K, key players of the signaling cascade downstream the BCR, as well as from the pro-proliferative effects observed for extracellular Galectin-1 on B cells [Tsai et al., 2014]. On the same line, Galectin-1 produced by B cells upon activation is required for their differentiation into plasma cells and has been described to support cell survival and thus required to maintain Ag-specific Ig titers [Anginot et al., 2013]. Of note, Galectin-1 has also been involved in the modulation of B cell responses since it induces T cell apoptosis, thus negatively impacting on B cell/T cell cooperation [Zuniga et al., 2001].

In T cells, the formation of Galectin lattices within the extracellular space has been described to mainly possess inhibitory properties on cell proliferation and/or activation by preventing ligand-independent TCR activation or by modulating the strength of TCR signaling (reviewed in [Seminario and Bunnell, 2008, Grigorian et al., 2009]). In line with these observations, Galectin-8 has been shown to negatively regulate T cell activation by counter-acting LFA-1 function and inducing T cell apoptosis [Vicuna et al., 2013]. Conversely, some studies report a positive effect of this Galectin in promoting regulatory T cell differentiation by impacting on IL-2 and TGF-β signaling [Sampson et al., 2016], providing co-stimulatory signals required for the proper antigen-mediated activation of T cells or inducing their antigen-independent proliferation [Schroeder et al., 2016]. Altogether these observations highlight a key role for Galectins in the regulation of both B and T cell functions.

However, some work is still needed to better understand how Galectins, and more generally extracellular proteins, regulate lymphocyte responsiveness to antigenic stimulation and how they act (sequentially, protein renewal, neo-secretion…?) to ensure the proper

coordination of the different cell types they act on. The large spectrum of effects induced by these proteins necessarily implies that their action must be tightly regulated in time and space. How such spatio-temporal regulation is orchestrated remains to be discovered and represents an interesting field for future investigations that might shed light on unexpected coordinated processes in the modulation of lymphocyte functions.

Over the two last decades, the idea that B cells encounter their cognate antigens in an immobilized form, e.g. at the surface of $CD169^+$ SCS macrophages, has emerged and is now well-accepted. In contrast to what has been described for soluble antigens, engagement of BCRs with surface-tethered antigens results in the establishment of close cell-cell interactions at the site of antigen contact. This leads to the formation of what is now known as the B cell immune synapse that might be viewed as a particular adhesive structure supporting specific cellular functions. The formation of the immune synapse at the antigen-contact site results in the asymmetric organization of B cells that ultimately induces B cell polarization. This process relies on the repositioning of the centrosome towards the immune synapse and the subsequent recruitment and secretion of lysosomes within the synaptic cleft. B cell polarization is strictly required for these cells to extract, process and present antigenic peptides loaded onto MHC-II molecules to primed $CD4^+$ T cells. Although the first molecular players regulating B cell polarization have been identified by former members of the lab, the precise mechanism governing centrosome repositioning towards the immune synapse remained to be elucidated. We here highlight an unexpected role for the pool of centrosome-associated F-actin in regulating the ability of the centrosome to polarize in B cells. This work represents the first description of such mechanism whereby F-actin nucleation at the centrosome, regulated by the availability of the Arp2/3 complex, determines the capacity of the centrosome to polarize in response to external stimuli.

In addition, the increasing pieces of data suggesting that tissue microenvironment might regulate various steps of B cell differentiation, activation and functions prompted us to investigate whether such cues could modulate the ability of B cells to polarize in response to immobilized antigen stimulation. In that context, we found that the presence of the glycan-binding protein Galectin-8 in the extracellular space enhanced lysosome secretion at the immune synapse, thus providing B cells with an enhanced capacity to extract and present immobilized antigens to primed $CD4^+$ T cells. These data describe for the first time the involvement of such extracellular cues in the modulation of B cell polarization and subsequently in tuning B cell functions. They further suggest that by modulating B cell adhesion/spreading onto antigen-presenting cells, proteins present within the lymphoid microenvironment might allow B cell tuning their responses to extracellular stimuli.

Taken together, these findings highlight the complex mechanisms used by a cell to efficiently respond to stimuli. First, the identification of the centrosome as being both an actin- and microtubule-organizing center highlights once again the pivotal role played by the crosstalk between both the actin and microtubule cytoskeletons in regulating cellular functions. Indeed, our data suggesting that actin and microtubule nucleation at the centrosome are co-regulated illustrate how a cell is able to finely tune precise cellular functions supported by the same structure/organelle to promote specific function. Second, the concept that the immune synapse might be seen as an adhesive structure that support specific cellular functions has important implications in our understanding of lymphocyte responses. Indeed, beyond its function in orienting cell polarization and responses, the immune synapse might play key roles in sensing lymphoid microenvironment allowing cells to adapt their adhesive properties to finely regulate their specific effector functions. Third, the existence of an effective competition for the cytosolic pool of Arp2/3 between distinct subcellular localizations to ensure the proper effector functions of a cell opens new roads for future investigations. This might have a major impact in cell biology since centrosome-associated F-actin might control cell polarization in many different cellular systems that rely on centrosome repositioning to achieve their specific cellular functions.

This work brings new pieces in the puzzle of the basic cell biological events governing B cell polarization but further studied are still needed to fully understand the exact mechanisms regulating this process. It would be of particular interest to better define how the different mechanisms described in this manuscript – i.e. the role of the PAR polarity complex and Dynein, the HS1-dependent recruitment of Arp2/3 at the immune synapse as well as the effect of extracellular cues – cooperate to ensure that B cells respond at the good time, at the right place and in the appropriate manner to antigenic stimulation. The study of such mechanisms in *in vivo* models would also represent another level of investigations that should highlight unexpected (and perhaps under-estimated) relationships between B cell responsiveness and functions and neighboring cells, such as stromal or other immune cells, present within the tissue microenvironment.

In addition, the preliminary results obtained from the medium throughput screening I performed during my thesis suggest that the mechanisms regulating B cell polarization is not as simple as we have thought but rather might result from complex interconnections between

different pathways. Additional work is here also required to fully understand the interdependencies that govern organelle repositioning in B cells.

How is organelle polarization tightly coordinated in time and space in B cells? How B cells integrate the various incoming signals, such as antigen recognition and extracellular cues, to self-reorganize and adapt their response? What is the impact of B cell polarity on the humoral immune response in animals and Humans? The answers to these questions represent the next challenges to be addressed…

MATERIAL AND METHODS

Cells and Cell Culture. The mouse IgG^+ B lymphoma cell line IIA1.6 (derived from the A20 cell line [ATCC #: TIB-208]) and the LMR7.5 T cell hybridoma that recognizes I-Ad-$Lack_{156–173}$ complexes (from and described in [Malherbe et al., 2000]) were cultured as previously reported [Yuseff et al., 2011] in CLICK medium (RPMI 1640 – GlutaMaxTM-I supplemented with 10% fetal calf serum, 1% penicillin–streptomycin, 0.1% β-mercaptoethanol, and 2% sodium pyruvate). All cell culture products were purchased from GIBCO/Life Technologies. All experiments were conducted in 50% CLICK / 50% RPMI 1640 – GlutaMaxTM-I.

siRNA. Protein silencing was achieved using the Neon transfection system (Invitrogen, Life Technologies). Briefly, B cells were washed in PBS, resuspended in Buffer R at a density of $50x10^6$ cells/ml and pre-designed ON-TARGETplus SMARTpool Non-targeting (siCtrl), HS1-, Arp2-, Arp3- or WASH-targeting siRNA (Dharmacon, GE Healthcare) were added at a final concentration of 200 nM. Cells were then electroporated (1300 Volts, 2 pulses, 20 ms/pulse) using 10 µl tips and incubated in CLICK medium for 60 to 72 h. Silencing efficiency was analysed by Western blot as described below.

Plasmids. The eGFP-Centrin1 and Utrophin-RFP plasmids were obtained from M. Bornens and M. Piel, respectively (Institut Curie, Paris, France). The eGFP-Centrin1-VCA plasmid was obtained by sub-cloning in frame the VCA domain of WASH at the C-terminus of the eGFP-Centrin1 construct. Briefly, the Centrin1 cDNA deleted from its stop codon was amplified from the eGFP-Centrin1 plasmid using the following primers: Forward: 5'-ctaggtaccatggcttccggcttcaaga-3' and Reverse: 5'-gcaggatccgtaa aggctggtcttcttcat-3' (which include KpnI and BamHI restriction sites (underlined), respectively). The WASH VCA cDNA was amplified from a previously home-made (A. Gautreau) WASH plasmid by using the primers: Forward: 5'-ttaggatccTCCGGACTCAGA TCTCGAGCTCAAGCTTCGAATTCTGCAGTCGACcagggagcccctaagga-3' (which includes BamHI restriction site (underlined) and the sequence for a peptide linker (upper-case)) and Reverse: 5'-gattctagaTCAggactcccagtcctcct-3' (which includes XbaI restriction site (underlined) and a stop codon (upper-case)). Both fragments were then sub-cloned in frame within the original vector using KpnI and XbaI restriction enzymes. BamHI restriction enzyme was used to orient the two fragments. The resulting eGFP-Centrin1-VCA plasmid was sequenced to ensure sequence integrity. The LINC-DN (Nesprin-2 SRKASH) plasmid

was obtained from E.R. Gomes and described in [Luxton et al., 2010]. Plasmid expression was achieved by electroporating $2x10^6$ B lymphoma cells with 1 or 3 µg of plasmid using the Amaxa Cell Line Nucleofactor Kit R (T-016 program, Lonza). Cells were incubated in CLICK medium for 16 to 20 h before analysis.

Reagents. The Lack antigen was produced and purified by the Recombinant Protein platform (UMR144, Institut Curie, Paris, France) and Lack peptide (aa 156-173) was synthetized by PolyPeptide Group. Cytochalasin D and Nocodazole used from centrosome purification were from Sigma Aldrich. For inhibition of Arp2/3 and Formin activity, cells were pre-treated with 25 µM CK666 or Smifh2 (Tocris Bioscience) for 30 min prior to be stimulated for indicated time in presence of the drug, respectively. Recombinant Galectin-8 was purchased from Sigma Aldrich.

Antibodies. The following primary antibodies were used for immunofluorescence: rabbit anti-γ-Tubulin (Abcam, #Ab11317, 1/2000), FITC-conjugated mouse anti-α-Tubulin (Abcam, #Ab64503, 1/100), rabbit anti-Arp2 (Abcam, #Ab47654, 1/200), rabbit anti-HS1 and rabbit anti-phospho-HS1 (both from Cell Signaling Technologies, #4557S and #8714P, respectively, 1/50), rabbit anti-WASH (home-made as previously described [Derivery et al., 2009], 1/250), human anti-GFP and anti-RFP (Recombinant antibodies platform, Institut Curie, Paris, France, 1/200). The following secondary antibodies were used: AlexaFluor488-, AlexaFluor568-, Cy3-, Cy5- and AlexaFluor647-conjugated $F(ab')_2$ donkey anti-rabbit (Jackson ImmunoResearch, 1/300) and AlexaFluor488- and Cy3- conjugated donkey anti-human (Life Technologies and Jackson ImmunoResearch, respectively, 1/200). F-actin was stained using AlexaFluor546- or AlexaFluor647-conjugated Phalloidin (Life Technologies, #A22283 and # A22287, respectively, 1/100). Nuclei were stained using 4′,6-Diamidino-2-phenyindole (DAPI, Sigma Aldrich, 1/5000).

For Western blotting, the following antibodies were used: mouse anti-γ-Tubulin (Sigma Aldrich, #T6557-.2ML, 1/500), rabbit anti-HS1, phospho-HS1 and phospho-Erk (Cell Signaling Technologies, #4557S, #8714P and #4377S, respectively, 1/1000), rabbit anti-Arp2 (Abcam, #Ab47654, 1/200), rabbit anti-WASH (home-made as previously described [Derivery et al., 2009], 1/250), mouse anti-Arp3 and anti-vinculin (Sigma Aldrich, #A5979-200UL , 1/200 and #V9264-200UL, 1/1000, respectively), followed by horseradish peroxidase (HRP)-conjugated donkey anti-mouse or rabbit (Jackson ImmunoResearch, 1/5000).

Preparation of BCR-ligand-coated beads. 4×10^7 3 µm latex NH2-beads (Polyscience) were activated with 8% glutaraldehyde (Sigma Aldrich) for 2 h at room temperature. Beads were washed with phosphate-buffered saline (PBS) and incubated overnight at 4ºC with different ligands: 100 µg.ml-1 of either $F(ab')_2$ goat anti-mouse IgG (BCR-ligand$^+$ beads) or $F(ab')_2$ goat anti-mouse IgM (BCR-ligand$^-$ beads) (MP Biomedical) in combination or not with 100 µg/ml of either ovalbumin (OVA), the *Leishmania major* antigen Lack and/or rGalectin-8.

B cell stimulation and immunofluorescences. Cells were plated on poly-L-lysine–coated slides and stimulated with indicated beads at a 1:2 ratio (cell:beads) for different time at 37°C and fixed in 4% paraformaldehyde for 12 min at room temperature. For γ-Tubulin staining, cells were further incubated with ice-cold 100% methanol for 2 min. Fixed cells were incubated 45-60 min with primary antibodies and 30 min with secondary antibodies in PBS-BSA-Saponin (1x/0.2%/0.05%).

Lysosome secretion. B cells were incubated with Cypher5E-BCR-ligand±Galectin-8-coated beads for 90 min and live cells imaging was performed. Cypher5E fluorescence signal was then measured and synapses displaying Cypher5E fluorescence intensity 10% higher than background value were considered that positive for lysosome secretion and acidification.

Lamp-1$^+$-rings and Antigen extraction. B cells were incubated with OVA±BCR-ligand±Galectin-8-coated beads for indicated time, fixed and stained for OVA and the lysosomes (Lamp-1). The amounts of OVA remaining on beads were quantified and normalized with respect to the initial OVA fluorescence intensity ($t=_{0\ min}$). Lamp-1$^+$-rings were manually counted.

Antigen presentation. B cells were incubated with Lack±BCR-ligand±Galectin-8-coated beads for 3 to 5 h or with peptide control for 1 h. Cells were washed with PBS, fixed in ice-cold PBS/0.01% glutaraldehyde for 1 min and quenched with PBS/100 µM glycine. B cells were then incubated with Lack specific T-cell hybridoma in a 1:1 ratio for 24 h. Supernatants were collected and IL-2 cytokine production was assessed using BD optEIA Mouse IL-2 ELISA set following manufacturer's instructions (BD Biosciences).

Time-lapse imaging. 1×10^5 B lymphoma cells co-expressing the centrosomal marker eGFP-Centrin1 and the F-actin probe Utrophin-RFP were seeded in 35 mm FD35 Fluorodish (World precision instruments, Inc). Cells were either treated with DMSO or CK666 (25 µM) or stimulated with either BCR-ligand$^-$ or BCR-ligand$^+$ beads and recorded at 37˚C, 5% CO_2 using an inverted spinning disk confocal microscope (Roper/Nikon) equipped with a 60x (1.4 NA) oil immersion objective and a CoolSNAP HQ2 camera. The images were acquired every 5 min and with z-stack of 1 µm. For the analysis, Fiji (ImageJ) software was used to reconstruct the 3D movies, correct bleaching (exponential fit correction) and analyze the amount of F-actin associated with the centrosome and the synapse focal plane.

Stable isotope labelling by amino acids in cell culture (SILAC). IIA1.6 cells were maintained in L-lysine-depleted SILAC RPMI 1640 (Thermo Scientific, Life Technologies) supplemented with 10% dialyzed FBS and 0.1 mg/ml heavy [$^{13}C_6$] or light [$^{12}C_6$] L-lysine (Thermo Scientific, Life Technologies). Every 3–4 days, cells were split and media replaced with the corresponding light or heavy labelling medium. After six to seven cell divisions, cells achieved ≥96% incorporation of amino acid isotopes.

Centrosome purification. Centrosomes were purified as previously described [Gogendeau et al., 2015] with slight modifications. Briefly, following stimulation with indicated beads for 60 min, cells were incubated on ice with 200 nM Nocodazole and 1 µg/ml Cytochalasin D for 90 min. Cells were washed and lysed in TicTac buffer (16 mM Pipes, 10 mM Hepes pH 7.5, 50 mM KCl, 1.2 mM EGTA, 5 mM MgCl2, 0.1% Triton X-100 and 0.1% β-mercaptoethanol) for 15 min. Centrosomes were isolated by sequential centrifugations at (1) 10.000 g for 30 min at 4°C on top of a 60% w/v sucrose cushion and (2) 40.000 g for 60 min at 4°C on top of a discontinuous sucrose gradient (40%-50%-70%, w/w). Finally, 10 fractions of 0.5 ml were recovered from the bottom of the tube and centrosome-containing fractions were identified by Western blot.

Proteomics. Proteins were separated by SDS-PAGE, and digested in-gel with rLys-C (recombinant endoproteinase, Promega). Peptides were extracted from gels and analyzed on a LTQ-Orbitrap XLTM mass spectrometer (Thermo Fisher Scientific, Bremen, Germany), essentially as described [Burgo et al., 2013]. Data were acquired using the Xcalibur software (version 2.0.7) and the resulting spectra where then analyzed via the MascotTM Software created with Proteome Discoverer (version 1.2, Thermo Scientific) using the SwissProt Mus

Musculus database. The resulting Mascot result files were further processed using myProMS [Poullet et al., 2007], allowing a maximum false discovery rate (FDR) of 1%. For SILAC-based protein quantification, peptides XICs (Extracted Ion Chromatograms) were retrieved from Proteome Discoverer™. Scale normalization was applied to compensate for mixing errors of the different SILAC cultures as described [Yang et al., 2002]. Protein ratios were computed as the geometrical mean of related peptides. To estimate ratio significance, a t test was performed with a Benjamini–Hochberg FDR control threshold set to 0.05. All quantified proteins have at least 3 peptides quantified (all peptides selected).

GO term enrichment analysis. Protein analysis by genome ontology (GO) term enrichment was computed based on annotation only and did not take into account the relative abundance of the 835 proteins in resting and activated lymphocytes. The frequency of each GO was computed in the mus musculus proteome (defined as the background, Slim Ontology file including all 21 283 mouse proteins) and compared to the set. GO enrichment factors were computed with the GO::TermFinder [Boyle et al., 2004] through myProMS.

***In vitro* nucleation assays.** In vitro nucleation assays were performed according to [Farina et al., 2016]. In brief, centrosomes isolated in TicTac buffer were incubated for 20 min on surface of a polydimethylsiloxane open chamber. The excess of centrosomes was washed with TicTac buffer supplemented with 1% BSA (TicTac-BSA). Microtubule and actin nucleation was induced by diluting tubulin dimers (labelled with ATTO-565, 30 µM final [Farina et al., 2016]) or actin monomers (labelled with Alexa-568, 1µM final [MacLean-Fletcher and Pollard, 1980, Isambert et al., 1995, Egile et al., 1999]) in TicTac buffer supplemented with 1 mM GTP, 2.7 mM ATP, 10 mM DTT, 20 µg/ml catalase, 3 mg/ml glucose, 100 µg/ml glucose oxidase and 0.25% w/v methylcellulose. In addition, a threefold molar equivalent of profilin to actin was added in the reaction mixture [Fedorov et al., 1994]. Time-lapse observations were performed by using a Total Internal Reflection Fluorescence (TIRF) microscope (Roper Scientific) equipped by an iLasPulsed system and an Evolve camera using a 60x 1.49 N.A. objective lens. For quantification of the actin nucleation activity by centrosomes, F-actin fluorescence intensity was integrated over a 2 µm diameter circle around the centrosome and normalized with respect to initial intensity. γ-Tubulin staining, needed for the efficiency calculation, was performed at the end of the movie recording under the microscope without prior fixation. Primary and secondary antibodies, diluted in TicTac-BSA buffer, were incubated for 60 min and 30 min, respectively. Arp2/3 complex inhibition

experiments were performed by adding 200 µM CK666 in reaction mixture. DMSO was used as control. Immunofluorescence staining of isolated centrosomes was performed by incubating centrosomes, seeded on a clean surface, with primary and secondary antibodies for 60 min and 30 min, respectively.

Western blotting. B cells were lysed at 4ºC in RIPA buffer (Thermo Scientific) supplemented with 1x Protease Inhibitor Cocktail (Roche) and 1x Halt Phosphatase Inhibitor Cocktail (Thermo Scientific). Supernatants were collected and loaded onto mini-PROTEAN TGX SDS–PAGE gels and transferred onto PVDF membranes (Trans-Blot Turbo Transfer). Membranes were blocked in 5% non-fat dry milk resuspended in 1xTBS–0.05% Tween-20 and incubated over-night at 4°C with primary antibodies followed by 60 min incubation with secondary antibodies. Western blots were developed with Clarity Western ECL substrate, and chemiluminescence was detected using the ChemiDoc imager (all from BioRad).

Quantitative RT-PCR. RNA extraction was performed from 30 mg of tissues or $10x10^6$ cells using Nucleospin RNA kit II according to manufacturer's instructions (Macherey Nagel). Reverse transcription was performed with 2 µg RNA using the SuperScript® VILO™ cDNA Synthesis Kit according to manufacturer's instructions (Invitrogen). Galectin-8 (primer: Mm01332239-m1 *Lgals8*, Life Technologies) mRNA levels were assessed using TaqMan Gene Expression Master Mix according to manufacturer's recommendations (Applied Biosystems). For LPS-induced systemic inflammation, mice received one retro-orbital injection of 50 µg LPS 6 hrs prior to RNA extraction.

Antigen presentation *in vivo*. HEL-specific B cells and OVA-specific $CD4^+$ T cells were purified from spleens of $CD45.2^+$ swHEL and OT-II transgenic mice using negative B cell and $CD4^+$ T cell isolation kits according to manufacturer's instructions, respectively (Miltenyi Biotec). $2x10^6$ swHEL B cells and $0.5x10^6$ OT-II CD4+ T cells were adoptively transferred by retro-orbital injection into $CD45.1^+$ wild-type recipient and mice were then immunized by footpad injection of indicated microspheres. 8 days later mice were sacrificed and the popliteal lymph nodes draining the site of immunization were harvested and treated with collagenase IV for 30 min at 37°C to obtain a single cell suspension. Cells were then labeled and the number of HEL-specific germinal center B cells and OVA-specific follicular helper T cells was assessed by flow cytometry (FACS Verse, BD).

Two-photon microscopy and cell tracking. One to three million IAβ-GFP-expressing MD4 (BCR^{MD4}) or WT (BCR^{WT}) B cells was adoptively transferred into wild-type recipient mice prior to be immunized with indicated red fluorescent-microspheres by footpad injection. 30 or 90 min post-immunization, mice were anesthetized and the popliteal lymph node draining the site of injection was prepared for two-photon imaging. The two-photon laser-scanning microscopy (TPLSM) setup used was a LSM510 Meta (Zeiss) coupled to a Maitai DeepSee femtosecond laser (690–1020 nm) (Spectra-Physics). The excitation wavelength was 900 nm. For analysis of cell migration, every 30 s during 30 min, six consecutive 230 × 230 μm^2 images, with 6 μm z spacing with a 40× (Zeiss) objective were taken. Images were average-projected with Image J software and automatic tracking of individual cells was performed with Imaris software. Individual tracks were manually checked and corrected when required.

Immunofluorescence acquisition, processing and analysis. All z-stack images (0.5 μm spacing) were acquired on an inverted spinning disk confocal microscope (Roper/Nikon) with a 60x/1.4 numerical aperture (NA) oil immersion objective. Image processing was performed with Fiji (Image J) software [Schindelin et al., 2012]. Single cell images shown in the figures were cropped from large fields, rotated and their contrast and brightness manually adjusted. Images shown are the average z-projection of 3 planes around the centrosome.

Centrosome Polarity Index was computed as described in Fig. 23a. Briefly, z-stacks were projected (SUM slice) and images were automatically threshold (Default) on the green channel to obtain the center of mass of the cell ($Cell_{CM}$). Then, the position of the centrosome and the bead geometrical center ($Bead_{GC}$) were manually selected. The position of the centrosome was then projected ($Cent_{proj}$) on the vector defined by the $Cell_{CM}$-$Bead_{GC}$ axis. The centrosome polarity index was calculated by dividing the distance between the $Cell_{CM}$ and the $Cent_{proj}$ by the distance between the $Cell_{CM}$ and the $Bead_{GC}$. The index ranges from −1 (anti-polarized) to 1 (fully polarized).

Centrosome- and synapse-associated Arp2 and F-actin were quantified as shown in Fig. 25b. Briefly, after manual selection of the centrosome, background subtraction (rolling ball 50px) on the z-projection (AVG) of the 3 planes around the centrosome was performed. We then computed the radial distribution of cytoplasmic Arp2 and F-actin fluorescence intensities from the centrosome of resting cells. The drop in fluorescence intensities (at 0.8 μm from the centrosome) was used as a threshold to define the radius of the centrosomal area that was further used to assess the amount of Arp2 and F-actin associated with the centrosome. The synaptic area was manually defined by positioning a fixed area at the cell-bead interface.

The distance between the centrosome and the nucleus was measured in three dimensions. For this, the nucleus was automatically threshold in 3D (Otsu) and the corresponding 3D-distance map was computed (Image 3D suite plugin). The 3D position of the centrosome was then manually selected on the cell stack and the shorter distance to the nucleus edge was measured on the 3D-distance map.

Statistics. All graphs and statistical analysis were performed with GraphPad Prism 5 (GraphPad Software). No statistical method was used to predetermine sample size. Kolmogorov–Smirnov test was used to assess normality of all data sets. Mann-Whitney test was used to determine statistical significance excepted when mentioned. Boxes in box plots extend from the 25^{th} to 75^{th} percentile, with a line at the median and whiskers extend from the 10^{th} to the 90^{th} percentile. Bar graphs show the mean ± s.e.m..

REFERENCES

ADIE, E. J., KALINKA, S., SMITH, L., FRANCIS, M. J., MARENGHI, A., COOPER, M. E., BRIGGS, M., MICHAEL, N. P., MILLIGAN, G. & GAME, S. 2002. A pH-sensitive fluor, CypHer 5, used to monitor agonist-induced G protein-coupled receptor internalization in live cells. *Biotechniques,* 33**,** 1152-4, 1156-7.

AHRINGER, J. 2003. Control of cell polarity and mitotic spindle positioning in animal cells. *Curr Opin Cell Biol,* 15**,** 73-81.

ALARCON, B., MESTRE, D. & MARTINEZ-MARTIN, N. 2011. The immunological synapse: a cause or consequence of T-cell receptor triggering? *Immunology,* 133**,** 420-5.

ALLEN, C. D., OKADA, T. & CYSTER, J. G. 2007. Germinal-center organization and cellular dynamics. *Immunity,* 27**,** 190-202.

AMANN, K. J. & POLLARD, T. D. 2001. Direct real-time observation of actin filament branching mediated by Arp2/3 complex using total internal reflection fluorescence microscopy. *Proc Natl Acad Sci U S A,* 98**,** 15009-13.

ANDRES-DELGADO, L., ANTON, O. M. & ALONSO, M. A. 2013. Centrosome polarization in T cells: a task for formins. *Front Immunol,* 4**,** 191.

ANDRES-DELGADO, L., ANTON, O. M., BARTOLINI, F., RUIZ-SAENZ, A., CORREAS, I., GUNDERSEN, G. G. & ALONSO, M. A. 2012. INF2 promotes the formation of detyrosinated microtubules necessary for centrosome reorientation in T cells. *J Cell Biol,* 198**,** 1025-37.

ANGINOT, A., ESPELI, M., CHASSON, L., MANCINI, S. J. & SCHIFF, C. 2013. Galectin 1 modulates plasma cell homeostasis and regulates the humoral immune response. *J Immunol,* 190**,** 5526-33.

ANGUS, K. L. & GRIFFITHS, G. M. 2013. Cell polarisation and the immunological synapse. *Curr Opin Cell Biol,* 25**,** 85-91.

ARANA, E., VEHLOW, A., HARWOOD, N. E., VIGORITO, E., HENDERSON, R., TURNER, M., TYBULEWICZ, V. L. & BATISTA, F. D. 2008. Activation of the small GTPase Rac2 via the B cell receptor regulates B cell adhesion and immunological-synapse formation. *Immunity,* 28**,** 88-99.

BABA, Y. & KUROSAKI, T. 2011. Impact of Ca2+ signaling on B cell function. *Trends Immunol,* 32**,** 589-94.

BADANO, J. L., MITSUMA, N., BEALES, P. L. & KATSANIS, N. 2006. The ciliopathies: an emerging class of human genetic disorders. *Annu Rev Genomics Hum Genet,* 7**,** 125-48.

BAJER, A. S., CYPHER, C., MOLE-BAJER, J. & HOWARD, H. M. 1982. Taxol-induced anaphase reversal: evidence that elongating microtubules can exert a pushing force in living cells. *Proc Natl Acad Sci U S A,* 79**,** 6569-73.

BAKKE, O. & DOBBERSTEIN, B. 1990. MHC class II-associated invariant chain contains a sorting signal for endosomal compartments. *Cell,* 63**,** 707-16.

BARNETT, B. E., CIOCCA, M. L., GOENKA, R., BARNETT, L. G., WU, J., LAUFER, T. M., BURKHARDT, J. K., CANCRO, M. P. & REINER, S. L. 2012. Asymmetric B cell division in the germinal center reaction. *Science,* 335**,** 342-4.

BAROIS, N., FORQUET, F. & DAVOUST, J. 1998. Actin microfilaments control the MHC class II antigen presentation pathway in B cells. *J Cell Sci,* 111 (Pt 13)**,** 1791-800.

BARTOLINI, F., MOSELEY, J. B., SCHMORANZER, J., CASSIMERIS, L., GOODE, B. L. & GUNDERSEN, G. G. 2008. The formin mDia2 stabilizes microtubules independently of its actin nucleation activity. *J Cell Biol,* 181**,** 523-36.

BATISTA, F. D. & HARWOOD, N. E. 2009. The who, how and where of antigen presentation to B cells. *Nat Rev Immunol,* 9**,** 15-27.

BATISTA, F. D., IBER, D. & NEUBERGER, M. S. 2001. B cells acquire antigen from target cells after synapse formation. *Nature,* 411**,** 489-94.

BATISTA, F. D. & NEUBERGER, M. S. 1998. Affinity dependence of the B cell response to antigen: a threshold, a ceiling, and the importance of off-rate. *Immunity,* 8**,** 751-9.

BAUDOIN, J. P., VIOU, L., LAUNAY, P. S., LUCCARDINI, C., ESPESO GIL, S., KIYASOVA, V., IRINOPOULOU, T., ALVAREZ, C., RIO, J. P., BOUDIER, T., LECHAIRE, J. P., KESSARIS, N., SPASSKY, N. & METIN, C. 2012. Tangentially migrating neurons assemble a primary cilium that promotes their reorientation to the cortical plate. *Neuron,* 76**,** 1108-22.

BAUM, B. & KUNDA, P. 2005. Actin nucleation: spire - actin nucleator in a class of its own. *Curr Biol,* 15**,** R305-8.

BELTZNER, C. C. & POLLARD, T. D. 2004. Identification of functionally important residues of Arp2/3 complex by analysis of homology models from diverse species. *J Mol Biol,* 336**,** 551-65.

BERTRAND, F., ESQUERRE, M., PETIT, A. E., RODRIGUES, M., DUCHEZ, S., DELON, J. & VALITUTTI, S. 2010. Activation of the ancestral polarity regulator protein kinase C zeta at the immunological synapse drives polarization of Th cell secretory machinery toward APCs. *J Immunol,* 185**,** 2887-94.

BLANCHOIN, L., BOUJEMAA-PATERSKI, R., SYKES, C. & PLASTINO, J. 2014. Actin dynamics, architecture, and mechanics in cell motility. *Physiol Rev,* 94**,** 235-63.

BOMBARDIER, J. P. & MUNSON, M. 2015. Three steps forward, two steps back: mechanistic insights into the assembly and disassembly of the SNARE complex. *Curr Opin Chem Biol,* 29**,** 66-71.

BORNENS, M. 2012. The centrosome in cells and organisms. *Science,* 335**,** 422-6.

BOYLE, E. I., WENG, S., GOLLUB, J., JIN, H., BOTSTEIN, D., CHERRY, J. M. & SHERLOCK, G. 2004. GO::TermFinder--open source software for accessing Gene Ontology information and finding significantly enriched Gene Ontology terms associated with a list of genes. *Bioinformatics,* 20**,** 3710-5.

BRINKLEY, B. R. 1985. Microtubule organizing centers. *Annu Rev Cell Biol,* 1**,** 145-72.

BROWN, B. K. & SONG, W. 2001. The actin cytoskeleton is required for the trafficking of the B cell antigen receptor to the late endosomes. *Traffic,* 2**,** 414-27.

BRUNATI, A. M., DEANA, R., FOLDA, A., MASSIMINO, M. L., MARIN, O., LEDRO, S., PINNA, L. A. & DONELLA-DEANA, A. 2005. Thrombin-induced tyrosine phosphorylation of HS1 in human platelets is sequentially catalyzed by Syk and Lyn tyrosine kinases and associated with the cellular migration of the protein. *J Biol Chem,* 280**,** 21029-35.

BURAKOV, A., NADEZHDINA, E., SLEPCHENKO, B. & RODIONOV, V. 2003. Centrosome positioning in interphase cells. *J Cell Biol,* 162**,** 963-9.

BURAKOV, A. V. & NADEZHDINA, E. S. 2013. Association of nucleus and centrosome: magnet or velcro? *Cell Biol Int,* 37**,** 95-104.

BURBAGE, M., KEPPLER, S. J., GASPARRINI, F., MARTINEZ-MARTIN, N., GAYA, M., FEEST, C., DOMART, M. C., BRAKEBUSCH, C., COLLINSON, L., BRUCKBAUER, A. & BATISTA, F. D. 2015. Cdc42 is a key regulator of B cell differentiation and is required for antiviral humoral immunity. *J Exp Med,* 212**,** 53-72.

BURGO, A., CASANO, A. M., KUSTER, A., AROLD, S. T., WANG, G., NOLA, S., VERRAES, A., DINGLI, F., LOEW, D. & GALLI, T. 2013. Increased activity of the vesicular soluble N-ethylmaleimide-sensitive factor attachment protein receptor TI-VAMP/VAMP7 by tyrosine phosphorylation in the Longin domain. *J Biol Chem,* 288**,** 11960-72.

BURKE, T. A., CHRISTENSEN, J. R., BARONE, E., SUAREZ, C., SIROTKIN, V. & KOVAR, D. R. 2014. Homeostatic actin cytoskeleton networks are regulated by assembly factor competition for monomers. *Curr Biol,* 24**,** 579-85.

BURNETTE, D. T., MANLEY, S., SENGUPTA, P., SOUGRAT, R., DAVIDSON, M. W., KACHAR, B. & LIPPINCOTT-SCHWARTZ, J. 2011. A role for actin arcs in the leading-edge advance of migrating cells. *Nat Cell Biol,* 13**,** 371-81.

CAMBIER, J. C., PLEIMAN, C. M. & CLARK, M. R. 1994. Signal transduction by the B cell antigen receptor and its coreceptors. *Annu Rev Immunol,* 12**,** 457-86.

CARCAMO, C., PARDO, E., OYANADEL, C., BRAVO-ZEHNDER, M., BULL, P., CACERES, M., MARTINEZ, J., MASSARDO, L., JACOBELLI, S., GONZALEZ, A. & SOZA, A. 2006. Galectin-8 binds specific beta1 integrins and induces polarized spreading highlighted by asymmetric lamellipodia in Jurkat T cells. *Exp Cell Res,* 312**,** 374-86.

CARLIER, M. F., PERNIER, J., MONTAVILLE, P., SHEKHAR, S., KUHN, S., CYTOSKELETON, D. & MOTILITY, G. 2015. Control of polarized assembly of actin filaments in cell motility. *Cell Mol Life Sci,* 72**,** 3051-67.

CARRASCO, Y. R. & BATISTA, F. D. 2007. B cells acquire particulate antigen in a macrophage-rich area at the boundary between the follicle and the subcapsular sinus of the lymph node. *Immunity,* 27**,** 160-71.

CARRASCO, Y. R., FLEIRE, S. J., CAMERON, T., DUSTIN, M. L. & BATISTA, F. D. 2004. LFA-1/ICAM-1 interaction lowers the threshold of B cell activation by facilitating B cell adhesion and synapse formation. *Immunity,* 20**,** 589-99.

CASEY, T. M., MEADE, J. L. & HEWITT, E. W. 2007. Organelle proteomics: identification of the exocytic machinery associated with the natural killer cell secretory lysosome. *Mol Cell Proteomics,* 6**,** 767-80.

CATTANEO, V., TRIBULATTI, M. V. & CAMPETELLA, O. 2011. Galectin-8 tandem-repeat structure is essential for T-cell proliferation but not for co-stimulation. *Biochem J,* 434**,** 153-60.

CHAINEAU, M., DANGLOT, L. & GALLI, T. 2009. Multiple roles of the vesicular-SNARE TI-VAMP in post-Golgi and endosomal trafficking. *FEBS Lett,* 583**,** 3817-26.

CHANG, J. T., PALANIVEL, V. R., KINJYO, I., SCHAMBACH, F., INTLEKOFER, A. M., BANERJEE, A., LONGWORTH, S. A., VINUP, K. E., MRASS, P., OLIARO, J., KILLEEN, N., ORANGE, J. S., RUSSELL, S. M., WENINGER, W. & REINER, S. L. 2007. Asymmetric T lymphocyte division in the initiation of adaptive immune responses. *Science,* 315**,** 1687-91.

CHERUKURI, A., CHENG, P. C. & PIERCE, S. K. 2001. The role of the CD19/CD21 complex in B cell processing and presentation of complement-tagged antigens. *J Immunol,* 167**,** 163-72.

CHESARONE, M. A. & GOODE, B. L. 2009. Actin nucleation and elongation factors: mechanisms and interplay. *Curr Opin Cell Biol,* 21**,** 28-37.

CHRISTENSEN, S. T., PEDERSEN, L. B., SCHNEIDER, L. & SATIR, P. 2007. Sensory cilia and integration of signal transduction in human health and disease. *Traffic,* 8**,** 97-109.

COMBS, J., KIM, S. J., TAN, S., LIGON, L. A., HOLZBAUR, E. L., KUHN, J. & POENIE, M. 2006. Recruitment of dynein to the Jurkat immunological synapse. *Proc Natl Acad Sci U S A,* 103**,** 14883-8.

COONROD, E. M. & STEVENS, T. H. 2010. The yeast vps class E mutants: the beginning of the molecular genetic analysis of multivesicular body biogenesis. *Mol Biol Cell,* 21**,** 4057-60.

CUENI, L. N. & DETMAR, M. 2009. Galectin-8 interacts with podoplanin and modulates lymphatic endothelial cell functions. *Exp Cell Res,* 315**,** 1715-23.
CUMMINGS, R. D. & LIU, F. T. 2009. Galectins. *In:* VARKI, A., CUMMINGS, R. D., ESKO, J. D., FREEZE, H. H., STANLEY, P., BERTOZZI, C. R., HART, G. W. & ETZLER, M. E. (eds.) *Essentials of Glycobiology.* 2nd ed. Cold Spring Harbor (NY).
CUNNINGHAM, A. F., GASPAL, F., SERRE, K., MOHR, E., HENDERSON, I. R., SCOTT-TUCKER, A., KENNY, S. M., KHAN, M., TOELLNER, K. M., LANE, P. J. & MACLENNAN, I. C. 2007. Salmonella induces a switched antibody response without germinal centers that impedes the extracellular spread of infection. *J Immunol,* 178**,** 6200-7.
CYSTER, J. G. 2010. B cell follicles and antigen encounters of the third kind. *Nat Immunol,* 11**,** 989-96.
DAGA, R. R., YONETANI, A. & CHANG, F. 2006. Asymmetric microtubule pushing forces in nuclear centering. *Curr Biol,* 16**,** 1544-50.
DANOWSKI, B. A. 1989. Fibroblast contractility and actin organization are stimulated by microtubule inhibitors. *J Cell Sci,* 93 (Pt 2)**,** 255-66.
DE LA ROCHE, M., RITTER, A. T., ANGUS, K. L., DINSMORE, C., EARNSHAW, C. H., REITER, J. F. & GRIFFITHS, G. M. 2013. Hedgehog signaling controls T cell killing at the immunological synapse. *Science,* 342**,** 1247-50.
DE SILVA, N. S. & KLEIN, U. 2015. Dynamics of B cells in germinal centres. *Nat Rev Immunol,* 15**,** 137-48.
DELAMARRE, L., PACK, M., CHANG, H., MELLMAN, I. & TROMBETTA, E. S. 2005. Differential lysosomal proteolysis in antigen-presenting cells determines antigen fate. *Science,* 307**,** 1630-4.
DELGADO, V. M., NUGNES, L. G., COLOMBO, L. L., TRONCOSO, M. F., FERNANDEZ, M. M., MALCHIODI, E. L., FRAHM, I., CROCI, D. O., COMPAGNO, D., RABINOVICH, G. A., WOLFENSTEIN-TODEL, C. & ELOLA, M. T. 2011. Modulation of endothelial cell migration and angiogenesis: a novel function for the "tandem-repeat" lectin galectin-8. *FASEB J,* 25**,** 242-54.
DELON, J. 2000. The immunological synapse. *Curr Biol,* 10**,** R214.
DENZIN, L. K. & CRESSWELL, P. 1995. HLA-DM induces CLIP dissociation from MHC class II alpha beta dimers and facilitates peptide loading. *Cell,* 82**,** 155-65.
DENZIN, L. K., SANT'ANGELO, D. B., HAMMOND, C., SURMAN, M. J. & CRESSWELL, P. 1997. Negative regulation by HLA-DO of MHC class II-restricted antigen processing. *Science,* 278**,** 106-9.
DEPOIL, D., WEBER, M., TREANOR, B., FLEIRE, S. J., CARRASCO, Y. R., HARWOOD, N. E. & BATISTA, F. D. 2009. Early events of B cell activation by antigen. *Sci Signal,* 2**,** pt1.
DERIVERY, E., SOUSA, C., GAUTIER, J. J., LOMBARD, B., LOEW, D. & GAUTREAU, A. 2009. The Arp2/3 activator WASH controls the fission of endosomes through a large multiprotein complex. *Dev Cell,* 17**,** 712-23.
DEWARD, A. D. & ALBERTS, A. S. 2008. Microtubule stabilization: formins assert their independence. *Curr Biol,* 18**,** R605-8.
DISKIN, S., CAO, Z., LEFFLER, H. & PANJWANI, N. 2009. The role of integrin glycosylation in galectin-8-mediated trabecular meshwork cell adhesion and spreading. *Glycobiology,* 19**,** 29-37.
DOGTEROM, M., KERSSEMAKERS, J. W., ROMET-LEMONNE, G. & JANSON, M. E. 2005. Force generation by dynamic microtubules. *Curr Opin Cell Biol,* 17**,** 67-74.
DONG, G. 2015. Building a ninefold symmetrical barrel: structural dissections of centriole assembly. *Open Biol,* 5.

DOYOTTE, A., RUSSELL, M. R., HOPKINS, C. R. & WOODMAN, P. G. 2005. Depletion of TSG101 forms a mammalian "Class E" compartment: a multicisternal early endosome with multiple sorting defects. *J Cell Sci,* 118**,** 3003-17.

DRIESSEN, C., BRYANT, R. A., LENNON-DUMENIL, A. M., VILLADANGOS, J. A., BRYANT, P. W., SHI, G. P., CHAPMAN, H. A. & PLOEGH, H. L. 1999. Cathepsin S controls the trafficking and maturation of MHC class II molecules in dendritic cells. *J Cell Biol,* 147**,** 775-90.

DUCHEZ, S., RODRIGUES, M., BERTRAND, F. & VALITUTTI, S. 2011. Reciprocal polarization of T and B cells at the immunological synapse. *J Immunol,* 187**,** 4571-80.

EGILE, C., LOISEL, T. P., LAURENT, V., LI, R., PANTALONI, D., SANSONETTI, P. J. & CARLIER, M. F. 1999. Activation of the CDC42 effector N-WASP by the Shigella flexneri IcsA protein promotes actin nucleation by Arp2/3 complex and bacterial actin-based motility. *J Cell Biol,* 146**,** 1319-32.

EGILE, C., ROUILLER, I., XU, X. P., VOLKMANN, N., LI, R. & HANEIN, D. 2005. Mechanism of filament nucleation and branch stability revealed by the structure of the Arp2/3 complex at actin branch junctions. *PLoS Biol,* 3**,** e383.

ELRIC, J. & ETIENNE-MANNEVILLE, S. 2014. Centrosome positioning in polarized cells: common themes and variations. *Exp Cell Res,* 328**,** 240-8.

ENNOMANI, H., LETORT, G., GUERIN, C., MARTIEL, J. L., CAO, W., NEDELEC, F., DE LA CRUZ, E. M., THERY, M. & BLANCHOIN, L. 2016. Architecture and Connectivity Govern Actin Network Contractility. *Curr Biol,* 26**,** 616-26.

ERICKSON, H. P. & O'BRIEN, E. T. 1992. Microtubule dynamic instability and GTP hydrolysis. *Annu Rev Biophys Biomol Struct,* 21**,** 145-66.

ESPELI, M., MANCINI, S. J., BRETON, C., POIRIER, F. & SCHIFF, C. 2009. Impaired B-cell development at the pre-BII-cell stage in galectin-1-deficient mice due to inefficient pre-BII/stromal cell interactions. *Blood,* 113**,** 5878-86.

ETIENNE-MANNEVILLE, S. 2004a. Actin and microtubules in cell motility: which one is in control? *Traffic,* 5**,** 470-7.

ETIENNE-MANNEVILLE, S. 2004b. Cdc42--the centre of polarity. *J Cell Sci,* 117**,** 1291-300.

FARINA, F., GAILLARD, J., GUERIN, C., COUTE, Y., SILLIBOURNE, J., BLANCHOIN, L. & THERY, M. 2016. The centrosome is an actin-organizing centre. *Nat Cell Biol,* 18**,** 65-75.

FAURE, S., SALAZAR-FONTANA, L. I., SEMICHON, M., TYBULEWICZ, V. L., BISMUTH, G., TRAUTMANN, A., GERMAIN, R. N. & DELON, J. 2004. ERM proteins regulate cytoskeleton relaxation promoting T cell-APC conjugation. *Nat Immunol,* 5**,** 272-9.

FEDOROV, A. A., POLLARD, T. D. & ALMO, S. C. 1994. Purification, characterization and crystallization of human platelet profilin expressed in Escherichia coli. *J Mol Biol,* 241**,** 480-2.

FINETTI, F., PACCANI, S. R., RIPARBELLI, M. G., GIACOMELLO, E., PERINETTI, G., PAZOUR, G. J., ROSENBAUM, J. L. & BALDARI, C. T. 2009. Intraflagellar transport is required for polarized recycling of the TCR/CD3 complex to the immune synapse. *Nat Cell Biol,* 11**,** 1332-9.

FLEIRE, S. J., GOLDMAN, J. P., CARRASCO, Y. R., WEBER, M., BRAY, D. & BATISTA, F. D. 2006. B cell ligand discrimination through a spreading and contraction response. *Science,* 312**,** 738-41.

FREEMAN, S. A. & GRINSTEIN, S. 2014. Phagocytosis: receptors, signal integration, and the cytoskeleton. *Immunol Rev,* 262**,** 193-215.

FREEMAN, S. A., LEI, V., DANG-LAWSON, M., MIZUNO, K., ROSKELLEY, C. D. & GOLD, M. R. 2011. Cofilin-mediated F-actin severing is regulated by the Rap GTPase and controls the cytoskeletal dynamics that drive lymphocyte spreading and BCR microcluster formation. *J Immunol,* 187**,** 5887-900.

GARDEL, M. L., KASZA, K. E., BRANGWYNNE, C. P., LIU, J. & WEITZ, D. A. 2008. Chapter 19: Mechanical response of cytoskeletal networks. *Methods Cell Biol,* 89**,** 487-519.

GAUTHIER, L., ROSSI, B., ROUX, F., TERMINE, E. & SCHIFF, C. 2002. Galectin-1 is a stromal cell ligand of the pre-B cell receptor (BCR) implicated in synapse formation between pre-B and stromal cells and in pre-BCR triggering. *Proc Natl Acad Sci U S A,* 99**,** 13014-9.

GOETZ, S. C. & ANDERSON, K. V. 2010. The primary cilium: a signalling centre during vertebrate development. *Nat Rev Genet,* 11**,** 331-44.

GOGENDEAU, D., GUICHARD, P. & TASSIN, A. M. 2015. Purification of centrosomes from mammalian cell lines. *Methods Cell Biol,* 129**,** 171-89.

GOLEY, E. D. & WELCH, M. D. 2006. The ARP2/3 complex: an actin nucleator comes of age. *Nat Rev Mol Cell Biol,* 7**,** 713-26.

GOMEZ, T. S., KUMAR, K., MEDEIROS, R. B., SHIMIZU, Y., LEIBSON, P. J. & BILLADEAU, D. D. 2007. Formins regulate the actin-related protein 2/3 complex-independent polarization of the centrosome to the immunological synapse. *Immunity,* 26**,** 177-90.

GOMEZ, T. S., MCCARNEY, S. D., CARRIZOSA, E., LABNO, C. M., COMISKEY, E. O., NOLZ, J. C., ZHU, P., FREEDMAN, B. D., CLARK, M. R., RAWLINGS, D. J., BILLADEAU, D. D. & BURKHARDT, J. K. 2006. HS1 functions as an essential actin-regulatory adaptor protein at the immune synapse. *Immunity,* 24**,** 741-52.

GONCZY, P. 2012. Towards a molecular architecture of centriole assembly. *Nat Rev Mol Cell Biol,* 13**,** 425-35.

GONDRE-LEWIS, T. A., MOQUIN, A. E. & DRAKE, J. R. 2001. Prolonged antigen persistence within nonterminal late endocytic compartments of antigen-specific B lymphocytes. *J Immunol,* 166**,** 6657-64.

GONZALEZ, S. F., LUKACS-KORNEK, V., KULIGOWSKI, M. P., PITCHER, L. A., DEGN, S. E., KIM, Y. A., CLONINGER, M. J., MARTINEZ-POMARES, L., GORDON, S., TURLEY, S. J. & CARROLL, M. C. 2010. Capture of influenza by medullary dendritic cells via SIGN-R1 is essential for humoral immunity in draining lymph nodes. *Nat Immunol,* 11**,** 427-34.

GRAKOUI, A., BROMLEY, S. K., SUMEN, C., DAVIS, M. M., SHAW, A. S., ALLEN, P. M. & DUSTIN, M. L. 1999. The immunological synapse: a molecular machine controlling T cell activation. *Science,* 285**,** 221-7.

GRIGORIAN, A., TOROSSIAN, S. & DEMETRIOU, M. 2009. T-cell growth, cell surface organization, and the galectin-glycoprotein lattice. *Immunol Rev,* 230**,** 232-46.

HAO, J. J., CAREY, G. B. & ZHAN, X. 2004. Syk-mediated tyrosine phosphorylation is required for the association of hematopoietic lineage cell-specific protein 1 with lipid rafts and B cell antigen receptor signalosome complex. *J Biol Chem,* 279**,** 33413-20.

HARTWIG, J. H., JUGLOFF, L. S., DE GROOT, N. J., GRUPP, S. A. & JONGSTRA-BILEN, J. 1995. The ligand-induced membrane IgM association with the cytoskeletal matrix of B cells is not mediated through the Ig alpha beta heterodimer. *J Immunol,* 155**,** 3769-79.

HARWOOD, N. E. & BATISTA, F. D. 2010. Early events in B cell activation. *Annu Rev Immunol,* 28**,** 185-210.

HARWOOD, N. E. & BATISTA, F. D. 2011. The cytoskeleton coordinates the early events of B-cell activation. *Cold Spring Harb Perspect Biol,* 3.

HAYDEN, J. H., BOWSER, S. S. & RIEDER, C. L. 1990. Kinetochores capture astral microtubules during chromosome attachment to the mitotic spindle: direct visualization in live newt lung cells. *J Cell Biol,* 111**,** 1039-45.

HEALD, R. & KHODJAKOV, A. 2015. Thirty years of search and capture: The complex simplicity of mitotic spindle assembly. *J Cell Biol,* 211**,** 1103-11.

HEASMAN, S. J. & RIDLEY, A. J. 2008. Mammalian Rho GTPases: new insights into their functions from in vivo studies. *Nat Rev Mol Cell Biol,* 9**,** 690-701.

HENG, Y. W. & KOH, C. G. 2010. Actin cytoskeleton dynamics and the cell division cycle. *Int J Biochem Cell Biol,* 42**,** 1622-33.

HENNE, W. M., STENMARK, H. & EMR, S. D. 2013. Molecular mechanisms of the membrane sculpting ESCRT pathway. *Cold Spring Harb Perspect Biol,* 5.

HIGGS, H. N., BLANCHOIN, L. & POLLARD, T. D. 1999. Influence of the C terminus of Wiskott-Aldrich syndrome protein (WASp) and the Arp2/3 complex on actin polymerization. *Biochemistry,* 38**,** 15212-22.

HIRONO, M. 2014. Cartwheel assembly. *Philos Trans R Soc Lond B Biol Sci,* 369.

HOEDT, E., ZHANG, G. & NEUBERT, T. A. 2014. Stable isotope labeling by amino acids in cell culture (SILAC) for quantitative proteomics. *Adv Exp Med Biol,* 806**,** 93-106.

HOWARD, J. & HYMAN, A. A. 2009. Growth, fluctuation and switching at microtubule plus ends. *Nat Rev Mol Cell Biol,* 10**,** 569-74.

HUBERT, T., VANDEKERCKHOVE, J. & GETTEMANS, J. 2011. Actin and Arp2/3 localize at the centrosome of interphase cells. *Biochem Biophys Res Commun,* 404**,** 153-8.

HUELSMANN, S. & BROWN, N. H. 2014. Spectraplakins. *Curr Biol,* 24**,** R307-8.

HUMPHRIES, J. D., WANG, P., STREULI, C., GEIGER, B., HUMPHRIES, M. J. & BALLESTREM, C. 2007. Vinculin controls focal adhesion formation by direct interactions with talin and actin. *J Cell Biol,* 179**,** 1043-57.

HURTADO, L., CABALLERO, C., GAVILAN, M. P., CARDENAS, J., BORNENS, M. & RIOS, R. M. 2011. Disconnecting the Golgi ribbon from the centrosome prevents directional cell migration and ciliogenesis. *J Cell Biol,* 193**,** 917-33.

ISAMBERT, H., VENIER, P., MAGGS, A. C., FATTOUM, A., KASSAB, R., PANTALONI, D. & CARLIER, M. F. 1995. Flexibility of actin filaments derived from thermal fluctuations. Effect of bound nucleotide, phalloidin, and muscle regulatory proteins. *J Biol Chem,* 270**,** 11437-44.

ISHIZAKI, T., MORISHIMA, Y., OKAMOTO, M., FURUYASHIKI, T., KATO, T. & NARUMIYA, S. 2001. Coordination of microtubules and the actin cytoskeleton by the Rho effector mDia1. *Nat Cell Biol,* 3**,** 8-14.

ISMAIL, A. M., PADRICK, S. B., CHEN, B., UMETANI, J. & ROSEN, M. K. 2009. The WAVE regulatory complex is inhibited. *Nat Struct Mol Biol,* 16**,** 561-3.

JAFFE, A. B. & HALL, A. 2005. Rho GTPases: biochemistry and biology. *Annu Rev Cell Dev Biol,* 21**,** 247-69.

JOBERTY, G., PETERSEN, C., GAO, L. & MACARA, I. G. 2000. The cell-polarity protein Par6 links Par3 and atypical protein kinase C to Cdc42. *Nat Cell Biol,* 2**,** 531-9.

JUNT, T., MOSEMAN, E. A., IANNACONE, M., MASSBERG, S., LANG, P. A., BOES, M., FINK, K., HENRICKSON, S. E., SHAYAKHMETOV, D. M., DI PAOLO, N. C., VAN ROOIJEN, N., MEMPEL, T. R., WHELAN, S. P. & VON ANDRIAN, U. H. 2007. Subcapsular sinus macrophages in lymph nodes clear lymph-borne viruses and present them to antiviral B cells. *Nature,* 450**,** 110-4.

KAJI, N., MURAMOTO, A. & MIZUNO, K. 2008. LIM kinase-mediated cofilin phosphorylation during mitosis is required for precise spindle positioning. *J Biol Chem,* 283**,** 4983-92.
KAKSONEN, M., TORET, C. P. & DRUBIN, D. G. 2006. Harnessing actin dynamics for clathrin-mediated endocytosis. *Nat Rev Mol Cell Biol,* 7**,** 404-14.
KARSENTI, E., KOBAYASHI, S., MITCHISON, T. & KIRSCHNER, M. 1984. Role of the centrosome in organizing the interphase microtubule array: properties of cytoplasts containing or lacking centrosomes. *J Cell Biol,* 98**,** 1763-76.
KAUFMANN, S. H. 2008. Immunology's foundation: the 100-year anniversary of the Nobel Prize to Paul Ehrlich and Elie Metchnikoff. *Nat Immunol,* 9**,** 705-12.
KEELING, J., TSIOKAS, L. & MASKEY, D. 2016. Cellular Mechanisms of Ciliary Length Control. *Cells,* 5.
KEMPHUES, K. J., PRIESS, J. R., MORTON, D. G. & CHENG, N. S. 1988. Identification of genes required for cytoplasmic localization in early C. elegans embryos. *Cell,* 52**,** 311-20.
KIM, D. H., CHO, S. & WIRTZ, D. 2014. Tight coupling between nucleus and cell migration through the perinuclear actin cap. *J Cell Sci,* 127**,** 2528-41.
KIM, D. I., BIRENDRA, K. C. & ROUX, K. J. 2015. Making the LINC: SUN and KASH protein interactions. *Biol Chem,* 396**,** 295-310.
KIRSCHNER, M. & MITCHISON, T. 1986. Beyond self-assembly: from microtubules to morphogenesis. *Cell,* 45**,** 329-42.
KOBAYASHI, T. & DYNLACHT, B. D. 2011. Regulating the transition from centriole to basal body. *J Cell Biol,* 193**,** 435-44.
KRENDEL, M., ZENKE, F. T. & BOKOCH, G. M. 2002. Nucleotide exchange factor GEF-H1 mediates cross-talk between microtubules and the actin cytoskeleton. *Nat Cell Biol,* 4**,** 294-301.
KUMAR, A., RAJENDRAN, V., SETHUMADHAVAN, R. & PUROHIT, R. 2014. Role of centrosome in regulating immune response. *Curr Drug Targets,* 15**,** 558-63.
KUOKKANEN, E., SUSTAR, V. & MATTILA, P. K. 2015. Molecular control of B cell activation and immunological synapse formation. *Traffic,* 16**,** 311-26.
KUPFER, A. & DENNERT, G. 1984. Reorientation of the microtubule-organizing center and the Golgi apparatus in cloned cytotoxic lymphocytes triggered by binding to lysable target cells. *J Immunol,* 133**,** 2762-6.
KUTSCHEIDT, S., ZHU, R., ANTOKU, S., LUXTON, G. W., STAGLJAR, I., FACKLER, O. T. & GUNDERSEN, G. G. 2014. FHOD1 interaction with nesprin-2G mediates TAN line formation and nuclear movement. *Nat Cell Biol,* 16**,** 708-15.
KWON, M., BAGONIS, M., DANUSER, G. & PELLMAN, D. 2015. Direct Microtubule-Binding by Myosin-10 Orients Centrosomes toward Retraction Fibers and Subcortical Actin Clouds. *Dev Cell,* 34**,** 323-37.
LAAN, L., ROTH, S. & DOGTEROM, M. 2012. End-on microtubule-dynein interactions and pulling-based positioning of microtubule organizing centers. *Cell Cycle,* 11**,** 3750-7.
LAMMERMANN, T. & SIXT, M. 2009. Mechanical modes of 'amoeboid' cell migration. *Curr Opin Cell Biol,* 21**,** 636-44.
LANZAVECCHIA, A. 1990. Receptor-mediated antigen uptake and its effect on antigen presentation to class II-restricted T lymphocytes. *Annu Rev Immunol,* 8**,** 773-93.
LANZAVECCHIA, A. & BOVE, S. 1985. Specific B lymphocytes efficiently pick up, process and present antigen to T cells. *Behring Inst Mitt***,** 82-7.
LARGHI, P., WILLIAMSON, D. J., CARPIER, J. M., DOGNIAUX, S., CHEMIN, K., BOHINEUST, A., DANGLOT, L., GAUS, K., GALLI, T. & HIVROZ, C. 2013.

VAMP7 controls T cell activation by regulating the recruitment and phosphorylation of vesicular Lat at TCR-activation sites. *Nat Immunol,* 14**,** 723-31.
LARSSON, J. & KARLSSON, S. 2005. The role of Smad signaling in hematopoiesis. *Oncogene,* 24**,** 5676-92.
LASSERRE, R. & ALCOVER, A. 2010. Cytoskeletal cross-talk in the control of T cell antigen receptor signaling. *FEBS Lett,* 584**,** 4845-50.
LE CLAINCHE, C. & CARLIER, M. F. 2008. Regulation of actin assembly associated with protrusion and adhesion in cell migration. *Physiol Rev,* 88**,** 489-513.
LE ROUX, D., LANKAR, D., YUSEFF, M. I., VASCOTTO, F., YOKOZEKI, T., FAURE-ANDRE, G., MOUGNEAU, E., GLAICHENHAUS, N., MANOURY, B., BONNEROT, C. & LENNON-DUMENIL, A. M. 2007. Syk-dependent actin dynamics regulate endocytic trafficking and processing of antigens internalized through the B-cell receptor. *Mol Biol Cell,* 18**,** 3451-62.
LEBENSOHN, A. M. & KIRSCHNER, M. W. 2009. Activation of the WAVE complex by coincident signals controls actin assembly. *Mol Cell,* 36**,** 512-24.
LEE, J. L. & STREULI, C. H. 2014. Integrins and epithelial cell polarity. *J Cell Sci,* 127**,** 3217-25.
LETTAU, M., KABELITZ, D. & JANSSEN, O. 2015. Lysosome-Related Effector Vesicles in T Lymphocytes and NK Cells. *Scand J Immunol,* 82**,** 235-43.
LEVY, Y., ARBEL-GOREN, R., HADARI, Y. R., ESHHAR, S., RONEN, D., ELHANANY, E., GEIGER, B. & ZICK, Y. 2001. Galectin-8 functions as a matricellular modulator of cell adhesion. *J Biol Chem,* 276**,** 31285-95.
LEVY, Y., RONEN, D., BERSHADSKY, A. D. & ZICK, Y. 2003. Sustained induction of ERK, protein kinase B, and p70 S6 kinase regulates cell spreading and formation of F-actin microspikes upon ligation of integrins by galectin-8, a mammalian lectin. *J Biol Chem,* 278**,** 14533-42.
LIM, J. P. & GLEESON, P. A. 2011. Macropinocytosis: an endocytic pathway for internalising large gulps. *Immunol Cell Biol,* 89**,** 836-43.
LIU, X., KAPOOR, T. M., CHEN, J. K. & HUSE, M. 2013. Diacylglycerol promotes centrosome polarization in T cells via reciprocal localization of dynein and myosin II. *Proc Natl Acad Sci U S A,* 110**,** 11976-81.
LOBERT, V. H. & STENMARK, H. 2011. Cell polarity and migration: emerging role for the endosomal sorting machinery. *Physiology (Bethesda),* 26**,** 171-80.
LOTTEAU, V., TEYTON, L., PELERAUX, A., NILSSON, T., KARLSSON, L., SCHMID, S. L., QUARANTA, V. & PETERSON, P. A. 1990. Intracellular transport of class II MHC molecules directed by invariant chain. *Nature,* 348**,** 600-5.
LUDFORD-MENTING, M. J., OLIARO, J., SACIRBEGOVIC, F., CHEAH, E. T., PEDERSEN, N., THOMAS, S. J., PASAM, A., IAZZOLINO, R., DOW, L. E., WATERHOUSE, N. J., MURPHY, A., ELLIS, S., SMYTH, M. J., KERSHAW, M. H., DARCY, P. K., HUMBERT, P. O. & RUSSELL, S. M. 2005. A network of PDZ-containing proteins regulates T cell polarity and morphology during migration and immunological synapse formation. *Immunity,* 22**,** 737-48.
LUXTON, G. W., GOMES, E. R., FOLKER, E. S., VINTINNER, E. & GUNDERSEN, G. G. 2010. Linear arrays of nuclear envelope proteins harness retrograde actin flow for nuclear movement. *Science,* 329**,** 956-9.
MACARA, I. G. 2004. Parsing the polarity code. *Nat Rev Mol Cell Biol,* 5**,** 220-31.
MACHESKY, L. M. 1999. Rocket-based motility: a universal mechanism? *Nat Cell Biol,* 1**,** E29-31.
MACHESKY, L. M., ATKINSON, S. J., AMPE, C., VANDEKERCKHOVE, J. & POLLARD, T. D. 1994. Purification of a cortical complex containing two

unconventional actins from Acanthamoeba by affinity chromatography on profilin-agarose. *J Cell Biol,* 127**,** 107-15.

MACLEAN-FLETCHER, S. & POLLARD, T. D. 1980. Identification of a factor in conventional muscle actin preparations which inhibits actin filament self-association. *Biochem Biophys Res Commun,* 96**,** 18-27.

MACLENNAN, I. C. 1994. Germinal centers. *Annu Rev Immunol,* 12**,** 117-39.

MALHERBE, L., FILIPPI, C., JULIA, V., FOUCRAS, G., MORO, M., APPEL, H., WUCHERPFENNIG, K., GUERY, J. C. & GLAICHENHAUS, N. 2000. Selective activation and expansion of high-affinity CD4+ T cells in resistant mice upon infection with Leishmania major. *Immunity,* 13**,** 771-82.

MARAVILLAS-MONTERO, J. L., GILLESPIE, P. G., PATINO-LOPEZ, G., SHAW, S. & SANTOS-ARGUMEDO, L. 2011. Myosin 1c participates in B cell cytoskeleton rearrangements, is recruited to the immunologic synapse, and contributes to antigen presentation. *J Immunol,* 187**,** 3053-63.

MARAVILLAS-MONTERO, J. L., LOPEZ-ORTEGA, O., PATINO-LOPEZ, G. & SANTOS-ARGUMEDO, L. 2014. Myosin 1g regulates cytoskeleton plasticity, cell migration, exocytosis, and endocytosis in B lymphocytes. *Eur J Immunol,* 44**,** 877-86.

MARCET-PALACIOS, M., ODEMUYIWA, S. O., COUGHLIN, J. J., GAROFOLI, D., EWEN, C., DAVIDSON, C. E., GHAFFARI, M., KANE, K. P., LACY, P., LOGAN, M. R., BEFUS, A. D., BLEACKLEY, R. C. & MOQBEL, R. 2008. Vesicle-associated membrane protein 7 (VAMP-7) is essential for target cell killing in a natural killer cell line. *Biochem Biophys Res Commun,* 366**,** 617-23.

MARO, B. & BORNENS, M. 1980. The centriole-nucleus association: effects of cytochalasin B and nocodazole. *Biol. Cellulaire,* 39**,** 287-290.

MARSHALL, W. F. 2001. Centrioles take center stage. *Curr Biol,* 11**,** R487-96.

MARTIN-COFRECES, N. B., BAIXAULI, F. & SANCHEZ-MADRID, F. 2014. Immune synapse: conductor of orchestrated organelle movement. *Trends Cell Biol,* 24**,** 61-72.

MARTIN-COFRECES, N. B., ROBLES-VALERO, J., CABRERO, J. R., MITTELBRUNN, M., GORDON-ALONSO, M., SUNG, C. H., ALARCON, B., VAZQUEZ, J. & SANCHEZ-MADRID, F. 2008. MTOC translocation modulates IS formation and controls sustained T cell signaling. *J Cell Biol,* 182**,** 951-62.

MARTINEZ-POMARES, L. & GORDON, S. 2007. Antigen presentation the macrophage way. *Cell,* 131**,** 641-3.

MASSARDO, L., METZ, C., PARDO, E., MEZZANO, V., BABUL, M., JARPA, E., GUZMAN, A. M., ANDRE, S., KALTNER, H., GABIUS, H. J., JACOBELLI, S., GONZALEZ, A. & SOZA, A. 2009. Autoantibodies against galectin-8: their specificity, association with lymphopenia in systemic lupus erythematosus and detection in rheumatoid arthritis and acute inflammation. *Lupus,* 18**,** 539-46.

MASTERS, T. A., PONTES, B., VIASNOFF, V., LI, Y. & GAUTHIER, N. C. 2013. Plasma membrane tension orchestrates membrane trafficking, cytoskeletal remodeling, and biochemical signaling during phagocytosis. *Proc Natl Acad Sci U S A,* 110**,** 11875-80.

MAYOR, S. & PAGANO, R. E. 2007. Pathways of clathrin-independent endocytosis. *Nat Rev Mol Cell Biol,* 8**,** 603-12.

METZGER, D. W., METZGER, C. A., LING, L. A., HURST, J. S. & VAN CLEAVE, V. H. 1992. Preparative isolation of murine CD5 B cells by panning and magnetic beads. *Ann N Y Acad Sci,* 651**,** 75-7.

MILLER, M. J., WEI, S. H., PARKER, I. & CAHALAN, M. D. 2002. Two-photon imaging of lymphocyte motility and antigen response in intact lymph node. *Science,* 296**,** 1869-73.

MITCHISON, N. A. 2004. T-cell-B-cell cooperation. *Nat Rev Immunol,* 4**,** 308-12.

MITCHISON, T. & KIRSCHNER, M. 1984. Dynamic instability of microtubule growth. *Nature,* 312**,** 237-42.

MONFREGOLA, J., NAPOLITANO, G., D'URSO, M., LAPPALAINEN, P. & URSINI, M. V. 2010. Functional characterization of Wiskott-Aldrich syndrome protein and scar homolog (WASH), a bi-modular nucleation-promoting factor able to interact with biogenesis of lysosome-related organelle subunit 2 (BLOS2) and gamma-tubulin. *J Biol Chem,* 285**,** 16951-7.

MOOREN, O. L., GALLETTA, B. J. & COOPER, J. A. 2012. Roles for actin assembly in endocytosis. *Annu Rev Biochem,* 81**,** 661-86.

MOREAU, H. D., LEMAITRE, F., TERRIAC, E., AZAR, G., PIEL, M., LENNON-DUMENIL, A. M. & BOUSSO, P. 2012. Dynamic in situ cytometry uncovers T cell receptor signaling during immunological synapses and kinapses in vivo. *Immunity,* 37**,** 351-63.

MORITA, E., COLF, L. A., KARREN, M. A., SANDRIN, V., RODESCH, C. K. & SUNDQUIST, W. I. 2010. Human ESCRT-III and VPS4 proteins are required for centrosome and spindle maintenance. *Proc Natl Acad Sci U S A,* 107**,** 12889-94.

MORITZ, M., BRAUNFELD, M. B., GUENEBAUT, V., HEUSER, J. & AGARD, D. A. 2000. Structure of the gamma-tubulin ring complex: a template for microtubule nucleation. *Nat Cell Biol,* 2**,** 365-70.

MORITZ, M., BRAUNFELD, M. B., SEDAT, J. W., ALBERTS, B. & AGARD, D. A. 1995. Microtubule nucleation by gamma-tubulin-containing rings in the centrosome. *Nature,* 378**,** 638-40.

MOSS, C. X., TREE, T. I. & WATTS, C. 2007. Reconstruction of a pathway of antigen processing and class II MHC peptide capture. *EMBO J,* 26**,** 2137-47.

MOSTOWY, S. & COSSART, P. 2012. Septins: the fourth component of the cytoskeleton. *Nat Rev Mol Cell Biol,* 13**,** 183-94.

MULLINS, R. D., HEUSER, J. A. & POLLARD, T. D. 1998. The interaction of Arp2/3 complex with actin: nucleation, high affinity pointed end capping, and formation of branching networks of filaments. *Proc Natl Acad Sci U S A,* 95**,** 6181-6.

NAGASAWA, T. 2006. Microenvironmental niches in the bone marrow required for B-cell development. *Nat Rev Immunol,* 6**,** 107-16.

NATKANSKI, E., LEE, W. Y., MISTRY, B., CASAL, A., MOLLOY, J. E. & TOLAR, P. 2013. B cells use mechanical energy to discriminate antigen affinities. *Science,* 340**,** 1587-90.

NOBES, C. D. & HALL, A. 1995a. Rho, rac and cdc42 GTPases: regulators of actin structures, cell adhesion and motility. *Biochem Soc Trans,* 23**,** 456-9.

NOBES, C. D. & HALL, A. 1995b. Rho, rac, and cdc42 GTPases regulate the assembly of multimolecular focal complexes associated with actin stress fibers, lamellipodia, and filopodia. *Cell,* 81**,** 53-62.

NOLEN, B. J., TOMASEVIC, N., RUSSELL, A., PIERCE, D. W., JIA, Z., MCCORMICK, C. D., HARTMAN, J., SAKOWICZ, R. & POLLARD, T. D. 2009. Characterization of two classes of small molecule inhibitors of Arp2/3 complex. *Nature,* 460**,** 1031-4.

OBINO, D., FARINA, F., MALBEC, O., SAEZ, P. J., MAURIN, M., GAILLARD, J., DINGLI, F., LOEW, D., GAUTREAU, A., YUSEFF, M. I., BLANCHOIN, L., THERY, M. & LENNON-DUMENIL, A. M. 2016. Actin nucleation at the centrosome controls lymphocyte polarity. *Nat Commun,* 7**,** 10969.

OBINO, D. & LENNON-DUMENIL, A. M. 2014. A critical role for cell polarity in antigen extraction, processing, and presentation by B lymphocytes. *Adv Immunol,* 123**,** 51-67.

OKADA, T., MILLER, M. J., PARKER, I., KRUMMEL, M. F., NEIGHBORS, M., HARTLEY, S. B., O'GARRA, A., CAHALAN, M. D. & CYSTER, J. G. 2005.

Antigen-engaged B cells undergo chemotaxis toward the T zone and form motile conjugates with helper T cells. *PLoS Biol,* 3**,** e150.

OLIVEIRA, F. L., BRAND, C., PAULA, A. A., ARCANJO, K. D., HSU, D. K., LIU, F. T., TAKIYA, C. M., BOROJEVIC, R., CHAMMAS, R. & EL-CHEIKH, M. C. 2011. Lack of galectin-3 disturbs mesenteric lymph node homeostasis and B cell niches in the course of Schistosoma mansoni infection. *PLoS One,* 6**,** e19216.

OLMOS, Y. & CARLTON, J. G. 2016. The ESCRT machinery: new roles at new holes. *Curr Opin Cell Biol,* 38**,** 1-11.

PALAZZO, A. F. & GUNDERSEN, G. G. 2002. Microtubule-actin cross-talk at focal adhesions. *Sci STKE,* 2002**,** pe31.

PAPE, K. A., CATRON, D. M., ITANO, A. A. & JENKINS, M. K. 2007. The humoral immune response is initiated in lymph nodes by B cells that acquire soluble antigen directly in the follicles. *Immunity,* 26**,** 491-502.

PARSONS, J. T., HORWITZ, A. R. & SCHWARTZ, M. A. 2010. Cell adhesion: integrating cytoskeletal dynamics and cellular tension. *Nat Rev Mol Cell Biol,* 11**,** 633-43.

PELLEGRIN, S. & MELLOR, H. 2007. Actin stress fibres. *J Cell Sci,* 120**,** 3491-9.

POLLARD, T. D., BLANCHOIN, L. & MULLINS, R. D. 2000. Molecular mechanisms controlling actin filament dynamics in nonmuscle cells. *Annu Rev Biophys Biomol Struct,* 29**,** 545-76.

POLLARD, T. D. & COOPER, J. A. 2009. Actin, a central player in cell shape and movement. *Science,* 326**,** 1208-12.

POULLET, P., CARPENTIER, S. & BARILLOT, E. 2007. myProMS, a web server for management and validation of mass spectrometry-based proteomic data. *Proteomics,* 7**,** 2553-6.

PREBLE, A. M., GIDDINGS, T. M., JR. & DUTCHER, S. K. 2000. Basal bodies and centrioles: their function and structure. *Curr Top Dev Biol,* 49**,** 207-33.

PRECIADO LOPEZ, M., HUBER, F., GRIGORIEV, I., STEINMETZ, M. O., AKHMANOVA, A., DOGTEROM, M. & KOENDERINK, G. H. 2014. In vitro reconstitution of dynamic microtubules interacting with actin filament networks. *Methods Enzymol,* 540**,** 301-20.

QI, H., EGEN, J. G., HUANG, A. Y. & GERMAIN, R. N. 2006. Extrafollicular activation of lymph node B cells by antigen-bearing dendritic cells. *Science,* 312**,** 1672-6.

RABINOVICH, G. A. & CROCI, D. O. 2012. Regulatory circuits mediated by lectin-glycan interactions in autoimmunity and cancer. *Immunity,* 36**,** 322-35.

RABINOVICH, G. A. & TOSCANO, M. A. 2009. Turning 'sweet' on immunity: galectin-glycan interactions in immune tolerance and inflammation. *Nat Rev Immunol,* 9**,** 338-52.

RAFTOPOULOU, M. & HALL, A. 2004. Cell migration: Rho GTPases lead the way. *Dev Biol,* 265**,** 23-32.

RANDALL, K. L., LAMBE, T., JOHNSON, A. L., TREANOR, B., KUCHARSKA, E., DOMASCHENZ, H., WHITTLE, B., TZE, L. E., ENDERS, A., CROCKFORD, T. L., BOURIEZ-JONES, T., ALSTON, D., CYSTER, J. G., LENARDO, M. J., MACKAY, F., DEENICK, E. K., TANGYE, S. G., CHAN, T. D., CAMIDGE, T., BRINK, R., VINUESA, C. G., BATISTA, F. D., CORNALL, R. J. & GOODNOW, C. C. 2009. Dock8 mutations cripple B cell immunological synapses, germinal centers and long-lived antibody production. *Nat Immunol,* 10**,** 1283-91.

RAYMOND, C. K., HOWALD-STEVENSON, I., VATER, C. A. & STEVENS, T. H. 1992. Morphological classification of the yeast vacuolar protein sorting mutants: evidence for a prevacuolar compartment in class E vps mutants. *Mol Biol Cell,* 3**,** 1389-402.

REAL, E., FAURE, S., DONNADIEU, E. & DELON, J. 2007. Cutting edge: Atypical PKCs regulate T lymphocyte polarity and scanning behavior. *J Immunol,* 179**,** 5649-52.

REIF, K., EKLAND, E. H., OHL, L., NAKANO, H., LIPP, M., FORSTER, R. & CYSTER, J. G. 2002. Balanced responsiveness to chemoattractants from adjacent zones determines B-cell position. *Nature,* 416**,** 94-9.

RETH, M. & WIENANDS, J. 1997. Initiation and processing of signals from the B cell antigen receptor. *Annu Rev Immunol,* 15**,** 453-79.

REVERSAT, A., YUSEFF, M. I., LANKAR, D., MALBEC, O., OBINO, D., MAURIN, M., PENMATCHA, N. V., AMOROSO, A., SENGMANIVONG, L., GUNDERSEN, G. G., MELLMAN, I., DARCHEN, F., DESNOS, C., PIEROBON, P. & LENNON-DUMENIL, A. M. 2015. Polarity protein Par3 controls B-cell receptor dynamics and antigen extraction at the immune synapse. *Mol Biol Cell,* 26**,** 1273-85.

RIDLEY, A. J. & HALL, A. 1992. The small GTP-binding protein rho regulates the assembly of focal adhesions and actin stress fibers in response to growth factors. *Cell,* 70**,** 389-99.

RIEDER, C. L. & ALEXANDER, S. P. 1990. Kinetochores are transported poleward along a single astral microtubule during chromosome attachment to the spindle in newt lung cells. *J Cell Biol,* 110**,** 81-95.

RIESE, R. J., WOLF, P. R., BROMME, D., NATKIN, L. R., VILLADANGOS, J. A., PLOEGH, H. L. & CHAPMAN, H. A. 1996. Essential role for cathepsin S in MHC class II-associated invariant chain processing and peptide loading. *Immunity,* 4**,** 357-66.

ROBBINS, E., JENTZSCH, G. & MICALI, A. 1968. The centriole cycle in synchronized HeLa cells. *J Cell Biol,* 36**,** 329-39.

ROBIN, C., OTTERSBACH, K., DE BRUIJN, M., MA, X., VAN DER HORN, K. & DZIERZAK, E. 2003. Developmental origins of hematopoietic stem cells. *Oncol Res,* 13**,** 315-21.

ROCHE, P. A. & CRESSWELL, P. 1990. Invariant chain association with HLA-DR molecules inhibits immunogenic peptide binding. *Nature,* 345**,** 615-8.

ROCHE, P. A. & CRESSWELL, P. 1991. Proteolysis of the class II-associated invariant chain generates a peptide binding site in intracellular HLA-DR molecules. *Proc Natl Acad Sci U S A,* 88**,** 3150-4.

RODRIGUEZ, O. C., SCHAEFER, A. W., MANDATO, C. A., FORSCHER, P., BEMENT, W. M. & WATERMAN-STORER, C. M. 2003. Conserved microtubule-actin interactions in cell movement and morphogenesis. *Nat Cell Biol,* 5**,** 599-609.

ROOZENDAAL, R., MEMPEL, T. R., PITCHER, L. A., GONZALEZ, S. F., VERSCHOOR, A., MEBIUS, R. E., VON ANDRIAN, U. H. & CARROLL, M. C. 2009. Conduits mediate transport of low-molecular-weight antigen to lymph node follicles. *Immunity,* 30**,** 264-76.

ROPER, K., GREGORY, S. L. & BROWN, N. H. 2002. The 'spectraplakins': cytoskeletal giants with characteristics of both spectrin and plakin families. *J Cell Sci,* 115**,** 4215-25.

ROSENBLATT, J., CRAMER, L. P., BAUM, B. & MCGEE, K. M. 2004. Myosin II-dependent cortical movement is required for centrosome separation and positioning during mitotic spindle assembly. *Cell,* 117**,** 361-72.

ROSSI, B., ESPELI, M., SCHIFF, C. & GAUTHIER, L. 2006. Clustering of pre-B cell integrins induces galectin-1-dependent pre-B cell receptor relocalization and activation. *J Immunol,* 177**,** 796-803.

ROTH, D. B. 2014. V(D)J Recombination: Mechanism, Errors, and Fidelity. *Microbiol Spectr,* 2.

ROTTY, J. D., WU, C. & BEAR, J. E. 2013. New insights into the regulation and cellular functions of the ARP2/3 complex. *Nat Rev Mol Cell Biol,* 14**,** 7-12.

ROUGERIE, P. & DELON, J. 2012. Rho GTPases: masters of T lymphocyte migration and activation. *Immunol Lett,* 142**,** 1-13.

SAEZ DE GUINOA, J., BARRIO, L. & CARRASCO, Y. R. 2013. Vinculin arrests motile B cells by stabilizing integrin clustering at the immune synapse. *J Immunol,* 191**,** 2742-51.

SAEZ DE GUINOA, J., BARRIO, L., MELLADO, M. & CARRASCO, Y. R. 2011. CXCL13/CXCR5 signaling enhances BCR-triggered B-cell activation by shaping cell dynamics. *Blood,* 118**,** 1560-9.

SAMPSON, J. F., SURYAWANSHI, A., CHEN, W. S., RABINOVICH, G. A. & PANJWANI, N. 2016. Galectin-8 promotes regulatory T-cell differentiation by modulating IL-2 and TGFbeta signaling. *Immunol Cell Biol,* 94**,** 220.

SANTOS-ARGUMEDO, L., MARAVILLAS-MONTERO, J. L. & LOPEZ-ORTEGA, O. 2013. Class I myosins in B-cell physiology: functions in spreading, immune synapses, motility, and vesicular traffic. *Immunol Rev,* 256**,** 190-202.

SCHINDELIN, J., ARGANDA-CARRERAS, I., FRISE, E., KAYNIG, V., LONGAIR, M., PIETZSCH, T., PREIBISCH, S., RUEDEN, C., SAALFELD, S., SCHMID, B., TINEVEZ, J. Y., WHITE, D. J., HARTENSTEIN, V., ELICEIRI, K., TOMANCAK, P. & CARDONA, A. 2012. Fiji: an open-source platform for biological-image analysis. *Nat Methods,* 9**,** 676-82.

SCHMORANZER, J., FAWCETT, J. P., SEGURA, M., TAN, S., VALLEE, R. B., PAWSON, T. & GUNDERSEN, G. G. 2009. Par3 and dynein associate to regulate local microtubule dynamics and centrosome orientation during migration. *Curr Biol,* 19**,** 1065-74.

SCHNEIDER, R. & PERSSON, S. 2015. Connecting two arrays: the emerging role of actin-microtubule cross-linking motor proteins. *Front Plant Sci,* 6**,** 415.

SCHNYDER, T., CASTELLO, A., FEEST, C., HARWOOD, N. E., OELLERICH, T., URLAUB, H., ENGELKE, M., WIENANDS, J., BRUCKBAUER, A. & BATISTA, F. D. 2011. B cell receptor-mediated antigen gathering requires ubiquitin ligase Cbl and adaptors Grb2 and Dok-3 to recruit dynein to the signaling microcluster. *Immunity,* 34**,** 905-18.

SCHROEDER, M. N., TRIBULATTI, M. V., CARABELLI, J., ANDRE-LEROUX, G., CARAMELO, J. J., CATTANEO, V. & CAMPETELLA, O. 2016. Characterization of a double-CRD-mutated Gal-8 recombinant protein that retains costimulatory activity on antigen-specific T cell response. *Biochem J.*

SEELEY-FALLEN, M. K., LIU, L. J., SHAPIRO, M. R., ONABAJO, O. O., PALANIYANDI, S., ZHU, X., TAN, T. H., UPADHYAYA, A. & SONG, W. 2014. Actin-binding protein 1 links B-cell antigen receptors to negative signaling pathways. *Proc Natl Acad Sci U S A,* 111**,** 9881-6.

SEMINARIO, M. C. & BUNNELL, S. C. 2008. Signal initiation in T-cell receptor microclusters. *Immunol Rev,* 221**,** 90-106.

SHARMA, S., ORLOWSKI, G. & SONG, W. 2009. Btk regulates B cell receptor-mediated antigen processing and presentation by controlling actin cytoskeleton dynamics in B cells. *J Immunol,* 182**,** 329-39.

SIMS, T. N., SOOS, T. J., XENIAS, H. S., DUBIN-THALER, B., HOFMAN, J. M., WAITE, J. C., CAMERON, T. O., THOMAS, V. K., VARMA, R., WIGGINS, C. H., SHEETZ, M. P., LITTMAN, D. R. & DUSTIN, M. L. 2007. Opposing effects of PKCtheta and WASp on symmetry breaking and relocation of the immunological synapse. *Cell,* 129**,** 773-85.

SMALL, J. V., KAVERINA, I., KRYLYSHKINA, O. & ROTTNER, K. 1999. Cytoskeleton cross-talk during cell motility. *FEBS Lett,* 452**,** 96-9.

SMYTHE, E. & AYSCOUGH, K. R. 2006. Actin regulation in endocytosis. *J Cell Sci,* 119**,** 4589-98.

SPRINGER, T. A. & DUSTIN, M. L. 2012. Integrin inside-out signaling and the immunological synapse. *Curr Opin Cell Biol,* 24**,** 107-15.

STINCHCOMBE, J. C. & GRIFFITHS, G. M. 2007. Secretory mechanisms in cell-mediated cytotoxicity. *Annu Rev Cell Dev Biol,* 23**,** 495-517.

STINCHCOMBE, J. C. & GRIFFITHS, G. M. 2014. Communication, the centrosome and the immunological synapse. *Philos Trans R Soc Lond B Biol Sci,* 369.

STINCHCOMBE, J. C., MAJOROVITS, E., BOSSI, G., FULLER, S. & GRIFFITHS, G. M. 2006. Centrosome polarization delivers secretory granules to the immunological synapse. *Nature,* 443**,** 462-5.

STINCHCOMBE, J. C., SALIO, M., CERUNDOLO, V., PENDE, D., ARICO, M. & GRIFFITHS, G. M. 2011. Centriole polarisation to the immunological synapse directs secretion from cytolytic cells of both the innate and adaptive immune systems. *BMC Biol,* 9**,** 45.

STODDART, A., DYKSTRA, M. L., BROWN, B. K., SONG, W., PIERCE, S. K. & BRODSKY, F. M. 2002. Lipid rafts unite signaling cascades with clathrin to regulate BCR internalization. *Immunity,* 17**,** 451-62.

STODDART, A., JACKSON, A. P. & BRODSKY, F. M. 2005. Plasticity of B cell receptor internalization upon conditional depletion of clathrin. *Mol Biol Cell,* 16**,** 2339-48.

SUETSUGU, S. 2013. Activation of nucleation promoting factors for directional actin filament elongation: allosteric regulation and multimerization on the membrane. *Semin Cell Dev Biol,* 24**,** 267-71.

SUMOZA-TOLEDO, A., GILLESPIE, P. G., ROMERO-RAMIREZ, H., FERREIRA-ISHIKAWA, H. C., LARSON, R. E. & SANTOS-ARGUMEDO, L. 2006. Differential localization of unconventional myosin I and nonmuscle myosin II during B cell spreading. *Exp Cell Res,* 312**,** 3312-22.

SUOZZI, K. C., WU, X. & FUCHS, E. 2012. Spectraplakins: master orchestrators of cytoskeletal dynamics. *J Cell Biol,* 197**,** 465-75.

SUZUKI, K., GRIGOROVA, I., PHAN, T. G., KELLY, L. M. & CYSTER, J. G. 2009. Visualizing B cell capture of cognate antigen from follicular dendritic cells. *J Exp Med,* 206**,** 1485-93.

TANG, N. & MARSHALL, W. F. 2012. Centrosome positioning in vertebrate development. *J Cell Sci,* 125**,** 4951-61.

TAPLEY, E. C. & STARR, D. A. 2013. Connecting the nucleus to the cytoskeleton by SUN-KASH bridges across the nuclear envelope. *Curr Opin Cell Biol,* 25**,** 57-62.

THAUNAT, O., GRANJA, A. G., BARRAL, P., FILBY, A., MONTANER, B., COLLINSON, L., MARTINEZ-MARTIN, N., HARWOOD, N. E., BRUCKBAUER, A. & BATISTA, F. D. 2012. Asymmetric segregation of polarized antigen on B cell division shapes presentation capacity. *Science,* 335**,** 475-9.

TOLAR, P., SOHN, H. W. & PIERCE, S. K. 2008. Viewing the antigen-induced initiation of B-cell activation in living cells. *Immunol Rev,* 221**,** 64-76.

TOURRET, M., GUEGAN, S., CHEMIN, K., DOGNIAUX, S., MIRO, F., BOHINEUST, A. & HIVROZ, C. 2010. T cell polarity at the immunological synapse is required for CD154-dependent IL-12 secretion by dendritic cells. *J Immunol,* 185**,** 6809-18.

TREANOR, B., DEPOIL, D., BRUCKBAUER, A. & BATISTA, F. D. 2011. Dynamic cortical actin remodeling by ERM proteins controls BCR microcluster organization and integrity. *J Exp Med,* 208**,** 1055-68.

TREANOR, B., DEPOIL, D., GONZALEZ-GRANJA, A., BARRAL, P., WEBER, M., DUSHEK, O., BRUCKBAUER, A. & BATISTA, F. D. 2010. The membrane skeleton controls diffusion dynamics and signaling through the B cell receptor. *Immunity,* 32**,** 187-99.

TRIBULATTI, M. V., CATTANEO, V., HELLMAN, U., MUCCI, J. & CAMPETELLA, O. 2009. Galectin-8 provides costimulatory and proliferative signals to T lymphocytes. *J Leukoc Biol,* 86**,** 371-80.

TSAI, C. M., CHIU, Y. K., HSU, T. L., LIN, I. Y., HSIEH, S. L. & LIN, K. I. 2008. Galectin-1 promotes immunoglobulin production during plasma cell differentiation. *J Immunol,* 181**,** 4570-9.

TSAI, C. M., GUAN, C. H., HSIEH, H. W., HSU, T. L., TU, Z., WU, K. J., LIN, C. H. & LIN, K. I. 2011. Galectin-1 and galectin-8 have redundant roles in promoting plasma cell formation. *J Immunol,* 187**,** 1643-52.

TSAI, C. M., WU, H. Y., SU, T. H., KUO, C. W., HUANG, H. W., CHUNG, C. H., CHEN, C. S., KHOO, K. H., CHEN, Y. J. & LIN, K. I. 2014. Phosphoproteomic analyses reveal that galectin-1 augments the dynamics of B-cell receptor signaling. *J Proteomics,* 103**,** 241-53.

UNGERER, C., QUADE-LYSSY, P., RADEKE, H. H., HENSCHLER, R., KONIGS, C., KOHL, U., SEIFRIED, E. & SCHUTTRUMPF, J. 2014. Galectin-9 is a suppressor of T and B cells and predicts the immune modulatory potential of mesenchymal stromal cell preparations. *Stem Cells Dev,* 23**,** 755-66.

URUNO, T., ZHANG, P., LIU, J., HAO, J. J. & ZHAN, X. 2003. Haematopoietic lineage cell-specific protein 1 (HS1) promotes actin-related protein (Arp) 2/3 complex-mediated actin polymerization. *Biochem J,* 371**,** 485-93.

UZBEKOV, R., KIREYEV, I. & PRIGENT, C. 2002. Centrosome separation: respective role of microtubules and actin filaments. *Biol Cell,* 94**,** 275-88.

VASCOTTO, F., LANKAR, D., FAURE-ANDRE, G., VARGAS, P., DIAZ, J., LE ROUX, D., YUSEFF, M. I., SIBARITA, J. B., BOES, M., RAPOSO, G., MOUGNEAU, E., GLAICHENHAUS, N., BONNEROT, C., MANOURY, B. & LENNON-DUMENIL, A. M. 2007. The actin-based motor protein myosin II regulates MHC class II trafficking and BCR-driven antigen presentation. *J Cell Biol,* 176**,** 1007-19.

VAUGHAN, S. & DAWE, H. R. 2011. Common themes in centriole and centrosome movements. *Trends Cell Biol,* 21**,** 57-66.

VICUNA, L., PARDO, E., CURKOVIC, C., DOGER, R., OYANADEL, C., METZ, C., MASSARDO, L., GONZALEZ, A. & SOZA, A. 2013. Galectin-8 binds to LFA-1, blocks its interaction with ICAM-1 and is counteracted by anti-Gal-8 autoantibodies isolated from lupus patients. *Biol Res,* 46**,** 275-80.

VILLADANGOS, J. A., RIESE, R. J., PETERS, C., CHAPMAN, H. A. & PLOEGH, H. L. 1997. Degradation of mouse invariant chain: roles of cathepsins S and D and the influence of major histocompatibility complex polymorphism. *J Exp Med,* 186**,** 549-60.

WICKSTEAD, B. & GULL, K. 2011. The evolution of the cytoskeleton. *J Cell Biol,* 194**,** 513-25.

WOODMAN, P. 2016. ESCRT-III on endosomes: new functions, new activation pathway. *Biochem J,* 473**,** e5-8.

WOODRUFF, J. B., WUESEKE, O. & HYMAN, A. A. 2014. Pericentriolar material structure and dynamics. *Philos Trans R Soc Lond B Biol Sci,* 369.

WUBBOLTS, R., FERNANDEZ-BORJA, M., JORDENS, I., REITS, E., DUSSELJEE, S., ECHEVERRI, C., VALLEE, R. B. & NEEFJES, J. 1999. Opposing motor activities of

dynein and kinesin determine retention and transport of MHC class II-containing compartments. *J Cell Sci,* 112 (Pt 6)**,** 785-95.

WUBBOLTS, R., FERNANDEZ-BORJA, M., OOMEN, L., VERWOERD, D., JANSSEN, H., CALAFAT, J., TULP, A., DUSSELJEE, S. & NEEFJES, J. 1996. Direct vesicular transport of MHC class II molecules from lysosomal structures to the cell surface. *J Cell Biol,* 135**,** 611-22.

WUBBOLTS, R. & NEEFJES, J. 1999. Intracellular transport and peptide loading of MHC class II molecules: regulation by chaperones and motors. *Immunol Rev,* 172**,** 189-208.

YANG, Y. H., DUDOIT, S., LUU, P., LIN, D. M., PENG, V., NGAI, J. & SPEED, T. P. 2002. Normalization for cDNA microarray data: a robust composite method addressing single and multiple slide systematic variation. *Nucleic Acids Res,* 30**,** e15.

YI, J., WU, X., CHUNG, A. H., CHEN, J. K., KAPOOR, T. M. & HAMMER, J. A. 2013. Centrosome repositioning in T cells is biphasic and driven by microtubule end-on capture-shrinkage. *J Cell Biol,* 202**,** 779-92.

YUSEFF, M. I., LANKAR, D. & LENNON-DUMENIL, A. M. 2009. Dynamics of membrane trafficking downstream of B and T cell receptor engagement: impact on immune synapses. *Traffic,* 10**,** 629-36.

YUSEFF, M. I., PIEROBON, P., REVERSAT, A. & LENNON-DUMENIL, A. M. 2013. How B cells capture, process and present antigens: a crucial role for cell polarity. *Nat Rev Immunol,* 13**,** 475-86.

YUSEFF, M. I., REVERSAT, A., LANKAR, D., DIAZ, J., FANGET, I., PIEROBON, P., RANDRIAN, V., LAROCHETTE, N., VASCOTTO, F., DESDOUETS, C., JAUFFRED, B., BELLAICHE, Y., GASMAN, S., DARCHEN, F., DESNOS, C. & LENNON-DUMENIL, A. M. 2011. Polarized secretion of lysosomes at the B cell synapse couples antigen extraction to processing and presentation. *Immunity,* 35**,** 361-74.

ZHANG, F., SOUTHWICK, F. S. & PURICH, D. L. 2002. Actin-based phagosome motility. *Cell Motil Cytoskeleton,* 53**,** 81-8.

ZHANG, X., LEI, K., YUAN, X., WU, X., ZHUANG, Y., XU, T., XU, R. & HAN, M. 2009. SUN1/2 and Syne/Nesprin-1/2 complexes connect centrosome to the nucleus during neurogenesis and neuronal migration in mice. *Neuron,* 64**,** 173-87.

ZHU, J., BURAKOV, A., RODIONOV, V. & MOGILNER, A. 2010. Finding the cell center by a balance of dynein and myosin pulling and microtubule pushing: a computational study. *Mol Biol Cell,* 21**,** 4418-27.

ZICK, Y., EISENSTEIN, M., GOREN, R. A., HADARI, Y. R., LEVY, Y. & RONEN, D. 2004. Role of galectin-8 as a modulator of cell adhesion and cell growth. *Glycoconj J,* 19**,** 517-26.

ZUNIGA, E., RABINOVICH, G. A., IGLESIAS, M. M. & GRUPPI, A. 2001. Regulated expression of galectin-1 during B-cell activation and implications for T-cell apoptosis. *J Leukoc Biol,* 70**,** 73-9.

APPENDICES

"Actin nucleation at the centrosome controls lymphocyte polarity"

Dorian Obino[1], Francesca Farina[2], Odile Malbec[1], Pablo J. Sáez[1], Mathieu Maurin[1], Jérémie Gaillard[2], Florent Dingli[3], Damarys Loew[3], Alexis Gautreau[4], Maria-Isabel Yuseff[5], Laurent Blanchoin[2], Manuel Théry[2,6] and Ana-Maria Lennon-Duménil[1]

Nature Communications, In press

[1]INSERM – U932 Immunité et Cancer, Institut Curie, PSL Research University, Paris, France
[2]Laboratoire de Physiologie Cellulaire et Végétale, Institut de Recherche en Technologie et Science pour le Vivant, UMR5168, CEA/INRA/CNRS/UGA, Grenoble, France
[3]Laboratoire de Spectrométrie de Masse Protéomique, Institut Curie, PSL Research University, Paris, France
[4]Ecole Polytechnique, CNRS UMR7654, Palaiseau, France
[5]Departamento de Biologia Cellular y Molecular, P. Universidad Catolica de Chile, Santiago, Chile
[6]Unité de Thérapie Cellulaire, Hôpital Saint Louis, Institut Universitaire d'Hématologie, UMRS1160, INSERM/AP-HP/Université Paris Diderot, Paris, France

nature COMMUNICATIONS

ARTICLE

Received 21 Dec 2015 | Accepted 5 Feb 2016 | Published 18 Mar 2016

DOI: 10.1038/ncomms10969 OPEN

Actin nucleation at the centrosome controls lymphocyte polarity

Dorian Obino[1], Francesca Farina[2], Odile Malbec[1], Pablo J. Sáez[1], Mathieu Maurin[1], Jérémie Gaillard[2], Florent Dingli[3], Damarys Loew[3], Alexis Gautreau[4], Maria-Isabel Yuseff[5], Laurent Blanchoin[2], Manuel Théry[2,6] & Ana-Maria Lennon-Duménil[1]

Cell polarity is required for the functional specialization of many cell types including lymphocytes. A hallmark of cell polarity is the reorientation of the centrosome that allows repositioning of organelles and vesicles in an asymmetric fashion. The mechanisms underlying centrosome polarization are not fully understood. Here we found that in resting lymphocytes, centrosome-associated Arp2/3 locally nucleates F-actin, which is needed for centrosome tethering to the nucleus via the LINC complex. Upon lymphocyte activation, Arp2/3 is partially depleted from the centrosome as a result of its recruitment to the immune synapse. This leads to a reduction in F-actin nucleation at the centrosome and thereby allows its detachment from the nucleus and polarization to the synapse. Therefore, F-actin nucleation at the centrosome—regulated by the availability of the Arp2/3 complex—determines its capacity to polarize in response to external stimuli.

[1] INSERM—U932 Immunité et Cancer, Institut Curie, PSL Research University, 75248 Paris Cedex 05, France. [2] CytoMorpho Lab, Biosciences & Biotechnology Institute of Grenoble, UMR5168, CEA/INRA/CNRS/Université Grenoble-Alpes, Grenoble 38054, France. [3] Laboratoire de Spectrométrie de Masse Protéomique, Institut Curie, PSL Research University, 75248 Paris Cedex 05, France. [4] Ecole Polytechnique, CNRS UMR7654, Palaiseau 91120, France. [5] Departamento de Biologia Celular y Molecular, Pontificia Universidad Catolica de Chile, Santiago 6513677, Chile. [6] CytoMorpho Lab, Hopital Saint Louis, Institut Universitaire d'Hematologie, UMRS1160, CEA/INSERM/Université Paris Diderot, Paris 75010, France. Correspondence and requests for materials should be addressed to A.-M.L.-D. (email: Ana-Maria.Lennon@curie.fr).

Cell polarity regulates a broad range of biological processes such as cell division, cell fate and cell migration[1–3]. It relies on the organization of the microtubule cytoskeleton, which defines the axis of cell division, as well as the directionality of intracellular trafficking[4]. As the centrosome drives the nucleation and organization of microtubules, this organelle was found to play an essential role in the polarization of a variety of cell types ranging from yeast to specialized cells in multicellular organisms[5]. In lymphocytes, centrosome reorientation to one cell pole was shown to be required for cell migration[6], asymmetric division[1,2,7] and immune synapse formation[8].

The term immune synapse refers to the zone of tight interaction that forms between lymphocytes and antigen-presenting cells towards which the centrosome polarizes[9]. It is viewed as a signalling platform where both exocytotic and endocytotic events needed for lymphocytes to perform their specific effector function take place[10]. These include the secretion of granules in both cytotoxic lymphocytes and natural killer cells[11], of cytokine-loaded vesicles in helper T cells[12,13] and of hydrolase-containing lysosomes in B cells[5,14]. Hence, centrosome polarization emerges as pivotal in the regulation of immunity, stressing the need to unravel the underlying molecular mechanisms. In that regard, PKC and Cdc42 signalling molecules as well as the microtubule minus-end motor Dynein were shown to regulate centrosome repositioning at the synapse of both B and T lymphocytes[14–20]. Regarding the actin cytoskeleton, Arp2/3-dependent nucleation of F-actin was shown to be dispensable for centrosome polarization in T lymphocytes, which rather requires the activity of Formins[21]. In general, whether and how centrosome-intrinsic components regulate its ability to polarize remains unexplored.

In this study, we show that Arp2/3-dependent F-actin nucleation at the centrosome of resting lymphocytes links this organelle to the nucleus. Clearance of centrosomal Arp2/3 upon lymphocyte activation promotes centrosome–nucleus separation and subsequent centrosome polarization to the immune synapse. F-actin nucleation at the centrosome therefore determines the ability of this organelle to polarize to one cell pole.

Results

Lymphocyte activation modifies the centrosome proteome. We aimed at investigating the role of centrosome-associated proteins in cell polarity by using B lymphocytes as a model. Centrosome polarization in these cells can be triggered by engaging their membrane antigen receptor—the B-cell antigen receptor (BCR)—with surface-tethered ligands coated on latex beads (Fig. 1a), planar surfaces or cells[14,17,22]. We hypothesized that changes in the composition of centrosome-associated proteins between non-polarized and polarized cells might reveal valuable candidates to be involved in this process. A stable isotope labelling by amino acids in cell culture (SILAC)[23]-based quantitative proteomic approach was therefore developed to identify proteins differentially associated with the centrosome of non-polarized and polarized B cells. For this, B cells were grown in cultures containing lysine labelled with light or heavy carbon isotopes and incubated for 60 min with BCR-ligand^{+} or BCR-ligand^{-} beads, respectively (Fig. 1b). Cells were lysed, centrosomes were isolated on sucrose gradient and the three main γ-tubulin-containing fractions were pooled for each sample (Fig. 1c). Resulting pools were mixed 1:1 to be separated by SDS–polyacrylamide gel electrophoresis (SDS–PAGE) followed by reverse-phase liquid chromatography and analysed by high-resolution mass spectrometry (LC–MS/MS) (Fig. 1b). This led to the quantification of 1,600 proteins (false discovery rate (FDR) of 1%, number of peptides used ≥ 3; Fig. 1d) among which 835 were differentially associated with the centrosome of activated lymphocytes (absolute fold change $\geq 10\%$ and adjusted P value of quantification ≤ 0.05; Fig. 1d, light red). To identify key networks, genome ontology (GO) term enrichment was performed on these 835 proteins. As expected, this analysis highlighted components of the microtubule-organizing centre (enrichment factor: 1.9; P value $= 3.56 \times 10^{-05}$) and the cytoskeleton (enrichment factor: 1.8; P value $= 2.65 \times 10^{-11}$) as two major groups of proteins enriched in centrosome preparations (Supplementary Table 1). More surprisingly, zooming on proteins belonging to the GO term 'Cytoskeleton' showed that while microtubule-related components were either increased or decreased in polarized cells, the majority of actin cytoskeleton components were reduced (69.8%; Fig. 1e and Supplementary Table 2). Noticeably, this particularly applied to three subunits of the branched actin-nucleating complex Arp2/3 (ref. 24; 10 and 12% decrease; Fig. 1e, red; and Supplementary Tables 3–5). Immunoblot analysis showed an even more pronounced reduction of the Arp2/3 subunit Arp2 in centrosomal fractions from activated lymphocytes (Supplementary Fig. 1a). No reduction in the total amount of Arp2 was observed between both conditions (Supplementary Fig. 1b). We conclude that BCR engagement induces multiple changes in the centrosome proteome including a significant reduction in the pool of associated Arp2/3. Although the presence of this complex at the centrosome had been described in the past[25], whether it regulates centrosome function remains unclear. We therefore focused our analysis on exploring the putative role of Arp2/3 reduction at the centrosome of activated lymphocytes in the polarization of this organelle.

Reduced centrosomal Arp2/3 in activated lymphocytes. We next asked whether reduction of Arp2/3 at the centrosome was equally observed in intact lymphocytes. Immunofluorescence analysis revealed the presence of two pools of Arp2/3 in resting B cells: a cortical pool (Fig. 2a, white arrow) and a cytosolic pool that surrounded the centrosome (Fig. 2a, white star). To accurately quantify this centrosome-associated pool of Arp2/3, we computed a radial line scan of Arp2 fluorescence intensity from the centrosome of resting lymphocytes and, based on this result, we defined a 'centrosomal area' (Fig. 2b). The amount of Arp2/3 in this centrosomal area was then quantified at different time points after BCR engagement. In agreement with our proteomic and immunoblot data, we found that this centrosome-associated pool of Arp2/3 gradually decreased in time upon lymphocyte stimulation with BCR-ligand^{+} beads (Fig. 2a,c). No reduction in the total amount of Arp2/3 was found (Supplementary Fig. 2a). Similarly, in resting B lymphocytes, we observed the presence of a pool of F-actin in close vicinity of the centrosome (Fig. 2d), which co-localized with Arp2/3 (Supplementary Fig. 2b). In contrast, in lymphocytes incubated for 30 min with BCR-ligand^{+} beads, F-actin was observed as patches dispersed in the cytosol rather than gathered around the centrosome (Fig. 2d). After 60 min of stimulation, the centrosome polarized to the cell–bead interface and was therefore found in proximity to the cortical F-actin pool. Nonetheless, the pool of centrosome-associated F-actin was decreased in these cells (Fig. 2b,d,e). No reduction in the total amount of F-actin was observed (Supplementary Fig. 2c). Of note, because methanol fixation required for γ-tubulin staining is not compatible with phalloidin labelling, the centrosome was stained with antibodies directed against α-tubulin, and images were processed (fluorescence intensity threshold) to visualize the centrosome but not the microtubules (Supplementary Fig. 2d). Altogether these results show that resting B cells display a pool of Arp2/3 and F-actin at their centrosome that decreases while this organelle polarizes to the immune synapse.

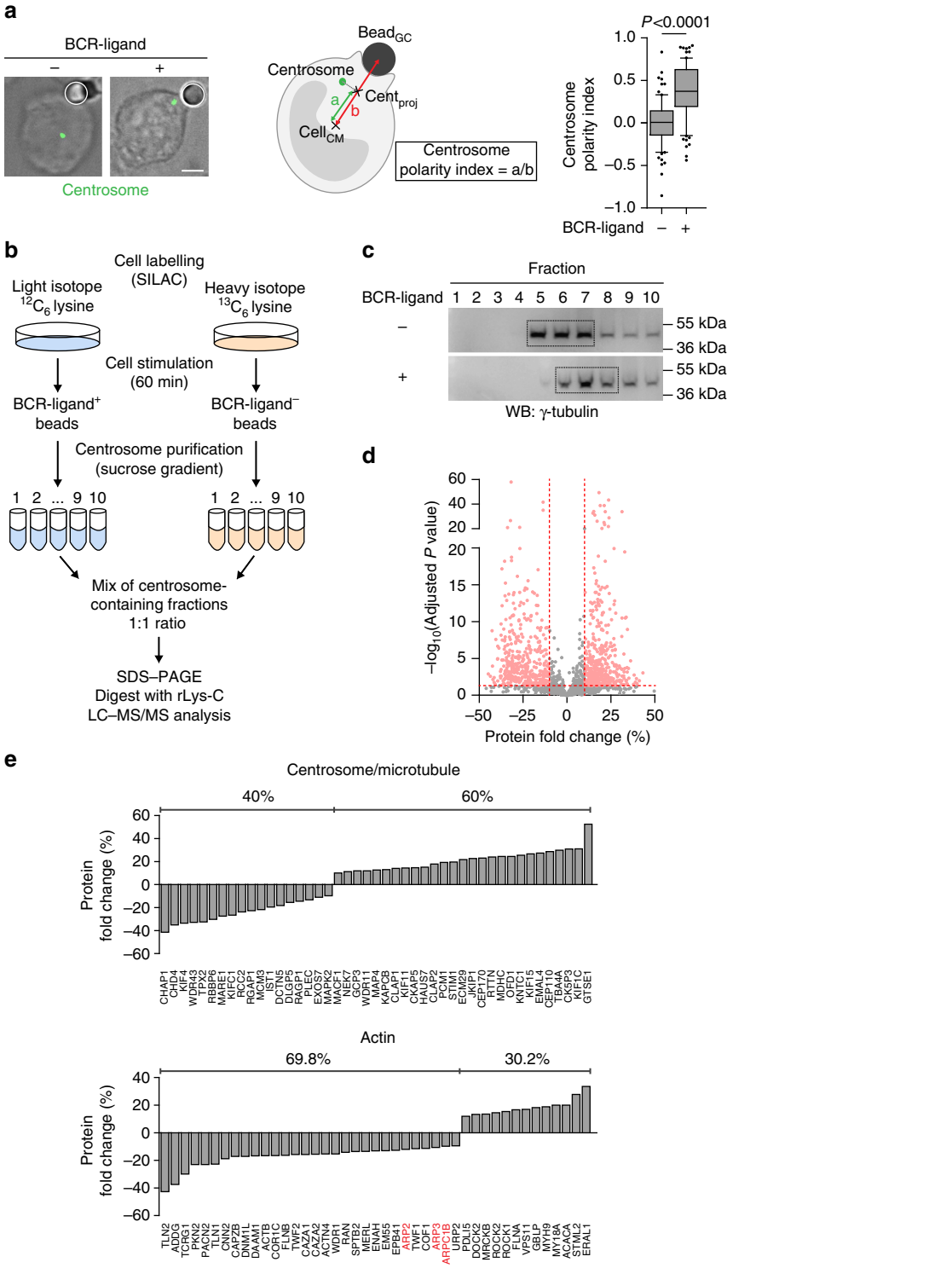

Figure 1 | Lymphocyte stimulation modifies the centrosome-associated proteome. (**a**) Left: representative images of non-polarized (BCR-ligand$^-$) and polarized (BCR-ligand$^+$) B cells. B cells were incubated for 60 min with beads coated with either BCR ligands or with proteins that do not engage the BCR, fixed and the centrosome was stained (γ-tubulin). White circles indicate bead position. Scale bar, 3 μm. Middle: schematics depicting centrosome polarity index measurement. Right: quantification of centrosome polarity index. Data are pooled from three independent experiments with $n=80$ and 85 cells for BCR-ligand$^-$ and BCR-ligand$^+$, respectively. Unpaired Student's *t*-test was used to determine statistical significance. (**b**) SILAC-based MS workflow used to identify proteins differentially associated with the centrosome of B cells stimulated with either BCR-ligand$^-$ or BCR-ligand$^+$ beads. (**c**) Western blots highlighting centrosome-containing fractions after centrosome isolation on discontinuous sucrose gradient. Immunoblots are representative of three independent experiments. (**d**) Volcano plot showing the 835 proteins considered for further analysis (light red) among the total of the 1,600 quantified proteins. Horizontal red line represents the threshold for statistical significance (adjusted *P* value ≤ 0.05). Vertical red lines represent the biological threshold used to select proteins (-10% and $+10\%$ of protein fold change). (**e**) Protein fold change (%) for each of the 45 proteins belonging to the 'centrosome/microtubule' subgroup (top) and the 43 belonging to the 'actin' one (bottom).

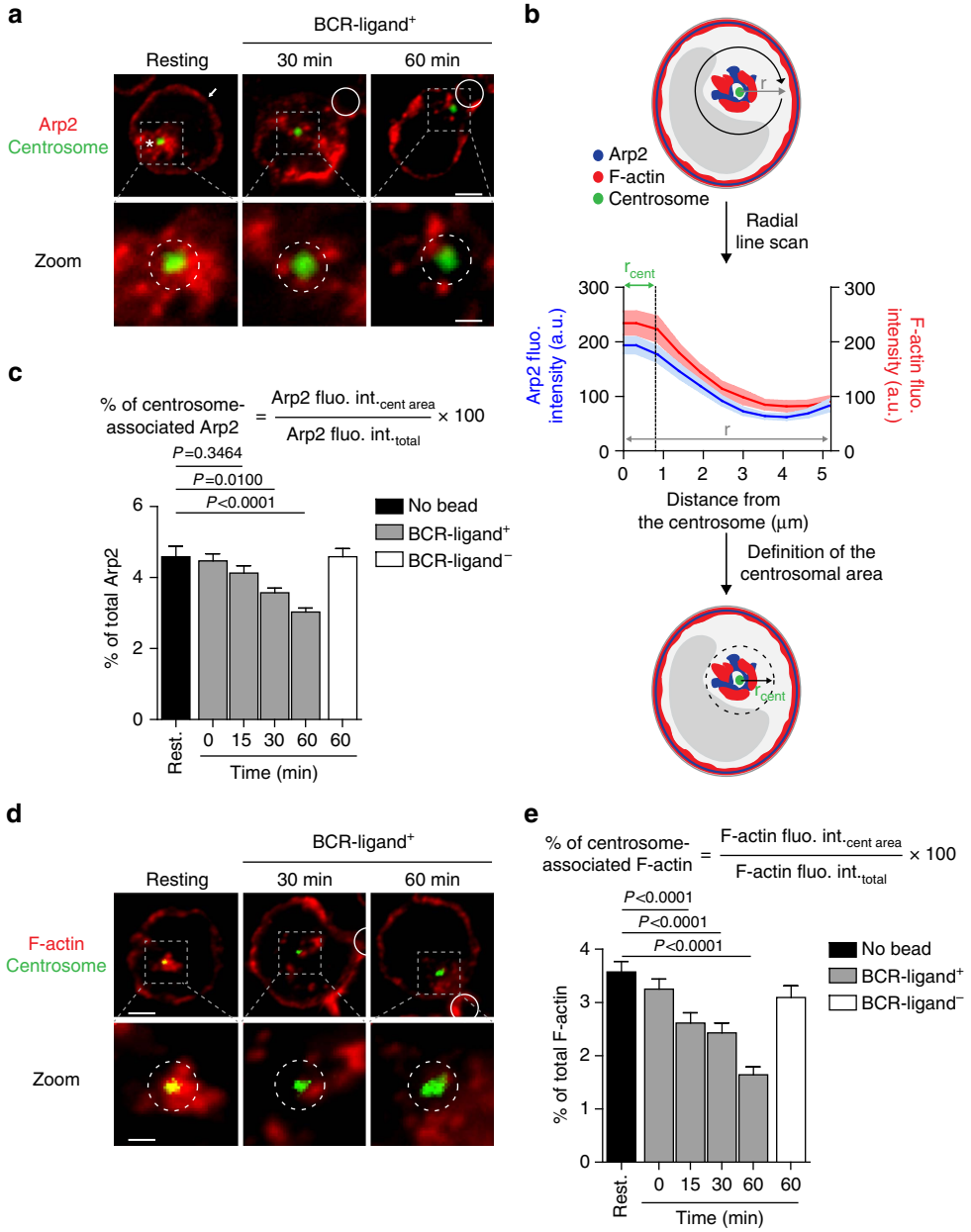

Figure 2 | Decreased association of Arp2/3 and F-actin with centrosomes of BCR-stimulated lymphocytes. (**a**,**d**) Representative images of B cells under resting conditions or stimulated with BCR-ligand$^+$ beads for indicated time, fixed and co-stained for Arp2 (white arrow: cortical pool; *: centrosomal pool) (**a**) or F-actin (phalloidin) (**d**) and the centrosome (α-tubulin). White circles indicate bead position. Dashed grey squares indicate the centrosomal region magnified below each image. Dashed circles on bottom panel highlight the centrosomal area used for quantification. Scale bars, top: 3 µm; bottom: 1 µm. (**b**) Schematics depicting the pipeline used to quantify centrosome-associated Arp2 and F-actin. (**c**,**e**) Quantification of centrosome-associated Arp2 (**c**) and F-actin (**e**) from cells shown in **a** and **d**, respectively. Data are pooled from three independent experiments with (**c**) $n=67$, 62, 64, 72, 61 and 69 cells, and (**e**) $n=54$, 63, 64, 62, 59 and 64 cells from left to right, respectively. fluo. int., fluorescence intensity. cent, centrosome. Rest., Resting.

Reduced F-actin nucleation at activated lymphocyte centrosomes. Having recently shown that centrosomes possess an intrinsic actin-nucleating activity in various cell types including T lymphocytes[26], we investigated whether the distinct amounts of centrosome-associated F-actin observed in resting and BCR-stimulated B lymphocytes reflected different actin nucleation capacities. For this, centrosomes purified from resting and activated B lymphocytes were compared for their ability to nucleate actin filaments *in vitro*. Strikingly, we observed that both centrosome preparations assembled actin asters from γ-tubulin spots (Fig. 3a), indicating that centrosomes possess an intrinsic actin nucleation capacity. In agreement with our hypothesis, actin nucleation by centrosomes purified from BCR-stimulated cells was strongly diminished as compared with centrosomes purified from resting lymphocytes. Indeed, both the number of actin asters and the actin fluorescence intensity at the aster centre were significantly decreased when using centrosomes from activated cells (Fig. 3b–d and Supplementary Movie 1). Importantly, centrosome integrity was not affected in preparations from activated lymphocytes, as shown by their ability to nucleate microtubules (Supplementary Fig. 3a). Consistent with these results and with our proteomic and immunofluorescence data, the amount of Arp2/3 associated with centrosomes purified from BCR-stimulated lymphocytes was also found to be strongly

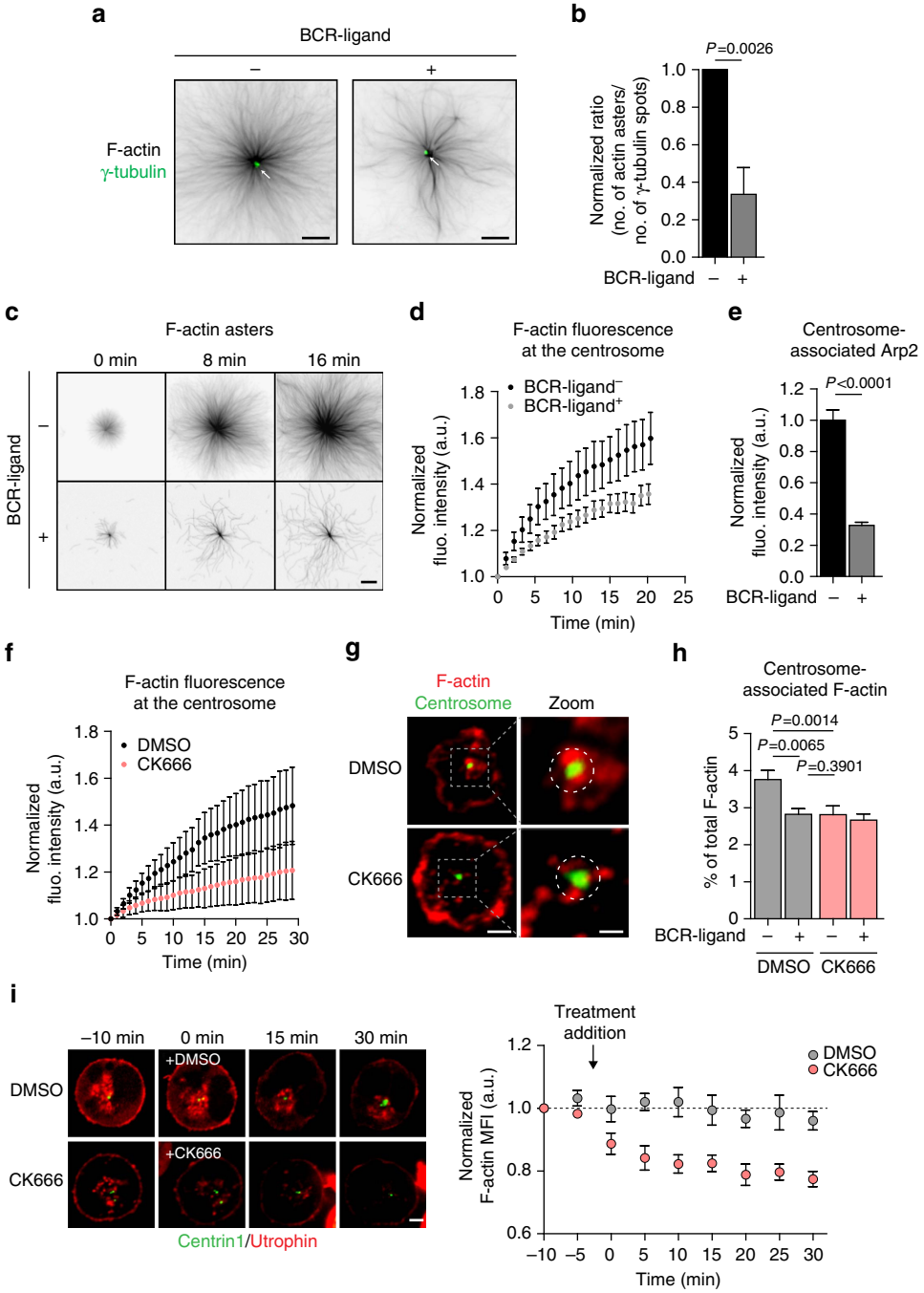

Figure 3 | F-actin nucleation by centrosomes is downregulated upon BCR stimulation. (**a**) Representative images of actin asters nucleated from isolated centrosomes (white arrow). Scale bar, 8 μm. (**b**) Actin nucleation efficiency was calculated as the ratio of the number of actin asters divided by the number of γ-tubulin spots (>200 actin asters and >450 γ-tubulin spots per condition pooled from four independent experiments). (**c**) Sequential images of F-actin assembly by centrosomes isolated from B cells stimulated with indicated beads. Scale bar, 5 μm. (**d**) Quantification of F-actin nucleation activity ($n=14$ and 12 actin asters per condition; data are representative of four independent experiments) (**e**) Quantification of Arp2 fluorescence (fluo.) intensity associated with purified centrosomes ($n=100$ and 190 centrosomes per condition pooled from two independent experiments). (**f**) Quantification of actin nucleation activity of centrosomes purified from resting lymphocytes in the presence of CK666 or dimethylsulfoxide (DMSO; $n=12$ and 22 actin asters, respectively; data are representative of two independent experiments). (**g**) Representative images of resting B cells treated with DMSO or CK666 for 60 min, fixed and co-stained for F-actin (phalloidin) and the centrosome (α-tubulin). Dashed grey squares indicate the region magnified on the right panel. Dashed circles on the right panel highlight the centrosomal area used for quantification. Scale bars, left: 3 μm; right: 1 μm. (**h**) Quantification of centrosome-associated F-actin of B cells pretreated for 30 min with DMSO or CK666 before being stimulated with indicated beads for 60 min in presence of the drug (>60 cells per condition pooled from three independent experiments). (**i**) Left: sequential images of resting B cells co-transfected with the centrosomal marker eGFP–Centrin1 and the F-actin probe Utrophin-RFP imaged by time-lapse spinning disk microscopy and treated with either DMSO or CK666 (between $t_{-5\,min}$ and $t_{0\,min}$). Scale bar, 3 μm. Right: quantification of centrosome-associated F-actin over time. Centrosomal F-actin mean fluorescence intensity (MFI) was normalized with respect to initial intensity ($t_{-10\,min}$) for each cell. Data are pooled from two independent experiments and graph shows the mean ± s.e.m. of $n=8$ and 10 cells for DMSO and CK666, respectively. *P* values determined by Mann–Whitney test.

decreased as compared with centrosomes of resting B cells (Fig. 3e).

The involvement of the Arp2/3 complex in F-actin nucleation by centrosomes purified from resting lymphocytes was confirmed by using the CK666 Arp2/3 inhibitor[27], which significantly reduced F-actin assembly (Fig. 3f). On the same line, treatment of resting B cells with CK666 decreased the amount of centrosome-associated F-actin to the levels observed in BCR-stimulated lymphocytes (Fig. 3g,h). Equivalent results were obtained when silencing Arp2/3 with two different siRNA (Supplementary Fig. 3b,c) or when using the Utrophin-red fluorescent protein (RFP) probe to label F-actin in live-imaging experiments: addition of CK666 resulted in decreased centrosomal F-actin in non-activated lymphocytes (Fig. 3i and Supplementary Movie 2). Interestingly, a significant reduction in the fraction of centrosome-associated Arp2/3 was also observed in CK666-treated resting B cells (Supplementary Fig. 3d), suggesting that Arp2/3 activity is required for its localization at the centrosome and/or that the presence of branched actin at the centrosome might help locally maintaining the complex. Of note, formin inhibition did not decrease F-actin nucleation at the centrosome, indicating that it most likely did not play a direct role in this process. Interestingly, formin inhibition even increased the amount of F-actin at the centrosome, what might result from the recently reported competition between Arp2/3 and formins[28] (Supplementary Fig. 3e,f). We conclude that lymphocyte centrosomes nucleate F-actin in an Arp2/3-dependent manner and that this property of centrosomes is downregulated upon lymphocyte activation as a result of Arp2/3 local depletion.

Arp2/3 recruitment to the immune synapse. We next searched for the molecular mechanisms responsible for this partial depletion of Arp2/3 from the centrosome of BCR-stimulated lymphocytes. It was shown that the Cortactin homologue haematopoietic lineage cell-specific protein (HS1), which is predominantly expressed in haematopoietic cells[29], recruits Arp2/3 to the BCR signalosome upon antigenic stimulation[30]. Consistently, we observed that BCR engagement with BCR-ligand^{+} beads induced HS1 phosphorylation and accumulation at the cell–bead interface (Fig. 4a,b). We therefore hypothesized that phospho-HS1-dependent recruitment of Arp2/3 at the immune synapse might lead to its partial depletion from the centrosome and thereby to a local decrease in F-actin nucleation. Consistent with this hypothesis, we found that the gradual decrease in the pool of centrosome-associated Arp2/3 and F-actin was concomitant to the accumulation of both proteins at the cell–bead interface (Fig. 4c–e and Supplementary Fig. 4a). This was also observed for F-actin in time-lapse imaging experiments: upon BCR stimulation, F-actin gradually decreased at the centrosome but progressively increased at the synapse (Fig. 4f and Supplementary Movie 3 and 4). Noticeably, both the decrease of Arp2/3 and F-actin at the centrosome and their increase at the synapse were severely impaired when silencing HS1 (Fig. 4g,h and Supplementary Fig. 4b). No reduction in centrosome-associated F-actin, nor in the total amount of F-actin was observed between control and HS1-silenced lymphocytes (Supplementary Fig. 4c,d). Hence, HS1-dependent recruitment of Arp2/3 at the cell–bead interface is associated with its partial depletion from the centrosome, thus decreasing the actin nucleation capacity of this organelle.

Centrosomal Arp2/3 and actin impair centrosome polarization. HS1-silenced lymphocytes that maintained high levels of centrosomal Arp2/3 and F-actin upon BCR stimulation were next used to investigate whether Arp2/3 and F-actin depletion from the centrosome regulates the ability of this organelle to polarize to the immune synapse. We found that most HS1 knockdown B cells did not reposition their centrosome at the cell–bead interface (Fig. 5a). However, because these cells displayed not only more Arp2/3 and F-actin at the centrosome but also less Arp2/3 and F-actin at the synapse as compared with control cells, we could not exclude that impaired centrosome polarization resulted from decreased Arp2/3 and F-actin at the synapse. To address this question, we investigated the effect of Arp2/3 inhibition on centrosome polarity. We found that both Arp2/3 silencing and inhibition with CK666 had no impact on centrosome polarization to the synapse (Fig. 5b and Supplementary Fig. 5a) and, even more importantly, rescued the non-polarized phenotype of HS1-silenced activated lymphocytes (Fig. 5c and Supplementary Fig. 5b,c). Of note, Arp2/3 inhibition in these cells reduced the centrosomal pool of F-actin (Fig. 5d–f) but had no significant effect on the amounts of synapse-associated F-actin (Supplementary Fig. 5d). CK666 treatment had no impact on BCR signalling (Supplementary Fig. 5e,f). These results suggest that the centrosomal pool of Arp2/3 and F-actin prevents centrosome polarization while its synaptic counterpart is not required for this process. In support of this conclusion, a significant correlation was found between the levels of centrosomal F-actin and the distance between this organelle and the bead geometrical centre (Fig. 5g). Hence, HS1-dependent recruitment of Arp2/3 at the synapse partially depletes this complex from the centrosome, leading to a local reduction in F-actin that is needed for centrosome polarization to the synapse.

We next sought for a strategy to directly assess whether actin nucleation by Arp2/3 at the centrosome prevents the polarization of this organelle to the immune synapse. Interestingly, WASH, an actin nucleation-promoting factor that activates Arp2/3 through its VCA (verprolin homology or WH2-connector-acidic) domain, was shown to associate to the centrosome[31]. In agreement, in resting lymphocytes, we observed WASH as discrete punctuated structures mainly gathered around the centrosome (Supplementary Fig. 5g). In addition, in resting cells, WASH silencing decreased the amount of F-actin at the centrosome to the levels observed in activated cells (Supplementary Fig. 5h–j), indicating that it participates to local Arp2/3 activation. We therefore reasoned that targeting the WASH VCA domain to the centrosome would result in the exacerbation of local Arp2/3 activity and F-actin nucleation. Accordingly, expression of the eGFP–Centrin1–VCA fusion protein strongly increased the amount of F-actin at the centrosome (Fig. 5h,i). More importantly, expression of the eGFP–Centrin1–VCA fusion protein compromised the ability of the centrosome to polarize to the immune synapse (Fig. 5j). As observed for Arp2/3 inhibition or silencing, WASH silencing had no impact on centrosome polarity (Supplementary Fig. 5k). Consistently, centrosome polarization in eGFP–Centrin1–VCA-expressing cells was rescued by inhibiting Arp2/3 activity (Fig. 5k). These data strongly support a model where F-actin nucleation at the centrosome prevents its translocation to the synapse and must therefore be downregulated upon lymphocyte activation.

Centrosomal F-actin tethers the centrosome to the nucleus. We next searched for the cellular basis of the negative impact of Arp2/3-dependent actin nucleation at the centrosome on its ability to polarize. In view of a recent work indicating that F-actin controls centrosome positioning by inducing the retrograde transport of the nucleus in polarized fibroblasts[32], we postulated that actin nucleation at the centrosome might regulate its physical interaction with the nucleus[33]. To test this hypothesis, we measured the distance between both organelles in lymphocytes that exhibited different levels of centrosomal

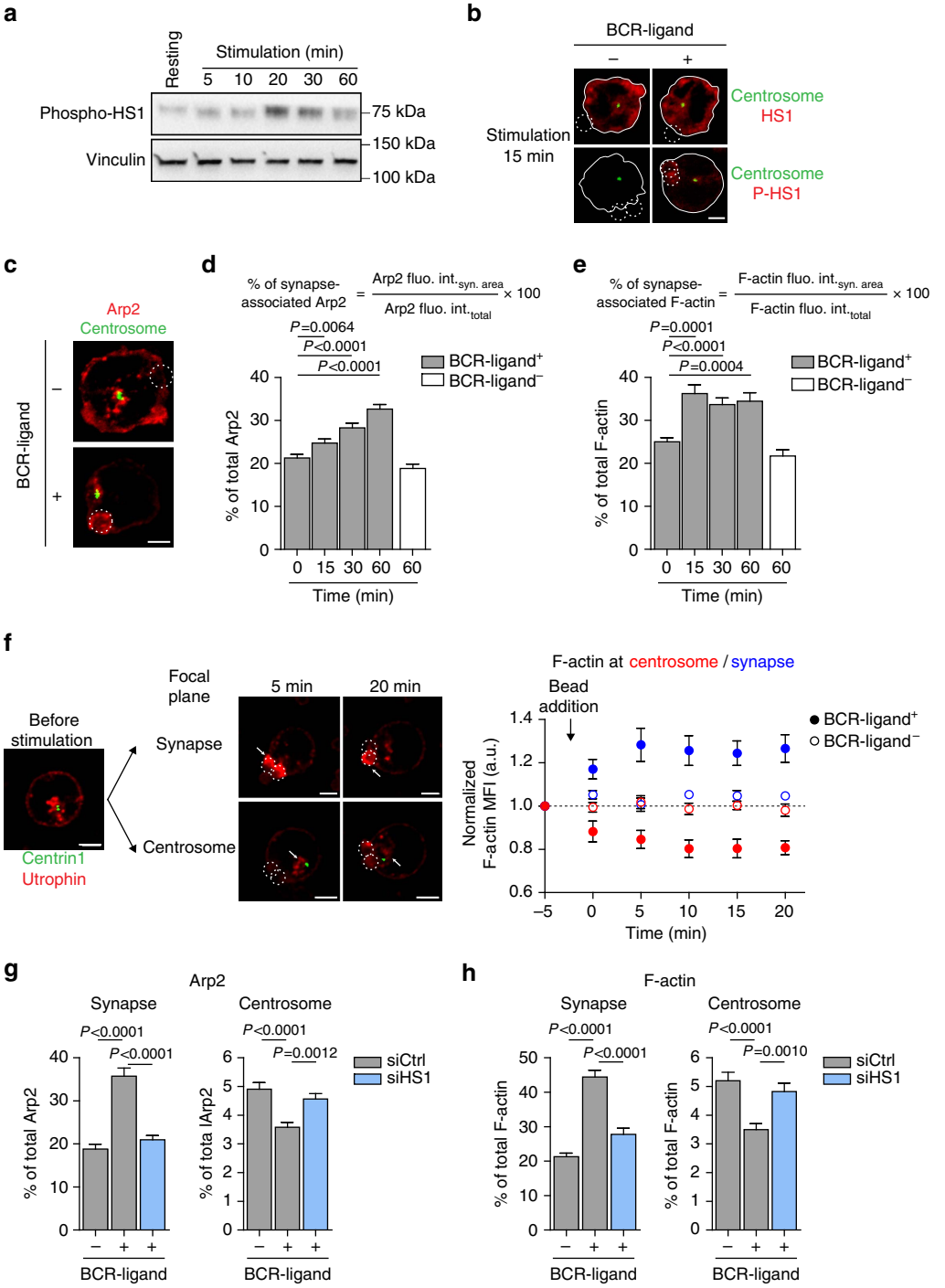

Figure 4 | Depletion of Arp2/3 from the centrosome results from its HS1-dependent recruitment at the immune synapse. (**a**) Western blot showing the phosphorylation of HS1 during the course of B-cell stimulation. Representative of two independent experiments. (**b**) Representative images of B cells stimulated with indicated beads for 15 min, fixed and co-stained for total HS1 (top) or phosphorylated HS1 (bottom) and the centrosome (α-tubulin). Dashed white circles indicate bead position. Scale bar, 3 μm. Images are representative of two independent experiments. (**c**) Representative images of B cells stimulated with indicated beads for 60 min, fixed and co-stained for Arp2 and the centrosome (α-tubulin). Dashed white circles indicate bead position. Scale bar, 3 μm. Representative of three independent experiments. (**d**,**e**) Quantification of synapse-associated Arp2 (**d**) and F-actin (**e**). (**d**) $n=71$, 64, 68, 72 and 69 cells and (**e**) $n=55$, 60, 66, 59 and 57 cells from left to right, pooled from three independent experiments. (**f**) Left: sequential images of B cells co-transfected with the centrosomal marker eGFP–Centrin1 and the F-actin probe Utrophin-RFP stimulated with BCR-ligand$^+$ beads and imaged by time-lapse spinning disk microscopy. White arrows indicate F-actin clearance from the centrosome (bottom) and its concomitant accumulation at the immune synapse (top) during the course of B-cell stimulation. Dashed white circles indicate bead position. Scale bar, 3 μm. Right: quantification of synapse- (blue) and centrosome- (red) associated F-actin of B cells stimulated with indicated beads. F-actin mean fluorescence intensity (MFI) was normalized with respect to initial intensity ($t_{-5\ min}$) for each cell. Data are pooled from two independent experiments and graph shows the mean ± s.e.m. of $n=7$ cells per condition. (**g**,**h**) Quantification of Arp2 (**g**) and F-actin (**h**) associated with the synapse (left) and the centrosome (right) in control and HS1-silenced B cells stimulated for 60 min with indicated beads. Data are pooled from two (**g**) and three (**h**) independent experiments with (**g**) synapse: $n=51$, 46 and 53 cells; centrosome: $n=51$, 52 and 47 cells; and (**h**) synapse: $n=72$, 74 and 66 cells; centrosome: $n=73$, 72 and 67 cells from left to right. *P* values determined by Mann–Whitney test. fluo. int., fluorescence intensity. syn, synapse.

F-actin. We found that reduction of centrosomal F-actin upon BCR engagement not only stimulated centrosome polarization but was also accompanied by an increase in the distance between the nucleus and this organelle (Fig. 6a). Strikingly, such increase was equally observed when depleting or inhibiting Arp2/3 in non-stimulated cells (Fig. 6b,c), indicating that the mere reduction of centrosomal F-actin is sufficient to induce its physical separation from the nucleus. Similarly, the distance between the centrosome and the nucleus of resting WASH-silenced cells, whose centrosome has low levels of centrosomal F-actin, was also increased (Supplementary Fig. 6a). In contrast, in activated HS1-silenced lymphocytes that maintained high levels of F-actin at their centrosome, the centrosome–nucleus distance was as short as in non-stimulated cells (Fig. 6d). This result equally applied to lymphocytes expressing the eGFP–Centrin1–VCA construct, which displayed increased centrosomal F-actin and impaired centrosome polarization (Fig. 6e,f). However, centrosome–nucleus separation was rescued in these cells by reducing centrosomal F-actin with CK666 or by silencing Arp2/3 (Fig. 6d–f and Supplementary Fig. 6b). These results strongly suggest that the pool of F-actin at the centrosome maintains it in close proximity to the nucleus and must therefore be depleted for these two organelles to physically separate. Important molecules involved in the physical association of the centrosome to the nucleus are components of the linker of nucleoskeleton and cytoskeleton (LINC) complex. This complex includes Nesprin proteins that bind both the microtubule and actin cytoskeleton networks. We therefore investigated whether detachment of the centrosome from the nucleus as a result of LINC complex disruption might rescue centrosome polarity. Over-expression of a dominant-negative mutant of Nesprin-2 that does not bind F-actin[32] was sufficient to increase the distance between the centrosome and the nucleus in resting cells without affecting the amounts of centrosome-associated F-actin (Fig. 6g and Supplementary Fig. 6c). More importantly, expression of this dominant-negative version of the LINC complex rescued both centrosome polarization and centrosome separation from the nucleus in HS1-silenced activated lymphocytes despite their high levels of centrosomal F-actin (Fig. 6h,i and Supplementary Fig. 6d,e). Hence, the need to deplete F-actin at the centrosome to detach it from the nucleus and allow its polarization to the immune synapse can be bypassed by disrupting the LINC complex. These results strongly suggest that F-actin nucleation at the centrosome is required for its physical association to the nucleus by the LINC complex. Altogether, these data further provide a putative mechanism for the need to deplete centrosomal Arp2/3 and F-actin to allow centrosome translocation to the immune synapse.

Discussion

We here found that BCR engagement with immobilized antigens induces the accumulation of the Cortactin-like protein HS1 at the immune synapse, which recruits Arp2/3, promoting the local enrichment of F-actin. Of note, although inhibition of Arp2/3 does not impair centrosome polarization, its activity is nonetheless required for B lymphocytes to process and present BCR-internalized antigens to T lymphocytes (Supplementary Fig. 6f), suggesting a function for this complex at the B-cell synapse. Recruitment of Arp2/3 at the synapse leads to its partial depletion from the centrosome, thereby reducing the pool of centrosome-nucleated F-actin. The centrosome would then be free to physically separate from the nucleus and move towards the immune synapse. Importantly, we found that an intact LINC complex is required for centrosomal F-actin to maintain centrosome attachment to the nucleus. Interestingly, although the molecular players that allow interaction between the LINC complex and the nucleoskeleton were described, the one that link this complex to the centrosome remained unclear[33]. Our results suggesting that F-actin nucleation at the centrosome might be a key player in this process therefore brings an interesting new piece to this puzzle.

Our findings strongly suggest that F-actin nucleation at the centrosome must decrease for this organelle to acquire a polarized localization. This might result, at least in part, from the role of centrosomal F-actin in retaining the centrosome in vicinity of the nucleus[33]. The idea that the actin cytoskeleton links the centrosome to the nucleus was initially proposed in the eighties based on observations showing that nucleus purification or cell enucleation required the addition of F-actin-depolymerizing drugs[34,35]. However, the precise nature and origin of this actin network remain unclear. Different F-actin structures had been reported in association to the centrosome and/or the nucleus. This includes 'actin clouds' that position centrosomes and mitotic spindles[36] and resemble the F-actin structures we observed at the centrosome of B lymphocytes. In addition, the nucleus of migrating fibroblasts associates to a 'perinuclear actin cap'[37] or to 'linear actin arrays' referred to as TAN lines, which regulate nucleus retrograde transport and centrosome polarity through the LINC complex[32,38]. Although we did not observe TAN lines in B lymphocytes, what might be due to their non-adherent properties, whether and how Arp2/3-dependent F-actin nucleation at the centrosome contributes to the formation and/or function of these actin structures will be an important point to investigate in the future.

Of note, we do not exclude that actin depletion at the centrosome may control additional processes required for efficient centrosome polarization than centrosome–nucleus

Figure 5 | Downregulation of centrosomal Arp2/3-dependent F-actin nucleation is required for centrosome polarization to the immune synapse. (**a**–**c**) Quantification of centrosome polarity index of control and HS1-silenced (**a**), CK666-treated (**b**) or HS1-silenced and CK666-treated (**c**) B cells stimulated with indicated beads for 60 min. (**a**) $n=77$, 71 and 75 cells; (**b**) $n=103$, 80 and 87 cells and (**c**) $n=77$, 69, 72 and 75 cells from left to right, pooled from three independent experiments. (**d**) Representative images of control and HS1-silenced B cells treated with dimethylsulfoxide (DMSO) or CK666, stimulated with BCR-ligand$^+$ beads for 60 min, fixed and co-stained for F-actin (phalloidin) and the centrosome (α-tubulin). Scale bars, left: 3 μm; right: 0.9 μm. (**e**) Quantification of centrosome-associated F-actin from cells shown in **d** ($n=41$, 47, 38 and 45 cells from left to right, pooled from two independent experiments). (**f**) Quantification of centrosomal F-actin of control, HS1- and HS1 plus Arp2-silenced B cells stimulated for 60 min with indicated beads ($n=58$, 65, 65 and 63 cells from left to right, pooled from three independent experiments). (**g**) Correlation analysis of centrosome-associated F-actin and the bead–centrosome distance ($n=185$ cells). Spearman correlation test, $P<0{,}0001$. (**h**) Left: schematics depicting the construct used to over-activate the Arp2/3 complex at the centrosome (bottom). Right: representative images of control and eGFP–Centrin1–VCA-expressing B cells, stimulated with indicated beads for 60 min, fixed and co-stained for F-actin (phalloidin) and the centrosome (GFP). Scale bar, 3 μm. (**d**,**h**) White circles indicate bead position. Dashed grey squares indicate the region magnified on the right. Dashed circles on magnifications highlight the centrosomal area used for quantification. (**i**,**j**) Quantification of centrosomal F-actin (**i**) and centrosome polarity index (**j**) of cells shown in **h**. (**i**) $n=74$, 66, 68 and 64 cells and (**j**) $n=75$, 71 and 64 cells from left to right, pooled from three independent experiments. (**k**) Quantification of centrosome polarity index of control and eGFP–Centrin1–VCA-expressing B cells, treated or not with CK666 and stimulated with indicated beads for 60 min ($n=41$, 39, 42 and 42 cells from left to right, pooled from two independent experiments). *P* values determined by Mann–Whitney test. Cent-VCA, eGFP-centrin1-VCA.

attachment. In particular, reduction of F-actin nucleation at the centrosome might induce local changes to favour its microtubule-dependent translocation to the synapse. For example, it may facilitate Dynein recruitment and/or local centrosome docking at the immune synapse. Consistent with these hypotheses, we and others have shown that Dynein is indeed required for centrosome reorientation to the synapse in both B and T lymphocytes[15,17,19,20]. Further work is needed to unravel the role played by centrosome-nucleated F-actin in the biology of resting lymphocytes, as well as to fully understand how depletion of this F-actin pool facilitates centrosome polarity.

Our data suggest that the centrosome and the immune synapse compete for Arp2/3. Although we cannot formally exclude that there is a direct exchange between centrosomal and synaptic Arp2/3, we think that this is unlikely in view of data showing that most Arp2/3 resides in the cytosol[39]. We therefore propose that

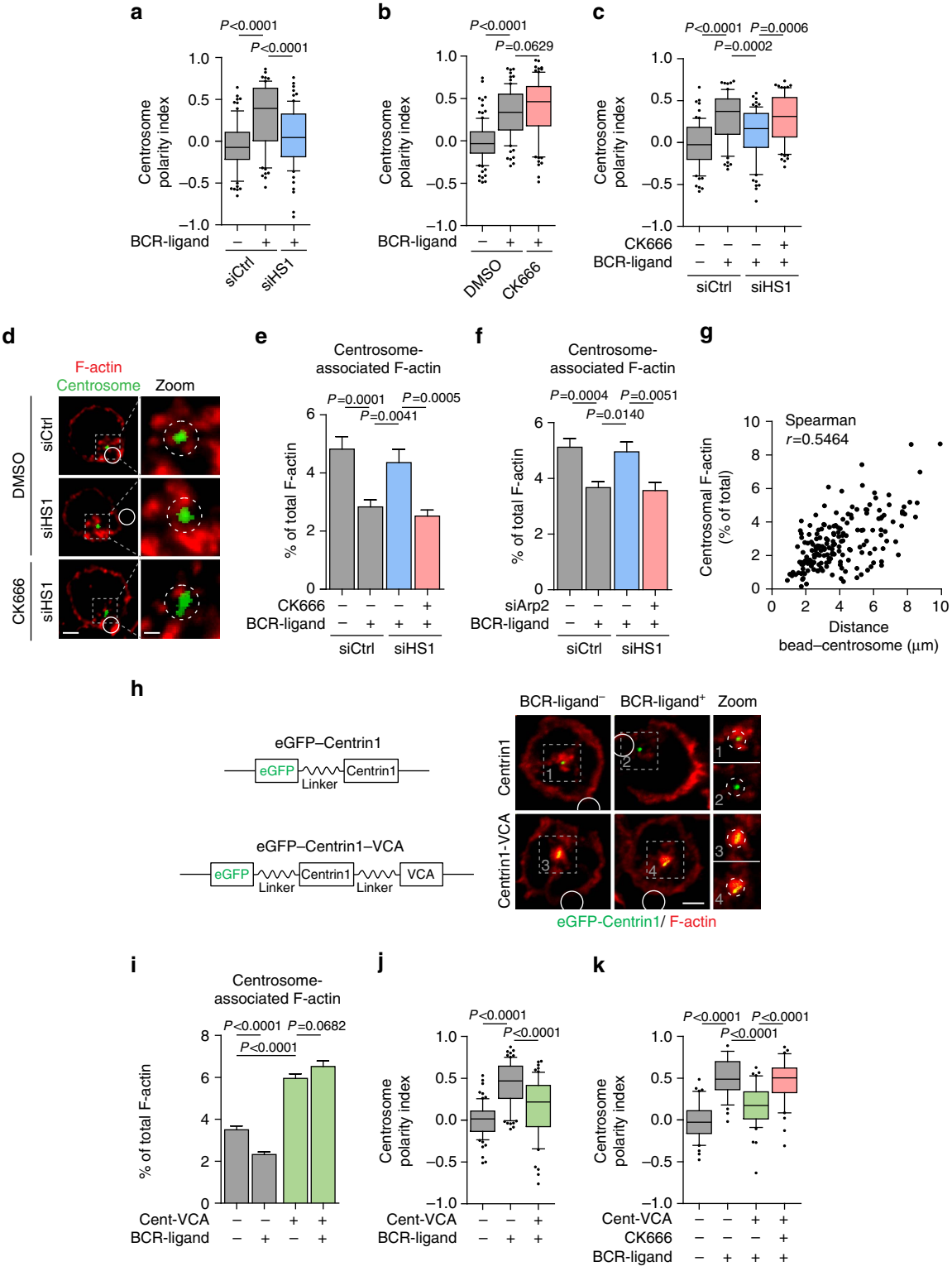

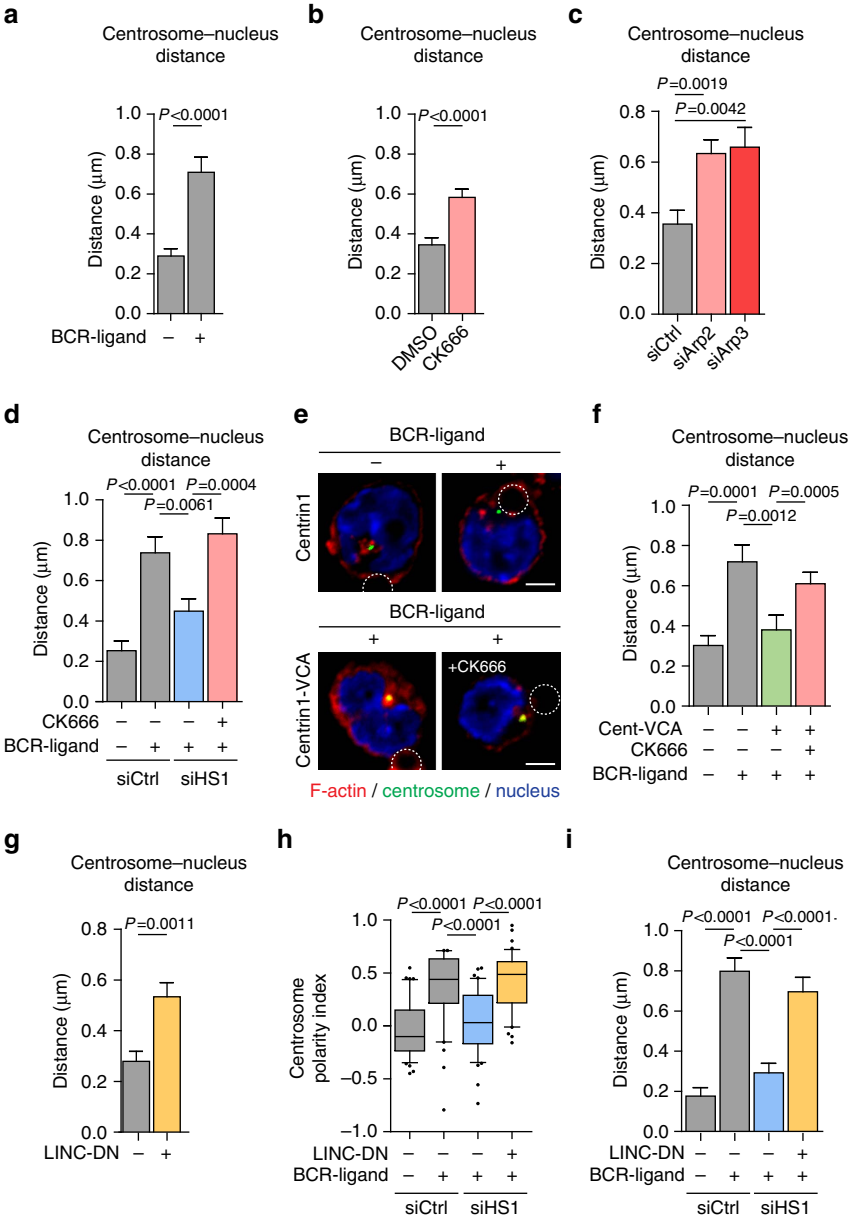

Figure 6 | Centrosomal Arp2/3-mediated F-actin nucleation links the centrosome to the nucleus through the LINC complex. (**a**–**d**) The shorter distance in three dimensions between the centrosome and the edge of the nucleus was measured in: (**a**) B cells stimulated with either BCR-ligand$^-$ or BCR-ligand$^+$ beads for 60 min; (**b**) resting B cells treated with dimethylsulfoxide (DMSO) or CK666 for 60 min; (**c**) control, Arp2- and Arp3-silenced resting B cells; and (**d**) control and HS1-silenced B cells, treated with either DMSO or CK666, and stimulated with indicated beads for 60 min. Data are pooled from two (**c**,**d**) and three (**a**,**b**) independent experiments with (**a**) $n=90$ cells per condition; (**b**) $n=93$ and 78 cells for DMSO and CK666, respectively; (**c**) $n=43$, 35 and 31 cells; and (**d**) $n=56$, 53, 52 and 54 cells from left to right. (**e**) Representative images of B cells over-expressing the eGFP–Centrin1 protein or the eGFP–Centrin1–VCA fusion protein treated or not with CK666, stimulated with indicated beads for 60 min, fixed and co-stained for F-actin (phalloidin), the centrosome (GFP) and the nucleus (DAPI). Dashed circles indicate bead position. Scale bar, 3 µm. (**f**) Quantification of the distance between the centrosome and the nucleus edge from cells shown in **e**. Data are pooled from two independent experiments with $n=41$, 39, 42 and 43 cells from left to right. (**g**) Quantification of the distance between the nucleus edge and the centrosome in resting B cells over-expressing or not the LINC-DN construct. Data are pooled from three independent experiments with $n=64$ cells per condition. (**h**,**i**) Quantification of centrosome polarity index (**h**) and centrosome–nucleus distance (**i**) of control and HS1-silenced B cells, over-expressing or not the LINC-DN construct and stimulated for 60 min with indicated beads. Data are pooled from two independent experiments with (**h**) $n=41$, 40, 42 and 42 cells and (**i**) $n=41$, 44, 41 and 45 cells from left to right. *P* values determined by Mann–Whitney test. DAPI, 4′,6-diamidino-2-phenyindole.

both the centrosome and the synapse are rather competing for the cytosolic pool of Arp2/3.

Anyhow, our data strongly suggest that there is an effective competition between distinct subcellular locations for this actin-nucleating complex. As a result of this competition, cells would respond to extracellular stimuli by favouring one biological process over another, what might provide a simple mechanism for cells to coordinate them in time and space. In addition, the existence of a competition for cytosolic Arp2/3 implies that the pool of centrosome-associated Arp2/3 might be minor in adherent cells as compared with lymphocytes, given that they use this complex to form adhesive structures such as lamellipodia.

Interestingly, it has been shown that immune synapses share many features with lamellipodia[40], suggesting that the competition between the centrosome and the immune synapse for Arp2/3 might also apply to the centrosome and the lamellipodium of migrating cells.

In conclusion, our results highlight an unexpected role for the regulation of centrosome-associated F-actin in the control of lymphocyte polarization. Whether and how this novel regulatory mechanism applies to additional biological systems that rely on cell polarity is an open question. This would be of particular interest in the context of cilium biogenesis that involves signalling pathways also used in immune synapse formation by lymphocytes[41,42].

Methods

Cells and cell culture. The mouse IgG$^+$ B-lymphoma cell line IIA1.6 (derived from the A20 cell line (American Type Culture Collection #: TIB-208)) and the LMR7.5 T-cell hybridoma that recognizes I-A^d-Lack$_{156-173}$ complexes (from and described in ref. 43) were cultured as reported[14] in CLICK medium (RPMI 1640—GlutaMax-I supplemented with 10% fetal calf serum, 1% penicillin–streptomycin, 0.1% β-mercaptoethanol and 2% sodium pyruvate). All cell culture products were purchased from GIBCO/Life Technologies. All experiments were conducted in 50% CLICK/50% RPMI 1640—GlutaMax-I.

siRNA. Protein silencing was achieved using the Neon transfection system (Invitrogen, Life Technologies). Briefly, B cells were washed in phosphate-buffered saline (PBS), resuspended in Buffer R at a density of 50×10^6 cells per ml and ON-TARGETplus SMARTpool Non-targeting (siCtrl), HS1- (siRNA#1: 5′-GGGCAUGAUGUAUCGGUUU-3′; siRNA#2: 5′-CCAAGGAGAGGGAAGCGAU-3′; siRNA#3: 5′-UGGAAGAGCCAGUGUACGA-3′; and siRNA#4: 5′-GUAAAGAUGAGCCGAGAAG-3′), Arp2- (siRNA#1: 5′-UGGUGUAACUGUUCGAUAA-3′; siRNA#2: 5′-GUUCUUUACUAAUGACGAA-3′; siRNA#3: 5′-GAUCAGUGCUUCUCGACAA-3′; and siRNA#4: 5′-CAUCGAGGUUGGAACGAGA), Arp3- (siRNA#1: 5′-GAAGAGAGCUAAGACGAUU-3′; siRNA#2: 5′-AAGCAGUGAAGGAACGCUA-3′; siRNA#3: 5′-GCUGACGGGUACAGUAAUA; siRNA#4: 5′-GAGUCAACGCCAUCUCAAA) or WASH- (siRNA#1: 5′-ACAGCAACACGGCGGAAUA-3′; siRNA#2: 5′-GAGGAGAAAUUGUUCGAUG-3′; siRNA#3: 5′-GCACAUUCAGGAACGUUUA-3′; and siRNA#4: 5′-GAAUACGGCUCCAUCUUUA-3′) targeting siRNA (Dharmacon, GE Healthcare) were added at a final concentration of 200 nM. Cells were then electroporated (1,300 V, 2 pulses, 20 ms per pulse) using 10-µl tips, and incubated in CLICK medium for 60–72 h. Silencing efficiency was analysed by western blot as described below.

Plasmids. The eGFP–Centrin1 and Utrophin-RFP plasmids were obtained from M. Bornens and M. Piel, respectively (Institut Curie, Paris, France). The eGFP–Centrin1–VCA plasmid was obtained by sub-cloning in frame the VCA domain of WASH at the C terminus of the eGFP–Centrin1 construct. Briefly, the Centrin1 cDNA deleted from its stop codon was amplified from the eGFP–Centrin1 plasmid using the following primers: forward: 5′-ctaggtaccatggcttccggcttcaaga-3′ and reverse: 5′-gcaggatccgtaaaggctggtcttcttcat-3′ (which include KpnI and BamHI restriction sites (underlined), respectively). The WASH VCA cDNA was amplified from a previously home-made (A. Gautreau) WASH plasmid by using the primers: forward: 5′-ttaggatccTCCGGACTCAGATCTCGAGCTCAAGCTTCGAATTCTGCAGTCGACcagggagcccctaagga-3′ (which includes BamHI restriction site (underlined) and the sequence for a peptide linker (upper case)) and reverse: 5′-gattctagaTCAggactcccagtcctcct-3′ (which includes XbaI restriction site (underlined) and a stop codon (upper case)). Both fragments were then sub-cloned in frame within the original vector using KpnI and XbaI restriction enzymes. BamHI restriction enzyme was used to orient the two fragments. The resulting eGFP–Centrin1–VCA plasmid was sequenced to ensure sequence integrity. The LINC-DN (Nesprin-2 SRKASH) plasmid was obtained from E.R. Gomes and described in ref. 32. Plasmid expression was achieved by electroporating 2×10^6 B-lymphoma cells, with 1 or 3 µg of plasmid using the Amaxa Cell Line Nucleofactor Kit R (T-016 programme, Lonza). Cells were incubated in CLICK medium for 16–20 h before analysis.

Reagents. The Lack antigen was produced and purified by the 'Recombinant Protein' platform (UMR144, Institut Curie, Paris, France), and Lack peptide (aa 156–173) was synthetized by PolyPeptide Group. Cytochalasin D and nocodazole used from centrosome purification were from Sigma Aldrich. For inhibition of Arp2/3 activity, cells were pretreated with 25 µM CK666 (Tocris Bioscience) for 30 min before being stimulated for indicated time in presence of the drug.

Antibodies. The following primary antibodies were used for immunofluorescence: rabbit anti-γ-tubulin (Abcam, #Ab11317, 1/2000); fluorescein isothiocyanate (FITC)-conjugated mouse anti-α-tubulin (Abcam, #Ab64503, 1/100); rabbit anti-Arp2 (Abcam, #Ab47654, 1/200); rabbit anti-HS1 and rabbit anti-phospho-HS1 (both from Cell Signalling Technologies, #4557S and #8714P, respectively, 1/50); rabbit anti-WASH (home-made as previously described[44], 1/250); and human anti-green fluorescent protein (GFP) and anti-red fluorescent protein (RFP) (Recombinant Antibodies Platform, Institut Curie, Paris, France, 1/200). The following secondary antibodies were used: AlexaFluor488-, AlexaFluor568-, Cy3-, Cy5- and AlexaFluor647-conjugated F(ab′)$_2$ donkey anti-rabbit (Jackson ImmunoResearch, 1/300); and AlexaFluor488- and Cy3- conjugated donkey anti-human (Life Technologies and Jackson ImmunoResearch, respectively, 1/200). F-actin was stained using AlexaFluor546- or AlexaFluor647-conjugated phalloidin (Life Technologies, #A22283 and #A22287, respectively, 1/100). Nuclei were stained using 4′,6-diamidino-2-phenyindole (DAPI, Sigma Aldrich, 1/5,000).

For western blotting, the following antibodies were used: mouse anti-γ-tubulin (Sigma Aldrich, #T6557-.2ML, 1/500); rabbit anti-HS1, phospho-HS1 and phospho-Erk (Cell Signaling Technologies, #4557S, #8714P and #4377S, respectively, 1/1,000); rabbit anti-Arp2 (Abcam, #Ab47654, 1/200); rabbit anti-WASH (home-made as previously described[44], 1/250); and mouse anti-Arp3 and anti-vinculin (Sigma Aldrich, #A5979-200UL, 1/200, and #V9264-200UL, 1/1,000, respectively), followed by horseradish peroxidase-conjugated donkey anti-mouse or rabbit (Jackson ImmunoResearch, 1/5,000).

Preparation of BCR-ligand-coated beads. In all, 4×10^7 3-µm latex NH_2-beads (Polyscience) were activated with 8% glutaraldehyde (Sigma Aldrich) for 2 h at room temperature. Beads were washed with PBS 1x and incubated overnight at 4 °C with different ligands: 100 µg ml^{-1} of either F(ab′)$_2$ goat anti-mouse IgG (BCR-ligand$^+$ beads) or F(ab′)$_2$ goat anti-mouse IgM (BCR-ligand$^-$ beads; MP Biomedical) in combination or not with 100 µg ml^{-1} of the *Leishmania major* antigen Lack.

B-cell stimulation and immunofluorescences. Cells were plated on poly-L-lysine-coated slides and stimulated with indicated beads at a 1:2 ratio (cell:beads) for different time at 37 °C and fixed in 4% paraformaldehyde for 12 min at room temperature. For γ-tubulin staining, cells were further incubated with ice-cold 100% methanol for 2 min and quenched for 10 min with PBS/100 mM glycine. Fixed cells were incubated 45–60 min with primary antibodies and 30 min with secondary antibodies in PBS–BSA–Saponin (1x/0.2%/0.05%).

Time-lapse imaging. A total of 1×10^5 B-lymphoma cells co-expressing the centrosomal marker eGFP–Centrin1 and the F-actin probe Utrophin-RFP were seeded in 35-mm FD35 Fluorodish (World Precision Instruments, Inc). Cells were either treated with dimethylsulfoxide (DMSO) or CK666 (25 µM) or stimulated with either BCR-ligand$^-$ or BCR-ligand$^+$ beads and recorded at 37 °C, 5% CO_2 using an inverted spinning disk confocal microscope (Roper/Nikon) equipped with a ×60 (1.4 numerical aperture (NA)) oil immersion objective and a CoolSNAP HQ2 camera. The images were acquired every 5 min with *z*-stack of 1 µm. For the analysis, Fiji (ImageJ) software was used to reconstruct the three-dimensional (3D) movies, correct bleaching (exponential fit correction) and analyse the amount of F-actin associated with the centrosome and the synapse focal plane.

Stable isotope labelling by amino acids in cell culture. IIA1.6 cells were maintained in L-lysine-depleted SILAC RPMI 1640 (Thermo Scientific, Life Technologies) supplemented with 10% dialysed FBS and 0.1 mg ml^{-1} heavy [$^{13}C_6$] or light [$^{12}C_6$] L-lysine (Thermo Scientific, Life Technologies). Every 3–4 days, cells were split and media replaced with the corresponding light- or heavy-labelling medium. After six to seven cell divisions, cells achieved ≥96% incorporation of amino-acid isotopes.

Centrosome purification. Centrosomes were purified as previously described[45] with slight modifications. Briefly, following stimulation with indicated beads for 60 min, cells were incubated on ice with 200 nM nocodazole and 1 µg ml^{-1} cytochalasin D for 90 min. Cells were washed and lysed in TicTac buffer (16 mM PIPES, 10 mM HEPES (pH 7.5), 50 mM KCl, 1.2 mM EGTA, 5 mM $MgCl_2$, 0.1% Triton X-100 and 0.1% β-mercaptoethanol) for 15 min. Centrosomes were isolated by sequential centrifugations at (1) 10,000*g* for 30 min at 4 °C on top of a 60% w/v sucrose cushion and (2) 40,000*g* for 60 min at 4 °C on top of a discontinuous sucrose gradient (40–50–70%, w/w). Finally, 10 fractions of 0.5 ml were recovered from the bottom of the tube, and centrosome-containing fractions were identified by western blot.

Proteomics. *Sample preparation.* Proteins from centrosome preparations were separated on 10% SDS–PAGE gels (Invitrogen) and stained with colloidal blue staining (LabSafe GEL BlueTM GBiosciences). Gel slices were excised (20 fractions) and proteins were reduced with 10 mM dithiothreitol before alkylation with 55 mM iodoacetamide. After washing and shrinking of the gel fractions with 100% MeCN, in-gel digestion was performed using recombinant endoproteinase rLys-C (Promega) overnight in 25 mM NH_4HCO_3 at 30 °C.

MS analysis. Peptides were extracted and analysed by nano-LC–MS/MS using an Ultimate 3000 system (Dionex S.A.) coupled to a LTQ-Orbitrap XL mass spectrometer (Thermo Fisher Scientific), as described[46]. Samples were loaded on a

C18 pre-column (300 µm inner diameter × 5 mm; Dionex) at 20 µl min^{-1} in 5% MeCN and 0.1% TFA. After 3 min of desalting, the pre-column was switched on the C18 column (75 µm inner diameter × 15 or 50 cm, packed with C18 PepMap, 3 µm, 100 Å; LC Packings) equilibrated in solvent A (5% CH_3CN and 0.1% HCOOH). Bound peptides were eluted using a 97-min linear gradient (from 5 to 30% (v/v)) of solvent B (80% CH_3CN and 0.085% HCOOH) at a 150-nl min^{-1} flow rate and oven temperature of 40 °C. Data-dependent acquisition was performed on the LTQ-Orbitrap mass spectrometer in the positive-ion mode. Survey MS scans were acquired in the Orbitrap on the 480–1,200 m/z range with the resolution set to a value of 60,000. Each scan was recalibrated in real time by co-injecting an internal standard from ambient air into the C-trap (lock mass option). The five most intense ions per survey scan were selected for collision-induced dissociation (CID) fragmentation and the resulting fragments were analysed in the linear trap (LTQ). Target ions already selected for MS/MS were dynamically excluded for 180 s.

Data analysis. Data were acquired using the Xcalibur software (v2.0.7) and the resulting spectra were analysed via the Mascot Software (v2.3) with Proteome Discoverer (v1.2, Thermo Scientific) using the SwissProt *Mus musculus* database. Carbamidomethylation of cysteine, oxidation of methionine, N-terminal acetylation and heavy $^{13}C_6$-lysine (Lys6) were set as variable modifications. We set specificity of trypsin digestion and allowed two missed cleavage sites and mass tolerances in MS, and MS/MS were set to 2 p.p.m. and 0.8 Da, respectively. The resulting Mascot result files were further processed using *my*ProMS[47] (v3.0), allowing a maximum FDR of 1% by automatically filtering the Mascot score at the peptide level.

Protein quantification. For SILAC-based protein quantification, peptides XICs (extracted ion chromatograms) were retrieved from Proteome Discoverer. Scale normalization computed using the 'package limma' from R was applied to compensate for mixing errors of the different SILAC cultures as described[48]. Protein ratios were computed as the geometrical mean of related peptides. To estimate ratio significance, a *t*-test was performed with a Benjamini–Hochberg FDR control threshold set to 0.05. All quantified proteins have at least three peptides quantified (all peptides selected). Peptide intensity ratio outliers were removed when their value was too far from the median observed in the peptide intensity ratio set for a given protein. Protein quantification ratio outliers were not computed when the identified peptide number was too different between the two channels. Proteins displaying a minimal absolute fold change $\geq$10% that reaches statistical significance (adjusted P value of quantification $\leq$0.05) were considered as differentially associated with the centrosome of activated lymphocytes. This led to the selection of 835 proteins.

GO term enrichment analysis. Protein analysis by GO term enrichment was computed based on annotation only and did not take into account the relative abundance of the 835 proteins in resting and activated lymphocytes. The frequency of each GO was computed in the *Mus musculus* proteome (defined as the background, Slim Ontology file including all 21,283 mouse proteins) and compared with the set. We reported only the GO terms with the frequency statistically enriched in our protein set compared with the background. GO enrichment factors were computed with the GO::TermFinder[49] through *my*ProMS. Briefly, to determine whether any GO term annotates a specified list of proteins at a frequency greater than the one expected by chance, GO::TermFinder calculates a P value using a hyper-geometric distribution. For multiple testing corrections, FDR was controlled and set to 1% (Benjamini–Hochberg). A P value was associated to each GO term individually. The FDR corresponds to the cutoff applied to the list of all the GO terms.

***In vitro* nucleation assays.** *In vitro* nucleation assays were performed according to Farina *et al.*[26]. In brief, centrosomes isolated in TicTac buffer were incubated for 20 min on surface of a polydimethylsiloxane open chamber. The excess of centrosomes was washed with TicTac buffer supplemented with 1% BSA (TicTac-BSA). Microtubule and actin nucleation was induced by diluting tubulin dimers (labelled with ATTO-565, 30 µM final[26]) or actin monomers (labelled with Alexa-568, 1 µM final[50–52]) in TicTac buffer supplemented with 1 mM GTP, 2.7 mM ATP, 10 mM dithiothreitol, 20 µg ml^{-1} catalase, 3 mg ml^{-1} glucose, 100 µg ml^{-1} glucose oxidase and 0.25% w/v methylcellulose. In addition, a threefold molar equivalent of profilin to actin was added in the reaction mixture[53]. Time-lapse observations were performed by using a total internal reflection fluorescence microscope (Roper Scientific) equipped by an iLasPulsed system and an Evolve camera (EMCCD 512 × 512, pixel = 16 µm) using a × 60 1.49 NA objective lens. For quantification of the actin nucleation activity by centrosomes, F-actin fluorescence intensity was integrated over a 2-µm-diameter circle around the centrosome and normalized with respect to initial intensity. γ-Tubulin staining, needed for the efficiency calculation, was performed at the end of the movie recording under the microscope without prior fixation. Primary and secondary antibodies, diluted in TicTac-BSA buffer, were incubated for 60 and 30 min, respectively. Arp2/3 complex inhibition experiments were performed by adding 200 µM CK666 in reaction mixture. dimethylsulfoxide was used as control. Immunofluorescence staining of isolated centrosomes was performed by incubating centrosomes, seeded on a clean surface, with primary and secondary antibodies for 60 and 30 min, respectively.

Western blotting. B cells were lysed at 4 °C in RIPA buffer (Thermo Scientific) supplemented with 1 × protease inhibitor cocktail (Roche) and 1 × Halt phosphatase inhibitor cocktail (Thermo Scientific). Supernatants were collected and loaded onto mini-PROTEAN TGX SDS–PAGE gels and transferred onto polyvinylidene fluoride membrane (Trans-Blot Turbo Transfer). Membranes were blocked in 5% non-fat dry milk resuspended in 1 × TBS–0.05% Tween-20 and incubated overnight at 4 °C, with primary antibodies followed by 60 min incubation with secondary antibodies. Western blots were developed with Clarity Western ECL substrate, and chemiluminescence was detected using the ChemiDoc imager (all from BioRad). Full scans of unprocessed western blots are available in Supplementary Fig. 7.

Calcium measurement. A total of 1 × 10^6 B cells were loaded with 1 µM Fluo-4 AM and Fura Red AM (Life Technologies) for 15 min at 37 °C in RPMI 1640 and resuspended in CLICK medium. The fluorescence of Fluo-4 and Fura Red were analysed using a BD Accuri C6 flow cytometer (BD Biosciences). After 120-s recording to assess basal Ca^{2+} levels, BCR-ligand at a final concentration of 10 µg ml^{-1} was added to the cell suspension and the Ca^{2+} levels were measured for 300 s. Finally, the ratio Fluo-4/Fura Red and the geometric mean over time were calculated using FlowJo software (v10, BD Biosciences).

Antigen presentation. B cells were incubated with Lack ± BCR-ligand-coated beads for 5 h or with peptide control for 1 h. Cells were washed with PBS, fixed in ice-cold PBS/0.01% glutaraldehyde for 1 min and quenched with PBS/100 mM glycine. B cells were then incubated with Lack-specific T-cell hybridoma in a 1:1 ratio for 24 h. Supernatants were collected and interleukin-2 cytokine production was assessed using BD optEIA Mouse IL-2 ELISA set following the manufacturer's instructions (BD Biosciences).

Immunofluorescence acquisition and analysis. All z-stack images (0.5-µm spacing) were acquired on an inverted spinning disk confocal microscope (Roper/Nikon) with a × 60/1.4 NA oil immersion objective. Image processing was performed with Fiji (ImageJ) software[54]. Because methanol fixation required for γ-tubulin staining is not compatible with phalloidin labelling, the centrosome was stained with antibodies directed against α-tubulin, and a threshold was applied to visualize the centrosome but not the microtubules as described in Supplementary Fig. 2d. Single-cell images shown in the figures were cropped from large fields, rotated and their contrast and brightness manually adjusted. Images shown are the average z-projection of three planes around the centrosome.

Centrosome polarity index was computed as described in Fig. 1a. Briefly, z-stacks were projected (SUM slice) and images were automatically threshold (Default) on the green channel to obtain the centre of mass of the cell ($Cell_{CM}$). Then, the position of the centrosome and the bead geometrical centre ($Bead_{GC}$) were manually selected. The position of the centrosome was then projected ($Cent_{proj}$) on the vector defined by the $Cell_{CM}$–$Bead_{GC}$ axis. The centrosome polarity index was calculated by dividing the distance between the $Cell_{CM}$ and the $Cent_{proj}$ by the distance between the $Cell_{CM}$ and the $Bead_{GC}$. The index ranges from −1 (anti-polarized) to 1 (fully polarized).

Centrosome- and synapse-associated Arp2 and F-actin were quantified as shown in Fig. 2b and Supplementary Fig. 4a, respectively. Briefly, after manual selection of the centrosome, background subtraction (rolling ball 50 px) on the z-projection (AVG) of the three planes around the centrosome was performed. We then computed the radial distribution of cytoplasmic Arp2 and F-actin fluorescence intensities from the centrosome of resting cells. The drop in fluorescence intensities (at 0.8 µm from the centrosome) was used as a threshold to define the radius of the centrosomal area that was further used to assess the amount of Arp2 and F-actin associated with the centrosome. The synaptic area was manually defined by positioning a fixed area at the cell–bead interface.

The distance between the centrosome and the nucleus was measured in three dimensions. For this, the nucleus was automatically threshold in 3D (Otsu) and the corresponding 3D-distance map was computed (Image 3D suite plugin). The 3D position of the centrosome was then manually selected on the cell stack and the shorter distance to the nucleus edge was measured on the 3D-distance map.

Statistics. All graphs and statistical analysis were performed with GraphPad Prism 5 (GraphPad Software). No statistical method was used to predetermine sample size. Kolmogorov–Smirnov test was used to assess normality of all data sets. Mann–Whitney test was used to determine statistical significance excepted when mentioned. Boxes in box plots extend from the 25th to 75th percentile, with a line at the median and whiskers extend from the 10th to the 90th percentile. Bar graphs show the mean ± s.e.m.

References

1. Barnett, B. E. *et al.* Asymmetric B cell division in the germinal center reaction. *Science* **335,** 342–344 (2012).
2. Thaunat, O. *et al.* Asymmetric segregation of polarized antigen on B cell division shapes presentation capacity. *Science* **335,** 475–479 (2012).
3. Schmoranzer, J. *et al.* Par3 and dynein associate to regulate local microtubule dynamics and centrosome orientation during migration. *Curr. Biol.* **19,** 1065–1074 (2009).

4. Elric, J. & Etienne-Manneville, S. Centrosome positioning in polarized cells: common themes and variations. *Exp. Cell Res.* **328,** 240–248 (2014).
5. Yuseff, M. I., Pierobon, P., Reversat, A. & Lennon-Dumenil, A. M. How B cells capture, process and present antigens: a crucial role for cell polarity. *Nat. Rev. Immunol.* **13,** 475–486 (2013).
6. del Pozo, M. A. *et al.* The two poles of the lymphocyte: specialized cell compartments for migration and recruitment. *Cell Adhes. Commun.* **6,** 125–133 (1998).
7. Chang, J. T. *et al.* Asymmetric T lymphocyte division in the initiation of adaptive immune responses. *Science* **315,** 1687–1691 (2007).
8. Stinchcombe, J. C. & Griffiths, G. M. Communication, the centrosome and the immunological synapse. *Philos. Trans. R. Soc. Lond. B. Biol. Sci.* **369,** 20130463 (2014).
9. Kupfer, A., Swain, S. L. & Singer, S. J. The specific direct interaction of helper T cells and antigen-presenting B cells. II. Reorientation of the microtubule organizing center and reorganization of the membrane-associated cytoskeleton inside the bound helper T cells. *J. Exp. Med.* **165,** 1565–1580 (1987).
10. Harwood, N. E. & Batista, F. D. The cytoskeleton coordinates the early events of B-cell activation. *Cold Spring Harb. Perspect. Biol.* **3,** a002360 (2011).
11. Rak, G. D., Mace, E. M., Banerjee, P. P., Svitkina, T. & Orange, J. S. Natural killer cell lytic granule secretion occurs through a pervasive actin network at the immune synapse. *PLoS Biol.* **9,** e1001151 (2011).
12. Ritter, A. T. *et al.* Actin depletion initiates events leading to granule secretion at the immunological synapse. *Immunity* **42,** 864–876 (2015).
13. Stinchcombe, J. C., Majorovits, E., Bossi, G., Fuller, S. & Griffiths, G. M. Centrosome polarization delivers secretory granules to the immunological synapse. *Nature* **443,** 462–465 (2006).
14. Yuseff, M. I. *et al.* Polarized secretion of lysosomes at the B cell synapse couples antigen extraction to processing and presentation. *Immunity* **35,** 361–374 (2011).
15. Liu, X., Kapoor, T. M., Chen, J. K. & Huse, M. Diacylglycerol promotes centrosome polarization in T cells via reciprocal localization of dynein and myosin II. *Proc. Natl Acad. Sci. USA* **110,** 11976–11981 (2013).
16. Quann, E. J., Liu, X., Altan-Bonnet, G. & Huse, M. A cascade of protein kinase C isozymes promotes cytoskeletal polarization in T cells. *Nat. Immunol.* **12,** 647–654 (2011).
17. Reversat, A. *et al.* Polarity protein Par3 controls B-cell receptor dynamics and antigen extraction at the immune synapse. *Mol. Biol. Cell* **26,** 1273–1285 (2015).
18. Yi, J. *et al.* Centrosome repositioning in T cells is biphasic and driven by microtubule end-on capture-shrinkage. *J. Cell Biol.* **202,** 779–792 (2013).
19. Combs, J. *et al.* Recruitment of dynein to the Jurkat immunological synapse. *Proc. Natl Acad. Sci. USA.* **103,** 14883–14888 (2006).
20. Martin-Cofreces, N. B. *et al.* MTOC translocation modulates IS formation and controls sustained T cell signaling. *J. Cell Biol.* **182,** 951–962 (2008).
21. Gomez, T. S. *et al.* Formins regulate the actin-related protein 2/3 complex-independent polarization of the centrosome to the immunological synapse. *Immunity* **26,** 177–190 (2007).
22. Schnyder, T. *et al.* B cell receptor-mediated antigen gathering requires ubiquitin ligase Cbl and adaptors Grb2 and Dok-3 to recruit dynein to the signaling microcluster. *Immunity* **34,** 905–918 (2011).
23. Hoedt, E., Zhang, G. & Neubert, T. A. Stable isotope labeling by amino acids in cell culture (SILAC) for quantitative proteomics. *Adv. Exp. Med. Biol.* **806,** 93–106 (2014).
24. Rotty, J. D., Wu, C. & Bear, J. E. New insights into the regulation and cellular functions of the ARP2/3 complex. *Nat. Rev. Mol. Cell Biol.* **14,** 7–12 (2013).
25. Hubert, T., Vandekerckhove, J. & Gettemans, J. Actin and Arp2/3 localize at the centrosome of interphase cells. *Biochem. Biophys. Res. Commun.* **404,** 153–158 (2011).
26. Farina, F. *et al.* The centrosome is an actin-organizing centre. *Nat. Cell Biol.* **18,** 65–75 (2016).
27. Nolen, B. J. *et al.* Characterization of two classes of small molecule inhibitors of Arp2/3 complex. *Nature* **460,** 1031–1034 (2009).
28. Burke, T. A. *et al.* Homeostatic actin cytoskeleton networks are regulated by assembly factor competition for monomers. *Curr. Biol.* **24,** 579–585 (2014).
29. Gomez, T. S. *et al.* HS1 functions as an essential actin-regulatory adaptor protein at the immune synapse. *Immunity* **24,** 741–752 (2006).
30. Hao, J. J., Carey, G. B. & Zhan, X. Syk-mediated tyrosine phosphorylation is required for the association of hematopoietic lineage cell-specific protein 1 with lipid rafts and B cell antigen receptor signalosome complex. *J. Biol. Chem.* **279,** 33413–33420 (2004).
31. Monfregola, J., Napolitano, G., D'Urso, M., Lappalainen, P. & Ursini, M. V. Functional characterization of Wiskott-Aldrich syndrome protein and scar homolog (WASH), a bi-modular nucleation-promoting factor able to interact with biogenesis of lysosome-related organelle subunit 2 (BLOS2) and gamma-tubulin. *J. Biol. Chem.* **285,** 16951–16957 (2010).
32. Luxton, G. W., Gomes, E. R., Folker, E. S., Vintinner, E. & Gundersen, G. G. Linear arrays of nuclear envelope proteins harness retrograde actin flow for nuclear movement. *Science* **329,** 956–959 (2010).
33. Burakov, A. V. & Nadezhdina, E. S. Association of nucleus and centrosome: magnet or velcro? *Cell Biol. Int.* **37,** 95–104 (2013).
34. Maro, B. & Bornens, M. The centriole-nucleus association: effects of cytochalasin B and nocodazole. *Biol. Cell.* **39,** 287–290 (1980).
35. Karsenti, E., Kobayashi, S., Mitchison, T. & Kirschner, M. Role of the centrosome in organizing the interphase microtubule array: properties of cytoplasts containing or lacking centrosomes. *J. Cell Biol.* **98,** 1763–1776 (1984).
36. Kwon, M., Bagonis, M., Danuser, G. & Pellman, D. Direct microtubule-binding by myosin-10 orients centrosomes toward retraction fibers and subcortical actin clouds. *Dev. Cell* **34,** 323–337 (2015).
37. Kim, D. H., Cho, S. & Wirtz, D. Tight coupling between nucleus and cell migration through the perinuclear actin cap. *J. Cell Sci.* **127,** 2528–2541 (2014).
38. Kutscheidt, S. *et al.* FHOD1 interaction with nesprin-2G mediates TAN line formation and nuclear movement. *Nat. Cell Biol.* **16,** 708–715 (2014).
39. Higgs, H. N., Blanchoin, L. & Pollard, T. D. Influence of the C terminus of Wiskott-Aldrich syndrome protein (WASp) and the Arp2/3 complex on actin polymerization. *Biochemistry* **38,** 15212–15222 (1999).
40. Sims, T. N. *et al.* Opposing effects of PKCtheta and WASp on symmetry breaking and relocation of the immunological synapse. *Cell* **129,** 773–785 (2007).
41. Finetti, F. *et al.* Intraflagellar transport is required for polarized recycling of the TCR/CD3 complex to the immune synapse. *Nat. Cell Biol.* **11,** 1332–1339 (2009).
42. de la Roche, M. *et al.* Hedgehog signaling controls T cell killing at the immunological synapse. *Science* **342,** 1247–1250 (2013).
43. Malherbe, L. *et al.* Selective activation and expansion of high-affinity CD4 + T cells in resistant mice upon infection with Leishmania major. *Immunity* **13,** 771–782 (2000).
44. Derivery, E. *et al.* The Arp2/3 activator WASH controls the fission of endosomes through a large multiprotein complex. *Dev. Cell* **17,** 712–723 (2009).
45. Gogendeau, D., Guichard, P. & Tassin, A. M. Purification of centrosomes from mammalian cell lines. *Methods Cell Biol.* **129,** 171–189 (2015).
46. Burgo, A. *et al.* Increased activity of the vesicular soluble N-ethylmaleimide-sensitive factor attachment protein receptor TI-VAMP/VAMP7 by tyrosine phosphorylation in the Longin domain. *J. Biol. Chem.* **288,** 11960–11972 (2013).
47. Poullet, P., Carpentier, S. & Barillot, E. myProMS, a web server for management and validation of mass spectrometry-based proteomic data. *Proteomics* **7,** 2553–2556 (2007).
48. Yang, Y. H. *et al.* Normalization for cDNA microarray data: a robust composite method addressing single and multiple slide systematic variation. *Nucleic Acids Res.* **30,** e15 (2002).
49. Boyle, E. I. *et al.* GO::TermFinder—open source software for accessing Gene Ontology information and finding significantly enriched Gene Ontology terms associated with a list of genes. *Bioinformatics* **20,** 3710–3715 (2004).
50. MacLean-Fletcher, S. & Pollard, T. D. Identification of a factor in conventional muscle actin preparations which inhibits actin filament self-association. *Biochem. Biophys. Res. Commun.* **96,** 18–27 (1980).
51. Isambert, H. *et al.* Flexibility of actin filaments derived from thermal fluctuations. Effect of bound nucleotide, phalloidin, and muscle regulatory proteins. *J. Biol. Chem.* **270,** 11437–11444 (1995).
52. Egile, C. *et al.* Activation of the CDC42 effector N-WASP by the Shigella flexneri IcsA protein promotes actin nucleation by Arp2/3 complex and bacterial actin-based motility. *J. Cell Biol.* **146,** 1319–1332 (1999).
53. Fedorov, A. A., Pollard, T. D. & Almo, S. C. Purification, characterization and crystallization of human platelet profilin expressed in Escherichia coli. *J. Mol. Biol.* **241,** 480–482 (1994).
54. Schindelin, J. *et al.* Fiji: an open-source platform for biological-image analysis. *Nat. Methods* **9,** 676–682 (2012).

Acknowledgements

We acknowledge P. Bousso, M. Bornens, P. Vargas, M. Chabaud, M. Bretou, V. Randrian and H. D. Moreau for critical discussions; M. Piel and C. Hivroz for critical reading of the manuscript; R. Basto and D. Gogendeau for advice on centrosome manipulation; G. Arras for his help with GO term enrichment analysis; and D. Lankar for technical advice and discussions. We thank Edgar R. Gomes for providing the Nesprin-2 SRKASH (LINC-DN) plasmid. We acknowledge the Nikon Imaging Center@CNRS-Institut Curie and PICT-IBiSA, Institut Curie, Paris, member of the France-BioImaging national research infrastructure, for support in image acquisition. D.O. was supported by fellowships from the Ecole Doctorale BioSPC, Université Paris Diderot and Université Paris Descartes and the Fondation pour la Recherche Médicale. M.I.-Y. was supported by a research grant from FONDECYT No. 1141182. Funding was obtained from the Association Nationale pour la Recherche (ANR-PoLyBex-12-BSV3-0014-001 to A.-M.L.-D. and ANR-12-BSV5-0004-01 to M.T. and L.B.) and the European Research Council (ERC-Strapacemi-GA 243103 to A.-M.L.-D. and Starting grant 310472 to M.T.).

Author contributions

D.O. designed, performed and analysed most of the experiments, assembled figures and participated in manuscript writing; F.F. and J.G. performed and analysed *in vitro* nucleation assays; O.M. assisted in cell culture, immunofluorescences, centrosome

purifications and performed biochemistry experiments; P.J.S. performed calcium measurements and time-lapse experiments; M.M. wrote Fiji (ImageJ) routines for image analysis; F.D. carried out the LC–MS/MS experimental work and D.L. supervised LC–MS/MS and proteomic data analysis; A.G. produced and provided the antibody against WASH; M.-I.Y. adapted the protocol for, assisted in centrosome purifications and proposed the original hypothesis of changes in the centrosome proteome triggered by BCR engagement; L.B. and M.T. designed and supervised *in vitro* nucleation assays and participated in manuscript writing; A.-M.L.-D. designed and supervised the overall research, funded it and wrote the manuscript.

Additional information

Supplementary Information accompanies this paper at http://www.nature.com/naturecommunications

Competing financial interests: The authors declare no competing financial interests.

Reprints and permission information is available online at http://npg.nature.com/reprintsandpermissions/

How to cite this article: Obino, D. *et al.* Actin nucleation at the centrosome controls lymphocyte polarity. *Nat. Commun.* 7:10969 doi: 10.1038/ncomms10969 (2016).

"Polarity protein Par3 controls B-cell receptor dynamics and antigen extraction at the immune synapse"

Reversat A[1]*, Yuseff MI[2]*, Lankar D[1†], Malbec O[1†], **Obino D**[1†], Maurin M[1], Penmatcha NV[1], Amoroso A[3], Sengmanivong L[4], Gundersen GG[5], Mellman I[6], Darchen F[7], Desnos C[7], Pierobon P[1‡] and Lennon-Duménil AM[1‡]

*, †, ‡ These authors contributed equally to this work.

Molecular Biology of the Cell, 2015, 26(7):1273-85

[1]INSERM U932, Institut Curie, Centre de Recherche, 75005 Paris, France.

[2]INSERM U932, Institut Curie, Centre de Recherche, 75005 Paris, France and Departamento de Biologia Celular y Molecular, P. Universidad Catolica de Chile, 6513677 Santiago, Chile.

[3]INSERM U932, Institut Curie, Centre de Recherche, 75005 Paris, France Facultad de Ciencias de la Salud, Universidad San Sebastián, 7510157 Santiago, Chile.

[4]Cell and Tissue Imaging Core Facility (PICT-IBiSA) and Nikon Imaging Centre, Institut Curie, UMR144, Centre de Recherche, 75005 Paris, France.

[5]Department of Pathology and Cell Biology, Columbia University, New York, NY 10032.

[6]Genentech, San Francisco, CA 94080.

[7]Université Paris Descartes, Sorbonne Paris Cité, CNRS UMR8250, 75270 Paris Cedex 06, France.

Polarity protein Par3 controls B-cell receptor dynamics and antigen extraction at the immune synapse

Anne Reversat[a,*], Maria-Isabel Yuseff[a,b,*], Danielle Lankar[a,†], Odile Malbec[a,†], Dorian Obino[a,†], Mathieu Maurin[a], Naga Venkata Gayathri Penmatcha[a], Alejandro Amoroso[a,c], Lucie Sengmanivong[d], Gregg G. Gundersen[e], Ira Mellman[f], François Darchen[g], Claire Desnos[g], Paolo Pierobon[a,‡], and Ana-Maria Lennon-Duménil[a,‡]

[a]INSERM U932, Institut Curie, Centre de Recherche, 75005 Paris, France; [b]Departamento de Biologia Celular y Molecular, Pontificia Universidad Catolica de Chile, 6513677 Santiago, Chile; [c]Facultad de Ciencias de la Salud, Universidad San Sebastián, 7510157 Santiago, Chile; [d]Cell and Tissue Imaging Core Facility (PICT-IBiSA) and Nikon Imaging Centre, Institut Curie, UMR144, Centre de Recherche, 75005 Paris, France; [e]Department of Pathology and Cell Biology, Columbia University, New York, NY 10032; [f]Genentech, San Francisco, CA 94080; [g]Université Paris Descartes, Sorbonne Paris Cité, CNRS UMR8250, 75270 Paris Cedex 06, France

ABSTRACT **B-cell receptor (BCR) engagement with surface-tethered antigens leads to the formation of an immune synapse, which facilitates antigen uptake for presentation to T-lymphocytes. Antigen internalization and processing rely on the early dynein-dependent transport of BCR–antigen microclusters to the synapse center, as well as on the later polarization of the microtubule-organizing center (MTOC). MTOC repositioning allows the release of proteases and the delivery of MHC class II molecules at the synapse. Whether and how these events are coordinated have not been addressed. Here we show that the ancestral polarity protein Par3 promotes BCR–antigen microcluster gathering, as well as MTOC polarization and lysosome exocytosis, at the synapse by facilitating local dynein recruitment. Par3 is also required for antigen presentation to T-lymphocytes. Par3 therefore emerges as a key molecule in the coupling of the early and late events needed for efficient extraction and processing of immobilized antigen by B-cells.**

Monitoring Editor
Xueliang Zhu
Chinese Academy of Sciences

Received: Sep 15, 2014
Revised: Jan 12, 2015
Accepted: Jan 20, 2015

INTRODUCTION

In lymph nodes, B-lymphocytes are activated through the engagement of their B-cell receptor (BCR) with antigens (Ags) tethered at the surface of neighboring cells (Batista and Harwood, 2009). BCR engagement leads to extraction and processing of these immobilized antigens for presentation onto major histocompatibility complex (MHC) class II molecules to primed $CD4^+$ T-cells (Mitchison, 2004). This process, referred to as T-B cooperation, is required for germinal center formation and production of high-affinity antibodies by B-lymphocytes.

Both efficient BCR signaling and extraction of surface-tethered antigens rely on the formation of an immune synapse that is reminiscent of the one described in T-lymphocytes (Kupfer *et al.*, 1987; Grakoui *et al.*, 1999). It includes a peripheral region, the pSMAC, into which coreceptors such as LFA-1 accumulate, and a central region, the cSMAC, toward which BCRs, organized into clusters containing signaling molecules (termed microclusters), are actively transported (Carrasco *et al.*, 2004; Harwood and Batista, 2008; Tolar *et al.*, 2009). Directed transport of microclusters to the cSMAC allows local gathering of BCR–antigen complexes and promotes their internalization (Fleire *et al.*, 2006, Schnyder *et al.*, 2011). Formation of signaling BCR microclusters relies on the local remodeling of the actin cytoskeleton by the small GTPase Rac2 and the ERM protein ezrin (Brezski and Monroe, 2007; Arana *et al.*, 2008;

This article was published online ahead of print in MBoC in Press (http://www.molbiolcell.org/cgi/doi/10.1091/mbc.E14-09-1373) on January 28, 2015.

*These authors contributed equally.

†These authors contributed equally.

‡These authors contributed equally.

The authors declare no conflicts of interest.

Address correspondence to: Paolo Pierobon (paolo.pierobon@curie.fr), Ana-Maria Lennon-Duménil (amlennon@curie.fr).

Abbreviations used: Ag, antigen; aPKC, atypical protein kinase C; BCR, B-cell receptor; MHC, major histocompatibility complex; MTOC, microtubule-organizing center; SIM, structured illumination microscopy; TIRFM, total internal reflection fluorescence microscopy.

Supplemental Material can be found at:
http://www.molbiolcell.org/content/suppl/2015/01/27/mbc.E14-09-1373v1.DC1.html

Treanor *et al.*, 2010). In addition, the directed movement of signaling BCR microclusters to the cSMAC requires their association with the microtubule motor protein dynein, which promotes antigen gathering, extraction, and presentation (Schnyder *et al.*, 2011).

Additional evidence for the involvement of the microtubule cytoskeleton in synapse organization and function is provided by our work demonstrating that the polarization of the microtubule-organizing center (MTOC) to the B-cell synapse allows the local secretion of lysosomal hydrolases that promote efficient antigen extraction (Yuseff *et al.*, 2011). Two other recent studies support the idea that B-cell polarity regulates B-lymphocyte function at several stages of activation. Indeed, it was shown that while migrating toward the T-cell zone, activated B-cells undergo asymmetric divisions, allowing segregation of the taken-up antigen to be presented to T-lymphocytes in one daughter cell only (Thaunat *et al.*, 2012). Asymmetric B-cell divisions were also described in germinal centers, where they might regulate the unequal inheritance of fate-associated molecules such as Bcl-6 by daughter cells (Barnett *et al.*, 2012). Control of cell polarity therefore emerges as a key mechanism involved in the regulation of B-lymphocyte responses.

In epithelial cells, establishment of cell polarity is driven by three conserved protein complexes: Scribble, Crumbs, and the partitioning-defective (Par) complex (Mellman and Nelson, 2008). Among the three, the Par polarity complex has the broadest function, controlling apicobasal polarity, asymmetric cell division, and directed cell migration. It is composed of three subunits—Par6, Par3, and atypical protein kinase Cζ (aPKCζ)—and is often activated downstream of the small GTPase Cdc42 (Iden and Collard, 2008). The mechanisms by which Par regulates cell polarity involve the redirection of both the actin and microtubule cytoskeletons toward precisely labeled intracellular locations. We demonstrated that MTOC and lysosome polarization induced upon BCR engagement with surface-tethered Ag relies on both Cdc42 and aPKCζ (Yuseff *et al.*, 2011). Of interest, it was highlighted that Par3 interacts with dynein in migrating fibroblasts (Schmoranzer *et al.* 2009). This has been shown to allow MTOC polarization in T-lymphocytes (Quann *et al.* 2009; Yi *et al.* 2013). Furthermore, Par3 transcription was shown to be under the control of Pax5, the master regulator of the B-cell lineage (Schebesta *et al.*, 2007). However, whether this ancestrally conserved polarity protein plays a role in B-lymphocyte function remains an open question.

Here we investigate the role of Par3 in formation and function of the B-cell synapse. We show that by facilitating the local recruitment of dynein, Par3 couples the early and late events required for presentation of immobilized Ag to T-lymphocytes: 1) the gathering of BCR-Ag microclusters at the synapse center and 2) the local exocytosis of lysosomes that delivers proteases and MHC class II molecules for Ag processing to take place.

RESULTS

BCR engagement with surface-tethered antigens triggers Par3 recruitment to the center of the immune synapse

To investigate whether Par3 is recruited at the B-cell synapse, we plated mouse B-lymphoma cells expressing Par3–green fluorescent protein (GFP) and LifeAct-CherryFP onto glass slides coated or not with specific BCR ligands and recorded them for 30 min by total interference reflection fluorescence time-lapse microscopy (TIRFM). As expected, we observed a flow of actin starting at the synapse periphery and moving toward its center, leading to lamellipodial extension and progressive contraction (Figure 1, A and B, and Supplemental Video S1). Of interest, Par3-GFP formed punctuated structures that, similar to actin, moved in a unidirectional manner to the synapse center. However, whereas these Par3-GFP dots ultimately concentrated at the level of the cSMAC, actin had a more peripheral distribution (Figure 1B). Of importance, no directional Par3-GFP movement (nor that of actin) was observed when B-cells were plated on slides noncoated with Ag (Figure 1B and Supplemental Figure S1), highlighting the specificity of this phenomenon. We conclude that Par3 is recruited at the B-cell synapse, undergoes centripetal movement, and concentrates at the level of the cSMAC.

Par3 is required for BCR-Ag microcluster gathering at the center of the immune synapse

The centripetal transport of BCR-Ag microclusters was shown to be essential for Ag gathering at the synapse center and uptake for presentation onto MHC class II molecules (Treanor *et al.*, 2010). Using planar lipid bilayers, we observed that BCR-Ag microclusters transiently overlapped with Par3-GFP–containing punctuated structures during centripetal transport (see arrows in Figure 2A and Supplemental Video S2). This result suggests that Par3 might be involved in the dynamics of these signaling structures. To address this question, we silenced Par3 expression using two Par3-specific short hairpin RNAs (shRNAs; Supplemental Figure S2A). Although Par3-silenced cells exhibited similar numbers of BCR-Ag microclusters as control cells, these microclusters often failed to gather at the cSMAC in the absence of the polarity protein, instead remaining dispersed at the cell periphery (Figure 2, B and C, and Supplemental Video S3). This was quantified by measuring the growth of microclusters during centripetal transport: whereas microcluster size increased in control B-cells as a result of their coalescence at the synapse center, this was not observed in Par3-silenced B-cells (Figure 2D). Of interest, a slight reduction in the phosphorylation of Erk and p38 was detected in Par3-silenced cells, suggesting that the mitogen-activated protein (MAP) kinase pathway requires microcluster centripetal transport for efficient activation (Supplemental Figure S2B). In addition, no significant difference in the mobility of single BCR molecules was observed between control and Par3-silenced resting B-lymphocytes (Supplemental Figure S3, A and B), suggesting that Par3 specifically regulates BCR dynamics upon engagement with immobilized antigens. We conclude that Par3 interacts with BCR-Ag microclusters and is required for their transport toward the center of the immune synapse.

Par3 regulates dynein dynamics at the B-cell synapse

The centripetal transport of BCR-Ag microclusters was shown to rely on dynein (Schnyder *et al.*, 2011). Of interest, this molecular motor was also described as interacting and partially colocalizing with Par3 in migrating fibroblasts (Schmoranzer *et al.*, 2009). We therefore hypothesized that Par3 regulates BCR microcluster transport by facilitating dynein recruitment at the B-cell synapse. To test this hypothesis, we investigated the localization of dynein IC74 (2C–red fluorescent protein [RFP]) in control and Par3-silenced B-cells. Spinning-disk microscopy analysis showed that dynein enrichment at the synapse was decreased in Par3-knockdown B-cells (Figure 3, A and B). In addition, analysis of the dynamics of the motor protein by TIRFM showed that the duration of single dynein trajectories was significantly reduced in Par3-silenced cells as compared with their control counterpart (Figures 3, C and D, and Supplemental Video S4), indicating that the time of presence of dynein at the immune synapse is decreased in the absence of the polarity protein. Of interest, this particularly concerned the dynein structures that localized at the synapse center (Figure 3E). Accordingly, transient colocalization events of Par3-GFP and dynein IC74 (2C-RFP) were observed in cotransfected B-cells (Figure 3F and Supplemental Video S5). Par3

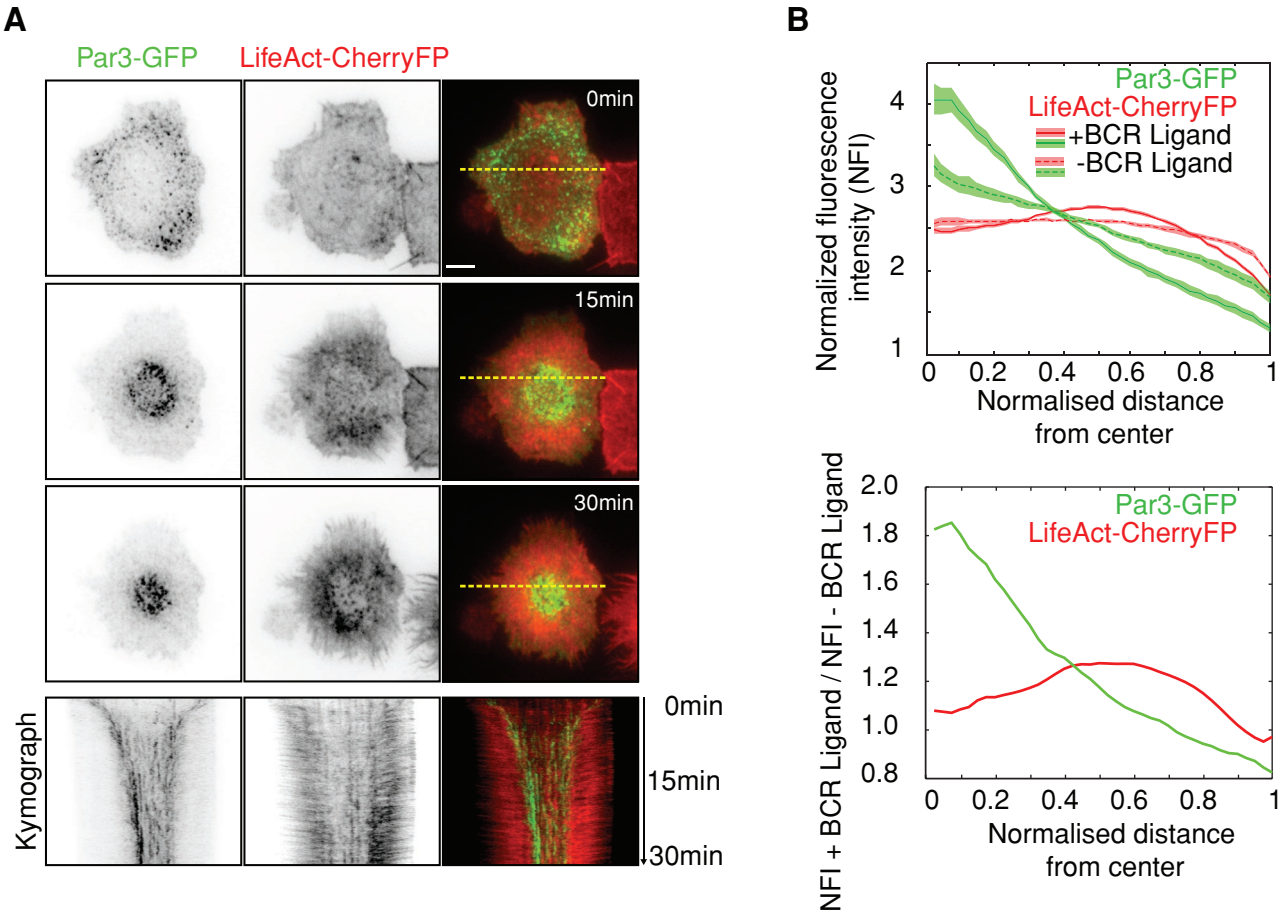

FIGURE 1: Par3 polarizes at the immune synapse. (A) Time-lapse imaging by TIRFM of B-cells expressing LifeAct-CherryFP and Par3-GFP, plated on glass slides coated with BCR ligand; bottom, kymographs of a line scan across the immune synapse (yellow dashed lines in top image). Scale bar, 3 μm. (B) Average of the integrated radial line scan (see *Materials and Methods*) normalized by the size of the cell and the fluorescence intensity (normalized fluorescence intensity [NFI]) measured for 65 and 34 cells plated on specific (+) and unspecific (–) BCR ligand, respectively, at $t = 30$ min after cell plating (at least two independent experiments). Shadow indicates the interval of confidence (±SEM). Bottom, ratio of the NFI averages (top) measured with and without antigen.

silencing had no effect on the endogenous expression levels of the dynein IC74 subunit (Supplemental Figure S3C). Thus, Par3 facilitates dynein enrichment at the center of the B-cell synapse, suggesting that Par3 might promote BCR-Ag microcluster centripetal transport by locally recruiting the motor protein.

Par3 and dynein regulate MTOC polarization to the B-cell synapse

Acquisition of surface-tethered Ag relies on 1) the early gathering of BCR-Ag microclusters at the cSMAC and 2) the later polarization of the MTOC and lysosomes at the immune synapse, which provide both the proteolytic enzymes and MHC class II molecules required for Ag extraction and processing (Yuseff *et al.*, 2011). Of interest, both Par3 and dynein are involved in MTOC polarization in a variety of cellular systems (Gérard *et al.*, 2007; Schmoranzer *et al.*, 2009). We therefore hypothesized that in addition to BCR-Ag microcluster gathering, Par3 and dynein might promote MTOC and lysosome polarization, thereby coupling the early and late events required for efficient Ag presentation.

To assess the role of Par3 and dynein in MTOC polarization to the B-cell synapse, we incubated B-lymphoma cells with 3-μm latex beads coated or not with BCR ligands, a system that is better suited than planar surfaces to study global cell polarity events (Yuseff *et al.*, 2011). We observed that Par3 and dynein were both enriched at the cell–bead interface and exclusively when beads were coated with specific BCR ligands (Figures 4, A–C). Partial colocalization of the two proteins was also observed (Figure 4A). Of importance, dynein polarization to Ag-coated beads was significantly reduced in Par3-silenced B-lymphocytes (Figure 4, D and E), whereas dynein inhibition did not alter Par3-GFP polarization (Supplemental Figure S4A). These results indicate that, as observed on planar surfaces, Par3 promotes the recruitment of dynein to the synapse that forms at the B-cell–bead interface.

Calculation of the MTOC polarity index showed that it was significantly reduced in Par3-silenced B-cells (Figure 5, A and B), indicating that Par3 is required for MTOC polarization in B-cells. Polarization was not observed in B-cells stimulated with beads coated with proteins that do not engage the BCR. Of importance, MTOC polarity was rescued by exogenously expressing human Par3-GFP in mouse B-cells silenced for the endogenous protein (McCaffrey and Macara, 2009), indicating that defective polarity in these cells did not result from shRNA off-targets (Supplemental Figure S4B). Dynein inhibition with ciliobrevin A also significantly impaired MTOC recruitment to the cell–bead interface (Supplemental Figure S5A). We conclude that Par3 and dynein are required for MTOC polarization to the B-cell synapse.

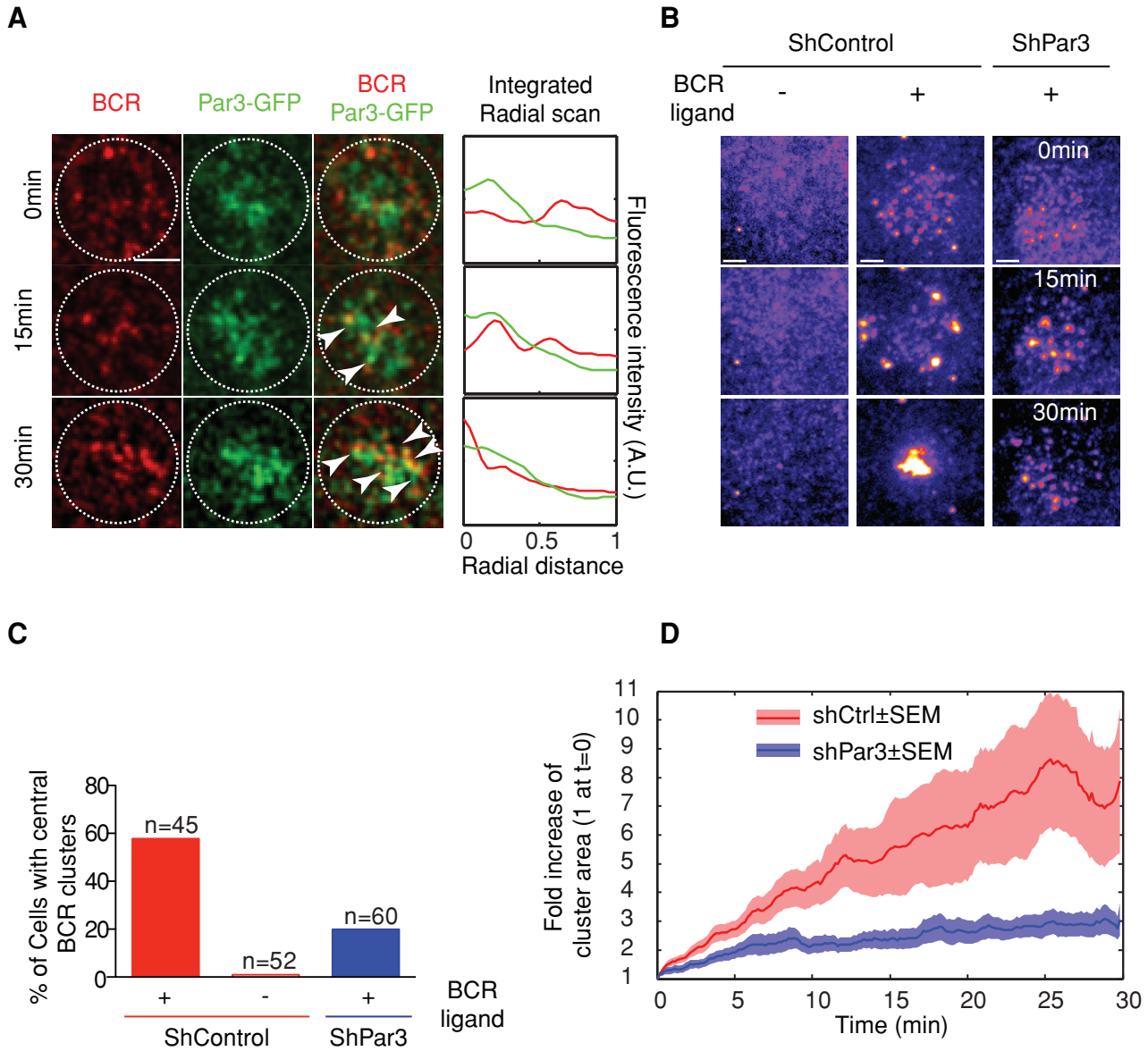

FIGURE 2: Par3 regulates BCR microcluster movement and gathering at the immune synapse. (A) TIRFM simultaneous images of Par3-GFP (green) and BCR clusters (red) of a cell (dashed circle) plated on supported lipid bilayer (scale bar, 3 μm); right, line scan integrated intensity signal of the two channels (as described in *Material and Methods*). (B) TIRFM images of control and Par3-silenced B-cells plated onto lipid bilayers containing ICAM-1 and specific (+) or nonspecific (–) fluorescent BCR ligand (see *Materials and Methods*). Scale bar, 3 μm. (C) Percentage of cells presenting BCR microclusters gathered at the center of the immune synapse after 30 min (qualitative comparison between images like the one displayed in B at $t = 0$ and 30 min). (D) Growth of BCR microclusters in time, shown as the fold increase of the size compared with time 0 (sizes are computed as described in *Materials and Methods*) in control and Par3-A– silenced B-cells (bold curves represent mean ± SEM for 45 samples for shCtrl and 60 samples for shPar3; three independent experiments).

Par3 and dynein regulate lysosome secretion at the B-cell synapse

Similar results were obtained when monitoring lysosome polarization to the cell–bead interface: both Par3 silencing and dynein inhibition significantly impaired lysosome recruitment to the synapse (Figure 5, A and C, and Supplemental Figure S5B). Analysis of dynein distribution in activated B-cells by structured-illumination microscopy (SIM) showed no major colocalization between the LAMP-1 lysosomal marker and the molecular motor, suggesting that the majority of the synaptic dynein pool was recruited independently of these vesicles (Figure 5D and Supplemental Video S6). The local density of lysosomes monitored by TIRFM was also reduced in Par3-silenced B-cells (Supplemental Figure S6A). In contrast, cell spreading measured on Ag-coated slides (Supplemental Figure S6B) or beads (Figures 6, A and B) remained unaffected. Similarly, the number of beads in contact with the control or silenced cells was not significantly different (Figure 6C). Lysosome exocytosis at the synapse was next assessed by measuring local acidification using beads coated with BCR ligands coupled to Cypher5E dye, which fluoresces at acidic pH (Milasta *et al.*, 2005; Yuseff at al., 2011). This experiment showed that synapse acidification was impaired in Par3-knockdown B-cells (Figure 6, D and E). In agreement with our previous findings (Yuseff *et al.*, 2011), no significant Cypher5E signal was observed in intracellular compartments, suggesting either that the

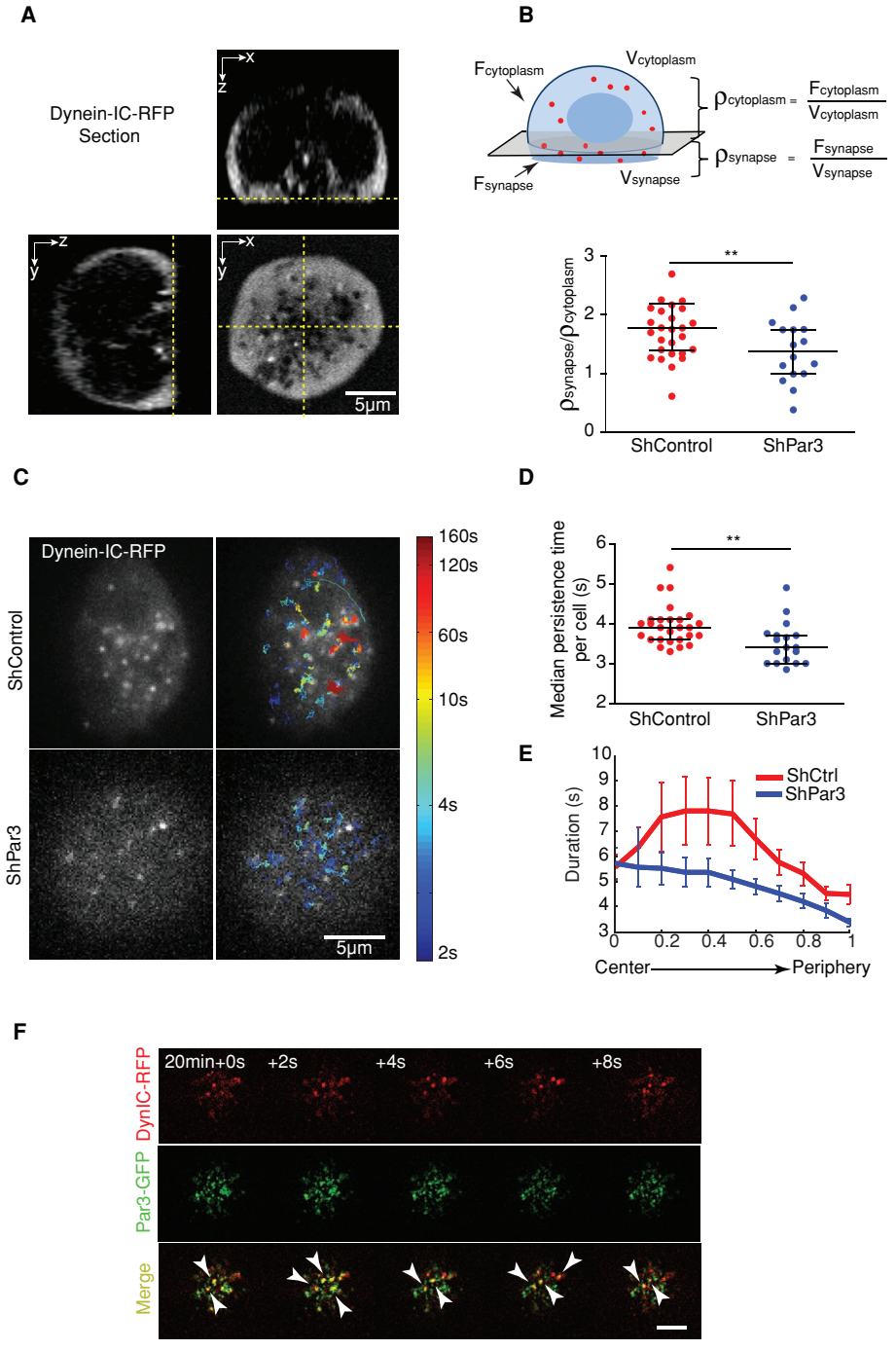

FIGURE 3: Par3 regulates dynein dynamics at the B-cell synapse. (A) B-cells expressing dynein-IC-RFP were plated on anti-IgG–coated coverslips and imaged 15 min to 1 h after stimulation by spinning-disk microscopy. The three images show three sections of a cell (bottom *xy* and two sagittal ones). (B) Method used to quantify dynein accumulation at the synapse: the ratio between fluorescence density of the signal (total fluorescence/volume) in the synapse to the fluorescence density in the cytoplasm was computed; a uniform distribution would give a ratio of 1. The measured fluorescence ratio is higher in shCtrl than in shPar3-A cells (shCtrl, $n = 27$; shPar3, $n = 18$; $p = 0.016$, Mann–Whitney test; three independent experiments), indicating Par3-dependent accumulation of dynein at the synapse. (C) The same pool of cells observed in B were previously observed in TIRFM, and the dynein puncta visible on each frame (left) were tracked with single-particle tracking (only puncta above background levels were considered); overlap of trajectories is color coded according to their duration. (D) Median duration of the trajectory computed in the same cell shows that in the control (shCtrl, $n = 27$) cells, dynein remains at the synapse significantly longer than in silenced ones (shPar3-A, $n = 18$; $p = 0.0028$, Mann–Whitney test); trajectories <2 s were discarded from statistics). (E) Average of the duration, with error bars (SEM), plotted along the normalized distance from the center of the cell for control and silenced cells (respectively, shCtrl, histogram computed for 4044 trajectories, 27 cells; and shPar3-A, for 2041 trajectories, 18 cells; three independent experiments). (F) Time-lapse imaging by TIRFM of B-cells expressing dynein-IC-RFP and Par3-GFP 20 min after being plated on glass slides coated with BCR ligand (scale bar, 5 μm).

fraction of taken-up Ag was not abundant enough to be detected or that Ag was internalized in early endosomal compartments whose pH is not compatible with Cypher5E fluorescence emission. Accordingly, Par3 silencing also reduced the extraction of immobilized Ag, as monitored by labeling the amount of ovalbumin remaining on beads in contact with B-cells (Figure 6F). Hence Par3 silencing impairs lysosome recruitment and secretion at the B-cell synapse as well as local Ag extraction.

Taken together, our results strongly suggest that Par3 regulates MTOC/lysosome recruitment at the synapse by locally recruiting dynein. To formally demonstrate this point, we assessed whether MTOC/lysosome polarity in Par3-silenced B-cells was rescued by expression of a Par3–yellow fluorescent protein (YFP) construct that lacks the N-terminal domain (Par3 Cter-YFP) responsible for its interaction with the motor protein (Schmoranzer *et al.*, 2009). Unfortunately, we found that this construct was mislocalized when transfected in B-cells, accumulating in their nucleus (Supplemental Figure S6C). Nevertheless, our data indicate that Par3 promotes the polarization of dynein to the B-cell synapse, which in turn is required for MTOC/lysosome local recruitment. We therefore conclude that Par3 promotes MTOC/lysosome polarization at least in part by facilitating dynein recruitment at the immune synapse, even though we cannot exclude that Par3-silenced B-cells might have additional defects that also contribute to their defective polarity phenotype.

Par3 is required for the processing and presentation of surface-tethered antigens to T-cells

Having shown that Par3 promotes both BCR-Ag microcluster gathering at the center of the synapse and the local secretion of lysosomes, we next investigated whether Par3 is required for presentation of surface-tethered Ag onto MHC class II molecules to $CD4^+$ T-lymphocytes. For this, we incubated B-cells with beads coated or not with specific BCR ligands plus the LACK antigen from *Leishmania major,* as previously described (Yuseff *et al.*, 2011). After 4 h, B-cells

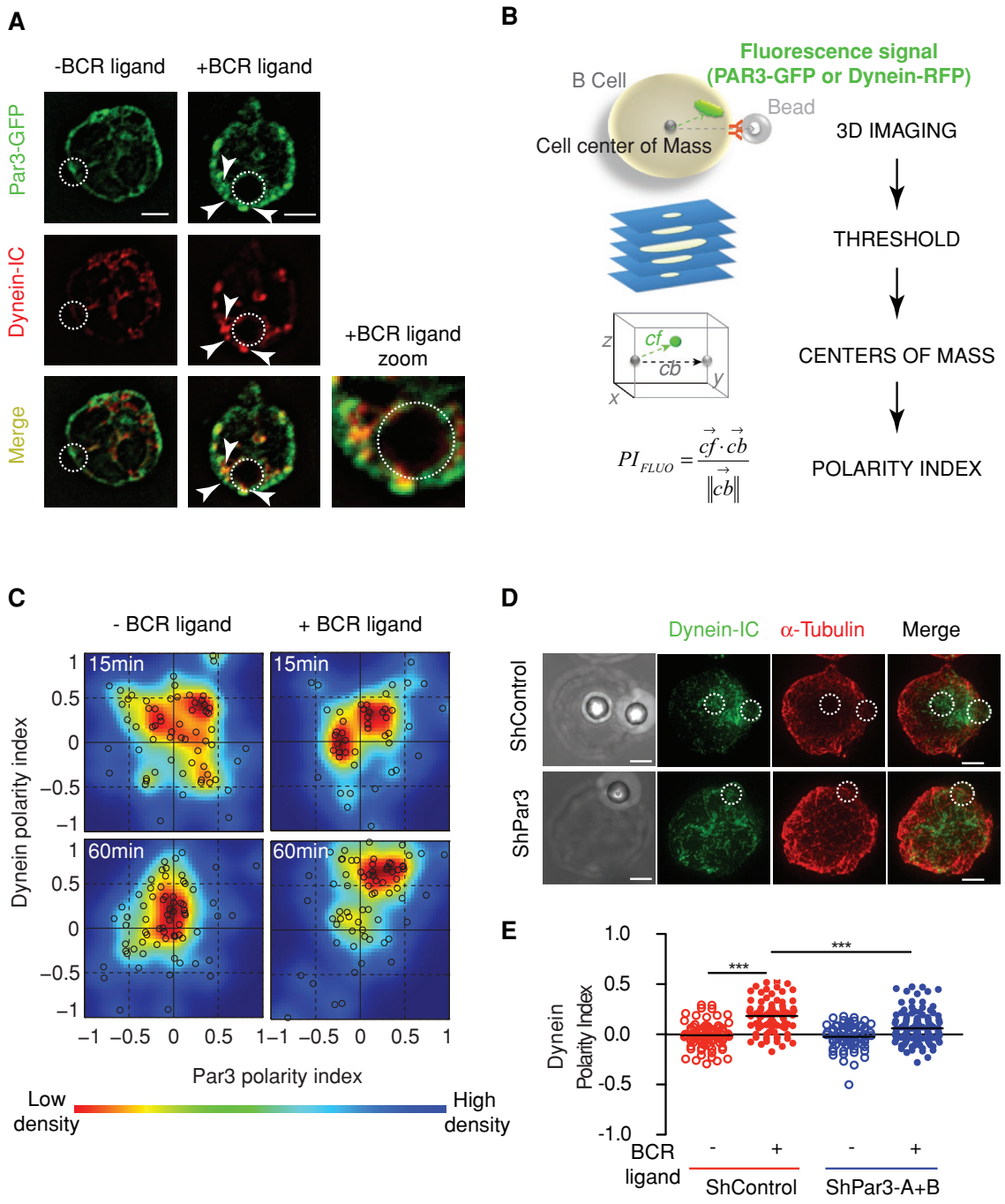

FIGURE 4: Par3 controls centrosome docking by recruiting dynein to the immune synapse. (A) Immunofluorescence staining of Par3-GFP (anti-GFP) and dynein (biotinylated anti–dynein-IC74) in B-cells previously incubated with anti-IgG–coated (+) or anti-IgM–coated (–, negative control) beads for 1 h. Scale bars, 3 μm. (B) The automated method used to quantify the degree of polarization of a cell: briefly, 1) the cell is imaged in three dimensions on different signals; 2) its center of mass and the center of mass of the signal of interest are obtained by suitable threshold methods; 3) the positions of the different centers of mass are computed relative to the center of the cell; and 4) the polarity index (PI) is obtained as described by the appropriate formula (see *Materials and Methods*). (C) Double polarity indexes were obtained for each condition (each black circle corresponds to a cell). Colored plot were obtained (using the dscatter.m Matlab routine; Eilers *et al.* 2004) from single-cell results (color code uses the Jet LUT: low density, blue; high density, red). The polarity index is measured at $t = 15$min (without [–] BCR ligand, $n = 88$; with [+] BCR ligand, $n = 76$) and $t = 60$ min (without [–] BCR ligand, $n = 95$; with [+] BCR ligand, $n = 95$; three independent experiments) after incubation (however, because we do not control the precise time at which cells interact with beads, this contact time might be slightly overestimated). (D) Control (shControl) and Par3-silenced (shPar3-B) B-cells were treated as described in A and stained for α-tubulin (red) and dynein-IC74 (green). Scale bars, 3 μm. (E) Dynein polarity indexes were obtained as described in *Materials and Methods* using single-cell analysis (respectively, $n = 80$, 83, 67, and 123; three independent experiments). Control stimulated cells (shControl, +) present increased polarity indexes compared with Par3 silenced and nonstimulated cells (p(shControl-ligand) < 0.0001, p(shPar3+ligand) < 0.0001; Mann–Whitney test against shControl+ligand).

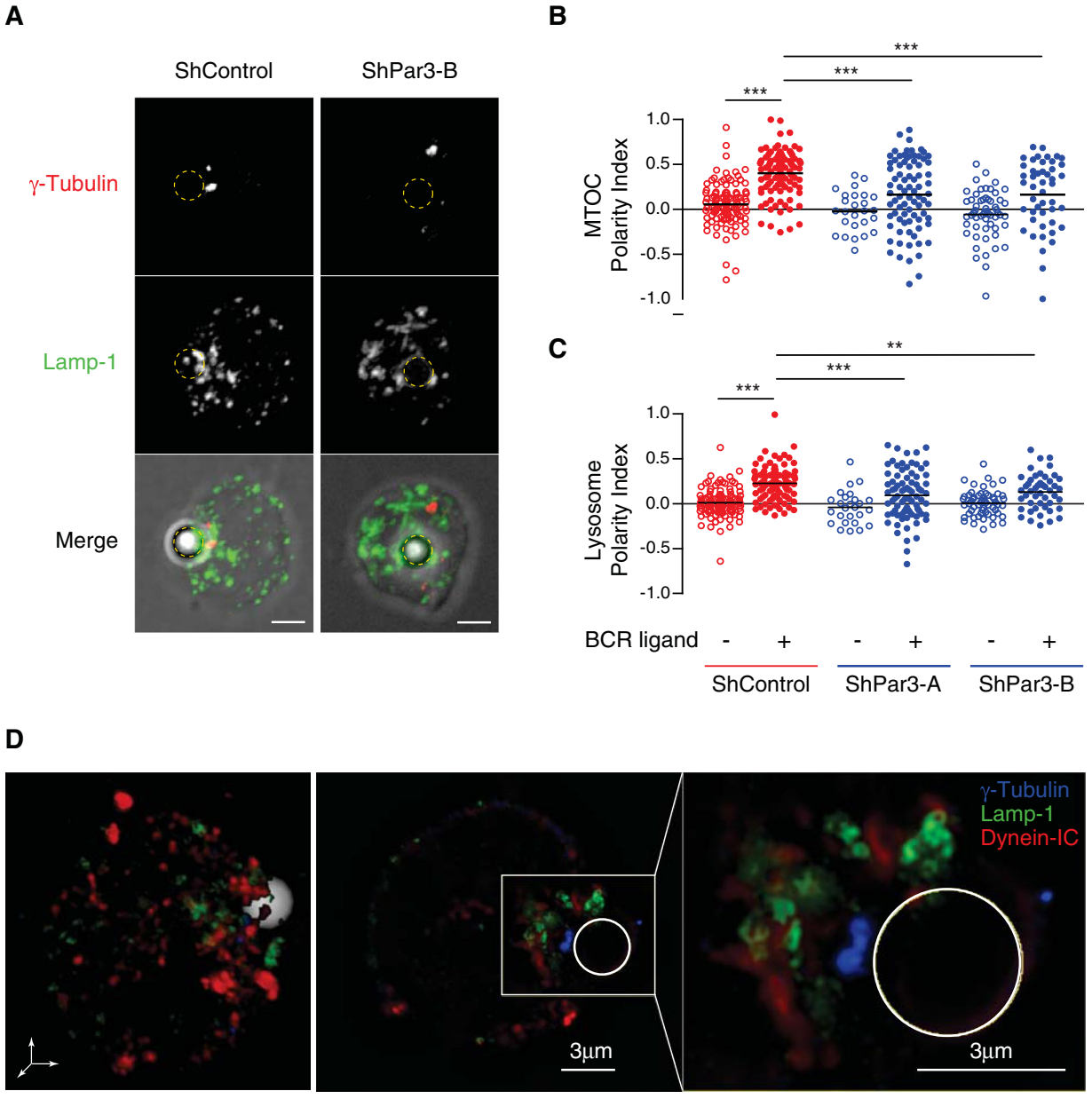

FIGURE 5: MTOC and lysosome polarization at the immune synapse relies on Par3. (A) Control (shControl) and Par3-silenced (shPar3-B) B-lymphoma cells were incubated with anti-IgG–coated beads (dotted circles) for 1 h and stained for γ-tubulin (red) and LAMP-1 (green) to label the MTOC and lysosomes, respectively. Scale bars, 3 µm. (B, C) Quantification of MTOC and lysosome polarization index, measured as described in Figure 4B in control (red circles) and Par3-silenced cells (blue circles, two different constructs) with and without specific antigen (empty and full dots, respectively). Quantification was performed using a single-cell analysis, according to *Materials and Methods* (n = 110, 103, 26, 81, 57, and 47, respectively; at least three independent experiments; for MTOC, p(shControl-BCR) < 0.0001, p(shPar3A+BCR) < 0.0001, and p(shPar3B+BCR) = 0.0005; for lysosomes, p(shControl-BCR) < 0.0001, p(shPar3A+BCR) = 0.0002, and p(shPar3B+BCR) = 0.0046; Mann–Whitney test against the control condition shControl+ligand). (D) SIM images showing a B-cell incubated with an anti-IgG–coated bead for 1 h and stained for γ-tubulin (blue), LAMP-1 (green), and dynein-IC74 (red); left, 3D view of the cell; middle, a planar section; right, zoom of the synapse, showing no colocalization between dynein-IC and LAMP-1 compartments.

were fixed and cultured in the presence of a T-cell hybridoma that recognizes the LACK peptide (amino acids 156–173) presented onto I-A^d MHC class II molecules, and their activation was measured by monitoring the secretion of interleukin-2 (IL-2). T-cell activation was observed only when using beads coated with BCR ligands, demonstrating that Ag must interact with the BCR to be efficiently presented to T-cells (Figure 6G). Ag presentation to T lymphocytes was compromised in Par3-silenced B-cells. Par3 silencing did not affect BCR cell surface levels at the steady state or the internalization of the BCR upon engagement (Supplemental Figure S7, A and B). These results indicate that impaired antigen processing did not result from altered BCR endocytic trafficking. Of importance, Par3 silencing had no effect on peptide presentation (Figure 6H), indicating that it does not affect surface expression levels of MHC class II or costimulatory molecules involved in B-cell–T-cell interactions. Equivalent results were obtained in purified mouse spleen B-cells

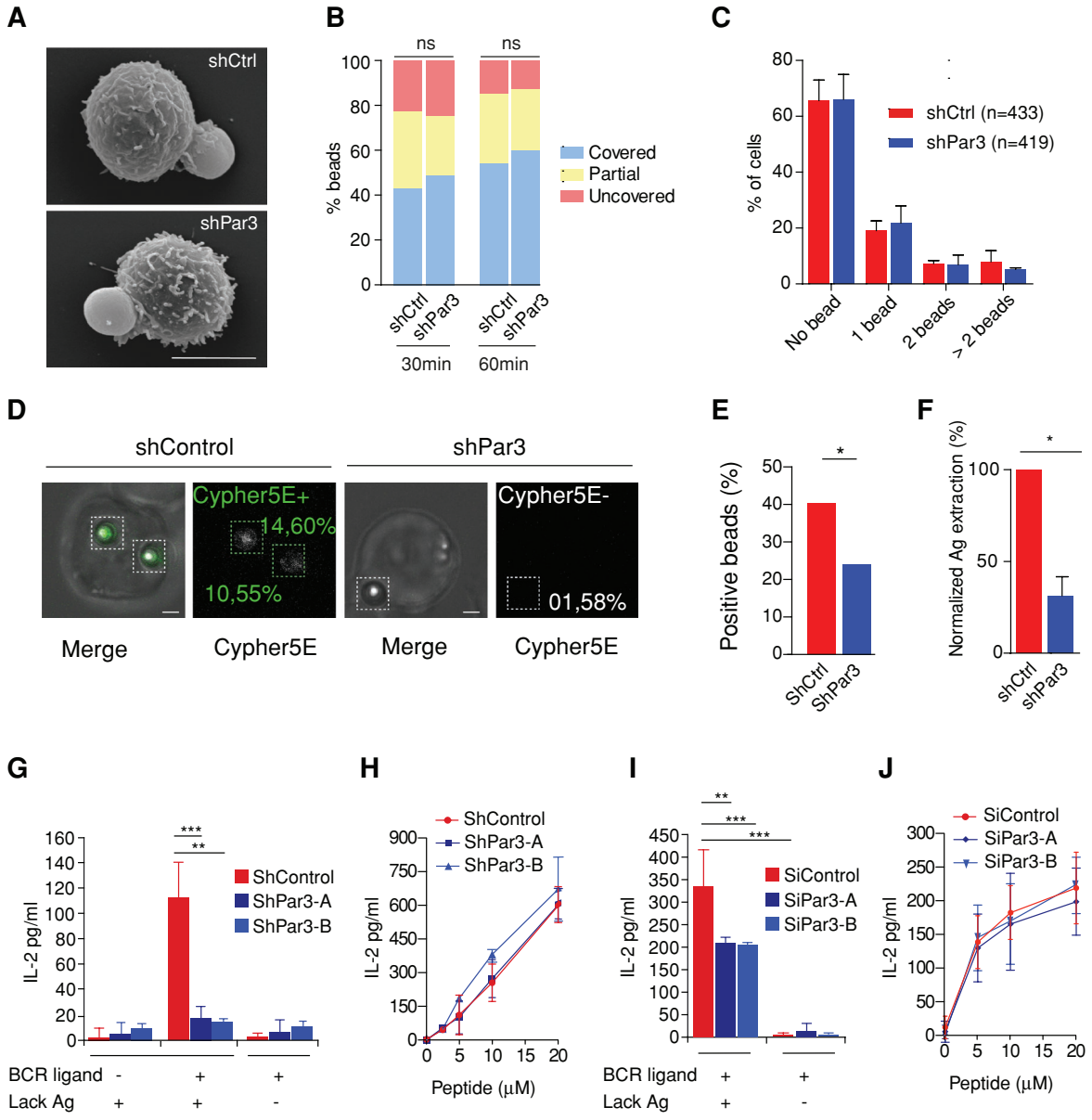

FIGURE 6: Par3-dependent lysosome recruitment and secretion at the immune synapse is required for antigen presentation to CD4+ T-cells. (A) Spreading of shCtrl and shPar3 cells on antigen-coated beads observed by scanning electron microscopy (scale bar, 5 µm). (B) Percentage of fully covered/partially covered/uncovered Ag-coated beads at 30 and 60 min (data pooled from three independent experiments; $n = 275$, 302, 426, and 420, respectively; chi-squared test, $p(30\text{min}) = 0.13$ and $p(60\text{min}) = 0.23$). (C) Percentage of cells in contact with no, one, two, or more Ag-coated beads showing no significant difference in shCtrl and shPar3 cells (data pooled from three independent experiments; two-way analysis of variance test, $p = 0.37$). (D) Representative images of an anti–IgG-Cypher5 bead associated to control (shCtrl) cell and Par3- silenced (shPar3-A) cells. The numbers indicate the increase in MFI of the bead above background. (E) Percentage of beads associated to anti–IgG-Cypher5 beads that showed a Cypher5 MFI of >10% above background ($p = 0.015$, Fisher's exact test) in control (shControl, $n = 130$) and silenced cells (shPar3, $n = 87$; pooled from more than three independent experiments). (F) Normalized antigen extraction measured by immunofluorescence (n(shCtrl) = 104, n(shPar3) = 95, pooled from three independent experiments). Antigen extraction in shPar3 cell is 70% weaker than in control cells (paired t test, $p = 0.022$). (G) Ag presentation assay with control and shPar3-silenced B-cells. Mean amounts of IL-2 ± SD were obtained by pooling triplicates from at least two independent experiments (p(shPar3A+Lack+ligand) < 0.0001, p(shPar3B+Lack+ligand) < 0.0001; one way analysis of variance [ANOVA] followed by Dunnett's multiple comparison test against control condition shControl+Lack+ligand; obvious significances are not shown). (H) Peptide control for B-cells used in the antigen presentation experiment (average value and SD computed on at least two independent experiments). (I) Ag presentation assay with control and siRNA Par3-silenced, spleen-derived primary B-cells. Mean amounts of IL-2 ± SD were obtained as average of triplicates from at least two independent experiments (p(siPar3A+Lack+ligand) < 0.0001, p(siPar3B+Lack+ligand) < 0.0001; two-way ANOVA, followed by Bonferroni post test, against control condition siControl+Lack+ligand; obvious significances are not shown). (J) Peptide control for primary B-cells used in the antigen presentation experiment (average value and SD computed on three independent experiments).

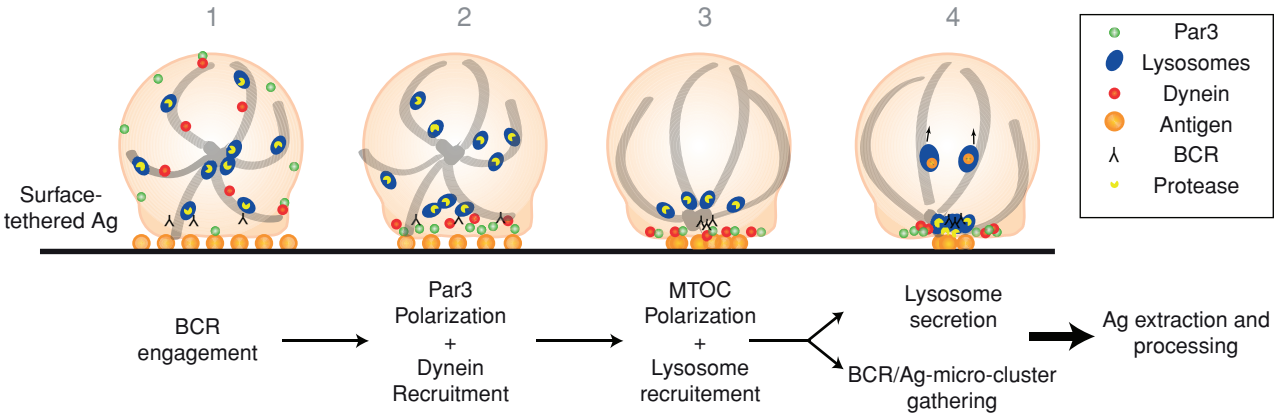

FIGURE 7: Model depicting the role of Par3 and dynein in extraction and processing of surface-tethered Ag by B-cells.

silenced for Par3 using two different siRNAs (Figure 6, I and J, and Supplemental Figure S7C). In addition, no difference was detected in the presentation of soluble Ag acquired by pinocytosis, even at higher concentrations (Supplemental Figure S7D). We conclude that the polarity protein Par3 is specifically required for the processing and presentation of surface-tethered antigens by promoting synapse formation and polarization of lysosomal trafficking.

DISCUSSION

B-cells rely on cell polarity to acquire their Ag-presentation function; however, the cellular mechanisms behind the establishment and maintenance of B-cell polarization during synapse formation remain incompletely resolved. In this study, we provided the first evidence for the implication of the ancestral polarity protein Par3 in the polarization of B-cells during synapse formation. Our results suggest that the localization of Par3 to the site of BCR-antigen interaction acts as a landmark of polarity that guides the further recruitment of molecules required for B-cell synapse organization and function. Indeed, we show that Par3 facilitates the recruitment of dynein to the B-cell synapse, which 1) allows the transport of BCR-Ag microclusters to the synapse center, where endocytosis takes place, and 2) drives MTOC polarization and local lysosome secretion. Although we do not formally demonstrate, as shown in fibroblasts, that the interaction between dynein and Par3 is direct in B-lymphocytes, impaired dynein recruitment at the synapse of Par3-silenced B-cells provides a simple explanation for defective BCR microcluster centripetal transport and MTOC/lysosome polarization in these cells. We propose that by coordinating these two events, Par3 and dynein couple the early and late events required for Ag processing and presentation to T-lymphocytes (see model in Figure 7).

We observed that Par3 controls the early onset of MAP kinase signaling, consistent with impaired microcluster gathering at the center of the synapse in Par3-silenced cells. These cells also show a slight increment in ERK phosphorylation at later time points. However, this was not sufficient to overcome their defective polarization phenotype, indicating that perturbations in early signaling events affect later cytoskeleton dynamics. We found that the gathering of Par3 occurs concomitantly to an actin flow directed toward the center of the B-cell synapse. These observations were obtained by transfecting Par3-GFP in B-lymphocytes. Indeed, we could not visualize endogenous Par3, most likely due to low expression levels of the protein in B-cells, as well as to the poor quality of the antibodies for immunofluorescence staining. However, we verified that Ag presentation is not impaired upon Par3-GFP expression in B-cells, indicating that the fusion protein does not alter B-cell function (Supplemental Figure S7D). Of interest, it has been found that segregation of polarity proteins is promoted by an actomyosin flow during the establishment of the anteroposterior axis in *Caenorhabditis elegans* embryos (Goehring *et al.*, 2011). It is tempting to speculate that the actomyosin contractions induced upon BCR engagement (Vascotto *et al.*, 2007) generate a positive feedback loop that reinforces Par3 recruitment and downstream events of B-cell polarization. Accordingly, myosin II has recently been shown to be involved in MTOC reorientation to the T-cell synapse (Liu *et al.*, 2013). In this model, MTOC polarization results from the concerted forces of myosin II, which localizes at the rear of activated T-cells and exerts pushing forces on the microtubule network, and dynein, which is recruited at the T-cell front and pulls on microtubules. In addition, in these cells, MTOC polarization was shown to require the local production of diacylglycerol (DAG), which recruits and activates PKCs (Quann *et al.*, 2009). Of interest, DAG is converted by DAG kinase to phosphatidic acid, which interacts with the PDZ domain of Par3 (Yu et Harris, 2012). Whether DAG plays a role in Par3-dependent MTOC polarization in B-cells or whether Par3 is involved in DAG-induced MTOC polarization in T-cells needs to be investigated. Indeed, although several polarity proteins, including Par3, were shown to be enriched at the T-cell synapse (Ludford-Menting *et al.*, 2005), their role in local dynein recruitment and MTOC polarization was not addressed.

We showed that aPKCζ is associated with the lysosomes that polarize to the B-cell synapse (Yuseff *et al.*, 2011). We observed that aPKCζ was not required for MTOC per se but instead stabilized its polarization, as well as the local secretion of lysosomes. It can be envisioned that BCR engagement induces 1) polarization of Par3, which allows dynein recruitment at the B-cell synapse and provides the driving force to gather microclusters at the cSMAC, and 2) phosphorylation of aPKCζ (Yuseff *et al.*, 2011), which stabilizes polarity by facilitating the docking of the MTOC and the secretion of lysosomes, possibly through its ability to interact with Par3. In this context, the concerted action of aPKCζ and Par3 would create a stable platform for efficient extraction and processing of surface-tethered Ag through coordinated events of exocytosis and endocytosis. Indeed, the lysosomes that are recruited in an MTOC-dependent manner at the B-cell synapse not only provide the extracellular proteases to facilitate Ag extraction, but also further help to recruit the MHC class II molecules to be loaded with antigenic peptides (Yuseff *et al.*, 2011). Formation of MHC class II–peptide complexes might occur at the cell surface (Moss *et al.*, 2007), as well as in endocytic vesicles that would form upon lysosome secretion, as described at the T-cell synapse (Angus *et al.*, 2013) and during compensatory endocytosis in secretory neurons (Gundelfinger *et al.*, 2003). In agreement with

impaired lysosome secretion (as measured by synapse acidification), we found that antigen extraction is reduced in Par3-silenced B-cells but not completely abrogated, suggesting that the mechanical component of antigen extraction (Natkanski *et al.*, 2013) persists.

The sustained polarized phenotype induced during synapse formation could also control later stages of B-cell activation. Indeed, prolonged synaptic interactions between T-cells and Ag-presenting cells were shown to coordinate asymmetric T-cell division by guiding the segregation of ancestral polarity proteins, aPKCζ and Scribble, thereby giving rise to different T-cell progeny with effector or memory fates (Chang *et al.*, 2007). Asymmetric cell divisions were further described in B-cells within germinal centers, where unequal inheritance of fate-associated molecules such as Bcl-6 and aPKC by daughter cells was observed (Barnett *et al.*, 2012). Another recent study showed that the asymmetric distribution of antigen within B-cells is conserved throughout cell division, giving rise to daughter cells with unequal Ag loads and consequently providing them with differential capacities for antigen presentation (Thaunat *et al.*, 2012). Whether the generation of these asymmetric populations is influenced by initial polarity cues established during synapse formation upon Ag encounter remains to be elucidated. Future experiments aimed at analyzing the effect of polarity proteins at different stages of B-cell activation, such as Ag encounter, migration, or asymmetric cell division, should help to shed light on these important questions.

MATERIALS AND METHODS

Cells

The mouse lymphoma cell line IIA1.6 (Lankar *et al.*, 2002) and the LMR7.5 Lack T-cell hybridoma, which recognizes I-A^d-$LACK_{156–173}$ complexes, were cultured as reported previously (Vascotto *et al.*, 2007) in CLICK medium (RPMI 1640, 10% fetal calf serum, 1% penicillin–streptomycin, 0.1% β-mercaptoethanol, and 2% sodium pyruvate). HEK 293T cells were cultured for lentiviral production in DMEM/Glutamax-5% fetal bovine serum, 1 mM sodium pyruvate, MEM nonessential amino acids, and penicillin–streptomycin. All cell culture products were purchased from GIBCO/Life Technologies, Paisley, UK. Primary B-cells were extracted from the spleen of BALB/c mice by negative selection as previously described (Vascotto *et al.*, 2007) and activated for 24 h with 1 μM CpG (ODN 1826; Invivogen, Shatin, Hong Kong) in B-cell culture medium supplemented with nonessential amino acids.

Antibodies and reagents

We used rat anti-mouse LAMP-1 (BD Bioscience, San Jose, CA), anti–α-tubulin (clone YL1/2; Serotec, Oxford, UK), mouse anti–α-actin (clone C4; Merck Millipore, Darmstadt, Germany), biotinylated mouse anti–dynein-IC74 (clone 74.1; Santa Cruz Biotechnology, Dallas, TX), rabbit anti–γ-tubulin (kindly provided by Michel Bornens, Institut Curie, Paris, France), rabbit anti-GFP (Ozyme, Montigny le Bretonneux, France); rabbit anti-Par3 (Merck Millipore), and rabbit anti-dynein (Santa Cruz Biotechnology). We used the following secondary antibodies (Jackson ImmunoResearch, West Grove, PA): $F(ab')_2$ goat anti-mouse, $F(ab')_2$ donkey anti–rabbit-Cy3, $F(ab')_2$ goat anti–rabbit-Alexa Fluor 488, $F(ab')_2$ donkey anti–rat-Cy5, streptavidin–Alexa Fluor 488, streptavidin-Cy3, and streptavidin–Alexa Fluor 647. Ciliobrevin A (HPI-4; Sigma-Aldrich, St. Louis, MO) and CypHer5E (Amersham Bioscience, Little Chalfont, UK) were used according to manufacturers' instructions. Ovalbumin was purchased from Sigma-Aldrich.

Preparation of Ag-coated beads

We activated 4×10^7 3-μm latex NH2-beads (Polyscience, Eppelheim, Germany) with 8% glutaraldehyde for 2 h at room temperature. Beads were washed with phosphate-buffered saline (PBS) and incubated overnight at 4°C with different ligands: 100 μg/ml of either $F(ab')_2$ goat anti-mouse immunoglobulin G (IgG) or $F(ab')_2$ goat anti-mouse IgM (MP Biomedical, Santa Ana, CA).

Preparation of Ag-coated surfaces

Fluorodishes (MatTek, Ashland, MA) were coated overnight with 10 μg/ml of either $F(ab')_2$ goat anti-mouse IgG or $F(ab')_2$ goat anti-mouse-IgM (MP Biomedicals) and 0.5 μg/ml rat anti-mouse CD45R/B220 (eBioscience, San Diego, CA) diluted in cold PBS.

Preparation of planar lipid bilayers

Planar lipid bilayers were prepared following Carrasco *et al.* (2004), with minor modifications. Biotinylated $(Fab')_2$ anti-IgG or IgM was added to the lipid bilayer (20 μg/ml), and cells were monitored upon contact with bilayers. The fluidity of the lipid bilayers was tested by fluorescence recovery after photo bleaching close to each cell of interest. For single-molecule experiments in steady state, bilayers contained biotinylated anti-B220 (40 ng/ml) to favor cell adhesion. Cells were previously incubated with monovalent Fab anti-IgG Alexa Fluor 555 at 1 nM and deposited in the lipid chamber.

DNA constructs

LifeAct-CherryFP was a kind gift from P. Chavrier (Institut Curie, Paris, France). The Par3-GFP construct and shRNA-Par3 were kindly provided by Ira Mellman (Genentech, South San Francisco, CA) and Ian Macara (University of Virginia, Charlottesville, VA), respectively. Mouse Par3-YFP and Par3-Cter-YFP were previously characterized (Schmoranzer *et al.*, 2009). The dynein-IC74-2C-RFP construct was a kind gift from F. Saudou (Institut Curie, Orsay, France) and previously characterized (Ha *et al.*, 2008).

Cell transfection

We electroporated 2.5×10^6 IIA1.6 B-lymphoma cells using Nucleofector R T16 (Lonza, Gaithersburg, MD) in the presence of 4 μg of plasmid DNA. Par3-GFP–transfected cells were cultured for 12–24 h before functional analysis. Transfection with shPar3 or shControl plasmids was done as previously described (Yuseff *et al.*, 2011). B-cells infected with shPar3 or shControl lentiviruses were selected in puromycin and transfected after 96 h with cathepsin D–monomeric RFP (mRFP), centrin-GFP, LifeAct-CherryFP, or dynein-IC-RFP and analyzed within 24 h.

We electroporated 4×10^6 CpG-treated primary B-cells using Mouse B Cell Nucleofector Kit (Lonza) in the presence of 100 nM of AllStars Negative Control siRNA (1027280; Quiagen, Hilden, Germany) for siControl or FlexiTube siRNA Mm_Pard3_4 and Mm_Pard3_2 (SI01369508 and SI01369494; Qiagen) for siPar3-A and siPar3-B, respectively. B-cells were resuspended in CpG-free prewarmed medium, and presentation experiments were performed 48 to 72 h after RNA interference transfection. Par3 levels were analyzed by Western blot as described later.

Lentiviral production and cell infection

The shRNAs used to silence Par3 in the IIA1.6 B-lymphoma cells were purified from MISSION shRNA Bacterial Glycerol Stocks (Sigma-Aldrich): shPar3-A TRCN0000094400, shPar3-B TRCN0000094401, and SHC002 as control (where not indicated in the figure legends, the data from shPar3-A and shPar3-B were pooled). Lentiviruses were produced by transfection in a 1:2.5:3 ratio of the envelope (pMD2G), the packaging (pPAX-2), and shRNA-encoding plasmids in 293T cells with Gene juice (Merck Millipore). Supernatants were harvested 72 h after transfection and

ultracentrifuged at 100,000 × *g* for 90 min at 4°C. Pellets were resuspended in 2% bovine serum albumin (BSA)/PBS and frozen at –80°C for later use. IIA1.6 B-cells were infected (multiplicity of infection 20) with spin centrifugation with Polybrene (5 µg/ml). After 24 h, puromycin selection (5 µg/ml) was performed, and cells were assayed after 72–120 h. Par3 levels were analyzed by Western blot as described.

Western blotting

B-cells were lysed at 4°C in buffer containing 0.5% NP-40, 50 mM Tris-HCl, pH 7.4, 150 mM NaCl, 1 mM dithiothreitol, Protease Inhibitor Cocktail (Roche, Basel, Switzerland), and Phosphatase Inhibitor Cocktail 2 (Sigma-Aldrich). Supernatants were collected and loaded onto NuPAGE SDS–PAGE gels (Invitrogen, Life Technologies) and transferred onto polyvinylidene fluoride membrane. Membranes were blocked in 5% nonfat dry milk and PBS–0.05% Tween-20 and incubated with antibodies against Par3 (1:1000; Millipore), pERK (1:1000; Cell Signaling, Danvers, MA), actin (1:5000; Millipore), or α-tubulin (1:5000; Serotec) as protein loading control, followed, respectively, by anti-rabbit (2X), -mouse, or -rat horseradish peroxidase–conjugated antibodies (Jackson ImmunoResearch). Western blots were developed with ECL reagents (Amersham), and chemiluminescence was detected with the LAS-3000 image analysis system (FujiFilm).

Rescue of Par3-silenced cells

Rescue of polarity in Par3-silenced cells was shown by measuring the polarity index of the MTOC in control (shCtrl) and silenced cells (shPar3) transfected 24 h after infection with either GFP- or Par3GFP-expressing plasmid. The images were taken with a spinning-disk microscope. To properly compare differently transfected cells, the analysis was restricted to cells presenting a GFP signal between 20 and 100% above the background.

Ag presentation assay

This was done as previously described (Yuseff *et al.*, 2011). Briefly, after incubation of B-cells with Lack-coated beads containing or not BCR ligands for 4 h, cells were washed, and the B-cell line was fixed in ice-cold PBS/0.01% glutaraldehyde for 1 min and quenched with PBS/100 µM glycine. B-cells were incubated with Lack T-cell hybridoma overnight (ratio B-cell:T-cell, 2:1). Supernatants from each condition were collected, and IL-2 cytokine production assays were performed (BD Bioscience).

Activation of B-cells and immunofluorescence analysis

Cells were plated on poly-L-lysine–coated glass coverslips and activated with Ag-coated beads at a 1:1 ratio for different time points at 37°C and then fixed in 4% paraformaldehyde for 10 min at room temperature. Fixed cells were incubated with antibodies in PBS/0.2% BSA/0.05% saponin. Immunofluorescence images were acquired on a confocal microscope (LSM510 inverted laser scanning confocal [Carl Zeiss Micro-Imaging] and inverted spinning disk confocal [Roper/Nikon]) with a 60×/1.4 numerical aperture (NA) oil immersion objective.

BCR internalization assay

Control and Par3-silenced cells were washed with PBS and resuspended in 50% CLICK/50% RPMI-1640 at a density of 10^6 cells/ml. Cells were incubated with 10 µg/ml $F(ab')_2$ goat anti-mouse IgG premixed to 20 µg/ml $F(ab')_2$ donkey anti-goat IgG for 30 min at 4°C. Cells were washed twice with cold CLICK/RPMI to remove the excess ligand and incubated or not (negative control) at 37°C for the indicated time. Internalization was stopped by incubating the cells on ice and adding cold PBS plus 5% BSA. To detect receptors remaining on the cell surface, cells were stained for 30 min on ice with donkey–anti-goat IgG Alexa Fluor 488 and washed with PBS plus 5% BSA. Flow cytometry was performed on an AccuriC6 flow cytometer (BD Biosciences), and data were analyzed with Flowjo software. The percentage of BCR on the cell surface was calculated as (MFI at 37°C)/(MFI at 4°C) × 100, where MFI is mean fluorescence intensity.

Antigen extraction assay

Ovalbumin (OVA) and $F(ab')_2$ anti-mouse IgM or anti-mouse IgG fragments were coupled to NH2 beads in equal concentrations. Cells incubated in a 1:1 ratio with Ag-coated beads were plated on poly-L-lysine slides at 37°C, fixed, and stained for OVA with a polyclonal antibody. The amount of OVA present on the beads was calculated by establishing a fixed area around beads in contact with cells and measuring fluorescence on three-dimensional (3D) projections obtained from the sum of each plane (ImageJ). The percentage of antigen extracted was estimated by the percentage of fluorescence intensity lost by the beads after 1 h.

Membrane-spreading assay

The IgG+ B-lymphoma cells were incubated with Ag-coated beads for different time points at 37°C on poly-L slides. At the end of each time point, warm medium was quickly replaced by ice-cold PBS/0.2% BSA, and cells were left on ice, where the staining with the first antibody (anti-goat IgG coupled to Cy5) and membrane staining with WGA-Alexa Fluor 488 (Invitrogen) were performed. After 1 h, cells were washed on ice with cold PBS/0.2% BSA and fixed with 4% paraformaldehyde for 10 min on ice. Cells were permeabilized with PBS/0.2% BSA/0.05% saponin for 20 min at room temperature before staining with the second antibody (anti-goat IgG coupled to Cy3). Membrane spreading around the Ag-coated bead was determined qualitatively by estimating the number of beads nonprotected, partially protected, or completely protected from the first antibody staining under nonpermeabilized conditions.

Time-lapse imaging

Time-lapse confocal microscopy and live-imaging images were done of B-cells plated on poly-L-lysine–coated glass dishes (Fluorodish) for CypHer5E and Par3-GFP experiments. Images were acquired at 37°C/4.5% CO_2 on an inverted spinning disk confocal microscope (Eclipse Ti; Roper/Nikon) with a 60×/1.4 NA oil immersion objective with MetaMorph software.

TIRFM

TIRFM was performed on a Nikon Eclipse Ti inverted microscope equipped with a 100×/1.49 NA oil immersion objective and a Quantem512SC Roper electron-multiplying charge-coupled device (EMCCD) camera mounted on Dual-View system at 37°C/4.5% CO_2. Acquisition was made using MetaMorph. For analysis of Par3-GFP, LifeAct-CherryFP, and cathepsin D–mRFP polarization at the synapse, B-cells were plated onto Ag-coated glass-bottom dishes (Fluorodish), and images were acquired every 5 or 10 s for 30 min with an exposure time of 100 ms.

For dynein-IC74-RFP analysis, B-cells were plated with the same technique for 15 min before imaging, and frames were acquired by streaming at 10 Hz for 1 min.

SIM imaging

Acquisitions were performed in 3D SIM mode with an n-SIM Nikon microscope before image reconstruction using NIS-Elements software based on Gustafsson *et al.* (2008). The system was equipped

with an APO TIRF 100×/1.49 NA oil immersion objective and an EMCCD DU-897 Andor camera.

Scanning electron microscopy

For scanning electron microscopy, cells preincubated with Ag-coated beads were loaded on a polylysine-coated coverslip and fixed with 2% glutaraldehyde in phosphate buffer at room temperature for 1 h. Samples were vacuum dried and dehydrated by critical-point drying with CO_2. The specimens were mounted on metallic supports with carbon tape and ion sputtered with cathodic gold. Analysis of samples was performed on a Cambridge S 260 microscope at pressure of 10^{-7} torr.

Image deconvolution

Images were acquired with a wide-field Eclipse NiU Upright Microscope (Nikon) equipped for image deconvolution. Acquisition was performed using a 100× Plan Apo VC 1.4 oil objective and a highly sensitive cooled interlined CCD camera (CoolSnap HQ2; Roper). The deconvolution code we used is described in Sibarita (2005).

Image analysis

Analysis of Par3-GFP/Lifeact-mCherry TIRFM movies. TIRF images of Par3-GFP and LifeAct-CherryFP were quantified with a custom-made Matlab program applied to the dual-view TIRF images: at each time point, the cell was identified by Otsu threshold on the actin channel. A kymograph was built for each channel starting from this mask and computing the average fluorescence intensity in concentric rings of width 1 pixel obtained by eroding the mask progressively.

Radial line scan. The density of the BCR clusters and Par3 (Figure 7A) was quantified on TIRF images convolved with a Gaussian filter to reduce background salt-pepper noise; the average intensity over the radius was computed using the radial line scan plug-in of Fiji over the radius of the cell and averaging over 10 frames the three different time points ($t = 0$, 15, 30 min). The plotted lines were normalized over the total intensity on each channel.

Cluster dynamics. TIRF multipositioning time-lapse movies of anti-BCR–labeled supported lipid bilayers were quantified as follows: for each movie, an automatic threshold (triangle method) was applied and the particles statistics extracted using Fiji-based macro (particles <3 square pixels were discarded). For each cell at each time point, the average area of top 10% brightest clusters was computed. The fold increase was computed with respect to the first time point.

Dynein recruitment analysis in three dimensions. Dynein recruitment was estimated using a custom-made ImageJ routine. In both control and shPar3 cells, first the fluorescence signal density (obtained as the integrated signal divided by the volume in voxels of the region of interest) was computed for the cytoplasm and the synapse ($\rho_{cytoplasm}$ and $\rho_{synapse}$, respectively). The synapse was considered as three planes starting from the bottom plane. Dynein enrichment was defined as the ratio between fluorescence signal densities, $\rho_{synapse}/\rho_{cytoplasm}$ (1 = no enrichment).

Single-particle tracking. For the dynein tracking, cells transfected with dynein IC74-RFP plasmid were plated on IgG-coated coverslips and observed on a TIRF setup. Movies of 3 min were taken at 10 Hz. After a global background subtraction, dynein spots were tracked using Trackmate plug-in on Fiji (Schindelin *et al.*, 2012), and trajectories were further elaborated with custom-made Matlab software to get the average residence time distribution along the radius of the cells.

Single-molecule tracking. Cells were plated on planar lipid bilayers and filmed on the TIRF setup. Movies of 30 s at 20 Hz were taken, and single-particle tracking was performed with an adapted version of the multiple target tracking program MTT (Serge *et al.*, 2008). The pointing accuracy was measured on fluorophore attached to the coverslip as 40 nm. Trajectories <5 frames were discarded from statistics. Diffusion coefficients (D) were measured from a linear fit of the mean square displacement $MSD(t) = 4Dt$ on the number of points that minimizes the error in the coefficient, taking into account the pointing accuracy, according to Michalet (2010). Only diffusion coefficients with a relative SE of 33% were considered in the analysis. Particles were considered immobile when $D < 0.01\ \mu m^2/s$.

Polarity analysis. Three-dimensional stacks acquired with a spinning-disk microscope were quantified with a custom-made Matlab program. Briefly, the images were binarized in the GFP channel using the maximal entropy method on the whole 3D stack to obtain the geometrical center of mass of the cell. The maximal fluorescence was used to position the MTOC. The weighted center of mass of different channels was used to define the average position (x, y, z) of the cellular components (dynein, lysosomes). Cross-correlation with a previously acquired image of the bead was used to position the bead in three dimensions. After we extracted the positions of the bead (B), the cell center of mass (C), and the MTOC (M) or another fluorescent marker (F), we computed the polarity index as projection of the vector $\overrightarrow{CM}$ along the vector $\overrightarrow{CB}$ normalized by the distance of bead to center of mass:. The index ranges between –1 (antipolarized) and 1 (fully polarized, object on the bead). Analogously the index for another fluorescence channel (such as dynein or lysosomes) was computed as above, replacing the position (M) of the MTOC with the one (F) of the center of mass of the signal in the specific channel.

Cathepsin D–mRFP recruitment analysis. B-cells were plated onto Ag-coated cover slides 15 min before TIRFM imaging, and frames were acquired by streaming at 20 Hz in stacks of 600 images. Image segmentation and single-particle tracking were done with Multidimensional Image Analysis software (Racine *et al.*, 2007) as previously described (Desnos *et al.*, 2007). The diffusion coefficient D_{xy} was calculated by fitting the mean square displacement $MSD(t) = 4D_{xy}t$ extracted from each trajectory on the first 10 time points.

Statistical tests

Statistical analysis was performed with Prism (GraphPad Software) or Matlab (MathWorks). The p values were computed using different tests as indicated in the figure legends; $*0.01 < p < 0.05$, $**0.001 < p < 0.01$, $***p < 0.001$; ns, nonsignificant.

ACKNOWLEDGMENTS

We thank Yolanda Carrasco, Yohanns Bellaiche, and Matthieu Piel for critical reading of the manuscript. We gratefully acknowledge the Nikon Imaging Center, CNRS-Institut Curie, and PICT-IbiSA, Institut Curie, Paris, and members of the France-BioImaging national research infrastructure, especially P. Paul-Gilloteaux and V. Fraisier. We thank François-Xavier Gobert for help with lentiviral production. Scanning electronic microscopy was performed at the Service de Microscopie Électronique of Paris 6 University (Paris, France). A.R. and M.-I.Y. were supported by fellowships from the Ministère de l'Éducation Nationale, the Association pour la Recherche contre le

Cancer, and the Fondation pour la Recherche Médicale. This work was funded by grants from the Young Investigator Program from the City of Paris and the European Research Council (Strapacemi 243103) to A-M.L.-D. and the Association Nationale pour la Recherche (ANR-12-Polybex to A-M.L.-D. and F.D. and ANR-2010-JCJC-Immuphy to P.P.).

REFERENCES

Angus KL, Griffiths GM (2013). Cell polarisation and the immunological synapse. Curr Opin Cell Biol 25, 85–91.

Arana E, Vehlow A, Harwood NE, Vigorito E, Henderson R, Turner M, Tybulewicz VL, Batista FD (2008). Activation of the small GTPase Rac2 via the B cell receptor regulates B cell adhesion and immunological-synapse formation. Immunity 28, 88–99.

Barnett BE, Ciocca ML, Goenka R, Barnett LG, Wu J, Laufer TM, Burkhardt JK, Cancro MP, Reiner SL (2012). Asymmetric B cell division in the germinal center reaction. Science 335, 342–344.

Batista FD, Harwood NE (2009). The who, how and where of antigen presentation to B cells. Nat Rev Immunol 9, 15–27.

Brezski RJ, Monroe JG (2007). B cell antigen receptor-induced Rac1 activation and Rac1-dependent spreading are impaired in transitional immature B cells due to levels of membrane cholesterol. J Immunol 179, 4464–4472.

Carrasco YR, Fleire SJ, Cameron T, Dustin ML, Batista FD (2004). LFA-1/ICAM-1 interaction lowers the threshold of B cell activation by facilitating B cell adhesion and synapse formation. Immunity 20, 589–599.

Chang JT, Palanivel VR, Kinjyo I, Schambach F, Intlekofer AM, Banerjee A, Longworth SA, Vinup KE, Mrass P, Oliaro J, *et al.* (2007). Asymmetric T lymphocyte division in the initiation of adaptive immune responses. Science 315, 1687–1691.

Desnos C, Huet S, Fanget I, Chapuis C, Bottiger C, Racine V, Sibarita JB, Henry JP, Darchen F (2007). Myosin va mediates docking of secretory granules at the plasma membrane. J Neurosci 27, 10636–10645.

Eilers PHC, Goeman JJ (2004). Enhancing scatterplots with smoothed densities. Bioinformatics 20, 623–628.

Fleire SJ, Goldman JP, Carrasco YR, Weber M, Bray D, Batista FD (2006). B cell ligand discrimination through a spreading and contraction response. Science 312, 738–741.

Gérard A, Mertens AE, van der Kammen RA, Collard JG (2007). The Par polarity complex regulates Rap1- and chemokine-induced T cell polarization. J Cell Biol 176, 863–875.

Goehring NW, Trong PK, Bois JS, Chowdhury D, Nicola EM, Hyman AA, Grill SW (2011). Polarization of PAR proteins by advective triggering of a pattern-forming system. Science 334, 1137–1141.

Grakoui A, Bromley SK, Sumen C, Davis MM, Shaw AS, Allen PM, Dustin ML (1999). The immunological synapse: a molecular machine controlling T cell activation. Science 285, 221–227.

Gundelfinger ED, Kessels MM, Qualmann B (2003). Temporal and spatial coordination of exocytosis and endocytosis. Nat Rev Mol Cell Biol 4, 127–139.

Gustafsson MGL, Shao L, Carlton PM, Wang CJR, Golubovskaya IN, Cande WZ, Agard DA, Sedat JW (2008). Three-dimensional resolution doubling in wide-field fluorescence microscopy by structured illumination. Biophys J 94, 4957–4970.

Ha J, Lo KWH, Myers KR, Carr TM, Humsi MK, Rasoul BA, Segal RA, Pfister KK (2008). A neuron-specific cytoplasmic dynein isoform preferentially transports TrkB signaling endosomes. J Cell Biol 181, 1027–1039.

Harwood NE, Batista FD (2008). New insights into the early molecular events underlying B cell activation. Immunity 28, 609–619.

Iden S, Collard JG (2008). Crosstalk between small GTPases and polarity proteins in cell polarization. Nat Rev Mol Cell Biol 9, 846–859.

Kupfer A, Swain SL, Singer SJ (1987). The specific direct interaction of helper T cells and antigen-presenting B cells. II. Reorientation of the microtubule organizing center and reorganization of the membrane-associated cytoskeleton inside the bound helper T cells. J Exp Med 165, 1565–1580.

Lankar D, Vincent-Schneider H, Briken V, Yokozeki T, Raposo G, Bonnerot C (2002). Dynamics of major histocompatibility complex class II compartments during B cell receptor-mediated cell activation. J Exp Med 195, 461–472.

Liu X, Kapoor TM, Chen JK, Huse M (2013). Diacylglycerol promotes centrosome polarization in T cells via reciprocal localization of dynein and myosin II. Proc Natl Acad Sci USA 16 110, 11976–11981.

Ludford-Menting MJ, Oliaro J, Sacirbegovic F, Cheah ET, Pedersen N, Thomas SJ, Pasam A, Iazzolino R, Dow LE, Waterhouse NJ, *et al.* (2005). A network of PDZ-containing proteins regulates T cell polarity and morphology during migration and immunological synapse formation. Immunity 22, 737–748.

McCaffrey LM, Macara IG (2009). The Par3/aPKC interaction is essential for end bud remodeling and progenitor differentiation during mammary gland morphogenesis. Genes Dev 23, 1450–1460.

Mellman I, Nelson WJ (2008). Coordinated protein sorting, targeting and distribution in polarized cells. Nat Rev Mol Cell Biol 9, 833–845.

Michalet X (2010). Mean square displacement analysis of single-particle trajectories with localization error: Brownian motion in an isotropic medium. Phys Rev E Stat Nonlin Soft Matter Phys 82, 041914.

Milasta S, Evans NA, Ormiston L, Wilson S, Lefkowitz RJ, Milligan G (2005). The sustainability of interactions between the orexin-1 receptor and beta-arrestin-2 is defined by a single C-terminal cluster of hydroxy amino acids and modulates the kinetics of ERK MAPK regulation. Biochem J 387, 573–584.

Mitchison NA (2004). T-cell-B-cell cooperation. Nat Rev Immunol 4, 308–312.

Moss CX, Tree TI, Watts C (2007). Reconstruction of a pathway of antigen processing and class II MHC peptide capture. EMBO J 26, 2137–2147.

Natkanski E, Lee WY, Mistry B, Casal A, Molloy JE, Tolar P (2013). B cells use mechanical energy to discriminate antigen affinities. Science 340, 1587–1590.

Quann EJ, Merino E, Furuta T, Huse M (2009). Localized diacylglycerol drives the polarization of the microtubule-organizing center in T cells. Nat Immunol 10, 627–635.

Racine V, Sachse M, Salamero J, Fraisier V, Trubuil A, Sibarita JB (2007). Visualization and quantification of vesicle trafficking on a three-dimensional cytoskeleton network in living cells. J Microsc 225, 214–228.

Schebesta A, McManus S, Salvagiotto G, Delogu A, Busslinger Ga, Busslinger M (2007). Transcription factor Pax5 activates the chromatin of key genes involved in B cell signaling, adhesion, migration, and immune function. Immunity 27, 49–63.

Schindelin J, Arganda-Carreras I, Frise E, Kaynig V, Longair M, Pietzsch T, Preibisch S, Rueden C, Saalfeld S, Schmid B, *et al.* (2012). Fiji: an open-source platform for biological-image analysis. Nat Methods 9, 676–682.

Schmoranzer J, Fawcett JP, Segura M, Tan S, Vallee RB, Pawson T, Gundersen GG (2009). Par3 and dynein associate to regulate local microtubule dynamics and centrosome orientation during migration. Curr Biol 19, 1065–1074.

Schnyder T, Castello A, Feest C, Harwood NE, Oellerich T, Urlaub H, Engelke M, Wienands J, Bruckbauer A, Batista FD (2011). B cell receptor-mediated antigen gathering requires ubiquitin ligase Cbl and adaptors Grb2 and Dok-3 to recruit dynein to the signaling microcluster. Immunity 34, 905–918.

Serge A, Bertaux N, Rigneault H, Marguet D (2008). Dynamic multiple-target tracing to probe spatiotemporal cartography of cell membranes. Nat Methods 5, 687–694.

Sibarita JD (2005). Deconvolution microscopy. Adv Biochem Eng Biotechnol 95, 201–243.

Thaunat O, Granja AG, Barral P, Filby A, Montaner B, Collinson L, Martinez-Martin N, Harwood NE, Bruckbauer A, Batista FD (2012). Asymmetric segregation of polarized antigen on B cell division shapes presentation capacity. Science 335, 475–479.

Tolar P, Sohn HW, Liu W, Pierce SK (2009). The molecular assembly and organization of signaling active B-cell receptor oligomers. Immunol Rev 232, 34–41.

Treanor B, Depoil D, Gonzalez-Granja A, Barral P, Weber M, Dushek O, Bruckbauer A, Batista FD (2010). The membrane skeleton controls diffusion dynamics and signaling through the B cell receptor. Immunity 32, 1–13.

Vascotto F, Lankar D, Faure-Andre G, Vargas P, Diaz J, Roux D Le, Yuseff MI, Sibarita JB, Boes M, Raposo G, *et al.* (2007). The actin-based motor protein myosin II regulates MHC class II trafficking and BCR-driven antigen presentation. J Cell Biol 176, 1007–1019.

Yi J, Wu X, Chung AH, Chen JK, Kapoor TM, Hammer JA (2013). Centrosome repositioning in T cells is biphasic and driven by microtubule end-on capture-shrinkage. J Cell Biol 202, 779–792.

Yu CG, Harris TJC (2012). Interactions between the PDZ domains of Bazooka (Par-3) and phosphatidic acid: in vitro characterization and role in epithelial development. Mol Biol Cell 23, 3743–3753.

Yuseff MI, Reversat A, Lankar D, Diaz J, Fanget I, Pierobon P, Randrian V, Larochette N, Vascotto F, Desdouets C, *et al.* (2011). Polarized secretion of lysosomes at the B cell synapse couples antigen extraction to processing and presentation. Immunity 35, 361–374.

"A critical role for cell polarity in antigen extraction, processing and presentation by B lymphocytes"

Dorian Obino[1] and Ana-Maria Lennon-Duménil[1]

Advances in Immunology, 2014, 123:51-67

[1]INSERM – U932, Institut Curie, Paris, France

CHAPTER TWO

A Critical Role for Cell Polarity in Antigen Extraction, Processing, and Presentation by B Lymphocytes

Dorian Obino, Ana-Maria Lennon-Duménil[1]
INSERM U932, Institut Curie, Paris, France
[1]Corresponding author: e-mail address: ana-maria.lennon@curie.fr

Contents

Abstract

The activation of B lymphocytes in response to external stimuli represents a key step in the adaptive immune response, which is required for the production of high-affinity antibodies and for the generation of long-term memory. Because the dysregulation of B lymphocyte responses can lead to diverse pathological situations, B cells are considered today as valuable therapeutic targets for immunomodulation, in particular in the context of autoimmune reactions. Here, we review the fundamental molecular and cell biological mechanisms that enable B cells to efficiently sense, acquire, and respond to extracellular antigens. A special emphasis is given to cell polarity, which was shown to be critical for the regulation of antigen acquisition, processing, and presentation by B lymphocytes. How cell polarity coordinates the various steps of B lymphocyte activation and might impact the humoral immune response is further discussed.

Advances in Immunology, Volume 123
ISSN 0065-2776
http://dx.doi.org/10.1016/B978-0-12-800266-7.00001-7

1. INTRODUCTION

In the lymph nodes, B cells acquire antigens that are tethered at the surface of neighboring cells such as migrating or follicular dendritic cells or subcapsular sinus (SCS) macrophages (Carrasco & Batista, 2007; Junt et al., 2007; Qi, Egen, Huang, & Germain, 2006; Suzuki, Grigorova, Phan, Kelly, & Cyster, 2009). The recognition by B cells of such immobilized antigens through the engagement of their B-cell antigen receptors (BCRs) results in the establishment of an immune synapse (Batista, Iber, & Neuberger, 2001), which is a key step in the process of B-cell activation (Carrasco, Fleire, Cameron, Dustin, & Batista, 2004; Fleire et al., 2006). Antigen recognition is then followed by a rapid polarization of B cells where both the microtubule-organizing center (MTOC) and lysosomes are repositioned at the immune synapse (Yuseff et al., 2011). Lysosome recruitment and secretion at the synaptic interface promote antigen extraction and processing for further presentation to primed $CD4^+$ T cells (Yuseff et al., 2011). Upon activation, while a pool of B cells differentiates into short-lived plasmablasts producing antibodies with relative low affinity (Cunningham et al., 2007), another pool receives signals from T follicular helper cells. This cell-cell contact — known as T-cell/B-cell cooperation — is required for B cells to be fully activated, proliferate, and form germinal centers (GCs) (Mitchison, 2004). Here, B cells undergo affinity maturation and class switch recombination leading to their differentiation into either plasma cells, which produce high-affinity antibodies, or memory B cells (Allen, Okada, & Cyster, 2007; MacLennan, 1994). Thus, the outcome of the adaptive immune response relies on the ability of B cells to polarize upon antigen stimulation. In this chapter, a special emphasis is given to the crucial role for the spatio-temporal coordination of the membrane-trafficking and polarization events that are required for B cells to efficiently extract, process, and present antigens (Yuseff, Pierobon, Reversat, & Lennon-Duménil, 2013; Yuseff et al., 2011).

2. B-CELL ACTIVATION IN SECONDARY LYMPHOID ORGANS

2.1. Antigen encounter by B cells

Due to the antigenic specificity of each BCR, the probability for a given B cell to encounter its cognate antigen by patrolling the body is very

low. In contrast, the follicles of secondary lymphoid organs where B cells reside provide the appropriate environment for them to encounter their specific antigens. Antigens that are present in the peripheral tissues are collected within lymph nodes, which form an "antigen reservoir" for cognate B cells. The fate of antigens in the lymph nodes is mainly dependent on their nature (Batista & Harwood, 2009). Small antigens from afferent lymph vessels diffuse into the lymph node follicle where B cells acquire them in a soluble form (Pape, Catron, Itano, & Jenkins, 2007). The mechanisms by which soluble antigens gain access to B-cell follicles are not totally understood, but it has been proposed that their ingress is promoted by tiny pores (Batista & Harwood, 2009) and/or a conduit network that directly connects the subcapsular sinus (SCS) with B-cell follicles (Roozendaal et al., 2009). In contrast, large antigens (greater than 70 kDa) remain trapped at the SCS floor site where $CD169^+$ macrophages have been shown to capture and transfer them (Carrasco & Batista, 2007; Junt et al., 2007) to follicular B cells. How antigens are transferred from the SCS to B-cell follicles is unclear. Two routes have been suggested: First, the subcapsular $CD169^+$ macrophages that display a poor phagocytic capacity could recycle antigens and expose them in their native form at the cell surface. Second, antigens that are immobilized at the surface of $CD169^+$ macrophages could be translocated from the SCS to B-cell follicles through macrophage protrusions (Martinez-Pomares & Gordon, 2007). In all cases, antigens are presented to cognate B cells and the engagement of the BCR with such surface-tethered antigens triggers the establishment of an immune synapse between the antigen-carrying cell and the B cell.

2.2. The establishment of the immune synapse

The immune synapse formed by B cells after the engagement of their BCR with cell-surface-bound antigens resembles the one originally described in the T cells (Grakoui, 1999; Yuseff, Lankar, & Lennon-Duménil, 2009). The BCR is composed of a cell-surface immunoglobulin associated to a signaling module that comprises the Igα–Igβ dimer. This dimer contains immunoreceptor tyrosine-based activation motifs that are rapidly phosphorylated by Src family kinases upon antigen recognition (Cambier, Pleiman, & Clark, 1994; Reth & Wienands, 1997). This initiates a cascade of signaling events involving cytosolic molecules such as Syk, Lyn, and Vav (Depoil et al., 2009; Tolar, Sohn, & Pierce, 2008) and calcium flux that ultimately launches the transcription of genes required for B-cell function (Baba &

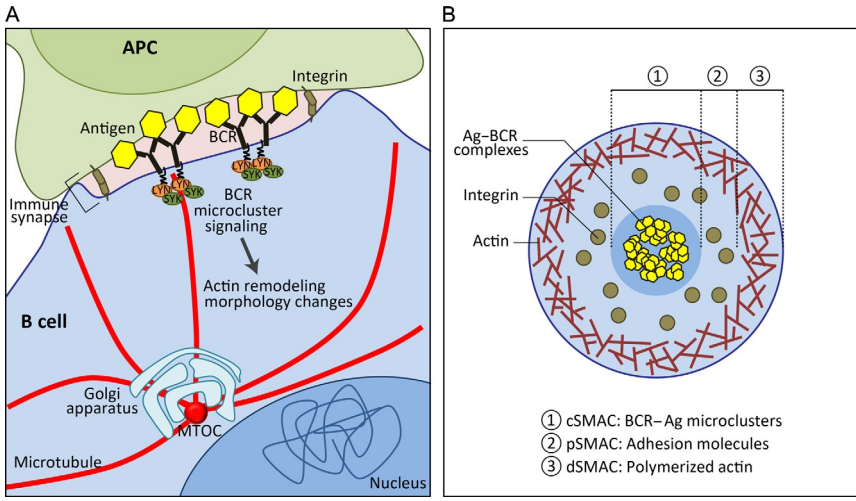

Figure 2.1 B cells form an immune synapse upon BCR engagement with immobilized antigens. (A) The engagement of the BCR with cell surface-tethered antigens leads to signaling events that trigger profound actin cytoskeleton remodeling: The B cell spreads on the antigen-presenting cell and the reorganization of its membrane at the antigen-contact site forms an immune synapse. (B) The immune synapse is a highly organized platform that includes three concentric areas: At the synapse center, antigen–BCR microclusters concentrate and form the central supramolecular activation cluster or cSMAC ①. This is surrounded by the peripheral SMAC where adhesion molecules such as LFA-1 localize ② and the distal SMAC where polymerized actin accumulates ③.

Kurosaki, 2011) (Fig. 2.1A). Concomitantly, drastic modifications of the B-cell actin cytoskeleton take place. First, BCR stimulation initiates a rapid cofilin-dependent actin cytoskeleton depolymerization at the antigen-contact site, allowing the local increase of BCR diffusion within the membrane (Freeman et al., 2011). This is followed by polarized actin repolymerization that promotes B-cell spreading onto the antigen-carrying cell. This process facilitates the formation of BCR microclusters that are required for sustained BCR signaling (Treanor et al., 2010). Then, BCR microclusters merge together in the center of the synapse to form the central supramolecular activation cluster (cSMAC) through a contraction phase mediated by myosin II (Fleire et al., 2006), which requires the coordinated action of the ezrin, radixin, and moesin proteins (Treanor, Depoil, Bruckbauer, & Batista, 2011) and the microtubule minus-end molecular motor dynein (Schnyder et al., 2011). Cortical actin rearrangements also trigger the formation of a second concentric region called the peripheral SMAC (pSMAC) that contains adhesion molecules such as LFA-1

(lymphocyte function-associated antigen 1, also known as $\alpha_L\beta_2$ integrin). The engagement of this integrin with its counterreceptor intercellular adhesion molecule 1 (also known as CD54) promotes B-cell adhesion to the antigen-presenting cell, facilitating the formation of the immune synapse and decreasing the antigen-affinity threshold required for BCR-mediated B-cell activation (Carrasco et al., 2004). Whereas the cSMAC and the pSMAC display very low concentration of polymerized actin, actin concentrates in a third concentric region called the distal SMAC (dSMAC) (Fig. 2.1B). Thus, reorganization of the actin cytoskeleton upon BCR engagement with surface-tethered antigen is a crucial stage in the early events of B-cell responses. In addition, the establishment of the immune synapse gives the first cues of asymmetrical cell organization leading *in fine* to the polarization of B-cell organelles towards the synaptic interface.

3. B-CELL POLARITY AND ANTIGEN PROCESSING AND PRESENTATION

3.1. B-cell polarization upon particulate antigen stimulation

Similarly to observations that were made in natural killer and cytotoxic T cells (Stinchcombe et al., 2011), upon BCR engagement, B cells rapidly polarize their MTOC towards the antigen-contact site. Concomitantly, MHC class II^+/Lamp-1^+ lysosomes are recruited to the immune synapse, where they cluster (Yuseff et al., 2011) (Fig. 2.2A). Interestingly, using MHC class II-expressing human melanoma cells, Wubbolts et al. had found that MHC class II^+ lysosomes traffic along microtubules to reach the plasma membrane (Wubbolts et al., 1996, 1999). Accordingly, we have shown that laser ablation of the MTOC following B-cell stimulation prevents polarized recruitment of lysosomes at the immune synapse (Yuseff et al., 2011). Although the molecular mechanisms underlying B-cell polarization upon BCR engagement with surface-tethered antigens are not fully understood, we identified the conserved polarity machinery cell division control protein 42 (Cdc42) and the atypical protein kinase C zeta-type (aPKC-ζ) (Yuseff et al., 2013) as required for B-cell polarization. Silencing of either Cdc42 or aPKC-ζ impairs MTOC and lysosome relocation at the synaptic interface, giving rise to a drastic decrease in antigen extraction, processing, and presentation (Yuseff et al., 2011).

B-cell polarization is not restricted to the MTOC and lysosomes. Indeed, we have found that upon BCR engagement with surface-tethered antigens, B cells polarize their Golgi apparatus and reorient their nucleus so that a

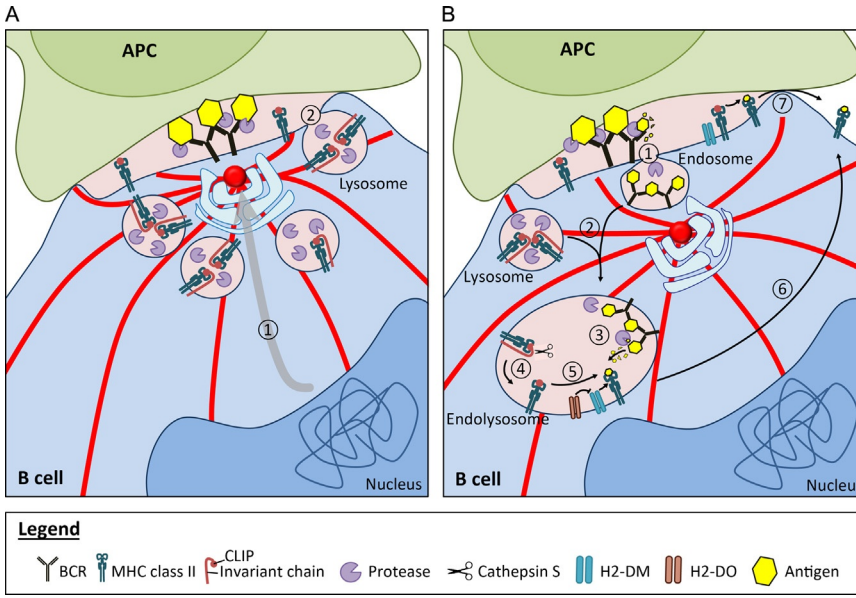

Figure 2.2 B cells polarize upon antigen stimulation. (A) Antigen stimulation initiates morphological changes within B cells. The microtubule-organizing center (MTOC) together with the Golgi apparatus reposition at the immune synapse ①. Concomitantly, lysosomes that were dispersed at the cell periphery cluster around the MTOC and are recruited at the antigen-contact site where they are secreted ②, resulting in synapse acidification (light pink) and the local release of proteases. (B) Synapse acidification and protease release promote efficient antigen extraction within the synaptic space leading to antigen internalization in B cell–endosomes ①. Endolysosomes that are formed by the fusion ② of antigen-containing endosomes with lysosomes that carry MHC class II molecules allow the efficient processing of antigens ③. In the same compartment, cathepsin S cleaves the invariant chain (Ii) ④ resulting in MHC class II–CLIP complex formation. Finally, H2-DM molecules promote the exchange between CLIP and antigenic peptides for them to be loaded onto MHC class II molecules ⑤. The catalysis of CLIP released by H2-DM is regulated by another nonclassical MHC II molecule, H2-DO. Peptide–MHC class II complexes are exported to the B-cell surface ⑥. It is important to note that antigenic peptides might also be generated within the synaptic space where they are directly loaded onto MHC class II molecules at the cell surface ⑦.

nucleus invagination faces the immune synapse (unplublished data and Fig. 2.2A). Interestingly, it has been recently described that during B-cell development, nuclear positioning of genes undergoes global changes that orchestrates B-cell fate (Lin et al., 2012). Taken together, it is tempting to speculate that antigenic stimulation leads to a global B-cell reorganization through the acquisition of polarity. In this context, BCR engagement with

surface-tethered antigens might coordinate (1) the polarization of the MTOC at the immune synapse to guide lysosome recruitment at the synaptic interface, (2) the repositioning of the Golgi apparatus in close proximity of the synapse to facilitate the export of neosynthetized proteins, and (3) the remodeling of chromatin to allow the transcription of genes required for B-cell function. How these events are coordinated in time and space remains to be determined. Is B-cell polarization established in a sequential manner? Does BCR stimulation initiate a "program" of global morphological changes that leads to the independent polarization of organelles? As discussed in the preceding text, we have shown that lysosome clustering at the immune synapse relies on the repositioning of the MTOC (Yuseff et al., 2011), providing the first clue on the interdependence of the polarization events observed upon BCR engagement.

3.2. Antigen extraction from antigen-presenting cell membranes

The immune synapse that forms at the interface between antigen-carrying cells and B lymphocytes corresponds to a dynamic structure where both endocytic and exocytic events take place. In T cells, it has been shown that effector molecules such as cytokines and lytic granules are secreted through the immune synapse towards target cells (Poo, Conrad, & Janeway, 1988; Stinchcombe et al., 2011). Exocytosis at the T-cell synapse occurs in specific domains that display very low levels of polymerized actin (Stinchcombe, Majorovits, Bossi, Fuller, & Griffiths, 2006), facilitating the local secretion of molecules (Chemin et al., 2012).

In B cells, upon BCR engagement with immobilized antigens, lysosomes are recruited at the immune synapse where they are locally secreted, thereby leading to the acidification of the extracellular synaptic space and the release of proteases in this confined environment (Yuseff et al., 2011) (Fig. 2.2A). Both synapse alkalinization and extracellular inhibition of proteases lead to a drastic decrease in the capacity of B cells to extract antigens, indicating that synapse acidification and protease secretion are required for efficient extraction of immobilized antigens (Yuseff et al., 2011). Whether exocytic events at the B-cell synapse specifically take place in areas displaying low concentration of polymerized actin has not been addressed so far.

The integration of mechanics into this biological process has recently been proposed by showing that B cells use myosin IIA-mediated pulling forces to discriminate between membrane-bound antigens displaying

different affinities for the BCR (Natkanski et al., 2013). Using flexible and fluid plasma membrane sheets that display mechanical properties close to those of dendritic cells, they have shown that upon BCR engagement, myosin II pulls on the presenting membrane leading to its invagination and subsequent antigen internalization into clathrin-coated pits. The lifetime of membrane invaginations and the probability of antigen internalization depend on the strength of antigen–BCR interactions. Using antigens with different affinities for the BCR, they further showed that myosin IIA activity impairs the internalization of relatively low-affinity antigens by disrupting antigen–BCR bonds. Myosin IIA activity is therefore critical for B cells to discriminate antigen affinities and later develop productive antibody responses (Natkanski et al., 2013). This work further raises the question of whether myosin II-dependent mechanical forces are generally required for endocytosis of immobilized molecules, what might be frequent *in vivo*. Interestingly, it has been reported that during epithelial morphogenesis in the *Drosophila* embryo, myosin IIA is asymmetrically distributed within cells where it concentrates at anterior–posterior boundaries of cells. Polarized actomyosin contractility in the ventrolateral region of the epithelium destabilizes the adherens junctions by promoting local clathrin-dependent endocytosis of E-cadherin and defines the axis of cell division (Levayer, Pelissier-Monier, & Lecuit, 2011). However, the mechanism(s) underlying myosin IIA asymmetrical distribution within cells and its anchorage at the plasma membrane remain elusive.

Taken together, these studies suggest that both proteases that are exocytosed into the synaptic space and myosin IIA-mediated pulling forces help in internalizing antigens at the B-cell synapse. Whether mechanical forces exerted by myosin IIA contractility are sufficient to break pieces of the presenting membrane leading to their internalization together with antigens remains to be precisely determined. In addition, the role of lysosomal lipases that are secreted at the immune synapse and might help in acquiring membrane-bound antigens should be investigated. We propose that the requirement for extracellular proteolysis and/or mechanical forces to internalize antigens into B cells might depend on their biochemical and physical properties.

3.3. Processing of antigen–BCR complexes

Antigenic peptides are generated from extracted antigens and loaded onto MHC class II molecules for presentation to primed $CD4^+$ T cells (Fig. 2.2B). This step — known as T-cell/B-cell cooperation — is pivotal for the ultimate formation of GCs and production of high-affinity antibodies by B lymphocytes (Mitchison, 2004).

BCR-dependent activation of the cytoplasmic tyrosine kinase Syk is required for actin cytoskeleton reorganization and efficient antigen–BCR trafficking to MHC class II^+ endolysosomes (Le Roux et al., 2007) (Fig. 2.2B ① and ②). There, antigens undergo limited proteolysis in order to preserve T-cell epitopes from excessive degradation (Delamarre, Pack, Chang, Mellman, & Trombetta, 2005) (Fig. 2.2B ③). Interestingly, in addition to its role in the uptake of immobilized antigens, myosin IIA was also shown to facilitate the arrival of antigen–BCR complexes into MHC class II^+ endolysosomes through its interaction with the cytosolic tail of invariant chain (Ii) (Vascotto et al., 2007). Ii associates to MHC class II molecules during biogenesis in the endoplasmic reticulum, preventing the premature binding of endogenous peptides onto MHC class II molecules (Bakke & Dobberstein, 1990; Lotteau et al., 1990; Roche & Cresswell, 1990, 1991). Once in endolysosome, Ii undergoes sequential proteolysis by aspartic and cysteine proteases including cathepsin S and the intramembrane endoprotease SPPL2a. This ultimately leads to the generation of the Ii CLIP fragment that occupies the MHC class II peptide-binding groove (Driessen et al., 1999; Riese et al., 1996; Villadangos, Riese, Peters, Chapman, & Ploegh, 1997) (Fig. 2.2B ④). Noticeably, SPPL2a knockout mice display a defect in B-cell development due to intracellular accumulation of Ii, suggesting that the last step of Ii cleavage is a checkpoint during B-cell differentiation (Beisner et al., 2013; Schneppenheim et al., 2013). CLIP exchange with antigenic peptides is catalyzed by the nonclassical MHC class II molecule, H2-DM (Denzin & Cresswell, 1995) (Fig. 2.2B ⑤). B cells express an additional nonclassical MHC class II molecule, H2-DO, which was shown to downregulate the catalysis of CLIP released by H2-DM (Denzin, 1997). Accordingly, H2-DO knockout B cells were found to exhibit increased amount of MHC class II–peptide complexes and compete wild-type B cells for the entry to GCs (Draghi & Denzin, 2010). Finally, peptide–MHC class II complexes are exported to the B-cell surface for further presentation to primed $CD4^+$ T cells (Fig. 2.2B ⑥). Remarkably, antigen processing and peptide loading onto MHC class II molecules can also directly take place at the B-cell surface, where H2-DM molecules are equally found (Moss, Tree, & Watts, 2007) (Fig. 2.2B ⑦).

3.4. Antigen presentation to helper T cells

Following antigen internalization and processing, B cells migrate towards the T-cell boundary, where they establish contacts with cognate T cells (Pereira, Kelly, & Cyster, 2010). B-cell migration is supported by the upregulation of CCR7 (CC chemokine receptor 7) that senses CCL19 and CCL21

(CC chemokine ligands 19 and 21) produced by stromal cells in the T-cell zone (Reif et al., 2002). While migrating towards the T-cell zone, B cells concentrate internalized antigens in their uropod (Carrasco & Batista, 2007), suggesting that they maintain the polarized phenotype acquired upon BCR engagement with immobilized antigens. This polarized concentration of antigens leads to their asymmetrical distribution among daughter B cells following cell division, providing them with differential antigen presentation capacities (Thaunat et al., 2012). Noticeably, the contact between B cells and T cells also results in the establishment of an immune synapse, where both cells harbor polarized phenotypes (Duchez, Rodrigues, Bertrand, & Valitutti, 2011). At the synapse, bidirectional exchanges take place, ultimately leading to the formation of GCs where B cells undergo affinity maturation and class switch recombination and differentiate into either plasma cells producing high-affinity antibodies or long-lived memory B cells (Allen et al., 2007; MacLennan, 1994). Interestingly, asymmetrical polarized division of B cells was also observed during the GC reaction and shown to regulate the survival of daughter cells through the unequal inheritance of Bcl-6, IL-21 receptor, and the polarity protein aPKC-ζ (Barnett et al., 2011). Thus, cell polarity is likely to play an essential role in shaping B-cell responses to surface-tethered antigens at their various activation stages. Whether the initial B-cell polarity established upon BCR engagement with immobilized antigens impacts on asymmetrical cell division and formation of the immune synapse with T cells shall now be investigated.

4. EXTRACELLULAR CUES THAT TUNE B-CELL POLARITY AND ACTIVATION

4.1. Chemokines involved in follicle patrolling by B cells

It is clear that the microenvironment of lymphoid tissues plays a key role in (1) modulating the ability of B cells to respond to antigens, (2) driving B-cell differentiation and fate, and (3) tuning the overall outcome of the adaptive immune response. Whereas numerous studies have focused their interest in understanding how the lymphoid microenvironment impacts B-cell homing within lymph nodes or the GC reaction, only few data are available on how it modifies the ability of B cells to initially respond to surface-bound antigens. Efficient antigen sampling by B cells relies on their capability to explore entire follicles within lymph nodes. This is achieved in response to the chemokine CXCL13 that induces CXCR5-expressing B cells to continuously migrate by random walking (Miller, Wei, Parker, & Cahalan, 2002; Sáez de Guinoa, Barrio, Mellado, & Carrasco, 2011). B-cell spreading

onto antigen-presenting cells and immune synapse establishment are coupled to an arrest phase in B-cell migration during which B cells acquire antigens (Carrasco & Batista, 2007; Junt et al., 2007). Thereby, the tight regulation of the interplay between cell motility and antigen internalization is critical for B-cell function. It has been recently shown that recruitment to the immune synapse of the scaffold protein vinculin, which links integrins at the plasma membrane with the actin cytoskeleton (Humphries et al., 2007), regulates adhesion between the B cell and the antigen-presenting cell (Saez de Guinoa, Barrio, & Carrasco, 2013). Vinculin is recruited to the immune synapse, in parallel to a phosphatidylinositol (4,5)-bisphosphate (PIP_2) wave, and stabilizes LFA-1 cluster within the pSMAC. This process relies on the activity of the myosin IIA motor, which is also required for CXCL13-mediated migration (Sáez de Guinoa et al., 2011). Vinculin and myosin IIA are therefore critical for B lymphocytes to switch between random motility and antigen internalization. Thus, B cells possess the machinery required to (1) integrate incoming information and (2) adapt their response to maximize antigen acquisition by regulating the balance between cell migration and cell adhesion to antigen-presenting cells. This leads to the formation either of a stable immune synapse characterized by a firm adhesion of the B cell to the antigen-presenting cell and very poor migratory capacities or of CXCL13- and LFA-1-mediated kinapses where B cells establish successive short interactions with multiple antigen-presenting cells, alternating between adhesion and motility phases. Interestingly, this resembles the intermittent search strategy displayed by dendritic cells where the coupling between antigen processing and cell motility by myosin II was proposed to enable dendritic cells to efficiently patrol peripheral tissues in search for antigens (Faure-andré et al., 2008; Heuzé et al., 2013). Myosin II activity therefore emerges as pivotal for many steps of B-cell activation: (1) It stabilizes vinculin by promoting LFA-1-mediated B-cell spreading onto the antigen-presenting cell and might thereby decrease B-cell velocity, (2) it provides a mechanical force to "test" for discrimination of antigen affinity, and (3) it ensures the proper trafficking of antigen–BCR complexes into MHC class II^+ lysosomes for antigen processing. Whether myosin II regulates B-cell polarity and whether B-cell polarity contributes to the switch between antigen uptake and cell migration remain to be addressed.

4.2. Galectins and B-cell function

Beyond chemokines, B-cell follicles contain a diversity of stromal cells and extracellular matrix components that might modulate the outcome of

B lymphocyte responses. Such cues have been poorly studied. During the last decade, glycan-binding proteins have emerged as key regulators of immune cell homeostasis and response to antigens (Rabinovich & Croci, 2012). Among these proteins is the galectin family (Rabinovich & Toscano, 2009) that has the ability to cross-link cell-surface glycol proteins in the extracellular space upon secretion, thereby impacting a wide range of biological processes. For instance, it was described that the lack of galectin-3 in *Schistosoma mansoni* chronically infected mice promotes plasma cell formation (Oliveira et al., 2011), suggesting a role for this galectin in negative regulation of B-cell responses. In contrast, galectin-1 and galectin-8 were shown to bind to mature B cells and promote the differentiation of LPS-treated B cells into antibody-secreting plasma cells *in vitro* (Tsai et al., 2008, 2011). It is interesting to note that while galectin-1 expression increases during the course of B-cell differentiation upon LPS stimulation, the expression of galectin-8 decreases (Tsai et al., 2011), suggesting an important role for galectin-8 in the early steps of B-cell activation. In addition, high concentration of galectin-8 was reported to trigger antigen-independent proliferation of $CD4^+$ T cells, whereas lower quantity of the protein provides costimulatory signals that synergize antigen-specific $CD4^+$ T-cell responses (Cattaneo, Tribulatti, & Campetella, 2011; Tribulatti, Cattaneo, Hellman, Mucci, & Campetella, 2009). Interestingly, galectin-8 was also described to promote cell adhesion (Cueni & Detmar, 2009) and migration of endothelial cells *in vivo* (Delgado et al., 2011). Moreover, the presence of function-blocking autoantibodies against galectin-8 in the sera of patients suffering from systemic lupus erythematosus correlates with acute lymphopenia (Massardo et al., 2009), suggesting that galectin-8 binding to glycosylated proteins might regulate B-cell homeostasis and function. Whether galectins or other glycan-binding proteins that are present within the lymphoid environment modulate specific steps of B-cell activation such as BCR signaling, B-cell adhesion, polarity, or migration remains to be explored.

5. CONCLUDING REMARKS

Although the signaling and genetic processes that enable B lymphocytes to form GCs and differentiate into long-lived plasma cells have been extensively studied in the past, the fundamental cell biological events that drive B-cell activation in response to antigen stimulation have recently started to be unraveled. Here, we have reviewed the fundamental molecular and cell biological mechanisms involved in B-cell function and

further highlighted how the acquisition of cell polarity critically regulates the various stages of B-cell responses to surface-tethered antigens. How B-cell polarity is controlled by extracellular cues in the context of lymphoid organs and whether the modulation of B-cell polarity can be used to tune humoral immune responses in pathological situations shall now be investigated.

ACKNOWLEDGMENTS

The authors acknowledge Maria-Isabel Yuseff, Anne Reversat, Paolo Pierobon, Odile Malbec, and Danielle Lankar for critical discussions. D. O. was supported by a PhD fellowship from the Ecole Doctorale B3MI, Université Paris Diderot. Funding was obtained from the Association Nationale pour la Recherche (ANR-PoLyBex-12-BSV3-0014-001) and the European Research Council (ERC-Strapacemi-GA 243103) to A- M. L- D.

REFERENCES

Allen, C. D. C., Okada, T., & Cyster, J. G. (2007). Germinal-center organization and cellular dynamics. *Immunity*, *27*(2), 190–202. http://dx.doi.org/10.1016/j.immuni.2007.07.009.

Baba, Y., & Kurosaki, T. (2011). Impact of Ca2+ signaling on B cell function. *Trends in Immunology*, *32*(12), 589–594. http://dx.doi.org/10.1016/j.it.2011.09.004.

Bakke, O., & Dobberstein, B. (1990). MHC class II-associated invariant chain contains a sorting signal for endosomal compartments. *Cell*, *63*(4), 707–716. Retrieved from, http://www.ncbi.nlm.nih.gov/pubmed/2121367.

Barnett, B. E., Ciocca, M. L., Goenka, R., Barnett, L. G., Wu, J., Laufer, T. M., et al. (2011). Asymmetric B cell division in the germinal center reaction. *Science (New York, N.Y.)*, *335*, 342–344. http://dx.doi.org/10.1126/science.1213495.

Batista, F. D., & Harwood, N. E. (2009). The who, how and where of antigen presentation to B cells. *Nature Reviews. Immunology*, *9*(1), 15–27. http://dx.doi.org/10.1038/nri2454.

Batista, F. D., Iber, D., & Neuberger, M. S. (2001). B cells acquire antigen from target cells after synapse formation. *Nature*, *411*(6836), 489–494. http://dx.doi.org/10.1038/35078099.

Beisner, D. R., Langerak, P., Parker, A. E., Dahlberg, C., Otero, F. J., Sutton, S. E., et al. (2013). The intramembrane protease Sppl2a is required for B cell and DC development and survival via cleavage of the invariant chain. *The Journal of Experimental Medicine*, *210*(1), 23–30. http://dx.doi.org/10.1084/jem.20121072.

Cambier, J. C., Pleiman, C. M., & Clark, M. R. (1994). Signal transduction by the B cell antigen receptor and its coreceptors. *Annual Review of Immunology*, *12*, 457–486.

Carrasco, Y. R., & Batista, F. D. (2007). B cells acquire particulate antigen in a macrophage-rich area at the boundary between the follicle and the subcapsular sinus of the lymph node. *Immunity*, *27*(1), 160–171. http://dx.doi.org/10.1016/j.immuni.2007.06.007.

Carrasco, Y. R., Fleire, S. J., Cameron, T., Dustin, M. L., & Batista, F. D. (2004). LFA-1/ICAM-1 interaction lowers the threshold of B cell activation by facilitating B cell adhesion and synapse formation. *Immunity*, *20*(5), 589–599. Retrieved from, http://www.ncbi.nlm.nih.gov/pubmed/15142527.

Cattaneo, V., Tribulatti, M. V., & Campetella, O. (2011). Galectin-8 tandem-repeat structure is essential for T-cell proliferation but not for co-stimulation. *The Biochemical Journal*, *434*(1), 153–160. http://dx.doi.org/10.1042/BJ20101691.

Chemin, K., Bohineust, A., Dogniaux, S., Tourret, M., Guégan, S., Miro, F., et al. (2012). Cytokine secretion by CD4+ T cells at the immunological synapse requires Cdc42-dependent local actin remodeling but not microtubule organizing center polarity. *Journal*

of Immunology (Baltimore, Md: 1950), *189*(5), 2159–2168. http://dx.doi.org/10.4049/jimmunol.1200156.

Cueni, L. N., & Detmar, M. (2009). Galectin-8 interacts with podoplanin and modulates lymphatic endothelial cell functions. *Experimental Cell Research*, *315*(10), 1715–1723. http://dx.doi.org/10.1016/j.yexcr.2009.02.021.

Cunningham, A. F., Gaspal, F., Serre, K., Mohr, E., Henderson, I. R., Scott-Tucker, A., et al. (2007). Salmonella induces a switched antibody response without germinal centers that impedes the extracellular spread of infection. *Journal of Immunology (Baltimore, Md: 1950)*, *178*(10), 6200–6207. Retrieved from, http://www.ncbi.nlm.nih.gov/pubmed/17475847.

Delamarre, L., Pack, M., Chang, H., Mellman, I., & Trombetta, E. S. (2005). Differential lysosomal proteolysis in antigen-presenting cells determines antigen fate. *Science (New York, N.Y.)*, *307*(5715), 1630–1634. http://dx.doi.org/10.1126/science.1108003.

Delgado, V. M. C., Nugnes, L. G., Colombo, L. L., Troncoso, M. F., Fernández, M. M., Malchiodi, E. L., et al. (2011). Modulation of endothelial cell migration and angiogenesis: A novel function for the "tandem-repeat" lectin galectin-8. *FASEB Journal: Official Publication of the Federation of American Societies for Experimental Biology*, *25*(1), 242–254. http://dx.doi.org/10.1096/fj.09-144907.

Denzin, L. K. (1997). Negative regulation by HLA-DO of MHC class II-restricted antigen processing. *Science*, *278*(5335), 106–109. http://dx.doi.org/10.1126/science.278.5335.106.

Denzin, L. K., & Cresswell, P. (1995). HLA-DM induces CLIP dissociation from MHC class II alpha beta dimers and facilitates peptide loading. *Cell*, *82*(1), 155–165. Retrieved from, http://www.ncbi.nlm.nih.gov/pubmed/7606781.

Depoil, D., Weber, M., Treanor, B., Fleire, S. J., Carrasco, Y. R., Harwood, N. E., et al. (2009). Early events of B cell activation by antigen. *Science Signaling*, *2*(63), pt1. http://dx.doi.org/10.1126/scisignal.263pt1.

Draghi, N. A., & Denzin, L. K. (2010). H2-O, a MHC class II-like protein, sets a threshold for B-cell entry into germinal centers. *Proceedings of the National Academy of Sciences of the United States of America*, *107*(38), 16607–16612. http://dx.doi.org/10.1073/pnas.1004664107.

Driessen, C., Bryant, R. A., Lennon-Duménil, A. M., Villadangos, J. A., Bryant, P. W., Shi, G. P., et al. (1999). Cathepsin S controls the trafficking and maturation of MHC class II molecules in dendritic cells. *The Journal of Cell Biology*, *147*(4), 775–790. Retrieved from, http://www.pubmedcentral.nih.gov/articlerender.fcgi?artid=2156161&tool=pmcentrez&rendertype=abstract.

Duchez, S., Rodrigues, M., Bertrand, F., & Valitutti, S. (2011). Reciprocal polarization of T and B cells at the immunological synapse. *Journal of Immunology (Baltimore, Md: 1950)*, *187*(9), 4571–4580. http://dx.doi.org/10.4049/jimmunol.1100600.

Faure-andré, G., Vargas, P., Yuseff, M., Heuzé, M., Vascotto, F., Boulanger, J., et al. (2008). Regulation of dendritic cell migration by CD74, the MHC class II-associated Invariant chain. *Science*, *322*, 1705–1710.

Fleire, S. J., Goldman, J. P., Carrasco, Y. R., Weber, M., Bray, D., & Batista, F. D. (2006). B cell ligand discrimination through a spreading and contraction response. *Science (New York, N.Y.)*, *312*(5774), 738–741. http://dx.doi.org/10.1126/science.1123940.

Freeman, S. A., Lei, V., Dang-Lawson, M., Mizuno, K., Roskelley, C. D., & Gold, M. R. (2011). Cofilin-mediated F-actin severing is regulated by the Rap GTPase and controls the cytoskeletal dynamics that drive lymphocyte spreading and BCR microcluster formation. *Journal of Immunology (Baltimore, Md: 1950)*, *187*(11), 5887–5900. http://dx.doi.org/10.4049/jimmunol.1102233.

Grakoui, A. (1999). The immunological synapse: A molecular machine controlling T cell activation. *Science*, *285*(5425), 221–227. http://dx.doi.org/10.1126/science.285.5425.221.

Heuzé, M. L., Vargas, P., Chabaud, M., Le Berre, M., Liu, Y.-J., Collin, O., et al. (2013). Migration of dendritic cells: Physical principles, molecular mechanisms, and functional implications. *Immunological Reviews*, *256*(1), 240–254. http://dx.doi.org/10.1111/imr.12108.

Humphries, J. D., Wang, P., Streuli, C., Geiger, B., Humphries, M. J., & Ballestrem, C. (2007). Vinculin controls focal adhesion formation by direct interactions with talin and actin. *The Journal of Cell Biology*, *179*(5), 1043–1057. http://dx.doi.org/10.1083/jcb.200703036.

Junt, T., Moseman, E. A., Iannacone, M., Massberg, S., Lang, P. A., Boes, M., et al. (2007). Subcapsular sinus macrophages in lymph nodes clear lymph-borne viruses and present them to antiviral B cells. *Nature*, *450*(7166), 110–114. http://dx.doi.org/10.1038/nature06287.

Le Roux, D., Lankar, D., Yuseff, M., Vascotto, F., Yokozeki, T., Faure-andre, G., et al. (2007). Syk-dependent actin dynamics regulate endocytic trafficking and processing of antigens internalized through the B-cell receptor. *Molecular Biology of the Cell*, *18*(September), 3451–3462. http://dx.doi.org/10.1091/mbc.E06.

Levayer, R., Pelissier-Monier, A., & Lecuit, T. (2011). Spatial regulation of Dia and Myosin-II by RhoGEF2 controls initiation of E-cadherin endocytosis during epithelial morphogenesis. *Nature Cell Biology*, *13*(5), 529–540. http://dx.doi.org/10.1038/ncb2224.

Lin, Y. C., Benner, C., Mansson, R., Heinz, S., Miyazaki, K., Miyazaki, M., et al. (2012). Global changes in the nuclear positioning of genes and intra- and interdomain genomic interactions that orchestrate B cell fate. *Nature Immunology*, *13*(12), 1196–1204. http://dx.doi.org/10.1038/ni.2432.

Lotteau, V., Teyton, L., Peleraux, A., Nilsson, T., Karlsson, L., Schmid, S. L., et al. (1990). Intracellular transport of class II MHC molecules directed by invariant chain. *Nature*, *348*, 600–605.

MacLennan, I. C. (1994). Germinal centers. *Annual Review of Immunology*, *12*, 117–139. http://dx.doi.org/10.1146/annurev.iy.12.040194.001001.

Martinez-Pomares, L., & Gordon, S. (2007). Antigen presentation the macrophage way. *Cell*, *131*(4), 641–643. http://dx.doi.org/10.1016/j.cell.2007.10.046.

Massardo, L., Metz, C., Pardo, E., Mezzano, V., Babul, M., Jarpa, E., et al. (2009). Autoantibodies against galectin-8: Their specificity, association with lymphopenia in systemic lupus erythematosus and detection in rheumatoid arthritis and acute inflammation. *Lupus*, *18*(6), 539–546. http://dx.doi.org/10.1177/0961203308099973.

Miller, M. J., Wei, S. H., Parker, I., & Cahalan, M. D. (2002). Two-photon imaging of lymphocyte motility and antigen response in intact lymph node. *Science (New York, N.Y.)*, *296*(5574), 1869–1873. http://dx.doi.org/10.1126/science.1070051.

Mitchison, N. A. (2004). T-cell-B-cell cooperation. *Nature Reviews. Immunology*, *4*(4), 308–312. http://dx.doi.org/10.1038/nri1334.

Moss, C. X., Tree, T. I., & Watts, C. (2007). Reconstruction of a pathway of antigen processing and class II MHC peptide capture. *The EMBO Journal*, *26*(8), 2137–2147. http://dx.doi.org/10.1038/sj.emboj.7601660.

Natkanski, E., Lee, W. Y., Mistry, B., Casal, A., Molloy, J. E., & Tolar, P. (2013). B cells use mechanical energy to discriminate antigen affinities. *Science (New York, N.Y.)*, *340*(6140), 1587–1590. http://dx.doi.org/10.1126/science.1237572.

Oliveira, F. L., Brand, C., Paula, A. A., Arcanjo, K. D., Hsu, D. K., Liu, F.-T., et al. (2011). Lack of galectin-3 disturbs mesenteric lymph node homeostasis and B cell niches in the course of Schistosoma mansoni infection. *PloS One*, *6*(5), e19216. http://dx.doi.org/10.1371/journal.pone.0019216.

Pape, K. A., Catron, D. M., Itano, A. A., & Jenkins, M. K. (2007). The humoral immune response is initiated in lymph nodes by B cells that acquire soluble antigen directly in the follicles. *Immunity*, *26*(4), 491–502. http://dx.doi.org/10.1016/j.immuni.2007.02.011.

Pereira, J. P., Kelly, L. M., & Cyster, J. G. (2010). Finding the right niche: B-cell migration in the early phases of T-dependent antibody responses. *International Immunology*, *22*(6), 413–419. http://dx.doi.org/10.1093/intimm/dxq047.

Poo, W. J., Conrad, L., & Janeway, C. A. (1988). Receptor-directed focusing of lymphokine release by helper T cells. *Nature*, *332*, 378–380.

Qi, H., Egen, J. G., Huang, A. Y. C., & Germain, R. N. (2006). Extrafollicular activation of lymph node B cells by antigen-bearing dendritic cells. *Science (New York, N.Y.)*, *312*(5780), 1672–1676. http://dx.doi.org/10.1126/science.1125703.

Rabinovich, G. A., & Croci, D. O. (2012). Regulatory circuits mediated by lectin-glycan interactions in autoimmunity and cancer. *Immunity*, *36*(3), 322–335. http://dx.doi.org/10.1016/j.immuni.2012.03.004.

Rabinovich, G. A., & Toscano, M. A. (2009). Turning "sweet" on immunity: Galectin-glycan interactions in immune tolerance and inflammation. *Nature Reviews. Immunology*, *9*(5), 338–352. http://dx.doi.org/10.1038/nri2536.

Reif, K., Ekland, E. H., Ohl, L., Nakano, H., Lipp, M., Förster, R., et al. (2002). Balanced responsiveness to chemoattractants from adjacent zones determines B-cell position. *Nature*, *416*(6876), 94–99. http://dx.doi.org/10.1038/416094a.

Reth, M., & Wienands, J. (1997). Initiation and processing of signals from the B cell antigen receptor. *Annual Review of Immunology*, *15*, 453–479.

Riese, R. J., Wolf, P. R., Brömme, D., Natkin, L. R., Villadangos, J. A., Ploegh, H. L., et al. (1996). Essential role for cathepsin S in MHC class II-associated invariant chain processing and peptide loading. *Immunity*, *4*(4), 357–366. Retrieved from, http://www.ncbi.nlm.nih.gov/pubmed/8612130.

Roche, P. A., & Cresswell, P. (1990). Invariant chain association with HLA-DR molecules inhibits immunogenic peptide binding. *Nature*, *345*, 615–618.

Roche, P. A., & Cresswell, P. (1991). Proteolysis of the class II-associated invariant chain generates a peptide binding site in intracellular HLA-DR molecules. *Proceedings of the National Academy of Sciences of the United States of America*, *88*(8), 3150–3154. Retrieved from, http://www.ncbi.nlm.nih.gov/pubmed/21772034.

Roozendaal, R., Mempel, T. R., Pitcher, L. A., Gonzalez, S. F., Verschoor, A., Mebius, R. E., et al. (2009). Conduits mediate transport of low-molecular-weight antigen to lymph node follicles. *Immunity*, *30*(2), 264–276. http://dx.doi.org/10.1016/j.immuni.2008.12.014.

Saez de Guinoa, J., Barrio, L., & Carrasco, Y. R. (2013). Vinculin arrests motile B cells by stabilizing integrin clustering at the immune synapse. *Journal of Immunology (Baltimore, Md: 1950)*, *191*(5), 2742–2751. http://dx.doi.org/10.4049/jimmunol.1300684.

Sáez de Guinoa, J., Barrio, L., Mellado, M., & Carrasco, Y. R. (2011). CXCL13/CXCR5 signaling enhances BCR-triggered B-cell activation by shaping cell dynamics. *Blood*, *118*(6), 1560–1569. http://dx.doi.org/10.1182/blood-2011-01-332106.

Schneppenheim, J., Dressel, R., Hüttl, S., Lüllmann-Rauch, R., Engelke, M., Dittmann, K., et al. (2013). The intramembrane protease SPPL2a promotes B cell development and controls endosomal traffic by cleavage of the invariant chain. *The Journal of Experimental Medicine*, *210*(1), 41–58. http://dx.doi.org/10.1084/jem.20121069.

Schnyder, T., Castello, A., Feest, C., Harwood, N. E., Oellerich, T., Urlaub, H., et al. (2011). B cell receptor-mediated antigen gathering requires ubiquitin ligase cbl and adaptors grb2 and dok-3 to recruit Dynein to the signaling microcluster. *Immunity*, *34*(6), 905–918. http://dx.doi.org/10.1016/j.immuni.2011.06.001.

Stinchcombe, J. C., Majorovits, E., Bossi, G., Fuller, S., & Griffiths, G. M. (2006). Centrosome polarization delivers secretory granules to the immunological synapse. *Nature*, *443*(7110), 462–465. http://dx.doi.org/10.1038/nature05071.

Stinchcombe, J. C., Salio, M., Cerundolo, V., Pende, D., Arico, M., & Griffiths, G. M. (2011). Centriole polarisation to the immunological synapse directs secretion from cytolytic cells of both the innate and adaptive immune systems. *BMC Biology*, *9*(1), 45. http://dx.doi.org/10.1186/1741-7007-9-45.

Suzuki, K., Grigorova, I., Phan, T. G., Kelly, L. M., & Cyster, J. G. (2009). Visualizing B cell capture of cognate antigen from follicular dendritic cells. *The Journal of Experimental Medicine*, *206*(7), 1485–1493. http://dx.doi.org/10.1084/jem.20090209.

Thaunat, O., Granja, A. G., Barral, P., Filby, A., Montaner, B., Collinson, L., et al. (2012). Asymmetric segregation of polarized antigen on B cell division shapes presentation capacity. *Science*, *335*(6067), 475–479. http://dx.doi.org/10.1126/science.1214100.

Tolar, P., Sohn, H. W., & Pierce, S. K. (2008). Viewing the antigen-induced initiation of B-cell activation in living cells. *Immunological Reviews*, *221*, 64–76. http://dx.doi.org/10.1111/j.1600-065X.2008.00583.x.

Treanor, B., Depoil, D., Bruckbauer, A., & Batista, F. D. (2011). Dynamic cortical actin remodeling by ERM proteins controls BCR microcluster organization and integrity. *The Journal of Experimental Medicine*, *208*(5), 1055–1068. http://dx.doi.org/10.1084/jem.20101125.

Treanor, B., Depoil, D., Gonzalez-Granja, A., Barral, P., Weber, M., Dushek, O., et al. (2010). The membrane skeleton controls diffusion dynamics and signaling through the B cell receptor. *Immunity*, *32*(2), 187–199. http://dx.doi.org/10.1016/j.immuni.2009.12.005.

Tribulatti, M. V., Cattaneo, V., Hellman, U., Mucci, J., & Campetella, O. (2009). Galectin-8 provides costimulatory and proliferative signals to T lymphocytes. *Journal of Leukocyte Biology*, *86*(2), 371–380. http://dx.doi.org/10.1189/jlb.0908529.

Tsai, C.-M., Chiu, Y.-K., Hsu, T.-L., Lin, I.-Y., Hsieh, S.-L., & Lin, K.-I. (2008). Galectin-1 promotes immunoglobulin production during plasma cell differentiation. *Journal of Immunology (Baltimore, Md: 1950)*, *181*(7), 4570–4579. Retrieved from, http://www.ncbi.nlm.nih.gov/pubmed/18802059.

Tsai, C.-M., Guan, C.-H., Hsieh, H.-W., Hsu, T.-L., Tu, Z., Wu, K. J., et al. (2011). Galectin-1 and galectin-8 have redundant roles in promoting plasma cell formation. *Journal of Immunology (Baltimore, Md: 1950)*, *187*(4), 1643–1652. http://dx.doi.org/10.4049/jimmunol.1100297.

Vascotto, F., Lankar, D., Faure-André, G., Vargas, P., Diaz, J., Le Roux, D., et al. (2007). The actin-based motor protein myosin II regulates MHC class II trafficking and BCR-driven antigen presentation. *The Journal of Cell Biology*, *176*(7), 1007–1019. http://dx.doi.org/10.1083/jcb.200611147.

Villadangos, J. A., Riese, R. J., Peters, C., Chapman, H. A., & Ploegh, H. L. (1997). Degradation of mouse invariant chain: Roles of cathepsins S and D and the influence of major histocompatibility complex polymorphism. *The Journal of Experimental Medicine*, *186*(4), 549–560. Retrieved from, http://www.pubmedcentral.nih.gov/articlerender.fcgi?artid=2199027&tool=pmcentrez&rendertype=abstract.

Wubbolts, R., Fernandez-Borja, M., Jordens, I., Reits, E., Dusseljee, S., Echeverri, C., et al. (1999). Opposing motor activities of dynein and kinesin determine retention and transport of MHC class II-containing compartments. *Journal of Cell Science*, *112*(Pt 6), 785–795. Retrieved from, http://www.ncbi.nlm.nih.gov/pubmed/10036229.

Wubbolts, R., Fernandez-Borja, M., Oomen, L., Verwoerd, D., Janssen, H., Calafat, J., et al. (1996). Direct vesicular transport of MHC class II molecules from lysosomal structures to the cell surface. *The Journal of Cell Biology*, *135*(3), 611–622. Retrieved from, http://www.pubmedcentral.nih.gov/articlerender.fcgi?artid=2121075&tool=pmcentrez&rendertype=abstract.

Yuseff, M.-I., Lankar, D., & Lennon-Duménil, A.-M. (2009). Dynamics of membrane trafficking downstream of B and T cell receptor engagement: Impact on immune synapses. *Traffic (Copenhagen, Denmark)*, *10*(6), 629–636. http://dx.doi.org/10.1111/j.1600-0854.2009.00913.x.

Yuseff, M.-I., Pierobon, P., Reversat, A., & Lennon-Duménil, A.-M. (2013). How B cells capture, process and present antigens: A crucial role for cell polarity. *Nature Reviews. Immunology*, *13*(7), 475–486. http://dx.doi.org/10.1038/nri3469.

Yuseff, M.-I., Reversat, A., Lankar, D., Diaz, J., Fanget, I., Pierobon, P., et al. (2011). Polarized secretion of lysosomes at the B cell synapse couples antigen extraction to processing and presentation. *Immunity*, *35*(3), 361–374. http://dx.doi.org/10.1016/j.immuni.2011.07.008.

"Innate control of actin nucleation determines two distinct migration behaviours in dendritic cells"

Vargas P[1,2], Maiuri P[2], Bretou M[1], Sáez PJ[1], Pierobon P[1], Maurin M[1], Chabaud M[1], Lankar D[1], **Obino D**[1], Terriac E[2], Raab M[2], Thiam HR[2], Brocker T[3], Kitchen-Goosen SM[4], Alberts AS[4], Sunareni P[5], Xia S[5], Li R[5], Voituriez R[6,7], Piel M[2], Lennon-Duménil AM[1].

Nature Cell Biology, 2016, 18(1):43-53

[1]Inserm U932, Institut Curie, 12 rue Lhomond, 75005 Paris, France.

[2]CNRS UMR144, Institut Curie, 12 rue Lhomond, 75005 Paris, France.

[3]Institute for Immunology, Ludwig-Maximilian University of Munich, 80336 Munich, Germany.

[4]Van Andel Research Institute, 333 Bostwick Avenue N.E., Grand Rapids, Michigan 49503, USA.

[5]Johns Hopkins University School of Medicine, 855 N. Wolfe Street, Baltimore, Maryland 21205, USA.

[6]CNRS UMR 7600, Université Pierre et Marie Curie, 4 Place Jussieu, 75005 Paris, France.

[7]CNRS FRE 3231, Université Pierre et Marie Curie, 4 Place Jussieu, 75005 Paris, France.

nature cell biology

Innate control of actin nucleation determines two distinct migration behaviours in dendritic cells

Pablo Vargas[1,2,9], Paolo Maiuri[2,8], Marine Bretou[1,8], Pablo J. Sáez[1], Paolo Pierobon[1], Mathieu Maurin[1], Mélanie Chabaud[1], Danielle Lankar[1], Dorian Obino[1], Emmanuel Terriac[2], Matthew Raab[2], Hawa-Racine Thiam[2], Thomas Brocker[3], Susan M. Kitchen-Goosen[4], Arthur S. Alberts[4], Praveen Sunareni[5], Sheng Xia[5], Rong Li[5], Raphael Voituriez[6,7], Matthieu Piel[2,8,9] and Ana-Maria Lennon-Duménil[1,8,9]

Dendritic cell (DC) migration in peripheral tissues serves two main functions: antigen sampling by immature DCs, and chemokine-guided migration towards lymphatic vessels (LVs) on maturation. These migratory events determine the efficiency of the adaptive immune response. Their regulation by the core cell locomotion machinery has not been determined. Here, we show that the migration of immature DCs depends on two main actin pools: a RhoA–mDia1-dependent actin pool located at their rear, which facilitates forward locomotion; and a Cdc42–Arp2/3-dependent actin pool present at their front, which limits migration but promotes antigen capture. Following TLR4–MyD88-induced maturation, Arp2/3-dependent actin enrichment at the cell front is markedly reduced. Consequently, mature DCs switch to a faster and more persistent mDia1-dependent locomotion mode that facilitates chemotactic migration to LVs and lymph nodes. Thus, the differential use of actin-nucleating machineries optimizes the migration of immature and mature DCs according to their specific function.

The activation of T lymphocytes depends on the capacity of dendritic cells (DCs) to internalize antigens at the site of infection and transport them to lymph nodes (LNs) as processed major histocompatibility complex–peptide complexes[1]. Sampling of peripheral tissues by immature DCs relies on their intrinsic antigen internalization capacity that includes both phagocytosis and macropinocytosis[2–4]. Tissue patrolling might also involve active DC locomotion as immature DCs have been shown to be motile in peripheral locations such as the mouse ear and gut[5,6]. On sensing of microbial stimuli, DCs acquire a mature phenotype that is associated with the Cdc42-dependent downregulation of macropinocytosis and the upregulation of co-stimulatory molecules for productive interaction with T lymphocytes[2,3,7]. Mature DCs also upregulate the chemokine receptor CCR7 at their surface[8], which allows them to respond to gradients of CCL21 secreted by the lymphatic endothelium, inducing their directional migration towards lymphatic vessels (LVs) and LNs (refs 9, 10). Extracellular molecules from the endothelium such as podoplanin were also shown to influence mature DC locomotion *in vivo*[11]. However, whether and how the core migration machinery of DCs is modified on innate sensing and impacts on their immune function remains unknown.

The mechanisms that enable cell migration have been extensively studied in adhesive cells moving on flat two-dimensional (2D) surfaces. In most cases, they involve cycles of cell front extension mediated by Arp2/3-dependent nucleation of branched filamentous actin, followed by cell rear retraction[12]. However, 2D migration rarely applies to immune cells, which mainly migrate in complex 3D environments *in vivo*. Although 3D environments are diverse in terms of molecular composition and geometry, they share a common property that does not apply to flat surfaces: cell confinement. Noticeably, DC locomotion was shown to be independent of integrin-mediated adhesion in 3D and 2D confined environments as well as *in vivo*[13–15], stressing the need to use experimental systems exhibiting the proper geometry to tackle the mechanisms underlying DC migration.

We used confining devices to investigate how sensing of microbial components regulates the intrinsic migratory capacity of DCs. We found that maturation of DCs in response to Toll-like receptor (TLR) 4–MyD88 signalling increases their migration speed and persistence by regulating actin-nucleation machineries. We further show that this cell-intrinsic change in DC motility is required for them to efficiently follow chemotactic gradients and reach LNs *in vivo*. We propose

[1]Inserm U932, Institut Curie, 12 rue Lhomond, 75005 Paris, France. [2]CNRS UMR144, Institut Curie, 12 rue Lhomond, 75005 Paris, France. [3]Institute for Immunology, Ludwig-Maximilian University of Munich, 80336 Munich, Germany. [4]Van Andel Research Institute, 333 Bostwick Avenue N.E., Grand Rapids, Michigan 49503, USA. [5]Johns Hopkins University School of Medicine, 855 N. Wolfe Street, Baltimore, Maryland 21205, USA. [6]CNRS UMR 7600, Université Pierre et Marie Curie, 4 Place Jussieu, 75005 Paris, France. [7]CNRS FRE 3231, Université Pierre et Marie Curie, 4 Place Jussieu, 75005 Paris, France. [8]These authors contributed equally to this work.
[9]Correspondence should be addressed to P.V., M.P. or A.-M.L.-D. (e-mail: pablo.vargas@curie.fr or mpiel@curie.fr or amlennon@curie.fr)

Received 11 December 2014; accepted 9 November 2015; published online 7 December 2015; corrected online 23 December 2015; DOI: 10.1038/ncb3284

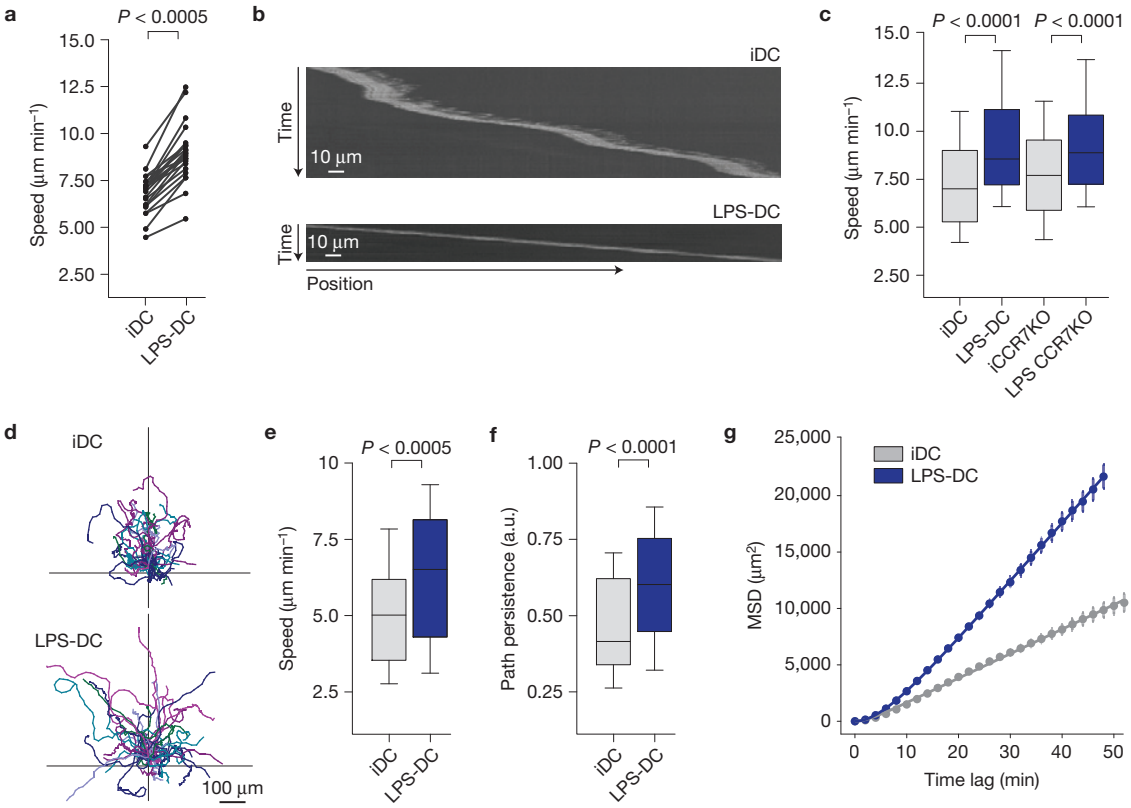

Figure 1 LPS activation induces fast and persistent DC migration. (**a**–**c**) Analysis of BMDCs migrating in 4 µm × 5 µm fibronectin-coated micro-channels. Cells were imaged between 6 and 16 h after LPS treatment (100 ng ml^{-1} for 30 min). (**a**) Mean instantaneous cell speed. Each dot represents the mean of one experiment (n = 29 experiments, >40 cells in each experiment). (**b**) Kymograph representative of an iDC and an LPS-DC migrating in micro-channels. (**c**) Analysis of CCR7KO DC migration in micro-channels (n = 150, 99, 145 and 151 cells for iDC, LPS-DC, iCCR7KO and LPS CCR7KO respectively). One representative experiment out of two is shown. (**d**–**g**) Analysis of DC migration under agarose. (**d**) Cell tracks of DCs migrating under agarose. Cells were imaged for 200 min. The starting point of each trajectory was translated to the origin of the plot. One representative experiment out of three is shown. (**e**,**f**) Mean instantaneous speed and path persistence of data depicted in **d** (n = 63 and 76 cells for iDC and LPS-DC respectively). (**g**) Mean square displacement (MSD) obtained from the data depicted in **d**. The Mann–Whitney test was applied for statistical analysis. In the box plots of **c**,**e**,**f** the bars include 90% of the points, the centre corresponds to the median and the box contains 75% of the data.

that regulation of the core cell migration machinery helps adapt the migratory behaviour of immature and mature DCs to their distinct functional requirements: environment sampling and antigen uptake for immature DCs and efficient migration to lymphoid organs for mature DCs.

RESULTS

Innate sensing induces fast and persistent DC migration

We asked whether innate sensing triggers cell-intrinsic changes in DC motility. To address this question, we compared the migration of immature DCs (iDCs) and LPS-treated mature DCs (LPS-DCs) in 1D confined micro-channels[15–17]. DCs pulsed with LPS for 30 min showed a significant increase in their migration speed after 6 h (Fig. 1a,b). This transient LPS treatment was sufficient to induce full DC maturation (Supplementary Fig. 1a,b). The increment in DC velocity was also observed in CCR7 knockout (KO) and pertussis toxin-treated cells (Fig. 1c and Supplementary Fig. 1c,d), excluding a role of G protein-coupled chemokine receptors. In contrast, both the LPS receptor TLR4 and its adaptor MyD88 (ref. 18) were needed for DC speed increment (Supplementary Fig. 1e,f). Hence, sensing of LPS triggers a TLR4–MyD88-dependent signalling cascade that promotes fast DC motility in 1D confined environments.

The trajectories of LPS-DCs were more continuous than those of iDCs, suggesting a more persistent locomotion mode (Fig. 1b). To measure cell migration persistence, we used the previously described 'under-agarose motility assay'[19], in which DCs are confined but freely move in two dimensions. LPS-DCs exhibited more directed trajectories as compared with iDCs (Fig. 1d). Accordingly, both their migration speed and path persistence were increased (Fig. 1e,f). As a consequence of that, LPS-DCs were more efficient in space exploration, as illustrated by their increased mean square displacement (Fig. 1g). Thus, TLR4 engagement triggers a cell-intrinsic response that results in mature DCs moving over larger distances as compared with their immature counterparts.

Innate sensing modifies actin dynamics in migrating DCs

We next investigated whether the impact of innate sensing on DC locomotion was associated with changes in their actin cytoskeleton. We have previously shown that iDCs alternate fast and slow motility phases when migrating in micro-channels[15]. Analysis of F-actin dynamics using DCs derived from LifeAct–GFP transgenic

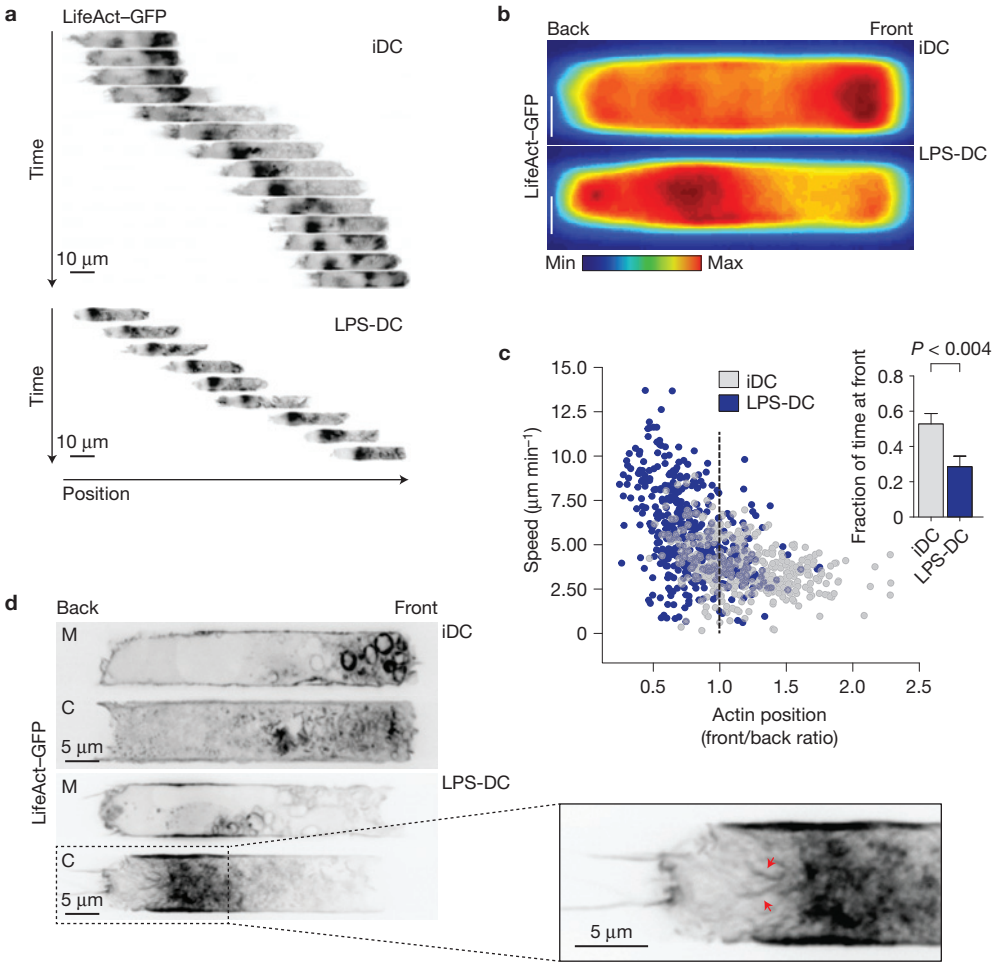

Figure 2 LPS activation of DCs modifies the dynamics of their actin cytoskeleton. (**a**–**d**) LifeAct–GFP imaging of BMDCs migrating in 8 μm × 5 μm fibronectin-coated micro-channels. (**a**) Sequential images of LifeAct–GFP DCs acquired on an epifluorescence microscope every 1 min with a ×20 objective. (**b**) LifeAct–GFP density maps. Scale bars, 2.5 μm. The signal recorded at each time point was integrated into a single image for single migrating cells (see Supplementary Fig. 2). The mean intensity obtained for each cell was then averaged into a single density map ($n = 31$ and 27 cells for iDC and LPS-DC respectively). One representative experiment out of four is shown. (**c**) Correlation between the LifeAct–GFP front/back ratio and instantaneous speed values from DCs migrating in micro-channels. Values were obtained from data shown in **b**. The inset shows the mean fraction of time spent by DCs with LifeAct–GFP concentrated at their front (first third of the cell). The Mann–Whitney test was applied for statistical analysis. Graphic shows mean and error bars correspond to s.e.m. (**d**) LifeAct–GFP DCs migrating in micro-channels and time lapsed on a spinning-disc microscope (×100). Middle (M) and cortical (C) planes were imaged. The red arrows on the zoomed image show actin cables formed at the rear of LPS-DC.

mice highlighted that iDCs concentrated F-actin at the cell front, particularly during phases of slow motion (Fig. 2a, upper panel). In contrast, the predominant F-actin pool of LPS-DCs was localized at the cell back. This pool of F-actin was also observed during phases of fast locomotion in iDCs (Fig. 2a, lower panel). These results were confirmed by quantifying the mean behaviour of the entire DC population using LifeAct–GFP density maps (Fig. 2b and Supplementary Fig. 2). Dynamic analysis showed that the presence of F-actin at the cell front inversely correlated with cell speed in both types of DC (Fig. 2c). However, iDCs spent significantly more time with actin at their front (Fig. 2c, inset). Noticeably, the predominant F-actin pool observed at the front of iDCs was mainly observed in ruffles and around macropinosomes[20] (Fig. 2d and Supplementary Videos 1 and 2). In contrast, the main F-actin structure present at the back of LPS-DCs localized at the cell cortex and included numerous actin cables (arrows in Fig. 2d and Supplementary Videos 1 and 3). Such cables were also occasionally observed in iDCs, in agreement with these cells exhibiting both slow and fast migration phases. These data highlight the existence of two main pools of F-actin in DCs: one at the cell front associated with slow motility, which is mainly observed in iDCs, and one at the cell back that correlates with fast migration.

F-actin at the front of iDCs depends on Arp2/3, limits migration but promotes antigen uptake

We next searched for the actin nucleators involved in the generation of these different actin pools. Branched actin nucleated by the Arp2/3 complex is known to promote migration by driving protrusion at the leading edge[21–23]. Arp2/3 has also been associated with membranes ruffling during macropinocytosis[24]. We therefore reasoned that Arp2/3 was needed for F-actin accumulation at the front of iDCs. Inhibiting Arp2/3 with CK666 (ref. 25) decreased the fraction of time iDCs spent with F-actin concentrated at their front (Fig. 3a,b). The

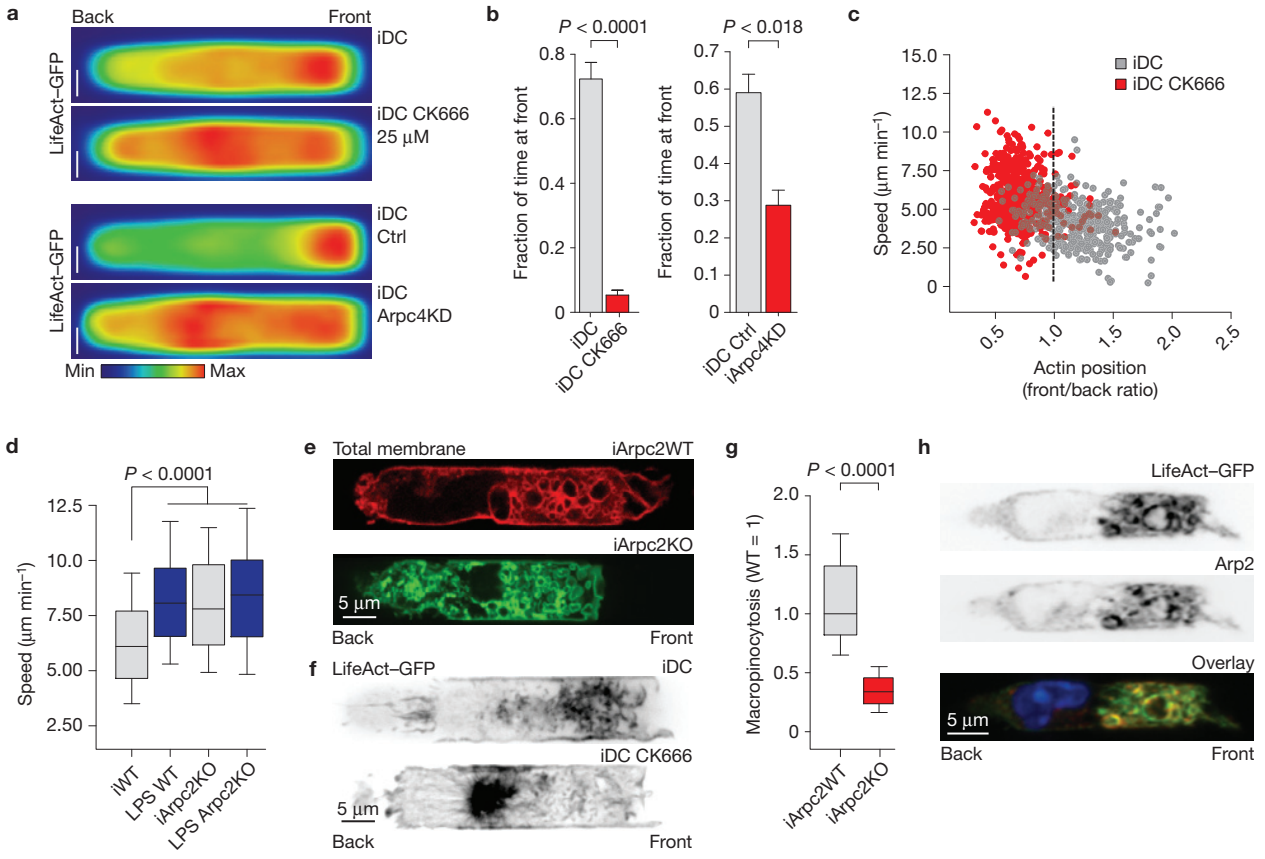

Figure 3 Arp2/3-dependent actin at the front of iDCs limits migration but promotes antigen uptake. (**a**) Mean LifeAct–GFP distribution in iDCs migrating in micro-channels and treated with the Arp2/3 inhibitor CK666 (25 μM) or silenced for Arpc4 ($n = 27$, 42, 28 and 26 cells for iDC, iDC CK666, iDC Ctrl and iArpc4KD respectively). Scale bars, 2.5 μm. One representative experiment out of three is shown. Internal controls are systematically used. (**b**) Dynamic analysis of the fraction of time spent by cells with LifeAct–GFP at their front obtained from data in **a**. Graphic shows mean and error bars correspond to s.e.m. (**c**) Correlation between the LifeAct–GFP front/back ratio and instantaneous speed values from DCs migrating in micro-channels obtained from data shown in **a**. (**d**) Mean instantaneous speed of WT or tamoxifen-induced Arpc2KO DCs migrating in micro-channels ($n = 308$, 255, 284 and 209 cells for iWT, LPS WT, iArpc2KO and LPS Arpc2KO respectively). One representative experiment out of three is shown. (**e**) Spinning-disc images (×100) of Arpc2 WT (TomatoFP$^+$) or KO (GFP$^+$) iDCs migrating in micro-channels. (**f**) Cortical LifeAct–GFP signal of control or CK666-treated iDCs migrating in micro-channels. (**g**) Quantification of fluorescent ovalbumin uptake in iDCs derived from WT and tamoxifen-induced Arpc2KO DCs migrating in micro-channels ($n = 36$ and 37 cells for Arpc2WT and Arpc2KO respectively). One representative experiment out of two is shown. (**h**) Immunofluorescence analysis of Arp2 in iDCs migrating in micro-channels analysed using a spinning-disc microscope (×100). The overlay shows LifeAct–GFP (green), Arp2 immunoreactivity (red) and DAPI staining (blue).The Mann–Whitney test was applied for all statistical analyses. In the box plots of **d** and **g** the bars include 90% of the points, the centre corresponds to the median and the box contains 75% of the data.

same result was observed when using siRNA targeting Arpc4, one of the actin-binding subunits of the Arp2/3 complex[26] (Fig. 3a,b and Supplementary Fig. 3a). Strikingly, high-resolution imaging showed that CK666 treatment led to the accumulation of cortical actin filaments at the rear of iDCs (Fig. 3f), which were organized in a similar structure to the one observed in LPS-DCs. None of these treatments significantly affected LifeAct–GFP distribution in LPS-DCs, showing that F-actin concentrates at their back independently of Arp2/3 (Supplementary Fig. 3b,c). Changes in F-actin distribution were not due to DC maturation induced by Arp2/3 inhibition (Supplementary Fig. 3d). Hence, Arp2/3 is required to maintain the pool of F-actin at the front of iDCs but is dispensable for F-actin enrichment at the rear of LPS-DCs.

Strikingly, Arp2/3 inhibition in iDCs not only decreased the accumulation of F-actin at their front but also increased their speed (Fig. 3c and Supplementary Fig. 3e). Although unexpected, this result is consistent with LPS-DCs lacking Arp2/3-dependent actin at the cell front and migrating faster than iDCs. A similar increase in cell velocity was observed in conditional Arpc2KO iDCs, which migrated as fast as LPS-DCs (Fig. 3d and Supplementary Fig. 3f). The speed of Arpc2KO DCs was also significantly increased in under-agarose migration assays (Supplementary Fig. 3g). This was independent of DC maturation (Supplementary Fig. 3h). Thus, unlike protrusion-based locomotion[21–23], the Arp2/3-dependent pool of F-actin present at the front of iDCs limits their migration.

Noticeably, the front of Arpc2KO iDCs contained small vesicles instead of large macropinosomes (Fig. 3e and Supplementary Fig. 3i), indicating that Arp2/3-dependent F-actin might be rather required for antigen macropinocytosis than for iDC locomotion. Accordingly, the amount of extracellular fluid enclosed in these vesicles was diminished when Arp2/3 was inhibited or knocked out (Fig. 3g and Supplementary Fig. 3j). Antigen uptake was also decreased

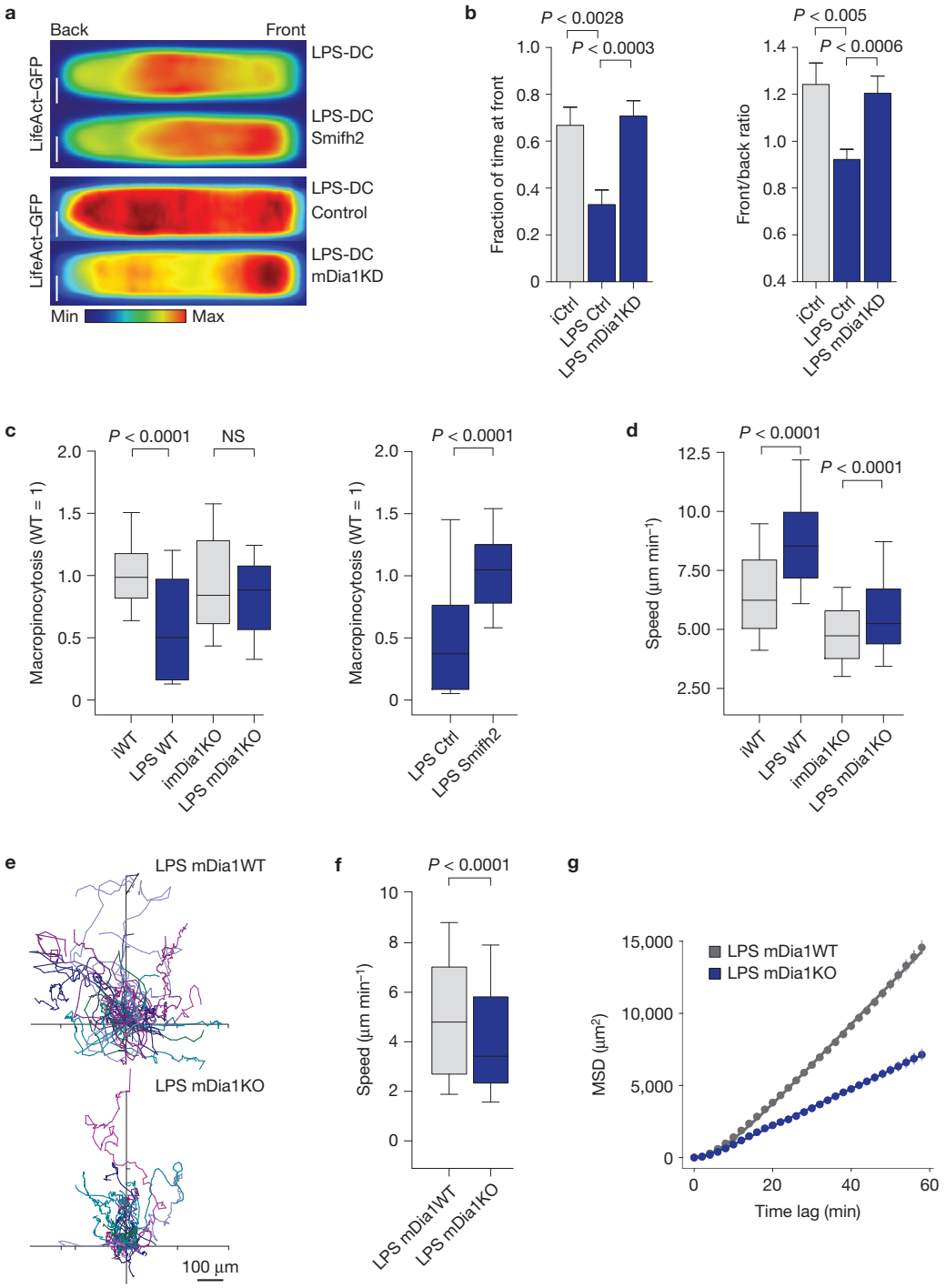

Figure 4 mDia1 is required for fast DC migration. (**a**,**b**) Analysis of DC migration in micro-channels. (**a**) Mean LifeAct–GFP distribution obtained from LPS-DCs migrating in micro-channels and treated with the formin inhibitor Smifh2 (25 µM) or silenced for mDia1. One representative experiment out of three is shown. Scale bars, 2.5 µm. (**b**) Dynamic analysis of the fraction of time spent by cells with LifeAct–GFP at their front obtained from data shown in **a** ($n = 21$, 22 and 31 for iCtrl, LPS Ctrl and LPS mDia1KD respectively). Graphic shows mean and error bars correspond to s.e.m. (**c**) Quantification of fluorescent ovalbumin uptake in DCs derived from WT and mDia1KO mice or treated with Smifh2 (25 µM) while migrating in micro-channels ($n = 33$, 36, 38, 45, 23 and 28 cells for WT, LPS DC, imDia1KO, LPS mDia1KO, LPS Ctrl and LPS Smifh2 respectively). One representative experiment out of two is shown. NS, not significant. (**d**) Mean instantaneous speed of control and mDia1KO DCs migrating in micro-channels ($n = 272$, 218, 192 and 310 cells for iWT, LPS WT, imDia1KO and LPS mDia1KO respectively). One representative experiment out of three is shown. (**e**–**g**) Analysis of DC migration under agarose. (**e**) Cell tracks of WT and mDia1KO LPS-DCs. Cells were imaged for 200 min. The starting point of each trajectory was translated to the origin of the plot. $n = 129$ and 69 cells for LPS mDia1WT and LPS mDia1KO respectively. One representative experiment out of three is shown. (**f**) Mean instantaneous speed obtained from data shown in **d**. (**g**) Mean square displacement (MSD) quantified from the data depicted in **e**. The Mann–Whitney test was applied for all statistical analyses. In the box plots of **c**,**d** and **f** the bars include 90% of the points, the centre corresponds to the median and the box contains 75% of the data.

in LPS-DCs, consistent with less actin accumulating at their front (Supplementary Fig. 3k). Immunofluorescence analysis showed that Arp2/3 was indeed enriched around macropinosomes at the front of iDCs (Fig. 3h). Density maps obtained from fixed cells highlighted that Arp2/3 exhibited a similar distribution in iDCs and LPS-DCs (Supplementary Fig. 3l). This observation suggests that the accumulation of F-actin at the back of LPS-DCs does not result from changes in Arp2/3 distribution. Together, our data indicate that antigen uptake—but not DC migration—requires Arp2/3.

mDia1-dependent actin nucleation at the cell rear controls fast DC migration

Arp2/3 inhibition or silencing had no major impact on actin distribution and migration of LPS-DCs, suggesting that the actin cables observed at their back result from alternative nucleating factors. We therefore investigated the possible involvement of formins, which nucleate non-branched actin filaments[27–29]. The broad formin inhibitor Smifh2 (ref. 30) induced the redistribution of actin from the back to the front of both iDCs and LPS-DCs (Fig. 4a and Supplementary Fig. 4a). This indicates that formin activity maintains F-actin at the DC rear. Among the 15 members of the formin family, mDia1 is known to be required for T-cell[31,32] and DC (ref. 33) migration from peripheral tissues to LNs. In addition, mDia1 is the main formin involved in nucleation of the bulk actin cortex[34]. Accordingly, analysis by immunofluorescence of mDia1 intracellular distribution showed that it was present all along the cortex in LPS-DCs (Supplementary Fig. 4b). As mDia1 staining required cell fixation with methanol, which did not preserve the predominant F-actin structure observed at the back of LPS-DCs, we could not observe whether mDia1 localized to it. Nonetheless, density maps showed that mDia1 localization followed F-actin distribution: whereas mDia1 was enriched at the front of iDCs, it increased at the back of LPS-DCs (Supplementary Fig. 4c). We therefore evaluated the specific contribution of mDia1 to LifeAct–GFP dynamics in migrating DCs. The pool of F-actin present at the rear of LPS-DCs was significantly reduced when silencing mDia1 (Fig. 4a and Supplementary Fig. 4d). In addition, the time spent by mDia1-silenced cells with F-actin concentrated at their front and their front/back F-actin ratio were increased (Fig. 4b). The effect of mDia1 was comparable to the one of Smifh2, suggesting that it is indeed the main formin involved. Of note, macropinocytosis was restored to levels comparable to the ones of iDCs in both mDia1KO and Smifh2-treated LPS-DCs, in agreement with F-actin accumulating at their front (Fig. 4c).

Knocking out the mDia1 gene[35] or inhibiting formins with Smifh2 reduced the migration speed and persistence of both iDCs and LPS-DCs (Fig. 4d and Supplementary Fig. 4e,f). However, the impact of mDia1 deficiency on cell speed was stronger in LPS-DCs. This result suggests that mDia1 is needed for fast DC migration and has therefore a greater impact on the speed of LPS-DCs, which predominantly migrate fast, than on iDCs, which alternate between fast and slow motility phases. Accordingly, we found that the highest speed reached by iDCs and LPS-DCs was significantly diminished in the absence of mDia1 (Supplementary Fig. 4g). In addition, under-agarose migration assays showed that mDia1-deficient LPS-DCs were slower and less efficient in space exploration as compared with wild-type cells (Fig. 4e–g). The migration defect of mDia1KO DCs was not due to impaired maturation (Supplementary Fig. 4h). Hence, unlike Arp2/3, mDia1 controls the maintenance of F-actin at the back of fast-moving DCs and is required for their persistent locomotion. Of note, inhibition of Arp2/3 in mDia1KO DCs had no effect on their migratory phenotype (Supplementary Fig. 4i). Thus, iDCs exhibit an mDia1-dependent F-actin pool at their rear needed for fast migration and an Arp2/3-dependent F-actin pool at their front that limits locomotion but is required for antigen uptake. In contrast, LPS-DCs predominantly exhibit mDia1-dependent F-actin at their back and therefore migrate faster and more persistently but do not efficiently take up extracellular material.

Actin nucleation at the front and back of DCs respectively relies on Cdc42 and RhoA

Our data show that inhibiting or knocking out Arp2/3 in iDCs is sufficient to recapitulate the phenotype of mature LPS-DCs in terms of migration and macropinocytosis, suggesting that LPS-induced DC maturation leads to the downregulation of Arp2/3 expression or activity. However, no change in the expression levels of Arp2/3 was observed on LPS treatment of DCs (Supplementary Figs 5a,b and 8a), implying that its actin-nucleation activity might rather be diminished in mature DCs. Downregulation of the small GTPase Cdc42, which activates Arp2/3 through the nucleation-promoting factor WASP (ref. 36), was shown to be responsible for reduced macropinocytosis in LPS-DCs (ref. 2). We therefore reasoned that down-modulation of Cdc42 activity might lead to reduced Arp2/3 activation and fast migration in mature DCs. To address this question, we used DCs generated from conditional Cdc42KO mice[37] or the Cdc42 inhibitor ML141. Cdc42KO and ML141-treated iDCs exhibited the same phenotype as Arp2/3-deficient DCs: they migrated as fast as LPS-DCs and spent less time with F-actin concentrated at their front (Fig. 5a–c and Supplementary Fig. 5c). As observed when inhibiting Arp2/3, inhibition of Cdc42 activity markedly decreased macropinocytosis in iDCs (Fig. 5d). No major effect of Cdc42 deficiency/inhibition was observed on F-actin distribution and migration of LPS-DCs (Fig. 5b,c). In sharp contrast, RhoAKO or RhoA-inhibited DCs exhibited a phenotype similar to the one of mDia1KO cells: their speed was decreased and, when treated with LPS, they accumulated F-actin at their front and internalized extracellular material by macropinocytosis (Fig. 5e–h). DC maturation was unaffected by both Cdc42 and RhoA deficiencies (Supplementary Fig. 5d). Therefore, downregulation of Cdc42 activity in mature LPS-DCs leads to decreased Arp2/3-mediated actin nucleation and macropinocytosis at their front. As a result of this, they adopt a fast migratory phenotype that relies on RhoA–mDia1-dependent actin nucleation.

mDia1 is required for chemotactic migration of mature DCs

In vivo, DCs increase their persistence when attracted to CCL21 gradients[10] on LVs. We therefore asked whether the mDia1-dependent migration increment observed in LPS-DCs affected their chemotactic migration (Supplementary Fig. 6a). Using collagen gels[13], we found that LPS-DCs but not iDCs—which do not express CCR7—migrated towards the CCL21 source (Supplementary Fig. 6b and Supplementary Video 4). Both, control and mDia1KO LPS-DCs expressed similar levels of surface CCR7 (Supplementary Fig. 6c) and sensed the direction of the gradient with similar efficiencies as shown by

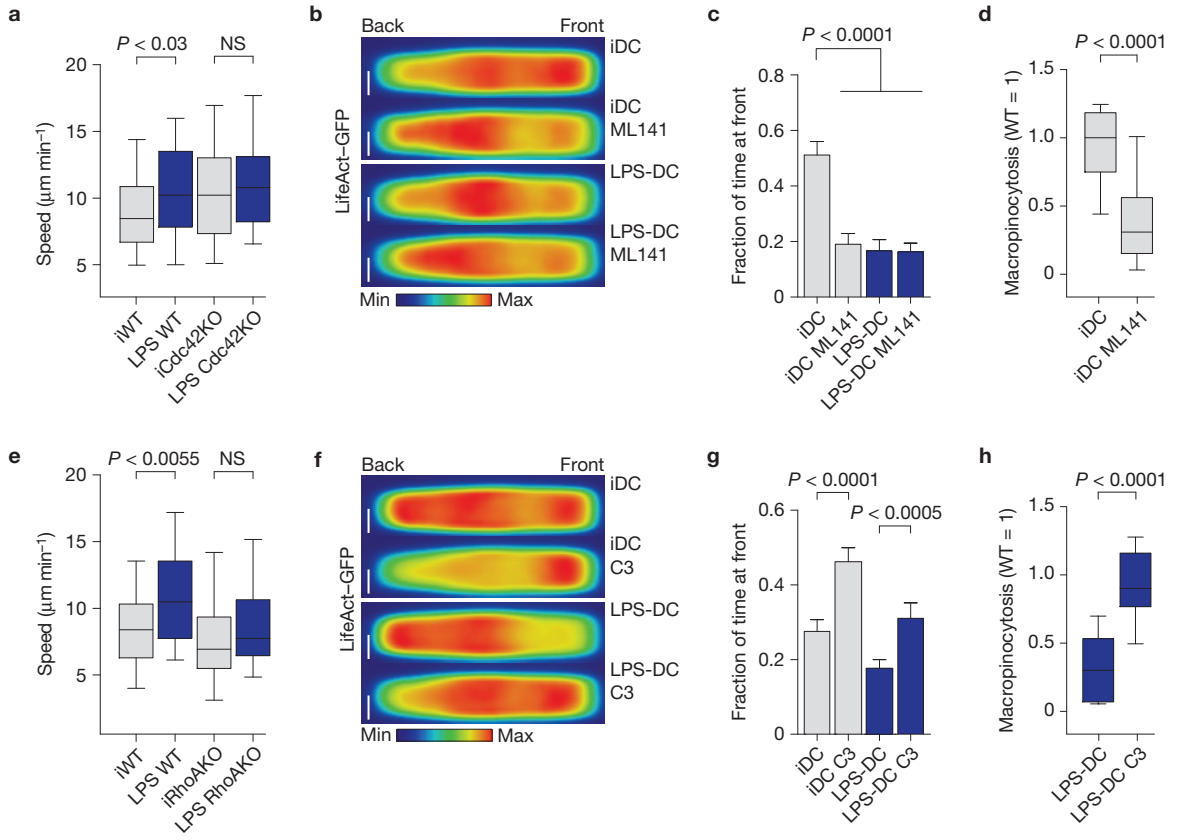

Figure 5 Cdc42 and RhoA respectively control the migration of iDCs and LPS-DCs. (**a**) Mean instantaneous speed of Cdc42WT and KO DCs migrating in micro-channels ($n=111$, 33, 129 and 110 cells for iWT, LPS WT, iCdc42KO and LPS Cdc42KO respectively). One representative experiment out of two is shown. NS, not significant. (**b**) Mean LifeAct–GFP distribution in DCs treated with the Cdc42 inhibitor ML141 (50 μM) ($n=25$, 32, 33 and 33 cells for iDC, iDC ML141, LPS-DC and LPS-DC ML141 respectively). One representative experiment out of two is shown. Scale bars, 2.5 μm. (**c**) Dynamic analysis of the fraction of time spent by cells with LifeAct–GFP at their front obtained from data in **b**. Graphic shows mean and error bars correspond to s.e.m. (**d**) Quantification of fluorescent ovalbumin uptake in iDCs treated with ML141 (50 μM) while migrating in micro-channels ($n=15$ and 29 cells for iDC and iDC ML141 respectively). One representative experiment out of two is shown. (**e**) Mean instantaneous speed of WT and RhoAKO DCs migrating in micro-channels ($n=86$, 102, 45 and 109 cells for iWT, LPS-DC, iRhoAKO and LPS RhoAKO respectively). One representative experiment out of two is shown. NS, not significant. (**f**) Mean LifeAct–GFP distribution in DCs migrating in micro-channels and treated with the RhoA inhibitor C3 convertase (1 μg ml^{-1}) ($n=42$, 97, 34 and 59 cells for iDC, iDC C3, LPS-DC and LPS-DC C3 respectively). One representative experiment out of two is shown. Scale bars, 2.5 μm. (**g**) Dynamic analysis of the fraction of time spent by cells with LifeAct–GFP at their front obtained from data shown in **f**. Graphic shows mean and error bars correspond to s.e.m. (**h**) Quantification of fluorescent ovalbumin uptake in iDCs treated with C3 convertase (1 μg ml^{-1}) while migrating in micro-channels ($n=23$ and 28 cells for LPS-DC and LPS-DC C3 respectively). One representative experiment out of two is shown. The Mann–Whitney test was applied for all statistical analyses. In the box plots of **a**,**d**,**e** and **h** the bars include 90% of the points, the centre corresponds to the median and the box contains 75% of the data.

the distribution of their trajectories (Fig. 6a,b and Supplementary Video 5). However, individual cell tracks were shorter in mDia1KO LPS-DCs (Fig. 6b). Further analysis highlighted that wild-type LPS-DCs increased both their speed and persistence while approaching the chemokine source (Fig. 6c,d and Supplementary Fig. 6b). No such increase was observed in the absence of chemokine (Fig. 6e). This process referred to as orthotaxis has been proposed as a mechanism by which chemokine gradients increase the efficiency of directional migration[38]. Strikingly, orthotaxis was impaired in mDia1KO LPS-DCs (Fig. 6c,d and Supplementary Fig. 7a–c). Hence, mDia1 not only increases the speed of LPS-DCs but is further required for their chemotactic migration, suggesting that the increment of DC migration induced on LPS sensing impacts chemokine-driven locomotion.

We found that Arp2/3 inhibition had no impact on directionality, speed or persistence of LPS-DCs migrating in CCL21 gradients (Fig. 6f,g), consistent with our result showing that LPS-DCs are insensitive to Arp2/3 inhibition in terms of F-actin distribution and migration speed. We conclude that mDia1 but not Arp2/3 controls the chemotactic movement of LPS-DCs in collagen gels. Surprisingly, none of them affected directionality, suggesting that alternative mechanisms might account for the regulation of cell orientation along CCL21 gradients.

mDia1 is required for arrival of LPS-DCs to lymphatic vessels and lymph nodes

So far, we have shown that mDia1 plays a key role in the TLR4–MyD88-dependent transition from slow to fast and persistent DC locomotion and is required for their chemotaxis *in vitro*. To evaluate whether this equally applies in tissues, we analysed the migration of LPS-DCs towards LVs in explanted ear epidermal

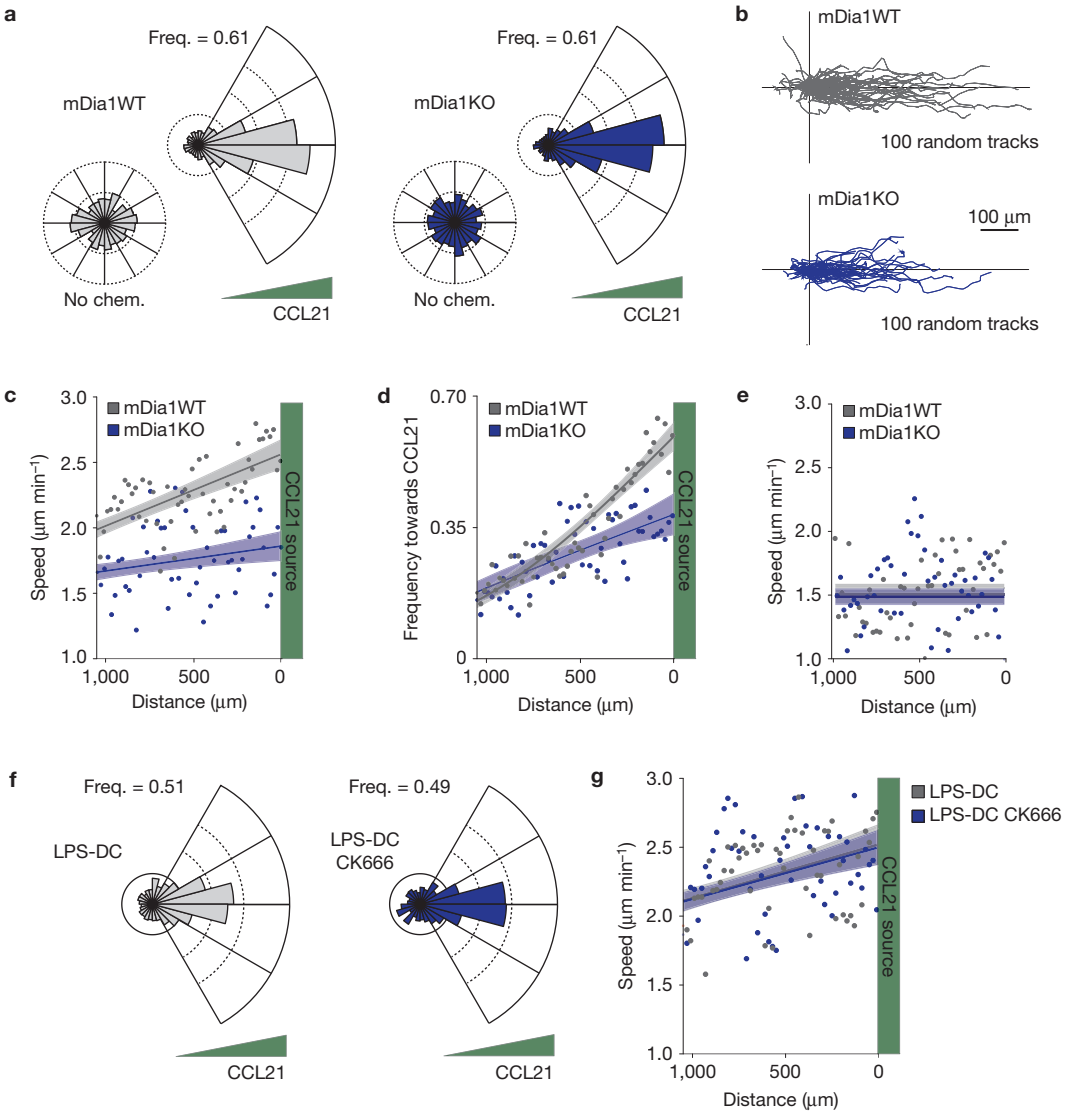

Figure 6 mDia1 is required for the chemotactic response of mature DCs. (**a**–**g**) Chemotactic response of LPS-DCs embedded in a collagen gel containing a CCL21 gradient. Frequency (Freq.) was calculated in 500 random tracks because of oversampling. One representative experiment out of three is shown. (**a**) Directionality of trajectories during the chemotactic response or in the absence of chemokines (No chem.) of mDia1WT and mDia1KO LPS-DCs. (**b**) One hundred random tracks of LPS-DCs undergoing chemotaxis. (**c**) Mean speed of LPS-DCs represented as a function of the distance to the CCL21 source. (**d**) Frequency of movement of LPS-DCs in the direction of the gradient represented as a function of the distance to the CCL21 source. (**e**) Speed of LPS-DCs in the absence of CCL21. (**f**) Directionality of trajectories of LPS-DCs treated or not with CK666 (25 µM) during chemotactic response as in **a**. (**g**) Mean speed of CK666-treated LPS-DCs represented as a function of the distance to the CCL21 source. Trend lines with 95% confidence interval are shown in **c**,**d**,**e** and **g**.

sheets[39] (Supplementary Fig. 7d). mDia1KO mature DCs exhibited decreased motility as compared with wild-type LPS-DCs when moving in the same tissue (Fig. 7a,b). Consequently, their ability to explore the space was reduced as depicted by their diminished mean square displacement (Fig. 7c). Analysis of cell tracks showed that control LPS-DCs exhibited a persistent random walk migration mode biased towards LVs whereas mDia1KO cells followed an isotropic diffusive pattern of locomotion (Fig. 7c and Supplementary Fig. 7e). As observed in collagen gels, wild-type LPS-DCs increased their speed and directionality while approaching LVs (Fig. 7d,e). In contrast, mDia1KO LPS-DCs migrated randomly, did not exhibit any significant directional bias towards LVs (Fig. 7b–e) and barely reached these vessels (Fig. 7f). Migration of Arpc2KO LPS-DCs to LVs was not altered (Fig. 7g), in agreement with these cells exhibiting wild-type migratory and chemotactic phenotypes *in vitro*. Hence, mDia1 is required for orthotaxis of mature DCs *in vivo*.

The absence of mDia1 had a stronger impact on DC migration in the skin than in collagen gels, suggesting that a persistent random walk is particularly critical for DC migration along chemokine gradients in the complex geometry of tissues. Consistent with these results, we found that the arrival of mDia1KO LPS-DCs to LNs on transfer into the footpad of wild-type recipients was also significantly decreased[33] (Fig. 7h and Supplementary Fig. 7f). We conclude that mature DCs must harbour an mDia1-dependent fast and persistent migration

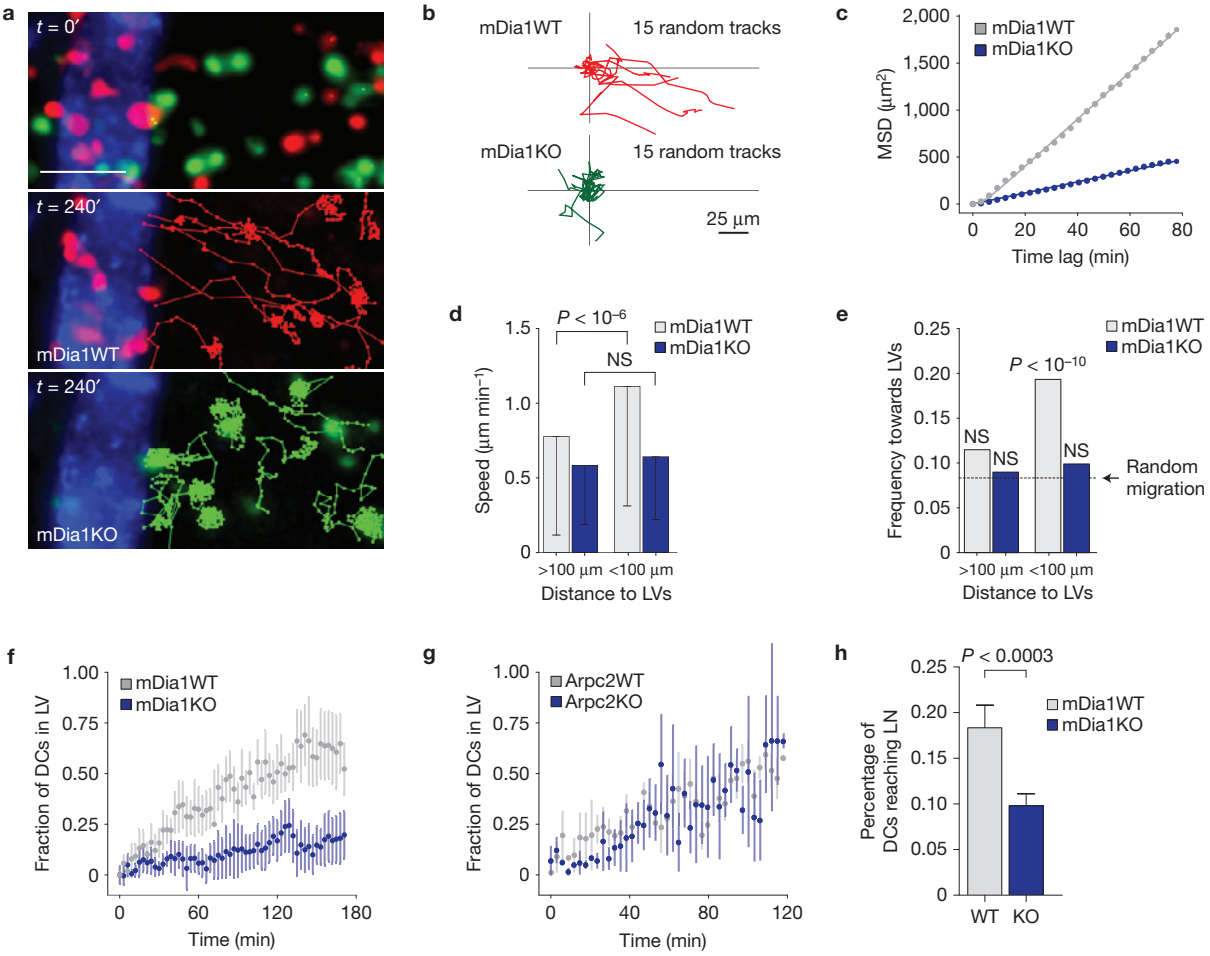

Figure 7 mDia1 is required for migration of mature DCs to LVs and LNs *in vivo*. (**a**–**f**) Migration of LPS-DCs in mouse ear explants ($n = 50$ and 59 cells for LPS mDia1WT and LPS mDia1KO respectively). Pool of three independent experiments. (**a**) Cell tracks from mDia1WT (red) or mDia1KO (green) LPS-DCs migrating in the proximity of LVs (stained with LYVE-1; blue) in a mouse epidermal ear sheet. Scale bar, 50 μm. (**b**) Fifteen randomly selected tracks of mDia1WT and mDia1KO LPS-DCs migrating in an epidermal ear sheet as shown in **a**. (**c**) Mean square displacement (MSD) of mDia1WT and mDia1KO LPS-DCs migrating in an epidermal ear sheet. The MSD curve of mDia1KO cells is fitted with a simple linear expression, reflecting the isotropic random walk-like behaviour of this population. Instead, the MSD curve of mDia1WT cells showed a first nonlinear increase followed by a linear dependency, as expected for biased persistent random walk and is fitted with Fürth's formula. (**d**) Mean instantaneous speed of LPS-DCs represented as a function of the distance to the closest LV. Error bars correspond to s.d. (**e**) Frequency of cell movements in the direction of the closest LV. Statistical analysis was performed comparing values with respect to random migration from data shown in **d**. Student's *t*-test and Pearson's χ^2 test were applied in **d** and **e**, respectively. NS, not significant. (**f**,**g**) Fraction of DCs that reach LVs plotted as a function of time. Error bars correspond to s.e.m. (**h**) *In vivo* migration of LPS-DCs to LNs. The number of mDia1WT and mDia1KO DCs that arrive at popliteal LNs after injection in the footpad was analysed by fluorescence-activated cell sorting after 16 h ($n = 9$ mice per condition pooled from three independent experiments). The Mann–Whitney test was applied for statistical analysis in **h**. Graphic shows mean and error bars correspond to s.e.m.

mode to follow chemotactic CCL21 gradients in peripheral tissues and reach LNs *in vivo*.

DISCUSSION

We here show that sensing of the microbial compound LPS increases the migration speed and persistence of DCs, a process required for efficient chemotaxis to LVs and homing to LNs. This relies on cell-intrinsic changes in F-actin distribution that result from the differential use of actin-nucleating machineries in immature and mature DCs. Thus, regulation of the core locomotion machinery on activation of the LPS–TLR4–MyD88 axis helps tune the migratory behaviour of immature and mature DCs according to their distinct functional requirements: environment sampling and antigen uptake for immature DCs and fast migration to LNs for mature DCs. Whether other microbial or inflammatory stimuli equally affect actin dynamics and chemotaxis of DCs shall now be addressed.

We found that Arp2/3 nucleates branched actin at the front of iDCs, which harbour a speed-fluctuating behaviour[15]. This F-actin pool compromised cell migration but promoted antigen capture by macropinocytosis. In mature LPS-DCs, which exhibited a poor macropinocytic capacity but migrated faster and more persistently than iDCs, F-actin was predominantly observed at the cell rear and relied on mDia1 and RhoA activities. Consistently, the levels of phosphorylated myosin II light chain, which are regulated by RhoA, were increased in LPS-DCs as compared with iDCs (Supplementary Figs 7g and 8b). These data suggest that mDia1-dependent actin

nucleation is used in both LPS-DCs and iDCs for locomotion, whereas Arp2/3-dependent actin nucleation is used by iDCs to integrate antigen uptake to cell migration. On LPS sensing, actin nucleation at the front by Arp2/3 is strongly reduced, allowing mature DCs to adopt a fast and directional migration mode. Strikingly, Cdc42, whose activity was shown to be downregulated after treatment of DCs with LPS (ref. 2), limited iDC migration but promoted macropinocytosis, as did Arp2/3. This result strongly suggests that Cdc42 inactivation is responsible for the loss of Arp2/3 activity in LPS-DCs.

Surprisingly, the presence of an Arp2/3-dependent F-actin pool at the front of iDCs reduced their motility. This result was unexpected given that Arp2/3 is described as promoting forward locomotion by generating protrusions at the cell front[21–23], showing that the branched actin network plays different roles in cell migration based on the environment geometry and the cell type. On 2D surfaces, cells exert forces parallel to the substratum owing to the presence of Arp2/3 at the cell front. In contrast, in confined environments, motility results from pushing forces exerted perpendicularly to the substratum[40]. Our data suggest that these forces are generated by formins and not by Arp2/3, consistent with findings made in HL-60 cells migrating in micro-channels[41]. Arp2/3 at the front of iDCs might impair migration by promoting the formation of macropinosomes, as suggested by results highlighting that migration and macropinocytosis are antagonistic in *Dictyostelium* and iDCs (refs 20,42). In iDCs, this antagonism results from the recruitment of myosin II to macropinosomes, which disrupts the back-to-front gradient of the motor protein and leads to speed reduction[20]. The present study therefore suggests that myosin II recruitment to the front of iDCs might rely on local Arp2/3 activity. Whether the presence of both mDia1 and Arp2/3 at the front of iDCs is needed to generate anti-polar actin filaments to which myosin II could bind should be explored.

We found that mature LPS-DCs must adopt an mDia1-dependent fast and persistent migration mode to efficiently migrate along CCL21 gradients. Of note, although Arp2/3 did not regulate chemotaxis of mature DCs, we cannot exclude that Arp2/3-dependent protrusion at the cell front is required for chemotaxis of iDCs. Remarkably, the impact of mDia1 deficiency on chemotaxis was more severe in epidermal ear sheets than in collagen gels. This was not due to impaired Clec2 expression in mDia1-deficient DCs (Supplementary Fig. 6b), a surface lectin that binds to podoplanin present on endothelial cells and is required for DC recruitment to LVs (ref. 11). This difference might rather result from the complex architecture of tissues that may locally modify the linearity of CCL21 gradients so that mature DCs must harbour a persistent random walk locomotion mode to not 'get distracted' and maintain their directionality. In that context, the presence of F-actin at the front of mDia1KO DCs could favour the sensing of such local gradient modifications, reducing their directional memory. Future experiments aimed at analysing the requirement for mDia1 in DCs migrating in irregular chemokine gradients *ex vivo* shall help address this hypothesis. □

METHODS

Methods and any associated references are available in the online version of the paper.

Note: Supplementary Information is available in the online version of the paper

ACKNOWLEDGEMENTS

The authors thank the PICT IBiSA platform at Institut Curie (CNRS UMR144, especially V. Fraisier) and the Institut Curie animal facility. P.V. thanks B. Goic for support, patience and critical reading of the manuscript. P.V. was supported by fellowships from Region Ile-de-France, Fondation pour la Recherche Médicale (FRM) and Institut Curie. M.B. and M.C. benefited from fellowships from Association pour la Recherche contre le Cancer and FRM respectively. S.M.K.-G. and A.S.A. were supported by the Grand Rapids Community and the Lunn Hope Foundations, the Van Andel Endowment, and the Purple Community. T.B. was supported by DFG SFB 1054-B03 and SFB 914-A06. This work was financially supported by grants from: the City of Paris, the European Research Council and the DCBIOL Labex (ANR-10-IDEX-0001-02-PSL* and ANR-11-LABX-0043) to A.-M.L.-D. (Strapacemi 243103) and the Association Nationale pour la Recherche (ANR-09-PIRI-0027-PCVI) and the InnaBiosanté foundation (Micemico) to A.-M.L.-D., M.P. and R.V.

AUTHOR CONTRIBUTIONS

P.V. designed, performed and analysed most experiments, prepared all manuscript figures and strongly participated in article writing and project conception. P.M. conceived and performed trajectory analyses and modelling. M.B. set up and assisted with siRNA-mediated silencing, qPCR and macropinocytosis experiments. P.J.S. and H.-R.T. assisted in optimizing micro-channel experiments. P.J.S. further helped P.V. with article revision. P.P. built the program for actin distribution analysis in migrating DCs. M.M. created all codes for quantification of macropinocytosis and arrival of DCs to LVs. M.C. carried out the initial observation of increased migration speed and decreased antigen uptake in CK666-treated iDCs. E.T. helped with micro-fabrication. D.L. assisted P.V. with immunofluorescence experiments. D.O. performed immunoblots. M.R. set up collagen gel experiments. T.B. generated and provided Cdc42 and RhoA conditional KO mice. S.M.K.-G. and A.S.A. generated and provided mDia1KO mice. S.X., P.S. and R.L. generated and provided Arpc2 conditional KO mice. R.V. conceived and performed migration modelling. M.P. and A.-M.L.-D. designed the overall research and wrote the manuscript.

COMPETING FINANCIAL INTERESTS

The authors declare no competing financial interests.

Published online at http://dx.doi.org/10.1038/ncb3284
Reprints and permissions information is available online at www.nature.com/reprints

1. Mellman, I. & Steinman, R. M. Dendritic cells: specialized and regulated antigen processing machines. *Cell* **106,** 255–258 (2001).
2. Garrett, W. S. *et al.* Developmental control of endocytosis in dendritic cells by Cdc42. *Cell* **102,** 325–334 (2000).
3. Cella, M., Sallusto, F. & Lanzavecchia, A. Origin, maturation and antigen presenting function of dendritic cells. *Curr. Opin. Immunol.* **9,** 10–16 (1997).
4. Sallusto, F., Cella, M., Danieli, C. & Lanzavecchia, A. Dendritic cells use macropinocytosis and the mannose receptor to concentrate macromolecules in the major histocompatibility complex class II compartment: downregulation by cytokines and bacterial products. *J. Exp. Med.* **182,** 389–400 (1995).
5. Farache, J. *et al.* Luminal bacteria recruit CD103+ dendritic cells into the intestinal epithelium to sample bacterial antigens for presentation. *Immunity* **38,** 581–595 (2013).
6. Ng, L. G. *et al.* Migratory dermal dendritic cells act as rapid sensors of protozoan parasites. *PLoS Pathog.* **4,** e1000222 (2008).
7. Turley, S. J. *et al.* Transport of peptide-MHC class II complexes in developing dendritic cells. *Science* **288,** 522–527 (2000).
8. Martln-Fontecha, A. *et al.* Regulation of dendritic cell migration to the draining lymph node: impact on T lymphocyte traffic and priming. *J. Exp. Med.* **198,** 615–621 (2003).
9. Tal, O. *et al.* DC mobilization from the skin requires docking to immobilized CCL21 on lymphatic endothelium and intralymphatic crawling. *J. Exp. Med.* **208,** 2141–2153 (2011).
10. Weber, M. *et al.* Interstitial dendritic cell guidance by haptotactic chemokine gradients. *Science* **339,** 328–332 (2013).
11. Acton, S. E. *et al.* Podoplanin-rich stromal networks induce dendritic cell motility via activation of the C-type lectin receptor CLEC-2. *Immunity* **37,** 276–289 (2012).
12. Pollard, T. D. & Borisy, G. G. Cellular motility driven by assembly and disassembly of actin filaments. *Cell* **112,** 453–465 (2003).
13. Lammermann, T. *et al.* Rapid leukocyte migration by integrin-independent flowing and squeezing. *Nature* **453,** 51–55 (2008).
14. Renkawitz, J. *et al.* Adaptive force transmission in amoeboid cell migration. *Nat. Cell Biol.* **11,** 1438–1443 (2009).
15. Faure-André, G. *et al.* Regulation of dendritic cell migration by CD74, the MHC class II-associated invariant chain. *Science* **322,** 1705–1710 (2008).
16. Heuzé, M. L. *et al.* Migration of dendritic cells: physical principles, molecular mechanisms, and functional implications. *Immunol. Rev.* **256,** 240–254 (2013).
17. Vargas, P., Terriac, E., Lennon-Dumenil, A. M. & Piel, M. Study of cell migration in microfabricated channels. *J. Vis. Exp.* **84,** e51099 (2014).

18. Barton, G. M. & Medzhitov, R. Toll-like receptor signaling pathways. *Science* **300,** 1524–1525 (2003).
19. Heit, B. & Kubes, P. Measuring chemotaxis and chemokinesis: the under-agarose cell migration assay. *Sci. STKE* **2003,** PL5 (2003).
20. Chabaud, M. *et al.* Cell migration and antigen capture are antagonistic processes coupled by myosin II in dendritic cells. *Nat. Commun.* **6,** 7526 (2015).
21. Bailly, M. *et al.* The F-actin side binding activity of the Arp2/3 complex is essential for actin nucleation and lamellipod extension. *Curr. Biol.* **11,** 620–625 (2001).
22. Blanchoin, L. *et al.* Direct observation of dendritic actin filament networks nucleated by Arp2/3 complex and WASP/Scar proteins. *Nature* **404,** 1007–1011 (2000).
23. Svitkina, T. M. & Borisy, G. G. Arp2/3 complex and actin depolymerizing factor/cofilin in dendritic organization and treadmilling of actin filament array in lamellipodia. *J. Cell Biol.* **145,** 1009–1026 (1999).
24. Koivusalo, M. *et al.* Amiloride inhibits macropinocytosis by lowering submembranous pH and preventing Rac1 and Cdc42 signaling. *J. Cell Biol.* **188,** 547–563 (2010).
25. Nolen, B. J. *et al.* Characterization of two classes of small molecule inhibitors of Arp2/3 complex. *Nature* **460,** 1031–1034 (2009).
26. Goley, E. D. *et al.* An actin-filament-binding interface on the Arp2/3 complex is critical for nucleation and branch stability. *Proc. Natl Acad. Sci. USA* **107,** 8159–8164 (2010).
27. Higashida, C. *et al.* Actin polymerization-driven molecular movement of mDia1 in living cells. *Science* **303,** 2007–2010 (2004).
28. Li, F. & Higgs, H. N. The mouse Formin mDia1 is a potent actin nucleation factor regulated by autoinhibition. *Curr. Biol.* **13,** 1335–1340 (2003).
29. Pruyne, D. *et al.* Role of formins in actin assembly: nucleation and barbed-end association. *Science* **297,** 612–615 (2002).
30. Rizvi, S. A. *et al.* Identification and characterization of a small molecule inhibitor of formin-mediated actin assembly. *Chem. Biol.* **16,** 1158–1168 (2009).
31. Eisenmann, K. M. *et al.* T cell responses in mammalian diaphanous-related formin mDia1 knock-out mice. *J. Biol. Chem.* **282,** 25152–25158 (2007).
32. Sakata, D. *et al.* Impaired T lymphocyte trafficking in mice deficient in an actin-nucleating protein, mDia1. *J. Exp. Med.* **204,** 2031–2038 (2007).
33. Tanizaki, H. *et al.* Rho-mDia1 pathway is required for adhesion, migration, and T-cell stimulation in dendritic cells. *Blood* **116,** 5875–5884 (2010).
34. Bovellan, M. *et al.* Cellular control of cortical actin nucleation. *Curr. Biol.* **24,** 1628–1635 (2014).
35. Peng, J., Wallar, B. J., Flanders, A., Swiatek, P. J. & Alberts, A. S. Disruption of the Diaphanous-related formin *Drf1* gene encoding mDia1 reveals a role for Drf3 as an effector for Cdc42. *Curr. Biol.* **13,** 534–545 (2003).
36. Machesky, L. M. *et al.* Scar, a WASp-related protein, activates nucleation of actin filaments by the Arp2/3 complex. *Proc. Natl Acad. Sci. USA* **96,** 3739–3744 (1999).
37. Luckashenak, N., Wahe, A., Breit, K., Brakebusch, C. & Brocker, T. Rho-family GTPase Cdc42 controls migration of Langerhans cells *in vivo*. *J. Immunol.* **190,** 27–35 (2013).
38. Sarris, M. *et al.* Inflammatory chemokines direct and restrict leukocyte migration within live tissues as glycan-bound gradients. *Curr. Biol.* **22,** 2375–2382 (2012).
39. Weber, M. & Sixt, M. Live cell imaging of chemotactic dendritic cell migration in explanted mouse ear preparations. *Methods Mol. Biol.* **1013,** 215–226 (2013).
40. Hawkins, R. J. *et al.* Pushing off the walls: a mechanism of cell motility in confinement. *Phys. Rev. Lett.* **102,** 058103 (2009).
41. Wilson, K. *et al.* Mechanisms of leading edge protrusion in interstitial migration. *Nat. Commun.* **4,** 2896 (2013).
42. Veltman, D. M. *et al.* PIP_3-dependent macropinocytosis is incompatible with chemotaxis. *J. Cell Biol.* **204,** 497–505 (2014).

DOI: 10.1038/ncb3284

METHODS

Cells. Mouse bone marrow-derived dendritic cells (BMDCs) were obtained by culturing bone marrow precursors for 10–12 days in IMDM medium containing FCS (10%), glutamine (20 mM), penicillin–streptomycin (100 U ml^{-1}), 2-ME (50 μM) and further supplemented with granulocyte-macrophage colony-stimulating factor (50 ng ml^{-1})-containing supernatant obtained from transfected J558 cells, as previously described[15]. iDCs were obtained by gentle recovery of semi-adherent cells from culture dishes. Mature DCs were obtained by treating iDCs with LPS (100 ng ml^{-1}) for 30 min and washing 3 times with complete medium. LPS-DC migration was recorded between 6 and 16 h post LPS treatment.

BMDCs and mice. LifeAct–GFP and CCR7KO BMDCs were originated from precursors purified from LifeAct–GFP and CCR7KO mice, and were a gift from M. Sixt (IST, Austria)[43,44]. mDia1KO BMDCs were obtained from precursors purified from mDia1KO mice that were generated in A.S.A.'s laboratory (Van Andel Institute)[35]. MyD88KO BMDCs were generated from precursors purified from MyD88KO mice (B6.129-MyD88 tm1*) and obtained from CDTA. Arpc2KO BMDCs were differentiated from precursors obtained from conditional tamoxifen-inducible Arpc2KO mice that were generated as follows: ARPC2FRT/LoxP mice were crossed to FLPeR mice to generate ARPC2 Loxp/+ animals in which the LacZ and neomycin genes had been deleted. ARPC2 Loxp/+ mice were crossed to EsrCre mice to generate ARPC2Loxp/+ EsrCre mice. These animals were crossed to Rosa26-targeted mice containing membrane-targeted tdTomato and membrane-targeted EGFP (mT/mG) reporter genes (Jackson Laboratory) to generate ARPC2Loxp/Loxp CreER mTmG mice. In these animals, tamoxifen-inducible Cre expression triggers both the depletion of Arpc2 and the exchange between tdTomato and GFP reporters, allowing the identification of recombined cells as GFP-positive[45]. This system was used to deplete Arpc2 *in vitro* from BMDC cultures by adding tamoxifen to bone marrow cultures from day 2–8. BMDCs KO for Cdc42 and RhoAKO were generated from mice obtained from T.B's laboratory. Cdc42KO animals were produced as previously described[37]. RhoAKO mice were generated following the same procedure as Cdc42KO mice. All animals are on a C57BL/B6 background and the corresponding breeding controls were systematically used. The experiments were performed on 6–8-week-old male or female mice. For animal care, we strictly followed the European and French National Regulation for the Protection of Vertebrate Animals used for Experimental and other Scientific Purposes (Directive 2010/63; French Decree 2013-118). The present experiments, which used mouse strains exhibiting non-harmful phenotypes, did not require a project authorization and benefited from guidance of the Animal Welfare Body, Research Centre, Institut Curie.

Antibodies and reagents. The following antibodies were used for immunofluorescence (IF) and immunoblot (western blot, WB) experiments: anti-Arpc2 (Millipore, 07-227, WB 1:500), -Arpc4 (Abcam, ab110770, WB 1:500), -Arp2 (Abcam, ab47654, IF 1:50), -Arp3 (Sigma, A5979, WB 1:500), -mDia1 (BD, 610849, IF 1:50, WB 1:200), -GFP (Sigma, GSN149, IF 1:100) and -tubulin (Serotec, MCA77G, WB 1:2,000). For FACS analysis anti-CD11c (HL3, 1:200), -CD86 (GL1, 1:200) and -CD40 (HM40-3, 1:200) were used (BD Biosciences). CCR7 expression was analysed by sequential incubation of DCs with mouse CCL19-Fc (eBioscience, 1:200) and a secondary anti-Fc antibody (Life Technologies, 1:400). To image DCs in micro-channels, we used Ovalbumin AlexaFluor-647 (0.4 mg ml^{-1}), and Hoechst 33342 (200 ng ml^{-1}) (Life Technologies). Pertussis toxin, CK666, Smifh2 and ML141 were obtained from Tocris Bioscience. Cell permeant C3 transferase was obtained from Cytoskeleton. BMDCs were activated using LPS from *Salmonella enterica* serotype typhimurium (Sigma).

Preparation of micro-channels. Micro-channels were prepared as described previously[15,17]. Briefly, polydimethylsiloxane (PDMS) (GE Silicones) was used. Their surface was coated with 10 μg ml^{-1} bovine plasma fibronectin (Sigma) for 1 h and then washed 3 times with PBS before introduction of cells in complete medium.

Velocity measurements in micro-channels. Migrating cells were imaged for 16 h on an epifluorescence video-microscope Nikon TiE microscope equipped with a cooled CCD (charge-coupled device) camera (HQ2, Photometrics) with a ×10 objective. A frequency of acquisition of 1 image per 2 min of transmission phase was used. Kymographs of the migrating cells were generated by subtracting from each frame the mean projection of the whole movie, generating clear objects in a dark background that were analysed using a custom program as described previously[15].

Under-agarose assay. Under-agarose migration was performed as described previously[19]. Briefly, a glass Petri dish was filled with 2 ml of 1.2% warm ultrapure agarose (Gibco) prepared in phenol red-free HBSS (Gibco). After polymerization at 37 °C a small hole was introduced at the centre of the agarose in which Hoechst 33342-stained DCs were loaded similarly to micro-channels experiments. DCs migrating between the agarose and the glass were imaged at ×10 for several hours, tracked following their nucleus and analysed using custom software.

siRNA silencing in BMDCs. BMDCs were transfected with siRNA specific for Arpc4 or mDia1 using the Amaxa mouse Dendritic Cell Nucleofector Kit (Lonza). Briefly, 2×10^6 BMDCs collected at day 7 of differentiation were transfected in 100 μl of Amaxa solution containing 10 μM of siRNA (all-star control or target specific). Nucleofected cells were further cultured for 48–72 h in BMDC medium. To test for specific depletion, 4 different siRNAs were tested in a first approach. Two of them were chosen on the basis of their capacity to deplete the corresponding target. LifeAct–GFP localization was evaluated for both siRNAs, but only the one with the highest depletion was chosen to show the data in the article. For mDia1 the siRNAs were obtained from Qiagen (Cat. no. GS13367, Product no. 1027416) and siRNA SI02686390 and SI02666706 were chosen. For Arpc4 the siRNAs were also obtained from Qiagen (Cat. no. GS68089, Product no. 1027416) and siRNA SI05382601 and SI00904141 were chosen.

qPCR. RNA extraction was performed using NucleoSpin RNA (Macherey-Nagel), according to the manufacturer's protocol. cDNA was obtained with the SuperScriptVILO cDNA synthesis kit (Life technologies), according to the manufacturer's protocol, starting from 1 μg of RNA. Quantitative PCR experiments were done with the Lightcycler 480 (Roche) using the Taqman Gene expression assay (Applied Biosystem) with the following primers: Mm01184552_m1 for Arpc4, Mm00492170_m1 for mDia1 and Mm99999915_g1 for GAPDH as a control.

Tamoxifen-induced depletion of Arpc2 gene. At day 4 of culture, bone marrow cells were seeded at 0.5×10^6 cells ml^{-1} in BMDC medium containing 1 μM tamoxifen (Sigma). This procedure was repeated at day 7 and cells were further cultured until day 10–11. The cells that had successfully recombined were identified as GFP-positive (∼50% of the cell). To evaluate the efficiency of *Arpc2* gene depletion, GFP$^+$ cells were isolated by FACS sorting and analysed for the expression of Arpc2 by immunoblot. About 75% gene depletion was usually obtained.

Macropinocytosis in migrating DCs. LifeAct–GFP DCs were incubated for 30 min in 200 ng ml^{-1} Hoechst 33342, washed and resuspended in BMDC medium containing 0.4 mg of ovalbumin (OVA) coupled to Alexa-647 (OVA–647). DCs were loaded in micro-channels and their nucleus, actin cytoskeleton and macropinosomes were simultaneously imaged on a Nikon TiE video-microscope with a ×20 objective. The LifeAct–GFP signal was used to generate a mask for each cell. This mask was used to measure the amount of OVA–647 located at the front of the nucleus with a custom ImageJ program to determine the amount of macropinocytosed material. The size and number of macropinosomes were evaluated by imaging cells at their central plane at ×100 magnification on an inverted spinning-disc confocal Roper/Nikon microscope.

LifeAct–GFP imaging and density maps. BMDCs generated from LifeAct–GFP knock-in mice were loaded in micro-channels and imaged for 6 h at 20× using an epifluorescence Nikon TiE video-microscope equipped with a cooled CCD camera (HQ2, Photometrics). On movie reconstruction, individual cells migrating in the channels were cropped using the ImageJ software. To map the LifeAct–GFP signal, the images obtained for each individual cell were aligned in a single column. Cell size normalization was applied to each time point according to the mean cell size and background subtraction. To obtain the mean behaviour of the cell, every time point was projected on average. The mean behaviour of the population was next obtained by projecting the mean signal of every individual cell (Supplementary Fig. 2). This procedure was performed using an ImageJ-compatible custom macro.

Immunofluorescence in micro-channels. Migrating BMDCs were allowed to migrate in micro-channels for 16 h. Cells were fixed with 4% paraformaldehyde (PFA) for 30 min at room temperature and blocked with PBS–2% BSA for 1 h. After blocking, the PDMS was carefully separated from the coverslip that formed the bottom part of the channel and on which most cells remained attached. Cells were next permeabilized with PBS containing 0.2% BSA and 0.05% saponin for 10 min and stained by sequential incubations with primary and secondary antibodies diluted in the permeabilization buffer. Slides were mounted using DAPI Fluoromount-G (SouthernBiotech) and visualized on an inverted spinning-disc confocal Roper/Nikon microscope with a 100× 1.4 NA oil immersion objective. In the case of Arp2 and mDia1 immunostaining, after PFA fixation cells were incubated with cold methanol for 30 s and then permeabilized using 0.02% Triton X-100 for 2 min before staining. To map Arp2 and mDia1 together with LifeAct–GFP signal DCs were stained with an anti-GFP antibody. Unfortunately, methanol fixation disrupted the actin patch observed in live LPS-DCs. To map Arp2 and mDia1 localization cells were imaged at ×20 using an epifluorescence Nikon TiE video-microscope and overlapped as described.

Immunoblotting. DCs were lysed for 2 min in a buffer containing 100 mM Tris, 150 mM NaCl, 0.5% NP-40 and a protease inhibitor cocktail tablet (Roche). Fifty micrograms of soluble extracts were loaded onto a 4–20% TGX gradient gel (BioRad) and transferred onto a Trans-Blot Turbo PVDF/Nitrocellulose membrane (BioRad). The membrane was blocked, incubated sequentially with the appropriate antibodies and revealed using the SuperSignal West Dura substrate (Thermo Scientific). Membranes were cut accordingly to the molecular weight of the protein of interest. This allowed us to evaluate different labelling in the same run. As consequence, full membranes were in most cases only fragments (Supplementary Fig. 8).

Migration in collagen gels. Collagen experiments were performed as described previously[46]. DCs were mixed at 4 °C with 1.6% bovine collagen type I (Advanced BioMatrix) at basic pH. Forty microlitres of the mix was deposited on a 35 mm glass -bottom dish and the drop was homogenized while covered with a 12 mm glass slide. The sample was incubated at 37 °C for 20 min to allow collagen polymerization. To generate the CCL21 gradient, 2 ml of BMDC medium containing 200 ng ml^{-1} of CCL21 was added to the plate. Cells were imaged (phase contrast) at a frequency of 1 image per 2 min using a ×10 objective overnight. Contiguous positions were stitched using the FIJI plugin Grid/collection stitching[47] and images were processed to extract cell tracks. The mean image of the movie was subtracted from every time point and white objects in a dark background were detected. Resulting movies were processed using the FIJI plugin Filter Mean (Intensity 3) and cells were tracked using custom software[48].

Migration in ear explants. Migration of DCs was performed as recently described, but modified to work with classic multi-position epifluorescence inverted microscopes[39]. Briefly, the epidermal sheet of isolated mice ears was removed, exposing the dermal part located just under the skin. After isolation, the dermal side was incubated sequentially with rat-anti Lyve1 (R&D) and anti-rat Alexa647 (Life technologies) for 1 h at 4 °C. CFSE (Life technologies) or CMTMR (Life technologies)-coloured LPS-DCs were added on top of the exposed dermal side of the skin for 1 h. Loosely attached cells were washed off and ears mounted on a PDMS block that kept the tissue flat. The block was inverted on top of a glass plate and immobilized to allow long-lasting cell recording on an epifluorescence Nikon TiE video-microscope equipped with a cooled CCD camera (HQ2, Photometrics). Tracks of migratory cells were obtained using the FIJI plugin MTrackJ.

Tracking analysis of ears DC migration. To analyse cell trajectories, custom C++ routines coupled with R (ref. 49) were developed[48]. The mean square displacement (MSD) was computed and fitted as previously described[50]. The squared distance between every two points of a cell track separated by a specific time lag was averaged over the entire population of trajectories. MSDs are ultimately plotted as a function of increasing time lag. The path persistence of a trajectory was defined as the ratio between the length of the cell path and the diameter of the theoretical disc containing the entire trajectory. It tends to 1 for very persistent tracks and to 0 for cells continuously changing their direction.

DCs homing to LNs. BMDCs generated from mDia1WT and KO mice were concentrated at 10×10^6 cells ml^{-1} in serum-free media and labelled for 10 min at 37 °C with either 2.5 μM CFSE (Invitrogen) or 2.5 μM CMTMR (Invitrogen) before stopping the reaction with complete medium. We stimulated BMDCs with 100 ng ml^{-1} LPS for 30 min at 37 °C, washed them twice and mixed them in equal numbers. Then, 20 μl of the mixed cell suspension containing 2×10^6 cells of each genotype was injected into the footpad of recipient C57BL/6 mice and 16 h later popliteal lymph nodes were collected, dissected and digested by incubating with 1 mg ml^{-1} collagenase D (Roche) for 30 min. To rule out any dye-specific effects, in each experiment cells from both genotypes were labelled by exchanging dies. For each genotype we calculated the homing index as the ratio of $CFSE_{LN}/CMTMR_{LN}$ to $CFSE_{Input}/CMTMR_{Input}$ to determine relative migratory capacity (LN: lymph node).

Statistics and reproducibility. Most of the experiments shown in figures correspond to representative experiments in which *n* cells were analysed as indicated in the legends. Migration experiments typically contained 40–100 cells per condition. An internal control (iDCs compared with LPS-DCs) was included in each migration experiment. Each experiment validated based on this internal control was repeated two or three times and conclusions were made only when results were reproduced in each individual experiment. Immunofluorescence experiments were systematically quantified using unbiased methods applied to data obtained from at least two independent experiments. In general, statistical comparison of internal samples was carried out using the non-parametric Mann–Whitney test except in collagen assays where the number of cells was extremely high (more than 2,000 tracks). In that case tracks were randomly selected and analysed with the appropriate statistical test (see figure legends). No statistical method was used to predetermine sample size. The experiments were not randomized and the investigators were not blinded to allocation during experiments and outcome assessment.

43. Forster, R. *et al.* CCR7 coordinates the primary immune response by establishing functional microenvironments in secondary lymphoid organs. *Cell* **99,** 23–33 (1999).
44. Riedl, J. *et al.* Lifeact mice for studying F-actin dynamics. *Nat. Methods* **7,** 168–169 (2010).
45. Muzumdar, M. D., Tasic, B., Miyamichi, K., Li, L. & Luo, L. A global double-fluorescent Cre reporter mouse. *Genesis* **45,** 593–605 (2007).
46. Wolf, K. *et al.* Physical limits of cell migration: control by ECM space and nuclear deformation and tuning by proteolysis and traction force. *J. Cell Biol.* **201,** 1069–1084 (2013).
47. Preibisch, S., Saalfeld, S. & Tomancak, P. Globally optimal stitching of tiled 3D microscopic image acquisitions. *Bioinformatics* **25,** 1463–1465 (2009).
48. Maiuri, P. *et al.* The first world cell race. *Curr. Biol.* **22,** R673–R675 (2012).
49. R-Core-Team. *R: A Language and Environment for Statistical Computing* (R Foundation for Statistical Computing, 2014); http://www.r-project.org
50. Selmeczi, D., Mosler, S., Hagedorn, P. H., Larsen, N. B. & Flyvbjerg, H. Cell motility as persistent random motion: theories from experiments. *Biophys. J.* **89,** 912–931 (2005).

Corrigendum: Innate control of actin nucleation determines two distinct migration behaviours in dendritic cells

Pablo Vargas, Paolo Maiuri, Marine Bretou, Pablo J. Sáez, Paolo Pierobon, Mathieu Maurin, Mélanie Chabaud, Danielle Lankar, Dorian Obino, Emmanuel Terriac, Matthew Raab, Hawa-Racine Thiam, Thomas Brocker, Susan M. Kitchen-Goosen, Arthur S. Alberts, Praveen Sunareni, Sheng Xia, Rong Li, Raphael Voituriez, Matthieu Piel and Ana-Maria Lennon-Duménil

Nat. Cell Biol. **18,** 43–53 (2015); published online 7 December 2015; corrected online 23 December 2015

In the version of this Article originally published, references 42 and 43 were incorrect. They have been replaced with the following single reference:

42. Veltman, D. M. *et al.* PIP_3-dependent macropinocytosis is incompatible with chemotaxis. *J. Cell Biol.* **204,** 497–505 (2014).

References 44–51 have been renumbered accordingly. These changes have been made in all online versions of the Article.

nature cell biology

DOI: 10.1038/ncb3284

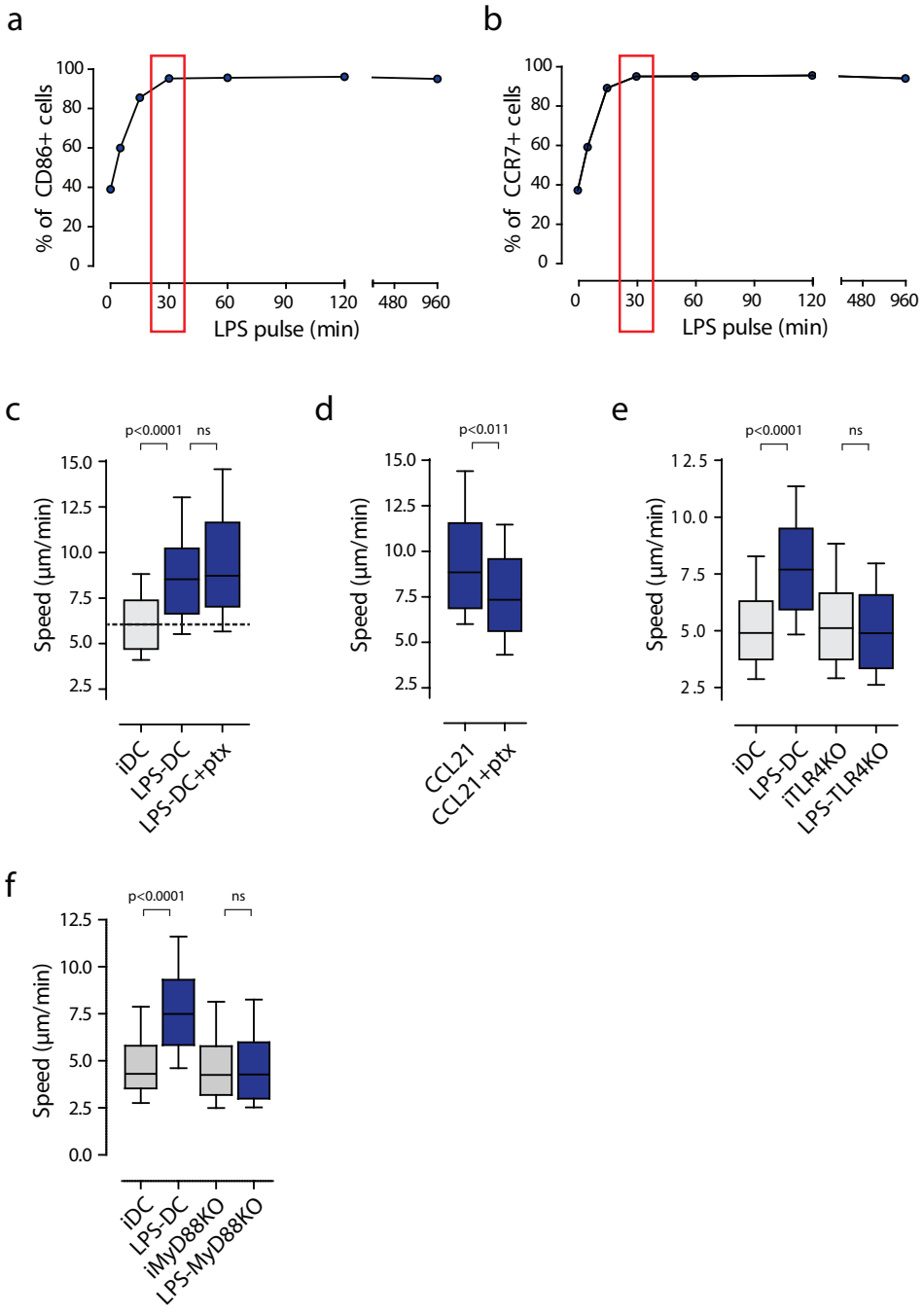

Supplementary Figure 1 DC migration becomes faster and more persistent upon LPS treatment. **a-b,** Analysis by flow cytometry of surface expression of the DC activation marker CD86 and the chemokine receptor CCR7. iDCs were incubated for different times with LPS (100 ng/ml), washed and cultured overnight. 30 min was found to be the minimal time to get the highest level of activation and CCR7 expression. 1 representative experiment out of 3 is shown. **c**, Mean instantaneous speed of migrating DCs in the presence of Pertussis toxin (Ptx, 200 µg/ml) in fibronectin- (c) or fibronectin plus CCL21- (d) coated micro-channels (n= 80, 94 and 91 for iDC, LPS-DC and LPS-DC Ptx respectively). 1 representative experiment out of 2 is shown. **d**, Ptx does not affect the LPS-induced increment in DC speed (c) but decreases the velocity of LPS-DCs migrating in the presence of CCL21 (d) (positive control for the activity of Ptx, n=92 and 100 for CCL21 and CCL21 Ptx respectively). 1 representative experiment out of 2 is shown. **e,** Mean instantaneous speed of WT and TLR4KO DCs migrating in micro-channels (n=150, 150, 152 and 122 for iDC, LPS-DC, iTLR4KO and LPS-TLR4KO cells respectively). 1 representative experiment out of 2 is shown. **f,** Mean instantaneous speed of control and Myd88KO DCs migrating in micro-channels (n=81, 74, 67 and 102 for iDC, LPS-DC, iMyd88KO and LPS-Myd88KO respectively). 1 representative experiment out of 3 is shown. The Mann-Whitney test was applied for statistical analyses in c-f. In the box plots of panels c-f the bars include 90% of the points, the center corresponds to the median and the box contains 75% of the data.

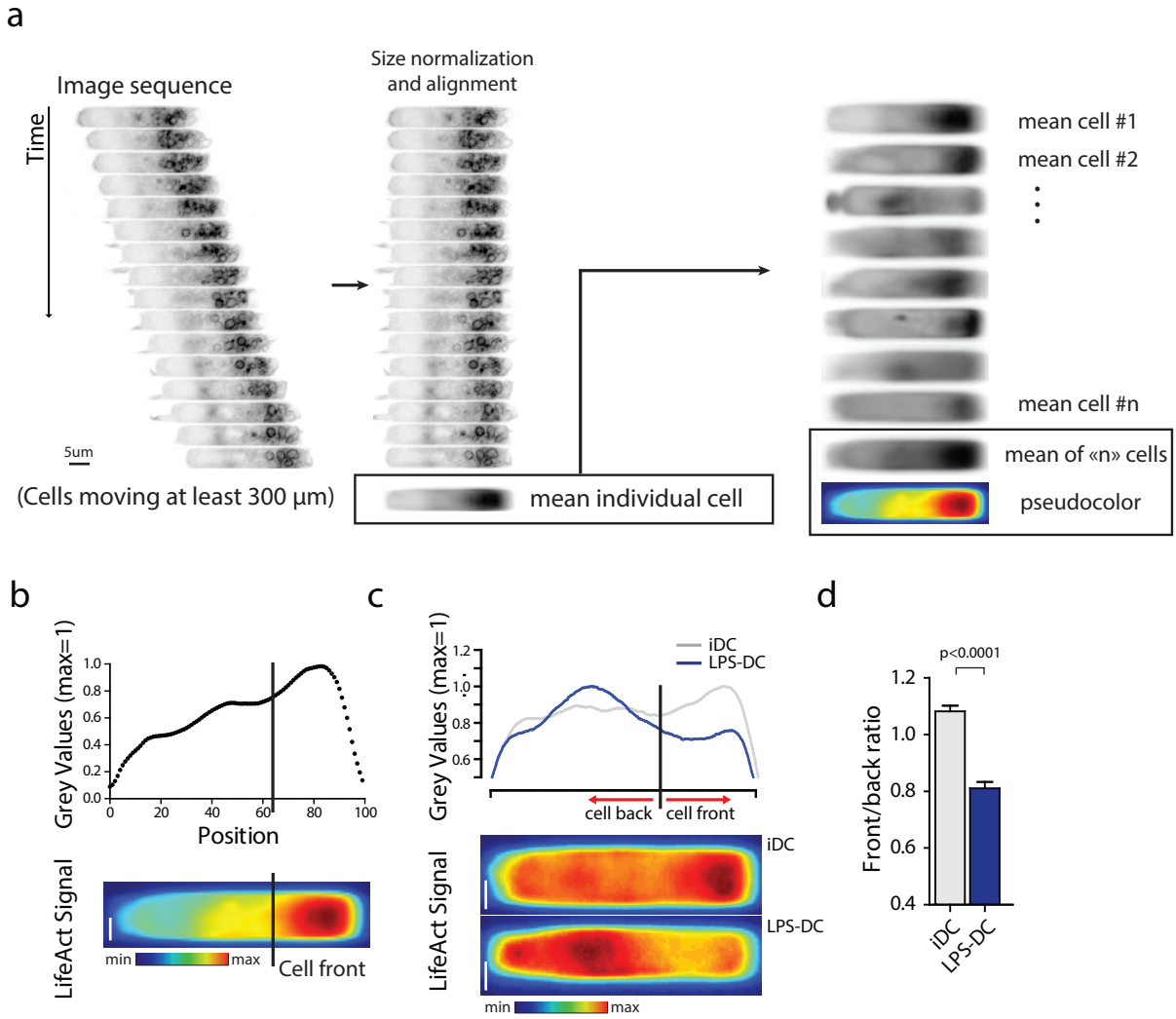

Supplementary Figure 2 Quantification of LifeAct-GFP dynamics in migrating DCs. **a-b,** Method used to quantify LifeAct-GFP localization in migrating DCs. Sequential images of LifeAct-GFP DCs were acquired on an epifluorescence microscope every 1min at 20x. Scale bar: 10µm. **a,** The LifeAct-GFP signal recorded at each time-point was integrated into a single image for all migrating cells. Cell alignment and cell size normalization were applied to generate the LifeAct-GFP density maps. Scale bar: 5 µm. **b**, Mean intensities obtained for each cell were averaged into a single LifeAct-GFP density map, assigning equivalent weight to each cell. Scale bar: 2.5 µm. **c-d,** Analysis of the LifeAct-GFP front/back ratio in iDCs and LPS-DCs migrating in micro-channels. The front was defined as the first third of the cell. Scale bar: 2.5 µm. Results obtained by analyzing the data showed in Fig. 2a-c (n=31 and 27 cells for iDC and LPS-DC respectively). 1 representative experiment out of 4 is shown. Graphic shows mean and error bars correspond to S.E.M. The Mann-Whitney test was applied for all statistical analysis.

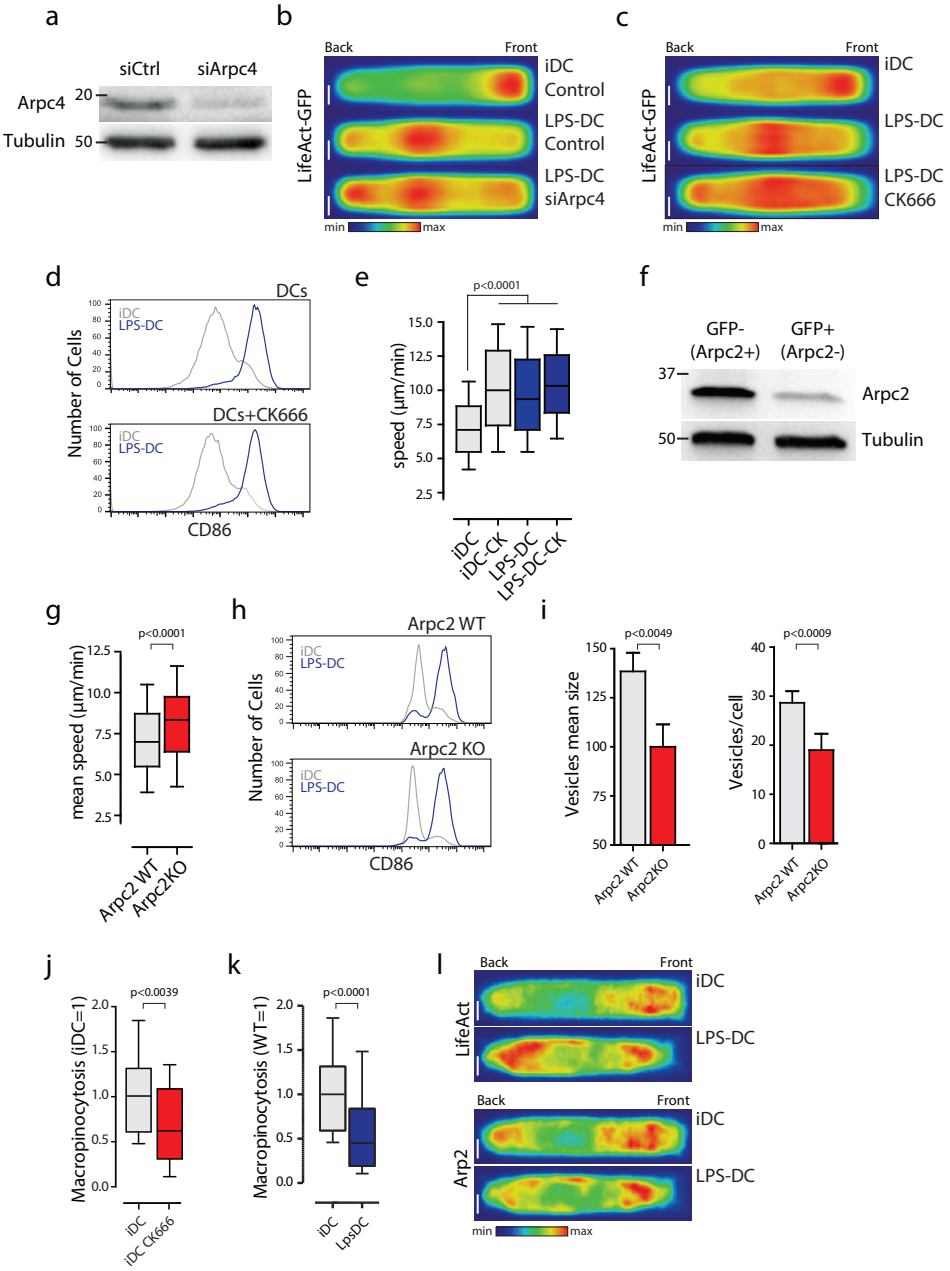

Supplementary Figure 3 Arp2/3 decreases the migration of iDCs but enhances their antigen uptake capacity. **a,** Immunoblot blot analysis of Arpc4 expression in BMDCs nucleofected with Arpc4-specific siRNA. **b, c,** LifeAct-GFP density maps obtained from iDC or LPS-DC silenced (**b**) or inhibited (**c**) for Arp2/3. LPS-DCs were treated with the Arp2/3 inhibitor CK666 (25 μM) or silenced for Arpc4. Scale bar: 2.5 μm. 1 representative experiment out of 2 is shown. **d,** Analysis by flow cytometry of surface expression of the DC activation marker CD86. iDCs were incubated 30 min with LPS (100 ng/ml), washed and cultured overnight. 1 experiment out of 4 is shown. **e**, Mean instantaneous speed of DCs migrating in micro-channels and treated or not with CK666 as in c (n=244, 192, 231 and 230 for iDC, iDC-CK666, LPS-DC and LPS-DC CK666 respectively). 1 representative experiment out of 3 is shown. **f**, Immunoblot analysis of Arpc2 and tubulin expression in tamoxifen-treated DCs. TomatoFP$^+$ (Arpc2WT) and conditional GFP$^+$ (Arpc2KO) iDCs were sorted from 10-days- DC cultures in which tamoxifen was added during the last 8 days. **g,** Analysis of the migration of Arpc2WT and KO iDCs under an agarose gel. Cells were imaged during 200 min and their cell speed was quantified after tracking. The analysis was performed on cells that had migrated >100 μm (n= 80 and 163 for Arpc2 WT and Arpc2 KO respectively). 1 representative experiment out of 2 is shown. **h,** Analysis by flow cytometry of surface expression of the DC activation marker CD86 performed as in d. **i**, Quantification of the size (left) and number (right) of vesicles present at the front of Arpc2WT and KO DCs migrating in micro-channels filled with fluorescent ovalbumin (n=36 and 37 for Arpc2WT and Arpc2 KO respectively). Graphics show mean and error bars correspond to S.E.M. **j,** Macropinocytic capacity of migrating DCs treated with the Arp2/3 inhibitor CK666 (n=62 and 41 for iDC and iDC CK666 respectively). 1 representative experiment out of 3 is shown. **k,** Macropinocytic capacity of iDCs and LPS-DCs (n=39 and 33 for iDC and LPS-DC respectively). 1 representative experiment out of 2 is shown. **l,** Density maps obtained from LifeAct-GFP DCs fixed while migrating in micro-channels and stained for Arp2 and GFP. Scale bar: 2.5 μm. In the box plots of panels e, g, j and k the bars include 90% of the points, the center corresponds to the median and the box contains 75% of the data. The Mann-Whitney test was applied for all statistical analyses.

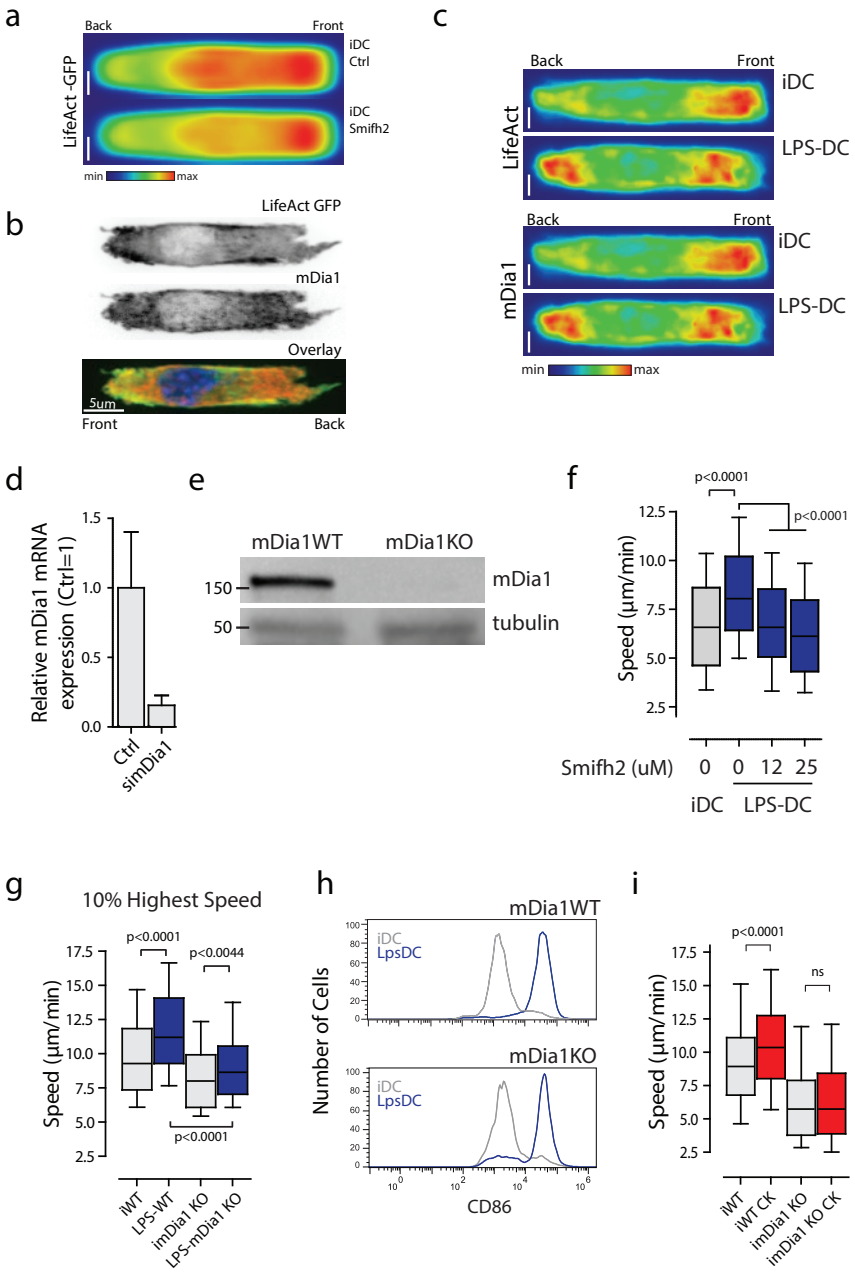

Supplementary Figure 4 Actin distribution at the back of DCs relies on the Formin mDia1 and is required for fast and persistent migration. **a,** LifeAct-GFP density maps of iDCs migrating in the presence or absence of the formin inhibitor Smifh2 (25 µM). 1 representative experiment out of 3 is shown. Scale bar: 2.5 µm. **b,** Immunofluorescence analysis of mDia1 expression in LPS-DCs migrating in micro-channels analyzed by spinning disk microscope (100x). Scale bar: 5 µm. **c**, Density maps obtained from LifeAct-GFP DC fixed while migrating in micro-channels and stained for mDia1 and GFP (2 independent experiments). Scale bar: 2.5 µm. **d**, Quantitative PCR analysis of mDia1 expression in DCs nucleofected with mDia1-specific siRNA. Graphic shows mean and error bars correspond to S.E.M. **e,** Immunoblot analysis of mDia1 and tubulin expression in immature mDia1WT and KO DCs. 1 representative experiment out of 3 is shown. **f,** Mean instantaneous speed of LPS-DCs migrating in micro-channels and treated with different doses of Smifh2 (n=125, 154, 134 and 141 for iDC, LPS-DC, LPS-DC 12 µM and LPS-DC 25 µM respectively). 1 representative experiment out of 3 is shown. **g**, 10% of the highest instantaneous speed values of DCs migrating in micro-channels (n=210, 238, 233 and 179 for iWT, LPS-WT, imDia1KO and LPS-mDia1KO respectively). 1 representative experiment out of 5 is shown. **h,** Analysis by flow cytometry of surface expression of the DC activation marker CD86. iDCs were incubated 30 min with LPS (100 ng/ml), washed and cultured overnight. 1 experiment out of 4 is shown. **i,** Mean instantaneous speed of mDia1WT and KO migrating in micro-channels and treated with CK666 (25 µM) (n=119, 107, 52 and 111 for iWT, iWT CK, imDia1KO and imDia1KO CK respectively). 1 representative experiment out of 2 is shown. In the box plots of panels f, g and i the bars include 90% of the points, the center corresponds to the median and the box contains 75% of the data. The Mann-Whitney test was applied for all statistical analyses.

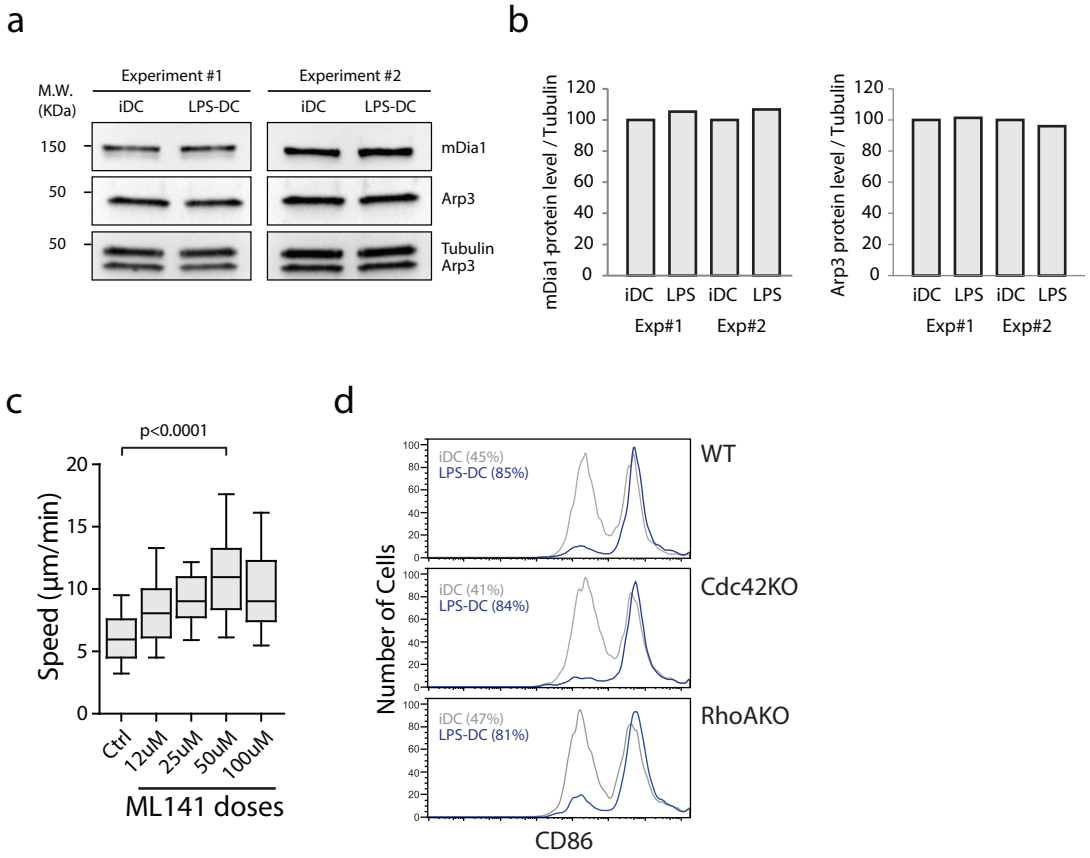

Supplementary Figure 5 Regulation of DC Arp2/3- and mDia1-dependent actin nucleation by Cdc42 and RhoA. **a, b**. iDCs were treated with LPS for 30 min, washed and further cultured at 37°C during 16h. **a**. Immunoblot analysis was performed as described in the supplementary experimental procedures. **b**. Normalized intensity obtained from data showed in panel a. Graphics show mean individual values. **c**, Mean instantaneous speed of iDCs migrating in micro-channels and treated with different doses of ML141 (n=164, 163, 142, 143 and 39 for iDC, iDC 12 µM, iDC 25 µM, iDC 50 µM and iDC 100 µM respectively). 1 experiment out of 3 is shown. In the box plot the bars include 90% of the points, the center corresponds to the median and the box contains 75% of the data. The Mann-Whitney test was applied for statistical analysis. **d**, Analysis by flow cytometry of surface expression of the DC activation marker CD86. iDCs were incubated 30 min with LPS (100 ng/ml), washed and cultured overnight.

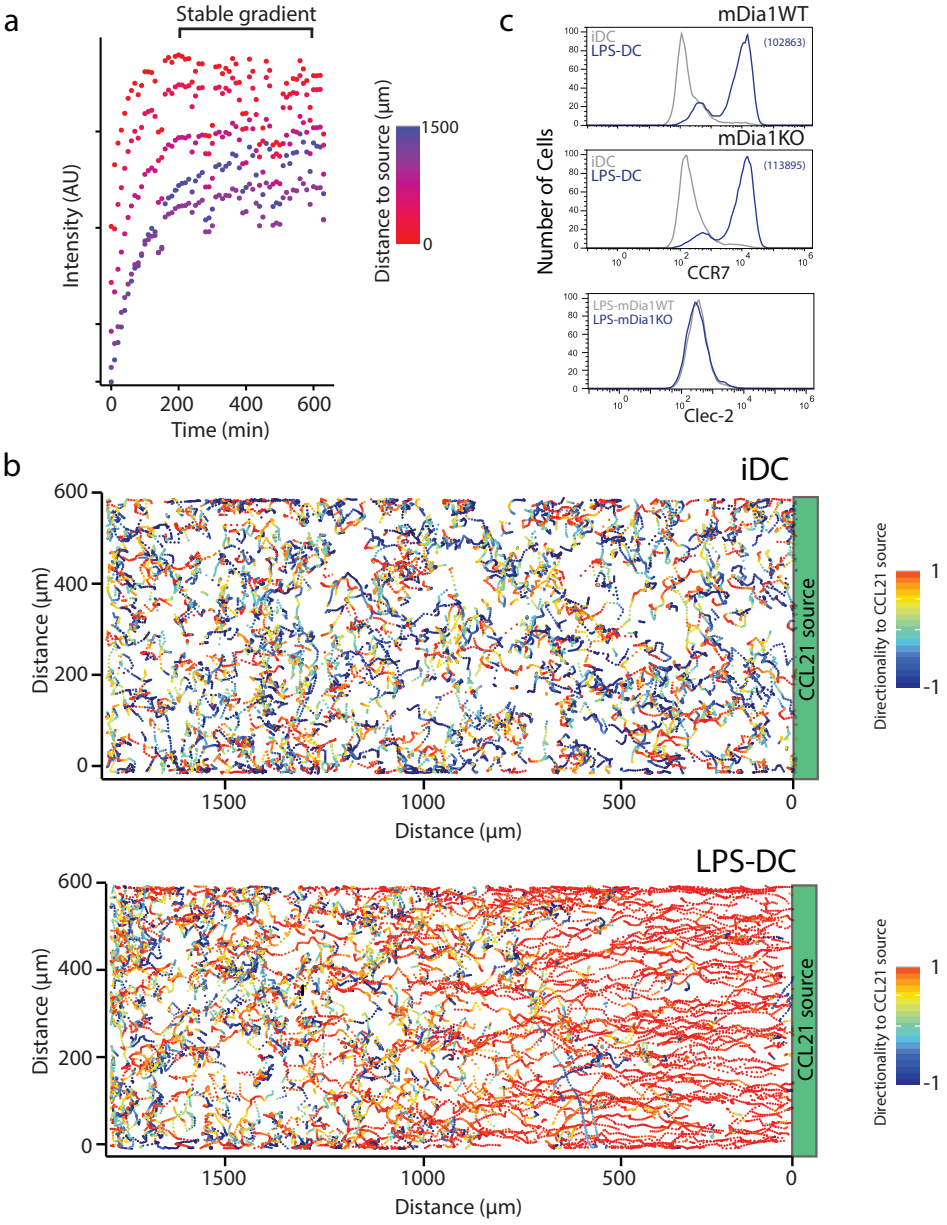

Supplementary Figure 6 Analysis of chemokine gradient sensing by iDCs and LPS-DCs. **a,** Collagen gels were bathed with a solution containing fluorescent ovalbumin (OVA), to evaluate protein penetration in the gel. Gradient steepness was evaluated by measuring the changes in fluorescence intensity according to the protein source using an epifluorescence microscope. Areas closer to the protein source (red) reached a plateau faster than distal areas (blue). After 200 min the gradient was considered as stable at any distance from the source. All the images showed in the paper correspond to analysis between 200 min and 600 min after addition of the chemokine. **b,** CCR7 and Clec-2 surface staining using flow cytometry was performed in DCs treated with LPS (100ng/ml) for 30 min and further cultured overnight. Geometric mean of fluorescence in the CCR7 positive population is depicted. **c**, Trajectories of iDCs (upper panel) and LPS-DCs (lower panel) along the CCL21 gradient formed in collagen gels. Directionality of segments of cell trajectories is shown in different colors: from red (toward the source) to blue (against it).

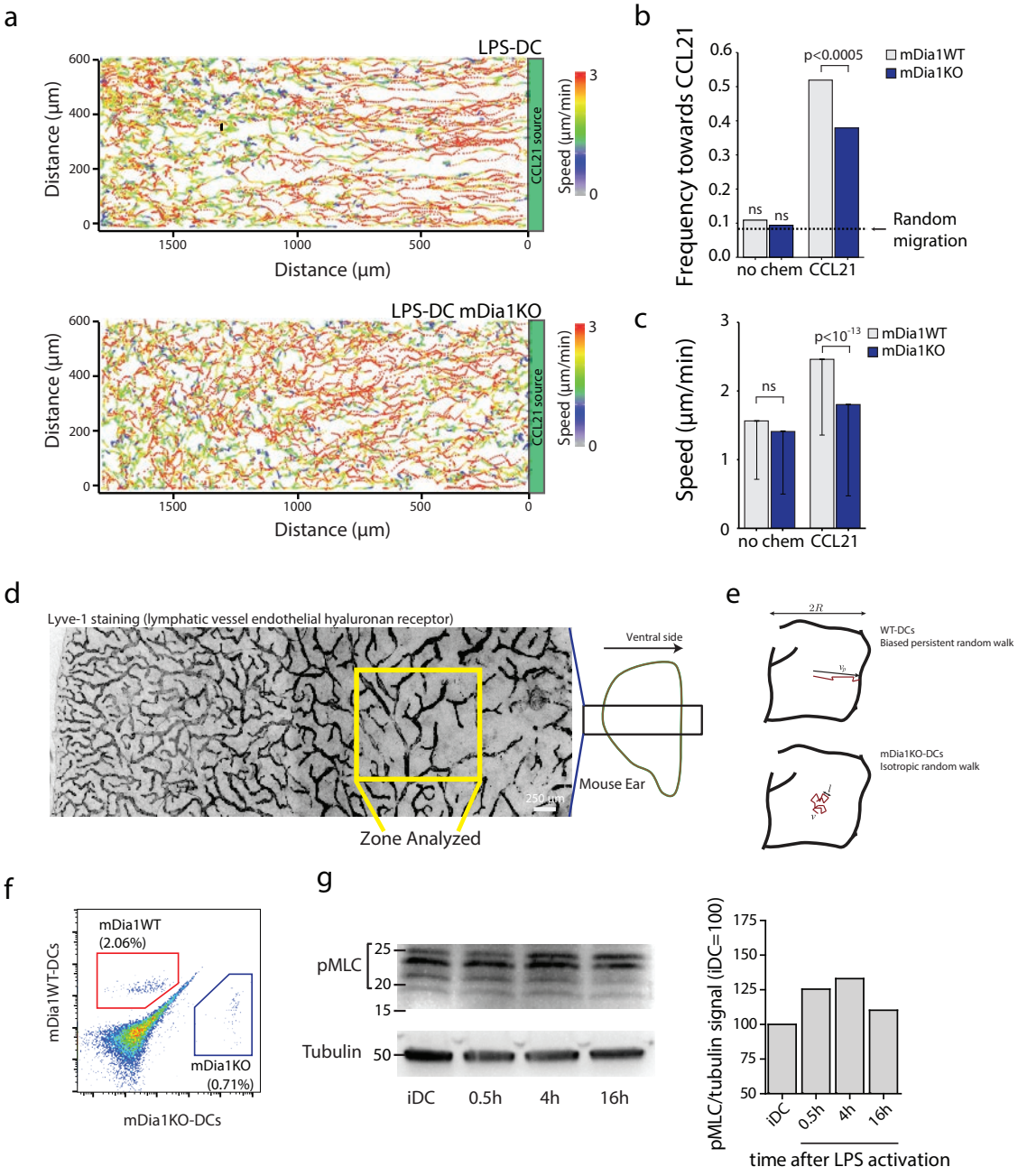

Supplementary Figure 7 Analysis of chemokine gradient sensing by mDia1KO LPS-DCs. **a,** Trajectories of WT (upper panel) and mDia1KO LPS-DCs (lower panel) along the CCL21 gradient formed in collagen gels. Speed of segments of cell trajectories is shown in different colors: from red (fast) to blue (slow). **b,** frequency of movement in the direction of the gradient in the 500 µm closer to the CCL21 source compared to random migration in absence of chemokines. Values are compared to equivalent position in the absence of chemokines. Analysis performed in 500 random tracks due to oversampling. **c**, Mean speed of DCs in the 500 µm closer to the CCL21 source. Analysis performed in 500 random tracks due to oversampling. Error bars correspond to S.D. Student's t-Test was applied for statistical analysis in b. Chi-squared Test was applied for statistical analysis in c. **d,** Ear explant stained with the anti-Lyve-1 marker to highlight LVs. The area enclosed in the yellow square corresponds to the zone analyzed when monitoring DC migration to LVs. Scale bar 250 µm. **e,** Scheme of different types of trajectories representing the behavior of mDia1WT and KO LPS-DCs in the ear explants. **f.** mDia1WT and KO LPS-DCs were stained with CMTRM or CFSE and co-injected in the footpad of WT recipient mice. Their presence in the popliteal lymph node 16 h later was analyzed by flow cytometry. Example representative of 3 experiments is shown. **g**, pMLC levels on DCs activated 30 min with LPS and cultured during the indicated time. The pMLC signal was normalized to tubulin levels.

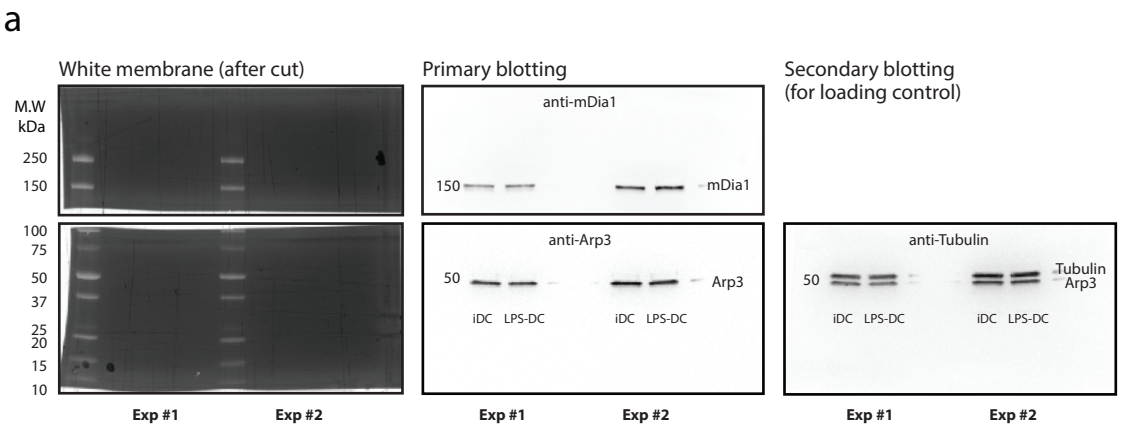

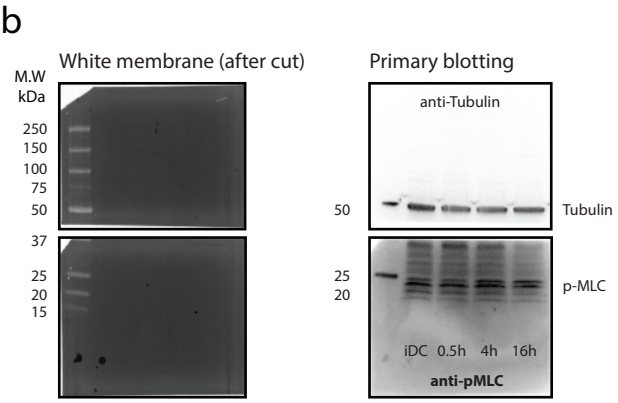

Supplementary Figure 8 Unprocessed full scans of key blots. **a**, Full scans of immunoblots showed in supplementary figure 5a. The whole membrane was divided in two based on the 100 kDa molecular weight marker (left panel). Each blot was sequentially incubated with the indicated primary antibody and the corresponding HRP-conjugated secondary antibody (central panel). For loading controls, the membrane containing the 50 kDa band was incubated sequentially with an anti-tubulin antibody and revealed with the corresponding HRP-conjugated secondary antibody (right panel). **b**, Full scans of immunoblots showed in supplementary figure 7g. Blots were obtained as described in a, except that the gel was cut based on the 37 kDa molecular weight marker, allowing detection of phospho-MLC and tubulin in the same run.

Supplementary Video Legends

Supplementary video 1: Distinct LifeAct-GFP dynamics in iDCs and LPS-DCs
LifeAct-GFP-expressing DCs migrating in 8 µm x 5µm fibronectin-coated micro-channels and time-lapsed on a spinning disk microscope (20x) at a frequency of 1 image/2min. Scale bar 5 µm.

Supplementary video 2: F-actin is enriched in ruffles at the front of iDCs
LifeAct-GFP-expressing iDCs migrating in 8 µm x 5µm fibronectin-coated micro-channels and time-lapsed on a spinning disk microscope (100x) at a frequency of 1 image/400ms. The cortex of a representative cell is shown. Scale bar 5 µm.

Supplementary video 3: F-actin is enriched at the rear of LPS-DCs
LifeAct-GFP-expressing LPS-DCs migrating in 8 µm x 5µm fibronectin-coated micro-channels and time-lapsed on a spinning disk microscope (100x) at a frequency of 1 image/400ms. The cortex of a representative cell is shown. Scale bar 5 µm.

Supplementary video 4: LPS-DCs but not iDCs respond to CCL21 gradients
iDCs and LPS-DC migrating along a CCL21 gradient in a collagen gel. The frequency of acquisition was 1 image/2 min (10x) on a video-microscope. The source of CCL21 is at the right of the movie. Scale bar 50 µm.

Supplementary video 5: Chemotaxis of wild-type and mDia1KO LPS-DCs in vitro
mDia1 wild-type and KO LPS-DCs migrating along a CCL21 gradient in a collagen gel. 1 image/2min (10x) was acquired on a video-microscope. The source of CCL21 is at the right of the movie. Scale bar 50 µm.

Supplementary video 6: Chemotaxis of wild-type and mDia1KO LPS-DCs in vivo
mDia1 wild-type (red) and KO (green) LPS-DCs migrating in an ear explant. 1 image/2min (20x) was acquired on a on a video-microscope. Scale bar 50 µm.

Abstract

In secondary lymphoid organs, B cells acquire antigens that are tethered at the surface of neighboring cells. Engagement of the B cell receptor (BCR) with such immobilized antigens leads to the formation of an immune synapse and the subsequent polarization of B cells. This includes the repositioning of the centrosome towards the immune synapse as well as the recruitment and local secretion of lysosomes required for efficient antigen extraction, processing and presentation onto class II major histocompatibility complex (MHC-II) molecules to primed CD4+ T cells. Pioneer work performed in the lab has highlighted the first molecular players involved in this process. However, the precise mechanism governing centrosome polarization remains to be fully elucidated. The work performed during this thesis aimed at identifying new regulators supporting centrosome polarization in B lymphocytes upon BCR engagement with immobilized antigens. In addition, in view of the emerging role played by the tissue microenvironment in shaping B cell activation and functions we investigated whether extracellular Galectin-8 modulates the ability of B cells to polarize, extract and present immobilized antigens.

We show here that, in resting lymphocytes, centrosome-associated Arp2/3 (actin related protein-2/3) locally nucleates F-actin, which is needed for centrosome tethering to the nucleus via the LINC (linker of nucleoskeleton and cytoskeleton) complex. Upon lymphocyte activation, Arp2/3 is partially depleted from the centrosome as a result of its HS1-dependent recruitment to the immune synapse. This leads to a reduction in F-actin nucleation at the centrosome and thereby allows its detachment from the nucleus and polarization to the synapse. In addition, we show that extracellular Galectin-8 favors lysosome recruitment and secretion at the immune synapse, hence providing B cells with an enhanced capacity to extract and present immobilized antigens.

Our findings highlight unexpected mechanisms that tune B cell polarity in response to antigenic stimulation and raise exciting questions concerning the coordinated regulation of these mechanisms to provide B cells with the capacity to efficiently extract, process and present surface-tethered antigens.

Résumé

Dans les organes lymphoïdes secondaires, les lymphocytes B acquièrent des antigènes immobilisés à la surface de cellules voisines. L'engagement du BCR (récepteur des cellules B) avec de tels antigènes induit la formation d'une synapse immunologique et la polarisation des lymphocytes B. Cette polarisation inclut le repositionnement du centrosome à la synapse immunologique ainsi que le recrutement et la sécrétion locale des lysosomes qui sont nécessaires à l'extraction, l'apprêtement et la présentation des antigènes sur les molécules du complexe majeur d'histocomptabilité de classe II (CMH-II) aux lymphocytes T CD4+ pré-activés. Des travaux précurseurs menés dans le laboratoire ont permis de mettre en évidence les premiers acteurs moléculaires impliqués dans ce processus. Cependant, le mécanisme précis gouvernant la polarisation du centrosome demeure encore aujourd'hui inconnu. Le travail réalisé pendant cette thèse avait pour objectif d'identifier de nouveaux régulateurs contrôlant la polarisation du centrosome dans les lymphocytes B après engagement du BCR avec des antigènes immobilisés. De plus, au regard du rôle grandissant joué par le microenvironnement tissulaire dans l'activation des lymphocytes B ainsi que dans la modulation de leurs fonctions, nous avons étudié l'effet de la protéine extracellulaire Galectine-8 sur la régulation de la capacité des lymphocytes B à se polariser et à extraire et présenter des antigènes immobilisés.

Le travail présenté dans ce manuscrit montre que la présence du complexe Arp2/3 au centrosome des lymphocytes B non activés permet la nucléation locale de filaments d'actine qui permettent, grâce à leur interaction avec le complexe LINC, de lier le centrosome au noyau. L'activation des lymphocytes B induit la déplétion partielle du complexe Arp2/3 du centrosome qui est recruté à la synapse immunologique par la protéine HS1. Ceci induit une diminution de la nucléation d'actine au centrosome entraînant la séparation entre le centrosome et le noyau et permettant la polarisation du centrosome vers la synapse. De plus, nous montrons que la présence de la protéine Galectine-8 dans le milieu extracellulaire favorise le recrutement et la sécrétion des lysosomes à la synapse immunologique, conférant aux lymphocytes B une meilleure capacité à extraire et présenter des antigènes immobilisés.

Nos résultats mettent en évidence des mécanismes inattendus régulant la polarisation des lymphocytes B en réponse à une stimulation antigénique et soulèvent des questions intéressantes concernant la régulation coordonnée de ces mécanismes qui confèrent aux lymphocytes B la capacité d'extraire, d'apprêter et de présenter des antigènes immobilisés efficacement.